




ADVERTIMENT. L'accés als continguts d'aquesta tesi queda condicionat a l'acceptació de les condicions d'ús establertes per la següent llicència Creative Commons:  <https://creativecommons.org/licenses/?lang=ca>

ADVERTENCIA. El acceso a los contenidos de esta tesis queda condicionado a la aceptación de las condiciones de uso establecidas por la siguiente licencia Creative Commons:  <https://creativecommons.org/licenses/?lang=es>

WARNING. The access to the contents of this doctoral thesis it is limited to the acceptance of the use conditions set by the following Creative Commons license:  <https://creativecommons.org/licenses/?lang=en>

CITIES GEOGRAPHICAL PATTERNS IN A CHANGING CLIMATE

A Perspective on Latin-American Settlements From Outer Space

UAB

Universitat Autònoma
de Barcelona



PhD Dissertation

CITIES GEOGRAPHICAL PATTERNS IN A CHANGING CLIMATE

A perspective on Latin-American settlements from outer space

Rafael VAN DER BORGHT

Directora y Tutora:

Dra. Montserrat Pallares-Barbera,
Departament de Geografia. Universitat Autònoma de Barcelona

Programa de Doctorat en Geografia
Departament de Geografia
Universitat Autònoma de Barcelona
Bellaterra, juny de 2024

À Xavier et Jacques.

Agradecimientos

Aunque los cuatro años de esta tesis a ratos se asemejaron a una travesía en solitario por un desierto, gran parte de lo que se presenta en las siguientes páginas no se hubiese podido escribir sin el apoyo de las personas que me han acompañado en este recorrido. A todas ellas les dedico las siguientes líneas a modo de agradecimiento.

Primero, a Montserrat Pallares-Barbera, Directora de esta tesis, por haber contestado al email enviado a inicios de abril del 2020. En ese momento, el planeta estaba inmerso en “la primera ola” de la Covid-19 y cada día traía su propia noticia surrealista. Para mí, una de esas noticias surrealista fue que Montserrat no descartara el proyecto de tesis Doctoral que le presentaba un desconocido que en ese momento residía en Santiago de Chile y que, para colmo, ni siquiera tenía una formación académica en Geografía. Por esa primera acogida, gracias. Y sobre todo gracias por las orientaciones, recomendaciones, consejos y oportunidades brindadas que, sin lugar a duda, han sido claves para poder llevar a cabo este proyecto.

Luego, a todas las personas que, de una manera u otra, me han encaminado hacia la tesis doctoral. José Eduardo Alatorre tiene una responsabilidad de peso en ello: sin las “pláticas” sobre economía del cambio climático y sus recomendaciones de usar R, este proyecto probablemente nunca hubiese visto la luz del día. Oscar Ishizawa, también es parcialmente responsable de lo que aquí se presenta. Su defensa del espíritu científico y del pensamiento crítico siempre han constituido una fuente de inspiración para mí. Igualmente, quisiera agradecer a los profesores que desde temprano han despertado mi inquietud intelectual e interés por entender el mundo. Entre ellos, Madame Machot, Madame Loquet, Madame Alam y Monsieur Cartapanis. Todos ellos han tenido una importancia fundamental en mi formación académica y algunas de sus enseñanzas han sido usadas en las investigaciones que conforman esta tesis.

Igualmente, quisiera extender un agradecimiento especial a Dominique Van der Borghet por compartirme algunas referencias claves para esta tesis y por su inagotable ímpetu humanista, fuente de admiración para mí. A Manu Vb Tintoré por dejarme usar uno de sus “*pixel organic*” para la portada de esta tesis y por compartir sus reflexiones sobre esta “*Terra, incógnita*”. Finalmente, a los amigos y compañeros de ruta que han nutrido este proyecto o que *sencillamente* han estado ahí para aguantar el desahogo durante los días difíciles. Laura Delgado, Younes Karroum, Paul Blanchard, Charly Andral, Román

Navalpotro, Loic Debet, Alexandre Bisquerra y Joaquín Muñoz; algunas de las cosas que conversamos en oportunidades diversas están reflejadas en este trabajo.

Last but not least, más allá de la investigación académica, los fundamentos de esta tesis lo constituyen mi familia. A Margarita y Philippe, mis padres, sin quienes no sería la persona que soy. Gracias también por el apoyo durante el taller de escritura organizado en Menorca para finalizar esta tesis. A mis hermanos Cédric, Guillermo y Hugues. A Carmen, mi esposa, quien sabe mejor que nadie lo que ha costado este proyecto. Te pido disculpas por todas las quejas de los malos momentos y te agradezco el apoyo incondicional y los ánimos con los que siempre me has invitado a seguir. Finalmente, a mi hija, Olivia. Ojalá el mundo no se haya convertido en algo demasiado fluctuante para cuando puedas leer estas líneas...

A todos los que leen estas líneas y he olvidado, a modo de excusa, están formalmente invitados a una copa de Malvasía en Sitges.

Abstract

The way we occupy the territory drives our relationship with the environment, with potentially important consequences for climate change mitigation and adaptation. To better understand these dynamics, this thesis assesses how the geographical patterns of Latin-American cities shape climate change challenges. To do so, it articulates an empirical perspective on two climate debates: (1) Whether and to what extent the spatial expansion of cities reduces CO₂ emissions and enables a shift towards low-carbon urban systems? (2) Whether and to what extent the greenness of the land cover reduces cities' vulnerability to extreme weather events and influences their capacity to adapt to climate change? These investigations rely on a novel methodology combining Earth Observations with a population-based definition of cities. This allows me to assemble a unique sample of more than 600 cities across seven Latin American countries. Findings indicate that altering the spatial distribution of urban population to promote a compact expansion pattern -characterized by simultaneous increases in density together with contained suburban sprawl- can significantly reduce regional urban CO₂ emissions. Likewise, this thesis finds that the negative effects of extreme rainfalls on urban economic activity -proxied through nighttime lights- are substantially reduced in cities displaying a greener land cover. Overall, this thesis sheds light on the pivotal role that urban and spatial planning policies -which provide the policy tools to shape cities' geographical patterns- play to curb CO₂ emissions and reduce climate vulnerability. In doing so, it intends to broaden the scope of climate discussions by promoting a system-perspective on the relationship between humans and the Earth system. This approach underscores the deep structural shifts that are required to navigate a more fluctuating world.

Resumen

La forma en la que habitamos el territorio condiciona nuestra relación con el medio ambiente, con consecuencias potencialmente importantes para la mitigación del cambio climático y la adaptación al mismo. Con el fin de entender mejor estas dinámicas, esta tesis evalúa cómo los patrones geográficos de las ciudades latinoamericanas configuran los desafíos climáticos que enfrenta la región. Para ello, se articula una perspectiva empírica sobre dos debates climáticos: (1) ¿En qué medida la expansión espacial de las ciudades reduce las emisiones de CO₂ e induce un cambio hacia sistemas urbanos bajos en carbono? (2) ¿En qué medida el verdor de la cubierta del suelo de las ciudades reduce su vulnerabilidad ante fenómenos meteorológicos extremos e influye en su capacidad de

adaptación al cambio climático? Estas investigaciones se basan en una metodología novedosa que combina observaciones de la Tierra con una definición de ciudades basada en la distribución espacial de la población. Esto permite constituir una muestra única de más de 600 ciudades repartidas en siete países latinoamericanos. Los análisis estadísticos indican que un patrón de expansión más compacto -caracterizado por un aumento de la densidad junto con una expansión suburbana contenida- puede limitar significativamente las emisiones de CO₂ urbano en la región. Esta tesis también evidencia que los efectos negativos de las precipitaciones extremas sobre la actividad económica urbana -medida mediante luces nocturnas- se reducen sustancialmente en las ciudades que presentan una cubierta de suelo más verde. Estos resultados ponen de relieve el papel fundamental que desempeñan las políticas de planificación urbana y territorial -que proporcionan los instrumentos para (re)configurar los patrones geográficos de las ciudades- para reducir tanto las emisiones de CO₂ como la vulnerabilidad climática. Se pretende así ampliar el horizonte del debate climático y promover un análisis sistémico de la relación entre seres humanos y sistema terrestre. Este enfoque recalca los profundos cambios estructurales que se requieren para poder navegar por un mundo más fluctuante.

Contents

Agradecimientos	i
Abstract	iv
Resumen	iv
Contents	vii
List of Figures.....	ix
List of Maps	x
List of Illustrations	xi
List of Tables.....	xi
List of Boxes.....	xi
List of Acronyms.....	xii

1 Framing the problem: the Anthropocene and climate change challenges in an urbanized world	2
1.1 The intertwined human-environment relationship is changing	2
1.2 Contemporaneous cities mirror the current Human-Environment Nexus	11
1.3 Shaping urbanization to confront climate change challenges?	16
2 Thesis objective and structure	22
2.1 Assessing how cities' geographical patterns shape climate change challenges ...	22
2.2 Setting the time-space resolution of the analysis	25
3 Cities Geographical Patterns in a changing climate: a review of literature.....	27
3.1 City spatial extent and CO2 emissions	28
3.2 City land cover and climate vulnerability	34
4 Methodology and data sources	41
4.1 An internationally harmonized approach to delineate “cities” across 7 Latin American countries	42
4.2 Overlaying the “city layer” on Earth Observations	48
4.3 Identifying causal relationships across a large sample of cities	62

5	Case study 1: Cities spatial expansion and CO2 emissions in seven Latin American countries	65
5.1	GHG emissions in Latin America: context and 2030 targets	68
5.2	The patterns of spatial expansion and CO2 emissions across Latin American cities 72	
5.3	A revamped STIRPAT model: The impact of spatial expansion dynamics on CO2 emissions	89
5.4	CO2 emissions pathways at the city-level and heterogeneity across cities	96
5.5	Projecting regional urban emissions under different spatial expansion scenarios 101	
5.6	Conclusion	110
5.7	Appendix.....	111
6	Case study 2: Cities land cover and vulnerability to extreme rainfall events in seven Latin American countries	115
6.1	Extreme rainfall in a changing climate: implication for Latin American cities	119
6.2	Urban economic activity and extreme rainfall impacts	130
6.3	The greenness of the land cover within Latin American cities	141
6.4	Empirical estimation of the impacts of extreme rainfall on night-time lights	145
6.5	The benefits of greener land cover	150
6.6	Conclusion	158
6.7	Appendix.....	160
7	Summary of findings: Spatial and urban planning as climate policy tools	174
7.1	Spatial and urban planning policies to enable low-carbon urban systems.....	174
7.2	Urban and spatial planning policies to reduce vulnerability to extreme rainfall...	179
7.3	Towards greener and more compact urban systems?	183
8	Future areas of investigation	188
9	Final considerations	191
10	References.....	196

List of Figures

Figure 1. Temperature evolution over the last 100,000 years	4
Figure 2. The “great acceleration” of human enterprise from 1750 to 2020	5
Figure 3. Latest status of the nine planet boundaries.	8
Figure 4. Climate change challenges result from the specific human-environment nexus that has consolidated during the Anthropocene	10
Figure 5. Higher urbanization rates positively correlate with higher GDP per capita (left) and higher greenhouses gas emissions (right).....	13
Figure 6. The emission gap until 2030	16
Figure 7. Temperature anomalies (in °C Celsius) relative to 1961-1990	18
Figure 8. Climate change will increase risks through more frequent extreme events (hazards), although ultimate impacts will depend on vulnerability and exposure conditions	19
Figure 9. Cities’ geographical patterns mediate the relationship between humans and the Earth system, thereby shaping climate change challenges	23
Figure 10. The spatial extent of Barcelona VS Atlanta, 1990	28
Figure 11. Conceptual approach to risk and impacts	34
Figure 12. Distribution of global GHG emissions by regions, 1990-2020 average.....	71
Figure 13. Average emissions per capita in LAC countries and selected comparators, 1990-2020.....	71
Figure 14. The patterns of spatial expansion in Latin America cities, 2000–2015	79
Figure 15. Distribution of estimated fossil fuel CO ₂ emissions per capita in 2015	84
Figure 16. Concentration of estimated fossil fuel CO _{2e} emissions by cities category	84
Figure 17. City population VS estimated fossil fuel CO ₂ emissions per capita in 2015	84
Figure 18. City GDP/cap VS estimated fossil fuel CO ₂ emissions in 2015	84
Figure 19. Moran’s plot of Ln city emissions, 2015. Moran’s I: 0.14***	88
Figure 20. Moran’s plot of Ln city emissions/cap, 2015. Moran’s I: 0.43***	88
Figure 21. Projected CO ₂ emissions pathways for an average city under three spatial expansion patterns	97
Figure 22. The heterogeneous effects of density and suburban ratios on CO ₂ emissions as a function of city population.....	99
Figure 23. The heterogeneous effects of density on CO ₂ emissions as a function of city GDP per capita	100
Figure 24. Evolution of the main drivers of CO ₂ emissions under the BaU VS the compact scenario, 2015-2030 (in %).....	105
Figure 25. Projected regional urban emissions in 2030 under a BaU VS a compact expansion scenario	107
Figure 26. Contribution of each driver to the evolution of CO ₂ emissions, by group of cities, 2015-2030 (in %).....	107
Figure 27. Temperature distribution in Latin America and the Caribbean: 1961-1990 VS 1991-2020.....	123
Figure 28. Time evolution of average temperature by subregions, 1961-2020	123
Figure 29. Changes in precipitation distribution (left) and probability of precipitation anomalies (right): 1961-1990 VS 1991-2020	123

Figure 30. Intensity-Frequency curves of extreme rainfall events for cities across seven Latin American countries, 1991-2005 VS 2006-2020	124
Figure 31. Heterogeneous precipitation patterns (Z-scores) in 4 selected cities.....	126
Figure 32. Change factor for the Annual Exceedance Probability of the 100-year return period largest monthly cumulative precipitation, 2070-2099, SSP5-8.5	128
Figure 33. Illustrative shift to the Intensity-Frequency curves for extreme rainfall events under SSP5-8.5	129
Figure 34. Predicted GDP using city NTLs vs actual GDP, 2013-2021	139
Figure 35. Evolution of flood frequency and damages in Latin America, 1965-2022 (5 year moving average).....	140
Figure 36. Nightlight time variation in Governador Valadares Brazil (left) and Santiago, Chile (right) before and after floods	140
Figure 37. Distribution of the greenness index across three categories of cities	142
Figure 38. Yearly variations of the greenness index across the full sample of cities (left) and selected cities (right), 2013-2021.....	144
Figure 39. Distribution of the mean greenness index by country	144
Figure 40. Mean greenness index VS mean precipitation at the city-level by city category ..	144
Figure 41. Annual probability of exceeding a given level of City NTL/cap reduction.....	148
Figure 42. Time dimension of the effects associated with extreme rainfall on city NTL/cap	149
Figure 43. Average city NTL/cap VS greenness index.....	151
Figure 44. Estimated effects of three models of extreme rainfall interacting with q-quantiles of greenness index (q=2, q=3 and q=4; left). (b) Distribution of the greenness index in each group of cities (right)	155
Figure 45. Observed vs simulated losses based on the 2015 distribution of extreme rainfall events	157
Figure 46. The distribution of the greenness index in each of the three spatial expansion patterns identified in this thesis.....	180
Figure 47. Summary of the policy options proposed to enhance low-carbon and climate-resilient urban systems in Latin America	183
Figure 48. From efficiency to robustness: a schematic view.....	194

List of Maps

Map 1. Potential routes of Homo Sapiens Out of Africa.....	3
Map 2. Land cover evolution around the city of Goiania, Brazil, in 1992, 2001, 2015.....	14
Map 3. Mismatch between my population-based “cities” and their respective administrative areas	46
Map 4. Global distribution of the main GHG emissions according to EDGAR	49
Map 5. Nighttime lights in the State of Sao Paulo, Brazil, 2018	56
Map 6. Visual comparison of two cities displaying differentiated greenness indexes.....	60
Map 7. The spatial expansion Santiago de Querétaro in Mexico, 2000 VS 2015.	73
Map 8. Urban centers and suburban areas in selected cities	76
Map 9. Estimated CO2 emissions per capita and spatial extent of selected cities in 7 Latin American countries.....	83

Map 10. Cities emissions/cap local indicators of spatial association (LISA).....	87
Map 11. Projected changes to maximum 5-day precipitations (in %) under different warming scenarios, rel. to 1850-1900	127
Map 12. Nighttime lights in northern coastal Peru during the March 2017 flooding (baseline VS March 2017).....	134
Map 13. Cities with geographical patterns conducive to a reduction of both CO2 emissions and climate vulnerability	184

List of Illustrations

Illustration 1. Examples of GI to address urban pluvial flood risk	37
Illustration 2. Diagram illustrating the Degree of Urbanization application for a population grid.....	45
Illustration 3. ODIAC Coverage compared to Global Greenhouse Gas Emissions in 2019 by Sector, End Use and Gases	50
Illustration 4. Schematic outline of the methodology used to estimate city-level CO2 emissions	52
Illustration 5. From extreme rainfall to nighttime light impacts: a schematic view	133
Illustration 6. Schematic outline of two coalitions of conflicting interests at the city-level..	185

List of Tables

Table 1. Pearson correlation coefficient and VIF of the independent variables	91
Table 2. Estimation results	93
Table 3. Direct, indirect and total city-level CO2 emissions elasticities	95
Table 4. Tailored elasticities for each group of cities	103
Table 5. The relationship between City NTLs and GDP	138
Table 6. Main estimations results.	147

List of Boxes

Box 1. Historical evolution of CO2 atmospheric concentration	6
Box 2. Tipping points in the Earth system	20
Box 3. Glossary of the terms used to refer to human settlements in this thesis	47
Box 4. How to account for Greenhouse Gas at city level?	54
Box 5. The NDVI: a quantitative measure of the amount of vegetation in a given area	61
Box 6. Extreme rainfall events according to the World Meteorological Organization	121
Box 7. The impacts of extreme rainfall on urban economic activity from a conceptual standpoint	136

List of Acronyms

AIC: Akaike information criterion
BaU: Business as usual
CEPAL: Comisión Económica para América Latina y el Caribe
CH₄: Methane
CHIRPS: Climate Hazards Group InfraRed Precipitation with Station data
CMIP-6: Coupled Model Intercomparison Project — phase 6
CO₂: Carbon dioxide
COP: United Nations Climate Change Conference of the Parties
C3S: Copernicus Climate Change Service
DMSP: Defense Meteorological Satellite Program
DoU: Degree of Urbanization
EEA: European Environment Agency
ENSO: El Niño–Southern Oscillation
EO: Earth Observations
ESA: European Space Agency
GADM: Global Administrative Areas
GDP: Gross Domestic Product
GHG: Greenhouse gas
GHS-POP: Global Human Settlement population grid
GI: Green Infrastructure
GtCO₂e: Gigatons of CO₂ equivalent
HEN: Human-Environment Nexus
IPCC: Intergovernmental Panel on Climate Change
LAC: Latin America and the Caribbean
LISA: local indicators of spatial association
NASA: The National Aeronautics and Space Administration
NDC: Nationally determined contributions
NDVI: Normalized Difference Vegetation Index
NO₂: Nitrogen dioxide
NTL: Night-time lights
ODIAC: The Open-Data Inventory for Anthropogenic Carbon dioxide
PB: Planet Boundary
PPM: Parts per million
RCB: Remaining carbon budget
STIRPAT: Stochastic Impacts by Regression on Population, Affluence and Technology
TFP: Total Factor Productivity (TFP).
TOA: Top-of-Atmosphere (TOA)
UNDESA: Department of Economic and Social Affairs of the United Nations Secretariat
UNEP: United Nations Environment Programme
UN-Habitat: United Nations Human Settlements Programme
VIF: Variance inflation factor
VIIRS: Visible Infrared Imaging Radiometer Suite
WMO: World Meteorological Organization

1 FRAMING THE PROBLEM: THE ANTHROPOCENE AND CLIMATE CHANGE CHALLENGES IN AN URBANIZED WORLD

1.1 The intertwined human-environment relationship is changing

Over the last 100,000 years, Homo Sapiens thrived and has proven to be extraordinarily creative in adapting to different geographies. Some 80,000 years before our age, a small group of hunter-gatherers moved out of Africa into the Eurasian continent (Oppenheimer 2003).¹ This marked the beginning of a larger evolution through which Sapiens started populating the entire planet. Although some scientific debate remains about how our ancestors left Africa and what routes they took (López, Van Dorp, and Hellenthal 2015), consistent evidence indicates that Homo sapiens spread across South Asia to reach the Australian continent perhaps as early as some 70,000 years before present. Later on, probably after 50,000 years ago, Sapiens started peopling Europe and West Asia (see Map 1). While other members of the Human family such as the Homo Neandertal extinguished around 30,000-25,000 years ago, Sapiens continued expanding its presence around the world. Eventually, Sapiens started settling across the American continent potentially between 30,000-22,000 years before present. In this very long endeavour, Sapiens displayed a remarkable ability to settle in diverse and extreme landscapes, from river valleys and coastal lands to large glacial ice sheets, steep mountains or dense forest.

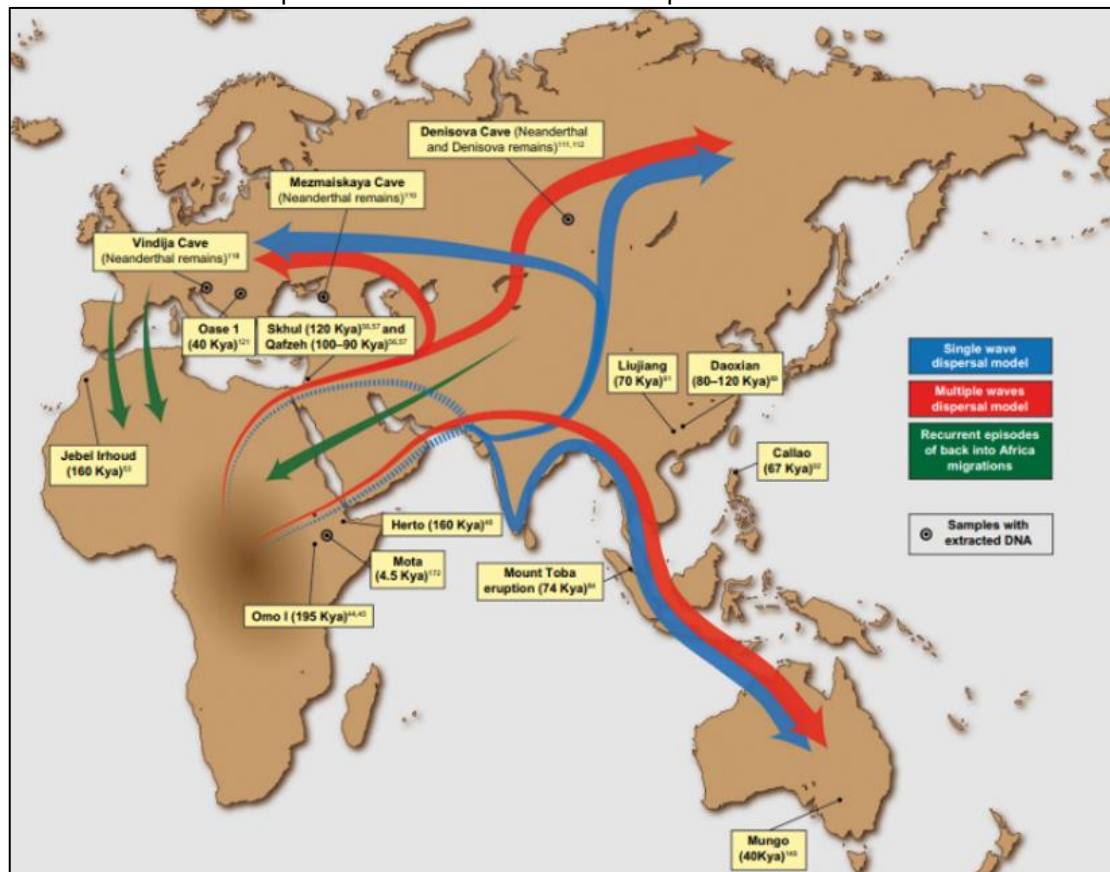
This evolution is all the more remarkable that it has happened while the Earth was oscillating between glacial and relatively warmer interglacial periods. Sapiens populated the planet during the last portion of the Pleistocene Epoch, a period often referred to as the “Ice Age”.² During this period, mean temperature on Earth was significantly lower than present day. During peak glaciation stages, it could reach 7°C below preindustrial levels (See Figure 1). This implied that much of North America, South America, Europe and Asia was covered by large glaciers and sea levels were much lower than nowadays. In that distant past, the mean temperature was not only lower but also exhibited strong volatility. In fact, these sharp temperature variations have played an important role in shaping the expansion of Sapiens around the world. For example, as a result of a relative warmer

¹ The dates reported in the first two paragraphs come from Oppenheimer (2003) and are obtained from a genetic analysis of anatomically modern humans. They might differ from the dates proposed by fossil and archaeological approaches.

² According to the [International Commission on Stratigraphy](#), the Pleistocene epoch goes from approximately 2.6 million to 11,700 years ago. It represents the Earth's most recent period of glaciations.

interglacial period around 50,000 years ago, ice sheets melted, opening a corridor from the Gulf region to the eastern Mediterranean countries, thereby facilitating the migrations of Sapiens towards these regions. By contrast, during peak glacial periods, sea-levels were lower, allowing Asia and North America to be connected by land via what is now called the Bering strait. This, in return, enabled the first migrations of Sapiens towards the American continent.

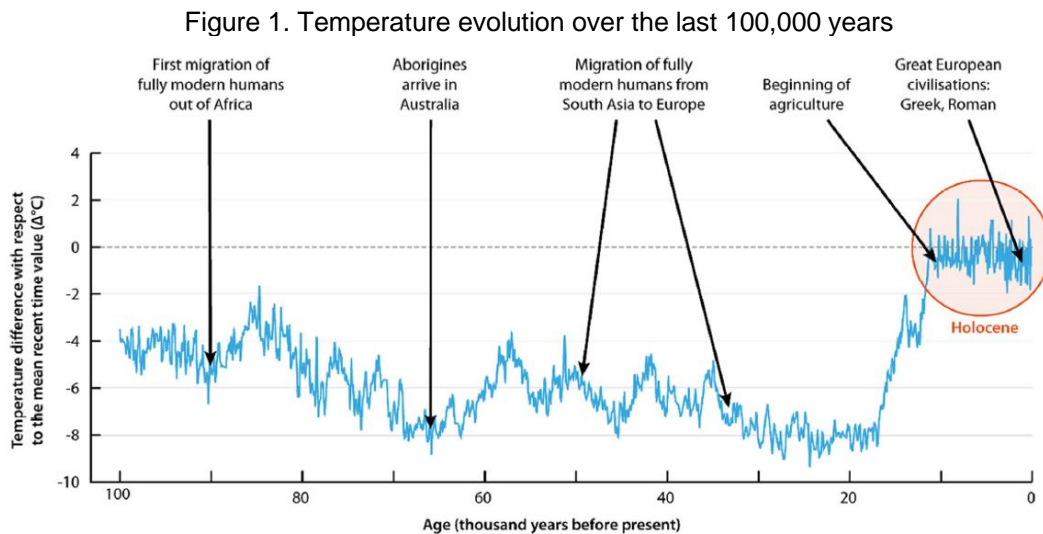
Map 1. Potential routes of Homo Sapiens Out of Africa



Note: Circles locate some of the most relevant ancient human remains. The placement of arrows is indicative.
Source: Extracted from López, Van Dorp, and Hellenthal (2015).

In this longer-timeframe, the flourishing of human civilization as we know it has taken place during a relatively short time-period called the Holocene. At the end of the last glacial maximum, some 18,000 years ago, mean temperature progressively increased, glaciers retreated and sea levels rise. Approximately 11,000 years ago, mean temperature reached a level close to its pre-industrial level (approximately 14°C), marking the beginning of the Holocene. Since then, Earth's climate has been relatively stable: global mean surface temperature increased by approximately 0.5°C from 9,000 years ago until the Industrial Revolution, with global temperature fluctuations contained in a range of at most 1.5 °C above and below the mean (Osman et al. 2021). It is during this period of relatively warm and stable climate that recorded human history has played out, from the beginning of

agriculture and writing to Antic Greek and Roman civilizations, until the XIX century industrial revolution.



Note: The red circle marks the last 11 000 years of the accommodating Holocene epoch. This figure is based on Vostok ice-core data. Ice-core samples taken at the Vostok station in Antarctica contain a record of atmospheric gas composition. These records come from air bubbles that have been trapped in snows and compressed into polar ice over 400,000 years. They allow to reconstruct historical fluctuations in greenhouse gases, such as CO₂, to proxy for temperature fluctuations.

Source: Extracted from Folke et al. (2021).

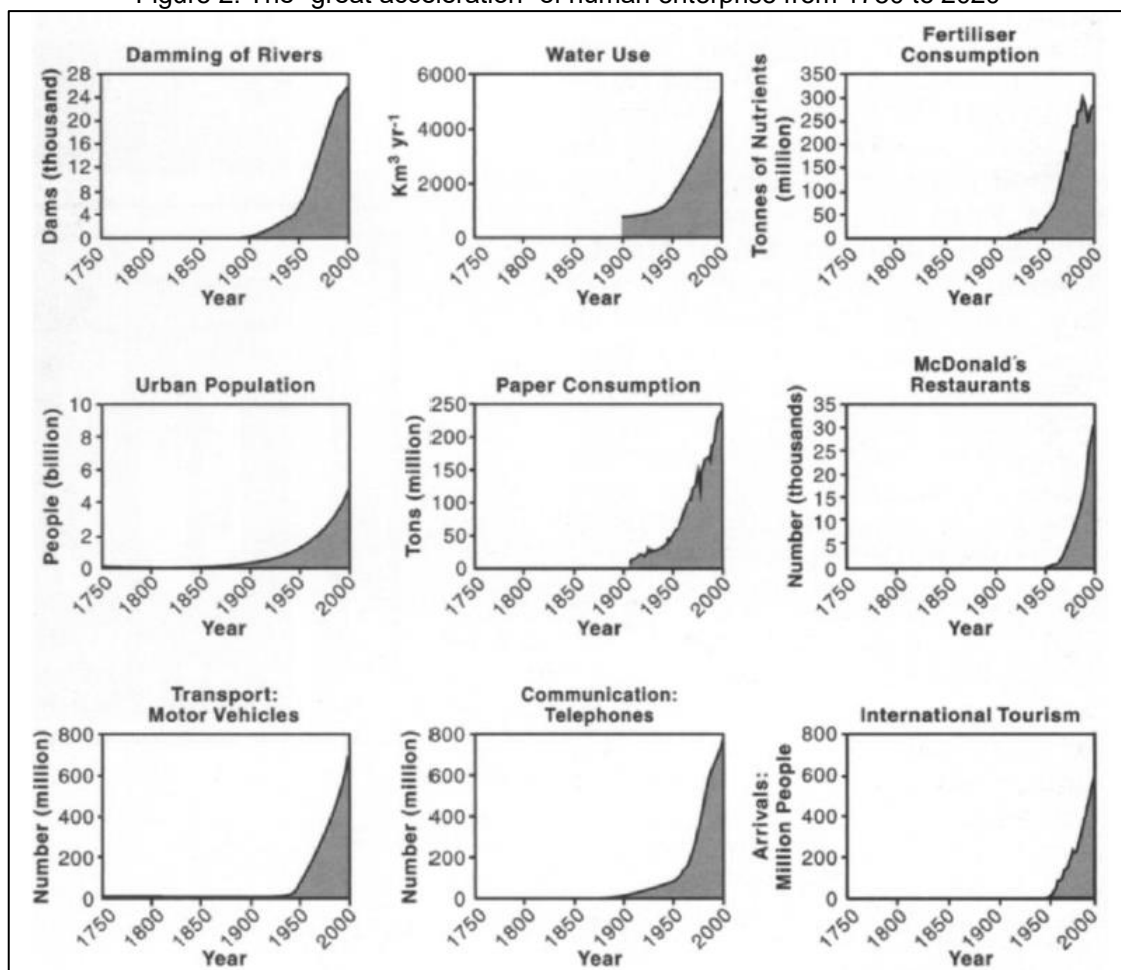
The last two hundred years of the Holocene have been characterized by an exponential increase in wealth and population. The human population reached one billion around 1800. It doubled to 2 billion around 1930 and doubled again to 4 billion around 1974. The global population is now approaching 8 billion and is expected to stabilize around 9–11 billion towards the end of this century (UNDESA 2019). Likewise, between 1820 and 2022, global GDP grew about 65-fold (Bolt and Van Zanden 2024). These evolutions have been documented in depth (see for example McNeill 2001). Remarkably, they displayed a sudden acceleration after the end of the second world war, with the rates of change of different components generating pressures on the environment intensifying sharply since the 1950s (see Figure 2).³ This has led Steffen, Crutzen, and McNeill (2007) to coin this recent period of human history “*the great acceleration*”. In fact, in 200 years, human influence on ecosystems and life-support systems have intensified more rapidly and extensively than in any other comparable period in human history.

This exponential growth has pushed us into the Anthropocene, with potentially huge consequences for human well-being and humanity as we know it. The Anthropocene term denotes the present geological time in which Humans represent such a dominant force

³ To give a few numbers based on Steffen, Crutzen, and McNeill (2007): petroleum consumption has grown by a factor of 3.5 since 1960, the number of motor vehicles increased from about 40million at the end of the War to nearly 700 million by 1996.

on Earth that many ecological conditions and processes are profoundly altered by human impacts (Crutzen 2002). This period of time is estimated to have started in the late eighteenth century, when global concentrations of carbon dioxide and methane started to increase.⁴ The Anthropocene contrasts with the impacts that preindustrial societies generated on ecosystems, which were largely local and reversible, producing fluctuations that remained within the bounds of the natural variability observed during the Holocene. This difference in magnitude and scale is perfectly illustrated when current changes in CO₂ atmospheric concentration are compared with those produced during the XVI century by land cover changes associated with widespread depopulation of the Americas after 1492 (see Box 1).

Figure 2. The “great acceleration” of human enterprise from 1750 to 2020



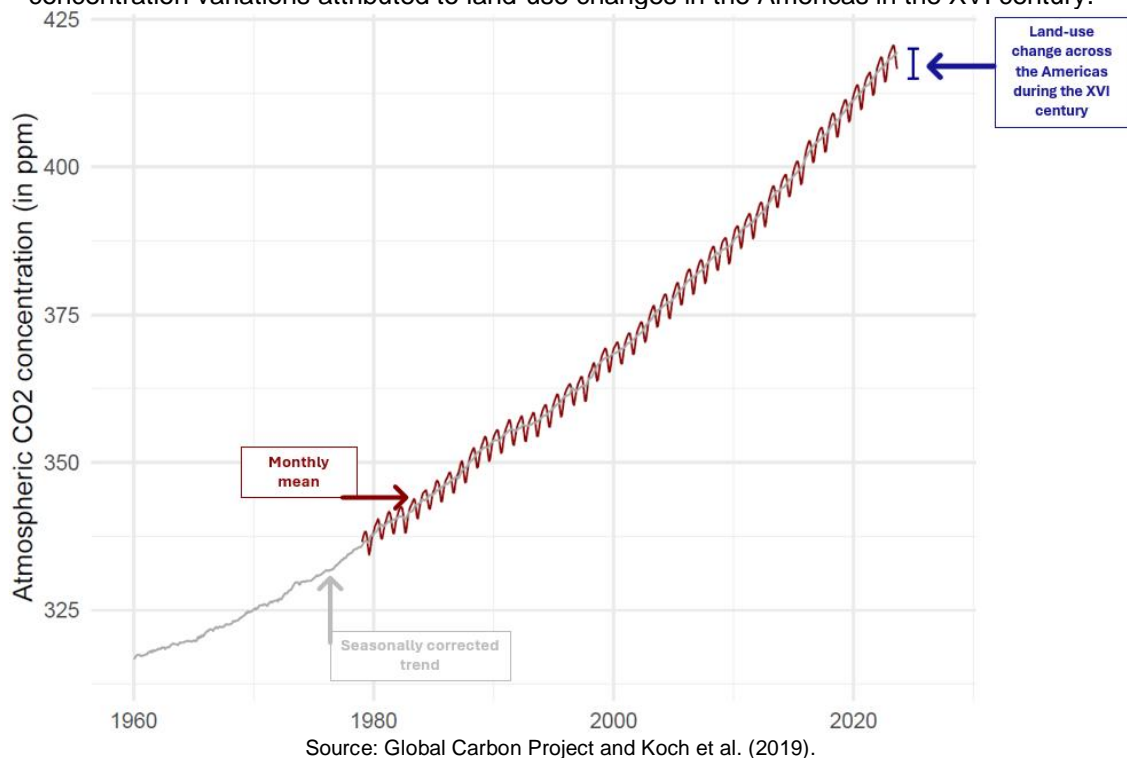
Source: Extracted from Steffen, Crutzen, and McNeill (2007).

⁴ The year 1784 is often mentioned as the beginning of the Anthropocene as it coincides with James Watt's design of the steam engine and the start of the industrial revolution. Importantly, human-induced alterations are not limited to greenhouse gases emissions in the atmosphere as they have also produced a signature in sediments and ice that is distinct from that of the Holocene. This confirms that the Anthropocene is stratigraphically a different epoch since at least the mid-20th century (Waters et al. 2016).

Box 1. Historical evolution of CO₂ atmospheric concentration

To give a sense of the magnitudes of human-induced impacts in the Anthropocene, I compare variations of atmospheric carbon dioxide (CO₂) concentration between two distant periods. The impact of large-scale depopulation of the Americas after 1492 might represent one of the largest human-driven environmental impact of preindustrial history. According to Koch et al. (2019), the “*Great Dying of the Indigenous Peoples of the Americas*” in the XVI century (estimated at approximately 54 million of persons or 90% of the pre-Hispanic population) has led to abandon considerable portions of the landscapes across the newly discovered continent. This massive land use change has resulted in a carbon uptake into the land estimated at an additional 5 parts per million (ppm), which contributes to explain the decline in global temperature by 0.15°C observed in the late 1500 - early 1600. The magnitude of this variation is illustrated by the blue bar in the figure below.

Figure Box 1. Evolution of atmospheric CO₂ concentration during 1960-2023 VS CO₂ concentration variations attributed to land-use changes in the Americas in the XVI century.



Current variations are of a different order of magnitude: only between 2020 and 2022, CO₂ concentration has increased by 7 ppm (i.e. from 411 ppm to 418 ppm). In the past 60 years, CO₂ concentration has increased by approximately 100 ppm. The annual rate of increase in atmospheric CO₂ during these past 60 years is estimated to be about 100 times faster than the increase at the end of the last ice age some 17,000 years ago. For the past 800,000 years, CO₂ concentration never exceeded 300 ppm (Lüthi et al. 2008).

The planet boundary (PB) approach provides a science-based analysis to better apprehend the impacts of human activities on Earth system under the Anthropocene. This approach -initially proposed by (Rockström et al. 2009)- builds upon Earth system science and seeks to delineate and quantify levels of anthropogenic perturbation that, if exceeded, would place the Earth system on a path that would strongly depart from a “Holocene-like” state. The PB framework operationalizes the Anthropocene concept by assessing whether and to which extent human activities are altering great natural equilibriums, putting Earth outside of the Holocene’s window of environmental variability.

Earth System: Following Steffen, Crutzen, and McNeill (2007), the term Earth system refers to the suite of interacting physical, chemical, biological and ecological global-scale cycles and energy fluxes that provide the life-support system for life at the surface of the planet. This definition implies that ecological processes referred to as “the Environment” or “Nature” are an integral and interacting part of the broader Earth System. The Earth system is a partially self-regulating system that can be forced by external drivers of change, such as varying flux of energy from the sun due to changes in Earth’s orbit or the increasing concentration of CO₂ in the atmosphere. Importantly, this systemic approach recognizes that Earth system can also be modified through feedback loops and interactions of different process within the system.

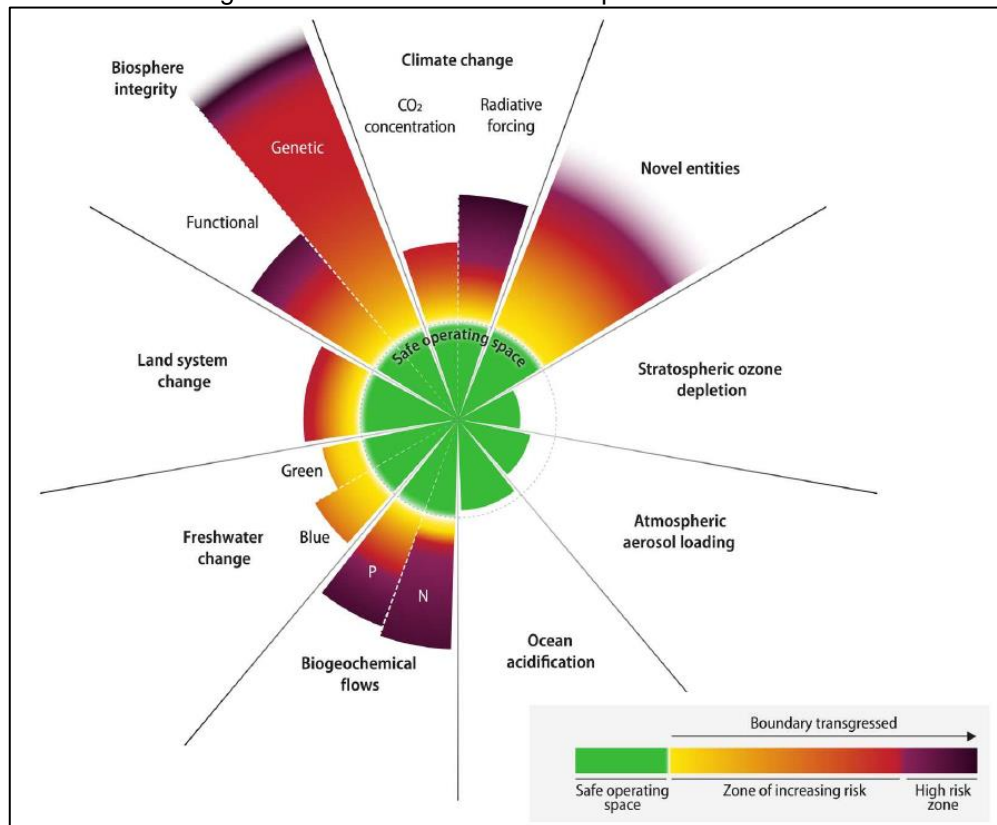
The message that emerges from the various PB assessment is clear and straightforward: “human activities are affecting Earth system functioning to a degree that threatens the resilience of the Earth System—its ability to persist in a Holocene-like state in the face of increasing human pressures and shocks.”⁵ The latest PB update found that six out of the nine processes identified as critical to “*maintain the stability and resilience of ES as a whole*” have now exceeded their thresholds values (see

Figure 3). Interest readers are referred to Richardson et al. (2023) for more details on each component of this latest update. It is nonetheless worth emphasizing that the remarkably stable Earth system state experienced over the past 10,000 years is the only one that modern civilizations have known. The end of Holocene-like conditions would thus open a period without equivalence in human history. In fact, the Holocene epoch is the only one that we know for sure can sustain modern human societies, leading authors to conclude that “*Earth is now well outside of the safe operating space for humanity*”⁶.

⁵ Source: Steffen et al. (2015), page 736 (page 1)

⁶ Source: Richardson et al. (2023), page 1

Figure 3. Latest status of the nine planet boundaries.



Note: "The green zone is the safe operating space (below the boundary). Yellow to red represents the zone of increasing risk. Purple indicates the high-risk zone where interglacial Earth system conditions are transgressed with high confidence. Values for control variables are normalized so that the origin represents mean Holocene conditions and the planetary boundary (lower end of zone of increasing risk, dotted circle) lies at the same radius for all boundaries (except for the wedges representing green and blue water, see main text). Wedge lengths are scaled logarithmically. The upper edges of the wedges for the novel entities and the genetic diversity component of the biosphere integrity boundaries are blurred either because the upper end of the zone of increasing risk has not yet been quantitatively defined (novel entities) or because the current value is known only with great uncertainty (loss of genetic diversity). Both, however, are well outside of the safe operating space. Transgression of these boundaries reflects unprecedented human disruption of Earth system but is associated with large scientific uncertainties".

Source: Figure and note extracted from Richardson et al. (2023).

Beyond numerical results, the systemic and integrated approach of this framework represents a key paradigm shift. The impacts of human activities on the global environment are often analysed as if they were separate issues. Climate change is for example treated apart from biodiversity loss, land system changes or global pollution. This fragmented approach to global environmental change fails to recognize (i) the systemic nature of the threats associated with the Anthropocene and (ii) the nonlinear interactions and compounding effects that different components can produce on the overall state of the Earth system. Instead, the PB framework is guided by an understanding that the planet is an integrated, partially self-regulating, system. It seeks to apprehend anthropogenic impacts on Earth system in this systemic context.

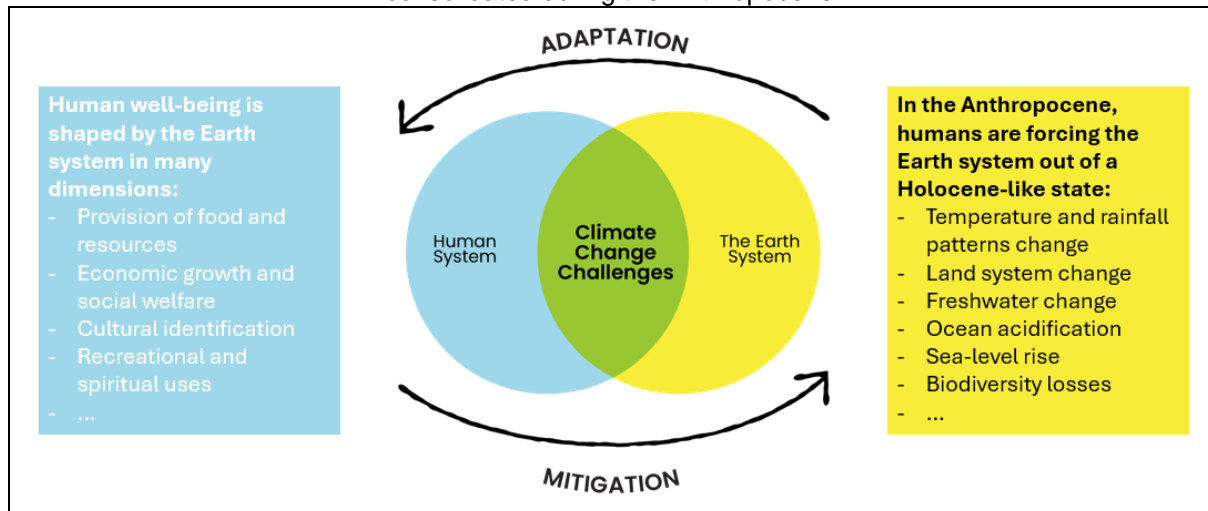
Inspired by the Planet Boundary framework, this thesis adopts a systemic perspective to examine climate change challenges resulting from tensions and frictions that have arisen between humans and the Earth system over the last 200 years. This thesis will refer to the relationships between humans and the Earth system as the **Human-Environment Nexus (HEN)**. Across time and space, different HEN have emerged. Anthropologists like Descola (2015) have for example shown that for indigenous societies living embedded within their direct environment, the divide between humans and the environment was less stringent than in modern societies.⁷ This strongly integrated HEN was also the one prevailing before the industrial revolution. Contrastingly, the scientific revolution initiated in the XVII century marked the emergence of a HEN where humans sought to extricate themselves from their environment and become as “*maitre and possesseur de la Nature*”.⁸ The concept of HEN is therefore used to depict the relationship that a given society has established with the environment, while emphasizing that Humanity is embedded within, intertwined with, and dependent upon the Earth system. Accordingly, the core focus of this thesis is not climate change as an environmental issue that would be separated from or would lie outside of the economic and social structure. Instead, this thesis focuses on the challenges associated with climate change from a human development perspective. Climate change challenges are viewed as the symptoms of the specific HEN that has consolidated during the Anthropocene.

From a schematic point of view, the concept of Human-Environment Nexus can be represented as two intertwined bubbles that are constantly interacting (see Figure 4). While the HEN before the industrial revolution could be represented by an almost perfect overlay of these two bubbles, modern societies have sought to separate these two bubbles by establishing a strong dichotomy between humans and ecosystems. This movement has generated the frictions. Climate change challenges are apprehended as the outcomes of these interactions and can be represented by the green area that forms the junction of the two bubbles in Figure 4. This thesis will therefore examine the nature of these interactions and the features of the prevailing HEN to better understand the underlying factors that produces climate change challenges. This conceptual framework underpins the different investigations proposed in this thesis.

⁷ In these societies animals and plants are often considered to have soul or spirit. In totemism, natural entities such as animals and plants are even considered to have a family connection with humans.

⁸ This can be translated as: “*master and possessor of Nature*”. René Descartes in *Discours de la méthode*, 1637. This sentence reflects the fact that the Environment is viewed as a domain governed by physical laws that can be understood and controlled by humans.

Figure 4. Climate change challenges result from the specific human-environment nexus that has consolidated during the Anthropocene



The HEN currently prevailing is generating two set of climate change challenges, which are the focus of this thesis. The HEN under the Anthropocene forms a circular relationship, which is a situation radically different from the one-way relationship observed during the Holocene. During the Holocene, human well-being was -to a large extent- determined by ecosystems regulated by the broader Earth system, but human systems had no capacity to significantly alter great natural equilibriums. In the Anthropocene, this relationship has become a tow-way relationship in which humans are forcing the Earth system out of the Holocene-like state it has been for the past 10,000 years. Two set of challenges arose from this circular HEN.⁹ On the one hand, fossil-fuelled human systems inherited from the industrial revolution and the great acceleration must be transformed to reduce GHG emissions and preserve the stability and resilience of the Earth system (i.e. **the mitigation challenge**); on the other, human systems have to adapt to an altered Earth system characterized by more erratic climate conditions together with more frequent extreme weather events (i.e. **the adaptation challenge**). This thesis will consistently refer to climate change challenges (or climate-related challenges) as the combination of both the mitigation and adaptation challenges.

⁹ As noted by Reyers et al. (2018), a major feature of the Anthropocene is that systems of people and nature are intertwined across temporal and spatial scales: human impacts on the Earth system in a specific place produce feedback effects at different location across the globe and at different moments in time. I acknowledge that this generates serious distributional and equity dimensions across countries, individuals and regions but decided not to include this dimension in

1.2 Contemporaneous cities mirror the current Human-Environment Nexus

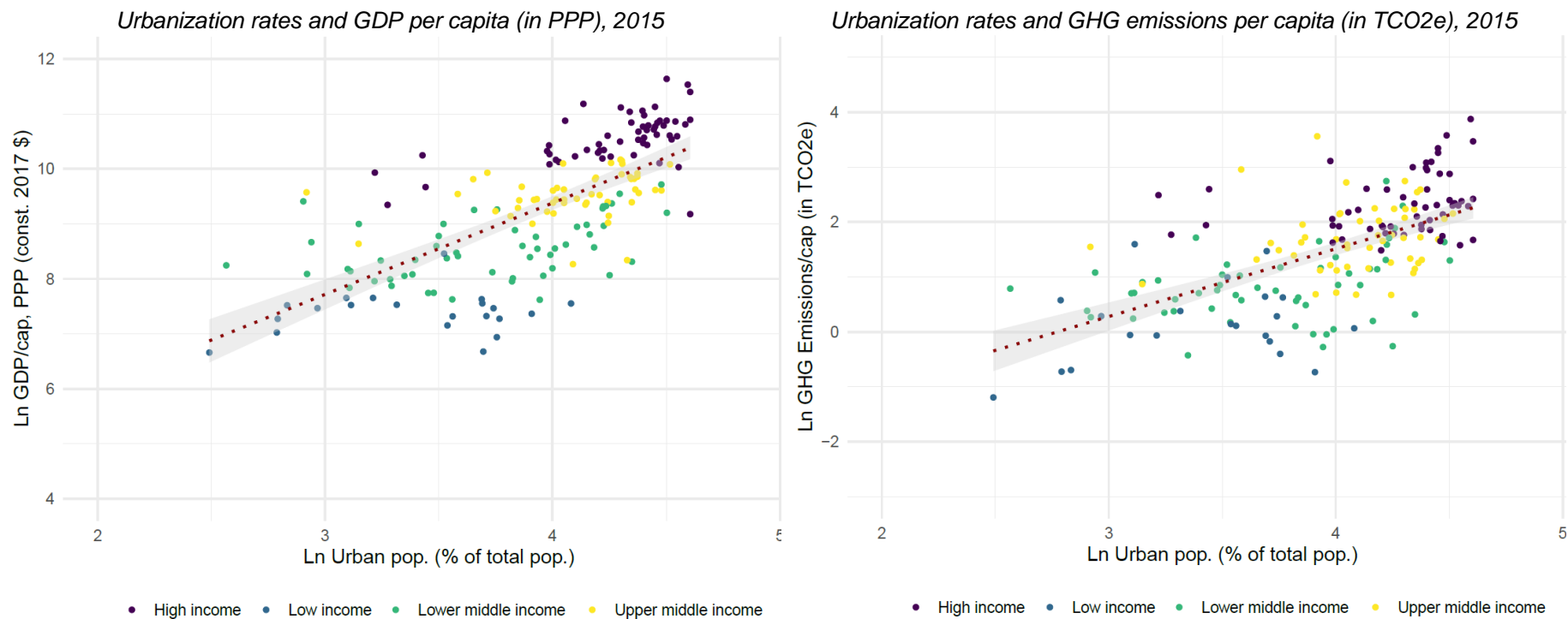
Of all the changes observed during the last 200 years, urbanization probably encapsulates the essence of the Anthropocene. For most of history, modern humans have been rural or living in small urban settlements *beyond the wall*. It is estimated that between the first century and the mid-XIX century, global urbanization levels were slowly fluctuating between 4% and 7% (Seto, Sánchez-Rodríguez, and Fragkias 2010). In fact, until the Industrial Revolution, walled cities were prevalent in both Europe and China, acting as barriers that not only restricted the city's expansion but also physically separated it from its surroundings. As the analysis of the case of Barcelona clearly revealed (Pallares-Barbera, Gisbert, and Badia 2021), this contained urban expansion was not motivated by environmental concerns but rather by security ones, with detrimental effects for the quality of life and health of this urban population. Additionally, even during phases of prosperity and relative expansion, urban structures predominantly consisted of raw natural materials, with minimal concrete urban infrastructure. Consequently, land cover changes produced by urban settlements were not only of a reduced spatial extent but were also reversible. A structurally different pattern is observed since the beginning of the Anthropocene. This has lead humanity to reach a major milestone in 2008: for the first time in history, the global urban population exceeded the rural population (UNDESA, 2019).

The Industrial Revolution and the great acceleration not only turned fossil fuels into the main source of energy; they also came along with significant changes in human settlements and urban development patterns. As an analogy to the Anthropocene, Seto and colleagues (2010) refer to the last 200 years as the “*new era of urbanization*” and evidence how both the demographic and land change process associated with urbanization differ from previous periods in at least three fundamental dimensions. First, the scale of urbanization is unprecedented, with cities being more populates, more spatially extensive and economically significant than ever before. At the dawn of the XIX century, when global population hovered around one billion, Beijing stood as the sole city with a population exceeding one million. A century later, 16 cities had a population of one million persons or more. In 2000, the number of cities with populations exceeding one million surged to 378 cities (UNDESA, 2019). Likewise, as a result of disperse urbanization patterns, during the period 1970–2010, urban land has expanded at a rate higher or equal to urban population growth in all regions of the world, leading to severe landscape transformations (Güneralp et al. 2020). Second, the speed at which population and land cover are becoming urban

surpasses any historical precedent. While it took the entirety of modern human history until 1960 for the global urban population to reach one billion, this figure doubled within the following 26 years. Third, the geographic distribution of urbanization is undergoing a notable shift. At the beginning of the XX century, the largest cities in the world were in Europe and the United States. In the *new era of urbanization*, Asia and South America host the largest cities in the world and could potentially be joined by Africa.

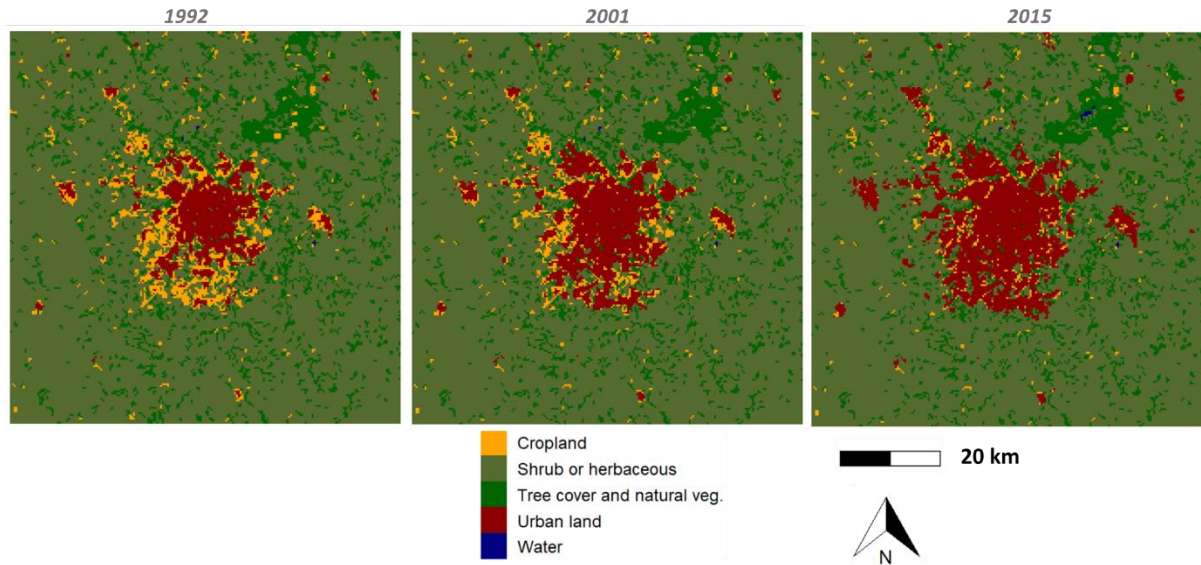
Humanity has now urbanized and cities are playing a pivotal role in shaping the HEN under the Anthropocene. In fact, modern capitalism is intrinsically linked to the rise of contemporary cities. At the national level, urbanization strongly and positively correlates with economic development and GHG emissions (Figure 5). This strong correlation is not to be interpreted as a causal relationship but rather helps illustrating how cities shape the HEN. More than a century ago, it was recognized that as people, firms and resources concentrate in close geographic space, multiple benefits arise (Marshall 1890; and Giuliano, Kang, and Yuan 2019; Glaeser 2010 for a more recent discussion). These *agglomeration economies* enhance productivity through various channels ranging from labour pooling, to spreading of costs and sharing of suppliers or innovation. However, cities also bring about negative congestion effects such as increasing prices of living and doing business or overcrowded public infrastructure and roads or pollution and public health issues. In each city, congestion and agglomeration effects constantly interact, explaining why countries are above or below the dotted trend line in red in Figure 5-left. When countries are able to fully reap the benefits of agglomeration, they display a higher GDP per capita than the average trend would otherwise indicate. Likewise, higher urbanization rates are unambiguously associated with higher GHG emissions per capita (Figure 5-right). However, countries can be below or above the trendline depending on a wide range of factors such as e.g. the carbon intensity of their GDP (i.e. GHG emissions per unit of GDP) or the expansion of their cities. A closer look at the city level is thus warranted to gain a refined understanding of these relationships.

Figure 5. Higher urbanization rates positively correlate with higher GDP per capita (left) and higher greenhouses gas emissions (right)



Note: the 182 countries of these two figures are classified according to the World Bank's income group classification. The dotted red line corresponds to a linear regression.
Source: own elaboration with World Bank, World Development Indicators.

Map 2. Land cover evolution around the city of Goiania, Brazil, in 1992, 2001, 2015.



Note: To improve map legibility, similar land cover classes provided in the underlying ESA raster have been consolidated into broader and more homogeneous land cover classes.

Source: Own elaboration. Basemap: ESA Land Cover Climate Change Initiative, Global Land Cover Maps, Version 2.0.7.

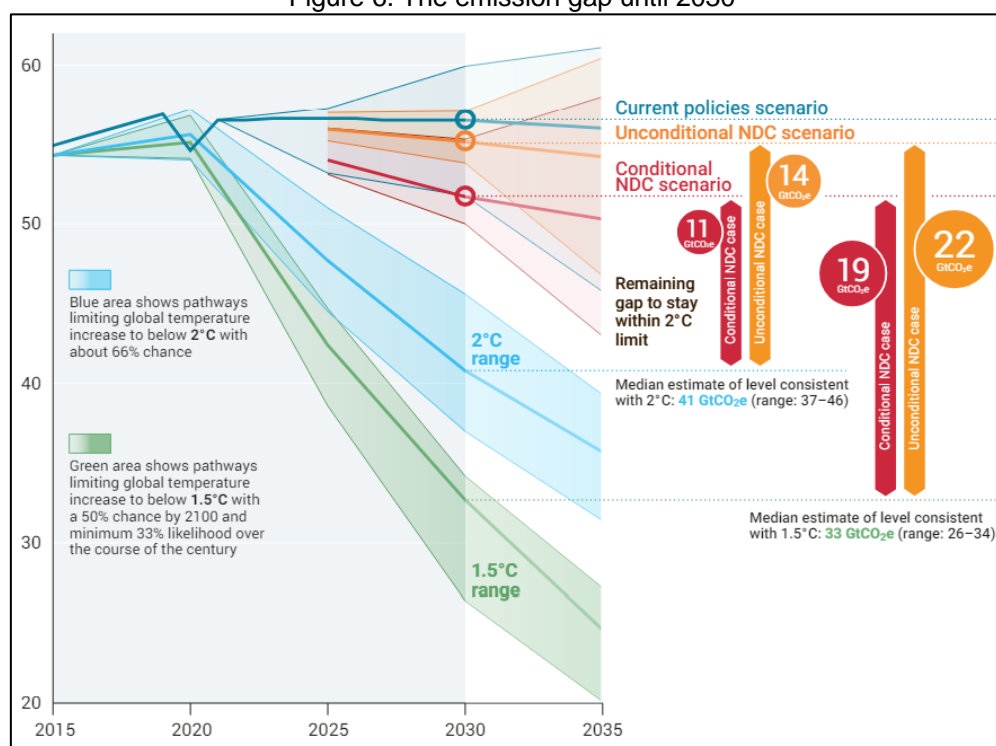
If we were to watch the last 200 years from outer space, contemporaneous cities would probably stand out as the most irreversible change on Earth surface with two salient features: (i) an exacerbated spatial expansion and (ii) a massive transformation of natural landscapes into man-made landscapes. Anecdotal evidence from the city of Goiania in Brazil perfectly illustrates this evolution. In 1933, as a result of an administrative decision, the city was created from scratch to replace the former capital of the State of Goiás -the town of Goiás. Goiania emerged as a meticulously planned urban center, with an original shape of a concentric radius designed to host 50,000 persons. It was located in a landscape known as the '*cerrado*' and marked by vast savanna expanses interwoven with forests and stream valleys, featuring diverse vegetation types. This gave Goiania its nickname -the *Capital of the Cerrado*- although, ironically, its consolidation as a state capital has profoundly transformed the original *cerrado* landscape. Today, Goiania is estimated to be the 10th largest city in Brazil, with a population exceeding 1,5 million inhabitants and an area spanning approximately 739 square kilometres (more than 7 times the size of Barcelona). The vicinity of Brasilia has further spurred the growth of the city and created a continuum of settlements along the Brasilia-Goiania axis, which now brings together about nine million people. Although this full historic evolution cannot be retraced from outer space, I leverage Earth observations to show recent land cover changes around the city of Goiania. Between 1992 and 2015, human settlements depicted in dark red in Map 2 have massively expanded, turning surrounding areas that were previously croplands, shrubs or tree covered areas into urban land and built-up structures. As this thesis will show, these alterations drive important changes to both Earth system and human well-being, with serious implications for the both the climate mitigation and climate adaptation challenges.

Examining the geographical patterns of cities might help elucidating the interactions between human well-being and Earth system. The spatial expansion of a city is one of the primary drivers of transportation needs and energy consumption within the city (see Chapter 3 for a review of literature). The spatial extent of a city might thus contribute to explain its level of GHG emissions, thereby influencing the mitigation challenge identified in Figure 4. Likewise, the land cover of a city and the prevalence of built-up and impervious surface directly influence the hydraulic response of a city (see Chapter 3 for a review of literature). Studying these land cover features can therefore help understanding how cities are affected by extreme rainfall events and provide relevant insight into the adaptation challenge (Figure 4). These aspects exemplify how the spatial expansion of a city or its land cover composition can shape climate-related challenges. More broadly, as I detail in the next chapter, the geographical patterns of a city can be viewed as mediating factor between human well-being and Earth system, thereby playing a crucial role in shaping climate change challenges (Figure 9).

1.3 Shaping urbanization to confront climate change challenges?

The way urban development will be shaped during the next decade is likely to have a decisive impact on greenhouse gas (GHG) emissions and our ability to withstand new climate patterns. This thesis will delve into these aspects from an empirical perspective. However, before delving into these aspects more in details, it is useful to quickly highlight the magnitude of changes required at the global level to mitigate and adapt to climate change. Unless otherwise indicated, all climate-related references included in this section are from the Intergovernmental Panel on Climate Change reports (IPCC 2018; 2021; 2023).

Figure 6. The emission gap until 2030



Profound changes to prevailing development pathways are required to maintain climate stability. The successive United Nations Climate Change Conference (COP) have focused on reaching a political consensus to limit global temperature increase to “*well below 2°C above preindustrial levels and to pursue efforts to limit the temperature increase even further to 1.5°C.*”¹⁰ The 1.5°C threshold represents the scientific consensus to avoid the worst impacts of climate change. Meeting this objective requires that greenhouse gas (GHG) emissions fall by about 45% by 2030 compared with 2010 levels and reach net zero by the middle of the century. Halving global GHG emissions in this timeframe will require fast, economy-wide, low-carbon development transformations, with a focus on the energy transition. Because of strong

¹⁰ This is the official terminology adopted in the 2015 Paris Agreement adopted during the COP21. This thesis will follow the climate-related literature and will refer to these goals as the long-term temperature goal of the Paris Agreement

inertia in the climate system, failure to get close to these GHG levels in 2030 will make it impossible to limit warming to 1.5°C with no or limited overshoot during this century and very challenging to limit warming to 2°C by the end of the century. The years that we have left until 2030 must be fully leveraged to foster immediate and large scale GHG emissions reductions.

However, in 2022 global GHG emissions increased by 1.2 per cent from 2021 and reached a new record of 57.4 gigatons of CO₂ equivalent (GtCO₂e).¹¹ The means that the reduction of global CO₂ emissions observed in 2020 as a result of the disruptions brought about by the Covid-19 pandemic have already been reversed. Even more concerning is the perspective until 2030. In the framework of the 2015 Paris Agreement, countries are committing to their own climate targets through their Nationally Determined Contributions (NDC). However, the collective reduction of emissions that could result from these NDC are largely insufficient to meet the objective indicate above: if left unaltered, current NDC will produce an emission gap that has been estimated at 14 GtCO₂e, for a 2°C goal and at 22 GtCO₂e for the 1.5°C goal (UNEP, 2023).¹² A gap of 14 GtCO₂e is broadly equivalent to the current annual emissions of the USA, the 27 countries of the European Union and India together. In hypothetical terms, meeting the 1.5°C goal thus implies that by 2030 the USA, the EU27 and India have stopped emitting, while other countries have stayed at their 2022 levels. Contrastingly, if current policies are continued, global warming could reach or even exceed 3°C above preindustrial levels by the end of the century. This is something that the Earth system has not experienced over the las 800,000 years.

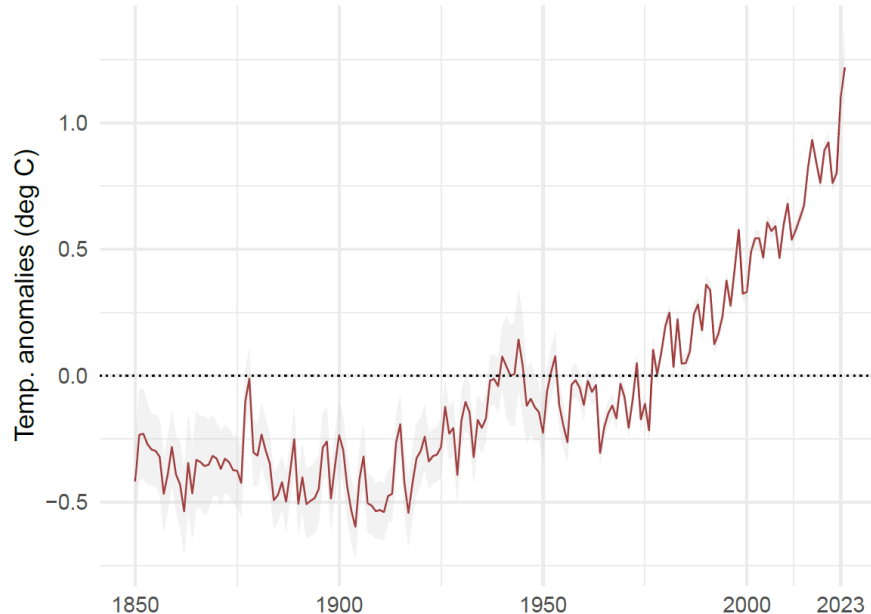
Emissions of GHG are already altering the Eart system. According to WMO (2024), the year 2023 set new and worrying records for key climate change indicators. Specifically, 2023 was the hottest year on record with global temperatures 1.45 ±0.12°C above pre-industrial, aggravating a trend that has been markedly departing from historical averages for at least the last 30 years (see Figure 7). Carbon dioxide concentrations in the atmosphere reached a record high (see Box 1) as methane and nitrous oxide did, placing the concentration of these three major greenhouse gases at unprecedentedly high levels. With these high temperatures, Antarctic sea-ice extent reached an absolute record low in February 2023 and the global average sea level has surged to an unprecedented peak. Moreover, the rate of sea level rise

¹¹ 1 Gigatonne is one billion tonnes. Carbon dioxide equivalent (CO₂e) is a metric used to compare emissions from various greenhouse gases on the basis of their global-warming potential (GWP) over 100 years. This is achieved by converting amounts of other gases to the equivalent amount of CO₂ in terms of global warming potential. For example, the GWP of methane and nitrous oxide is respectively 27-30 and 273 times higher than CO₂. Emissions of 1 million metric tonnes of methane (CH₄) and nitrous oxide (N₂O) are thus equivalent to emissions of 27-30 and 273 million metric tonnes of CO₂.

¹² The emissions gap is: *"the difference between the estimated global GHG emissions resulting from full implementation of the latest NDCs and those under least-cost pathways aligned with the long-term temperature goal of the Paris Agreement."* (UNEP, 2023). To realistically model a reduction of the magnitude required by the long-term temperature goal of the Paris Agreement - i.e. cutting in half GHG emissions by 2030- the large majority of models assume stringent emissions reductions starting in 2020, which current trends contradict. This emission gap here referenced is therefore likely to be a lower-bound estimate.

over the last decade (2014–2023) has more than doubled compared to the initial period of satellite observations (1993–2002). Eventually, over the 65-years of records, ocean heat content has never been so high.

Figure 7. Temperature anomalies (in °C Celsius) relative to 1961-1990



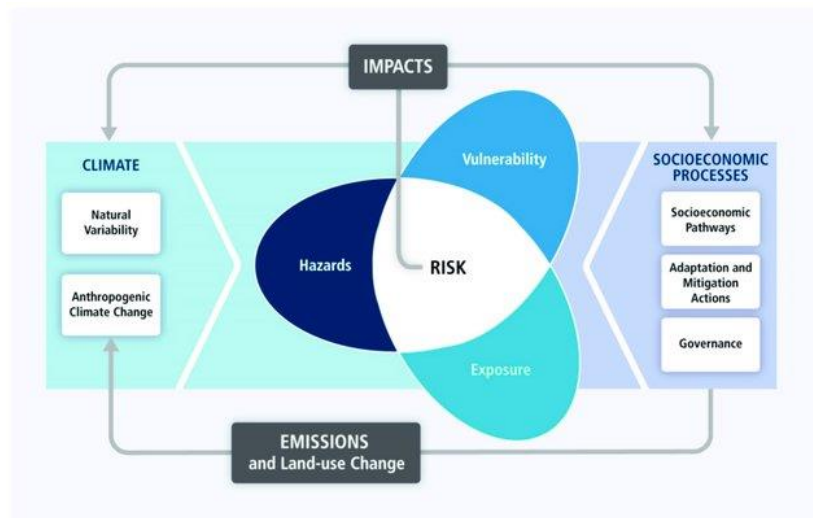
Note: uncertainties displayed in light grey account for uncertainty described by the 200 models used to reproduce this timeseries and uncertainty due to the fact that the analysis is not globally complete. See Morice et al. (2021) for more details.
Source: own elaboration.

The first impacts of a changing climate are being felt in the form of more frequent extreme events. Globally, more frequent and more severe weather and climate extremes have been recorded in recent years than in any other period before (WMO, 2024). Looking forward, projected changes in the intensity and frequency of climate extremes are very heterogeneous across regions, but they generally scale with global warming (IPCC 2023). Climate models now consistently indicate that global warming will cause statistically significant changes in extremes for (i) temperatures, (ii) heavy precipitation including that associated with tropical cyclones and (iii) a worsening of droughts in some regions. Projected percentage changes in frequency are higher for the rarer extreme events.

Besides extreme events, gradual changes to the climate system could bear far-reaching consequences. Increasing temperature will further accelerate the melting of ice in the poles, inducing a progressive rise of sea levels that can permanently flood small islands, low-lying coastal areas and deltas. Likewise, ocean warming leads to massive coral bleaching, severely undermining marine biodiversity and fisheries. If the global average temperature increases by 2°C, an alarming 99% of tropical corals are forecasted to vanish due to the combined effects of warming, ocean acidification, and pollution. On land, a warmer climate exacerbates the already fast species loss and extinction, further compounding biodiversity conservation

challenges. Worryingly, several climate tipping points are now more likely to be reached, which could unleash feedback loops and substantially disrupt critical processes for the stability of the Earth system as a whole (see Box 2). As evidenced by the PB framework, we are now endangering the self-regulation capacity of the Earth system and forcing this system out of a Holocene-like state.

Figure 8. Climate change will increase risks through more frequent extreme events (hazards), although ultimate impacts will depend on vulnerability and exposure conditions



Source: Extracted from (IPCC 2014).

The risks associated to climate change will depend on a wide range of factors including the magnitude and rate of warming, geographic location, development and vulnerability levels. More frequent extreme temperatures imply more frequent heat waves; more heavy precipitation events increase the likelihood of flood, while more frequent droughts exacerbate water stress episodes. All these evolutions increase risks to health, livelihoods, food security, water supply, human security and economic growth. These risks will increase as climate further warms but their outcomes will vary by locations and their ultimate impacts on human well-being will be modulated by a wide range of non-climatic determinants. From a schematic point of view, the impacts of extreme weather events are a function of exposure and vulnerability conditions, which are governed by socioeconomic process (see Figure 8). Managing the underlying socioeconomic process that determine exposure and vulnerability conditions is therefore key to limit the ultimate impacts of a warmer climate. Having said this, there is now enough scientific evidence to know that a global warming beyond 2°C will alter life-supporting systems so profoundly that human societies as we know them will not survive without profound and radical changes. In addition, we know that unless we drastically curb GHG emissions in the next five to ten years, we will very likely exceed a warming of 2°C. **The only open question that remains is whether the changes required to adapt to this new world will be deliberated and collectively organized or unintentional and chaotic.**

Box 2. Tipping points in the Earth system

While tipping points in the Earth System have traditionally been seen as unlikely and distant outcomes, recent scientific evidence has shown that they are becoming more likely and, importantly, are clearly interconnected across different natural process. As such, tipping points could interact among each other, producing feedback loops and self-reinforcing dynamics that would commit the world to long-term irreversible changes. To illustrate some of these dynamics, I provide a simplified view on how current levels of warming could trigger abrupt carbon release back to the atmosphere, thereby amplify global warming and its associated impacts on human systems.

As of January 2023, for a 50% chance of keeping warming to 1.5°C, the world's carbon budget has been estimated at about 250 GtCO₂ (see case study 1 and Lamboll et al. 2023). Major tipping points in the Earth system have the potential to totally erase this remaining carbon budget. First, with the Arctic warming at least twice as fast as the global average, the boreal forest in the subarctic is increasingly affected by fires, which could potentially turn the North American boreal forests from a carbon sink to a carbon source (Walker et al. 2019). Under the combined effects of deforestation and climate change, the Amazon Forest is undergoing similar changes. The dieback of the Boreal forests and the Amazon could release 110 Gt CO₂ and 90 Gt CO₂, respectively. Eventually, Permafrost across the Arctic is also beginning to defrost and releasing carbon dioxide and methane. It is estimated that permafrost emissions could release at least another 100 Gt CO₂ (Gasser et al. 2018).

Although harder to quantify, the melting of sea-ice in the poles is also amplifying regional warming in a feedback loop: glaciers, ice caps, and sea ice all have a high albedo, meaning they reflect a significant amount of sunlight back into space. When ice melts, it exposes darker surfaces like water or land, which absorb more sunlight instead of reflecting it. This absorption leads to increased heating of the Earth's surface, contributing to further melting in the surrounding areas. This feedback loop has already destabilized ice sheet in some sectors of the West Antarctic and could lead to domino effects over the rest of the West Antarctic (Feldmann and Levermann 2015). Palaeo-evidence indicates that such widespread ice discharge in the West Antarctic ice sheet has occurred repeatedly in the past, triggering massive sea level rise over long term horizons.

Not only sea ice collapse could amplify globally warming; it could also destabilise the self-regulating climate mechanisms at play during the Holocene. For example, Arctic and Greenland melting is releasing an important influx of fresh water into the North Atlantic, which contribute to slow down the Atlantic Meridional Overturning Circulation (AMOC) - commonly known as the Gulf Stream. Given the key role of the AMOC in global heat and salt transport by the ocean, its alteration could have far-reaching consequences including disrupting the West African monsoon, triggering drought in Africa's Sahel region, drying the Amazon and contributing to trap heat in the Southern Ocean, which could accelerate Antarctic ice loss. This has led Lenton et al. (2019) to refer to a "*global cascade*" of interconnected effects that could lead to a "*new, less habitable, 'hothouse' climate state*".

Note: this box largely builds upon and summarizes the information contained in Lenton et al. (2019).

To summarize this first chapter, it is worth remembering that over the last 100,000 years Sapiens has explored every corner of the world, showing an impressive ability to adapt to a highly fluctuating climate. Some 10,000 years ago, global temperatures rise to approximately pre-industrial levels and, until a few decades ago, have been remarkably stable. We are probably not yet fully aware of the deep links that exist between, on the one hand, the Earth system stability under the Holocene and, on the other, the rise of agricultural-based societies and the transition towards sedentary societies or the emergence of writing and the accumulation and transmission of knowledge over time. What we nonetheless know for certain is that the flourishing of all major civilizations -from Antic Greek and Romans to the XIX century capitalist society- has happened during this period of stable and relatively warm climate. In this very long timeframe, the last 200 years stand out as the beginning of a new era: human pressures on the Environment have increased so powerfully that we are now threatening the ability of the Earth-system to persist in a Holocene-like state, with profound consequences for the future of human societies as we know them.

In 1931, Paul Valéry wrote “*le temps du monde fini commence*”¹³. This sentence probably encapsulates some of the most important changes that have unfold during the last 200 years. It refers to the fact that, at the dawn of the XX century, every territory on the planet had been discovered and mapped out, opening a new era for Humanity. From a geographical point of view, this *finitude of the world* has marked a structural change to human settlements patterns. During most of history, human settlements were relatively smalls and scattered across natural landscapes separated by unknown territories. Nowadays, the entirety of the world has been mapped and humans have massively gathered in an unprecedent type of settlements: contemporaneous cities. This urbanization of humanity is likely to continue during the next decades, with wide-ranging consequences that encompasses economic productivity, innovation, our relationship to the Environment and probably other implications that we are still struggling to fully perceive. For what this thesis is interested in, the way we occupy the territory is also likely to shape climate change challenges.

¹³ This could be translated as “*The time of the finite world begins*”. Extracted from Valéry (1931).

2 THESIS OBJECTIVE AND STRUCTURE

This thesis is seeking to use geographical concepts – such as space, location and land cover– to the study of climate change challenges. Specifically, it focuses on the geographical patterns of cities. The concept of geographical patterns directly draws from Ahamer (2019) and is used in an evolutionary perspective: geographical patterns are similarities that repeat themselves in a natural or man-made environment to constitute structural trends that can be geo-mapped. By identifying and analysing these geographic patterns, this thesis intends to gain a better understanding of the interactions between humans and the Earth system. In this thesis, these geographical patterns principally relate to cities' (i) spatial expansion and (ii) land cover composition.

2.1 Assessing how cities' geographical patterns shape climate change challenges

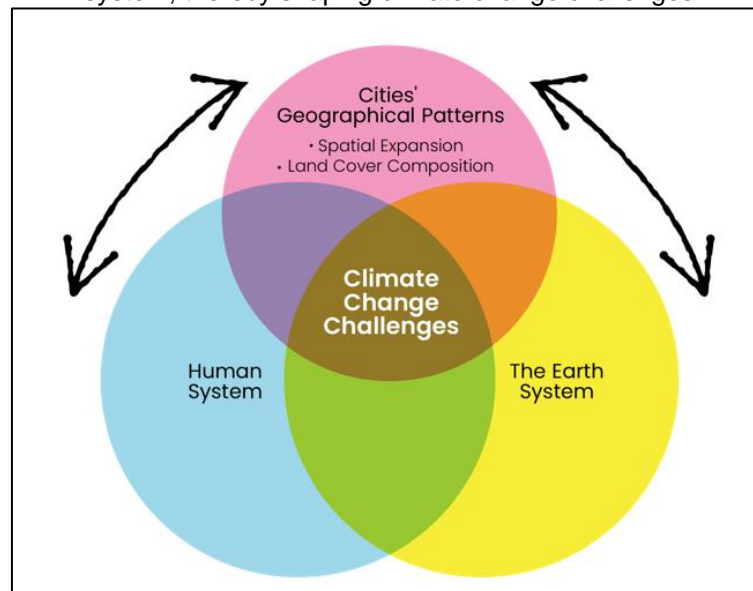
The overall objective of this thesis is to assess how the geographical patterns of Latin American cities shape climate change challenges. To do so, it articulates an empirical perspective on two climate debates: (1) Whether and to what extent cities' geographical patterns enable a shift towards low-carbon urban systems? (2) Whether and to what extent do geographical patterns reduce vulnerability to extreme weather events and influence cities' capacity to adapt to climate change?

The geographical patterns studied in this thesis capture two salient features of the *new era of urbanization*: the spatial expansion and land cover composition of contemporaneous cities. These two features are the focus of this thesis because they drive the interactions between humans and the Earth system. The unprecedented spatial expansion of contemporaneous cities has affected ecosystems across a wide array of dimensions, including the loss of agricultural land (G. Chen et al. 2020), reduced freshwater availability (McDonald et al. 2011) and the destruction of biodiversity hotspots and carbon sinks (Seto, Güneralp, and Hutyra 2012). The emergence of contemporaneous cities has also transformed natural landscapes into human-dominated landscapes, with a large predominance of built-up and impervious surface. These massive land cover changes significantly alter the hydrological cycle ((Arnold Jr. and Gibbons 1996) and the regulation of temperatures (Iungman et al. 2023). In return, these alterations can magnify the impacts of extreme weather events such as heatwaves or extreme rainfalls, further challenging adaptation to a changing climate.

Importantly, these geographical patterns are highly heterogeneous across Latin American cities. Large megalopolis in arid areas such as Mexico City do not display the same

spatial and land cover patterns than small towns in the tropical areas of Colombia or intermediary cities in the grasslands of Brazil. These strong differences have presumably important climate implications that could influence both climate mitigation and climate adaptation challenges. In fact, if almost all cities have spatially expanded, they have not all followed the same patterns of expansion, with probably different impacts in terms of GHG emissions. As detailed in the review of literature of the next chapter, compact cities could be instrumental to limit GHG emissions. Likewise, to varying degree, cities have been able to preserve green areas and natural parks, with potentially differentiated implications to adapt to more frequent extreme weather events. As detailed in the review of literature of the next chapter, the presence of green infrastructures and green areas within the city are key to enhance soil infiltration capacity and limit surface water runoff. A greener city land cover could therefore contribute to reduce vulnerability to extreme rainfall events.

Figure 9. Cities' geographical patterns mediate the relationship between humans and the Earth system, thereby shaping climate change challenges



Source: own elaboration.

Consequently, the overarching hypothesis of this thesis is that the geographical patterns of cities act as mediating factor between humans and the Earth system, thereby playing a crucial role in shaping climate change challenges. A graphical illustration of this approach and how it fits within the conceptual framework proposed in Chapter 1 is provided in Figure 9. Climate change challenges are the result of the specific Human-Environment Nexus (HEN) that has emerged during the Anthropocene -i.e. the green intersecting area in Figure 9. This specific HEN itself is shaped by the geographical patterns of cities. As such, a significant portion of climate change challenges is likely to be shaped by cities' geographical patterns. This portion of climate change challenges that can be influenced by cities' geographical patterns visually corresponds to the brown intersecting area in Figure

9. Informed by a multidisciplinary review of literature (detailed in Chapter 3), two working hypotheses have been derived from this overarching framework. These two hypotheses are empirically examined through the two case studies underpinning this thesis (Chapter 5 and 6, respectively). Although this thesis is not presented as a compendium of articles, a streamlined version of case study 1 has been published in the Journal *Cities* (article [available here](#)) and a streamlined version of case study 2 in the Journal *Global Environmental Change* (article [available here](#)). These working hypotheses and their accompanying research questions can be summarized as follows:

- The spatial expansion of a city influences its level of CO₂ emissions. Examining this hypothesis will help answering the following questions: is there a statistically significant relationship between spatial expansion and CO₂ emissions in Latin American cities? If yes, how future urbanization under different spatial expansion scenarios could impact CO₂ emission pathways? What does it entail for spatial and urban planning and how to promote a transition towards low-carbon urban systems in Latin America?
- The land cover composition of a city, particularly its greenness, influences its vulnerability to extreme rainfall events. Empirically testing this hypothesis will shed lights on the following questions: in Latin American cities, is the impact of extreme rainfall events significantly differentiated based on land-cover composition? If yes, can we quantify the benefits of a greener land-cover? What does it entail for spatial and urban planning and how to enable adaptation to climate change in the region?

To be able to empirically test these hypotheses, this thesis develops a novel methodology that leverages Earth Observations (EO) as its main source of data. This new source of information has proven particularly useful to capture the status and changes of land-cover, which allows me to tackle critical data constraints previously limiting a more comprehensive investigation of the two above-mentioned working hypothesis. Specifically, I combine data derived from EO with an internationally harmonized definition of cities (i.e. the *Degree of Urbanization*, see Chapter 4) to assemble a unique sample of more than 600 cities scattered across seven Latin American countries. This large sample of cities observed from outer space at various moments in time allow me to use fixed-effect econometric analysis to isolate the effect of geographical patterns from other time invariant city-specific characteristic (e.g. topography, elevation) or shocks commonly affecting all cities (e.g. international prices changes, variable quality of satellite imagery). This methodology is well-suited to uncover causal relationships and focus on structural trends that drive CO₂ emissions and climate vulnerability *everything else being equal*. Chapter 4 delves more in detail into these methodological aspects.

Another key feature of the methodology developed in this thesis is the population-based approach used to delineate cities and classify human settlements. This approach is fully detailed in Chapter 4 but, basically, has been designed to provide a more nuanced view on human settlements than the traditional “urban” VS “rural” binary categories. This approach based on the spatial distribution of the population is also more likely to depict the socioeconomic and functional reality of a city than its administrative boundaries. To ease communication, in this thesis I will often refer to “cities” although, from a conceptual point of view, it would be more accurate to refer to human settlements. The two terms are used interchangeably throughout the thesis. In fact, these “cities” encompass a large array of human settlements ranging from towns of 50,000 persons to megacities of more than 20 million persons.

In a nutshell, this thesis is proposing a new approach to better understand and quantify the impacts of cities’ geographical patterns on (i) CO₂ emissions and (ii) climate vulnerability. This enhanced understanding is used to show how the future spatial configuration and land cover composition of Latin American cities can have important impacts to address climate change challenges. This analysis also intends to reveal how the prevailing geographical patterns of Latin American cities have been driving unsustainability by boosting GHG emission and exacerbating climate vulnerability. In doing so, this thesis seeks to broaden the scope of climate discussions by providing empirical evidence on the role that spatial and urban planning policies -which provides the tools and instruments to shape cities’ geographical patterns- can play to address both climate mitigation and adaptation challenges.

2.2 Setting the time-space resolution of the analysis

This thesis investigates the role of cities geographical patterns across 7 Latin-American countries, namely Mexico, Colombia, Ecuador, Peru, Chile, Argentina, Brazil. Examining these relationships in Latin American cities is particularly relevant for three major reasons.

- First, while the Latin-American region already displays high urbanization rates, it is expected to continue urbanizing over the next years, although at a slower pace than in previous decades. The share of population living in urban areas in Latin American and the Caribbean is expected to grow from less than 80% in 2015 to almost 88% in 2050 (UNDESA, 2019). This suggest that, across the region, an additional 180 million persons could be living in cities in 45 years, with small and intermediate cities projected to display higher growth rates than large cities. During the next decades, cities geographical patterns will thus be modified to accommodate this influx of new city

dwellers. Simultaneously, available data indicates that Latin American cities are increasingly impacted by floods and this trend is likely to be further exacerbated under the combined effects of climate change and urbanisation (see case study 2). Better understanding how these evolutions could play out in terms of GHG emissions and climate vulnerability is key to inform future urban and spatial planning policies in the region.

- Secondly, cities' geographical patterns and development levels differ greatly across this region. This large diversity will allow me to replicate a quasi-experimental setting in which I assess whether and to what extent gradual changes in geographical patterns across a wide range of possibilities produce a causal impact on CO₂ emissions and climate vulnerability. The heterogeneity of cities in the region will also allow me to gain a refined understanding of the main relationship of interest in different development and geographical contexts.
- Finally, the limited amount of GHG inventories at the city level or the restrained information about urban flood impacts and climate vulnerability creates a very significant knowledge gap on climate-related challenges for the entire Latin-American region. This turns my methodology and the proxies' relying on Earth Observations all the more relevant.

From a temporal perspective, the use of Earth Observations constrains the temporal horizon that can be covered through the two empirical case studies. To ensure that the accuracy and quality of different EO sources is comparable, I will broadly focus on the last 30 years. From a statistical point of view, as explained more in detail in case study 2, this 30-year period is also necessary to detect possible changes in climate normal and extremes. Finally, this more recent period is also relevant because some of the first impacts of climate change are being felt throughout the region and can help better framing the problem.

3 CITIES GEOGRAPHICAL PATTERNS IN A CHANGING CLIMATE: A REVIEW OF LITERATURE

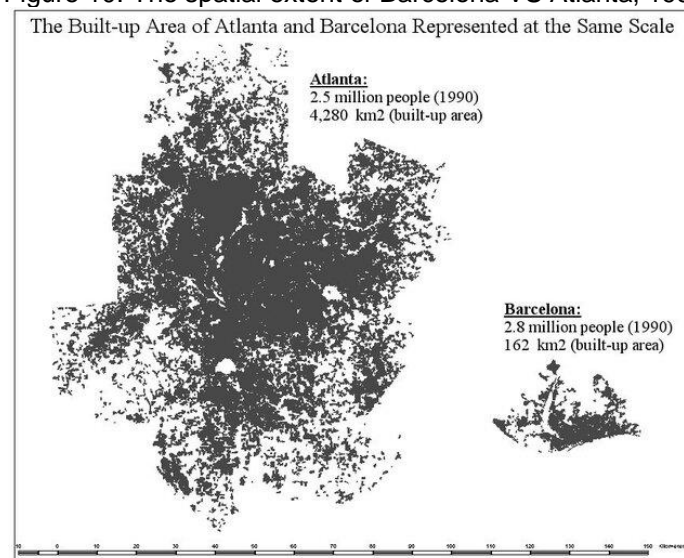
This chapter takes stock of the existing research investigating the relationship between cities' geographical patterns and climate change challenges to highlight the remaining knowledge gaps that this thesis is seeking to address. This literature review has informed the development of the conceptual approach and working hypothesis proposed in Chapters 1 and 2. As such, this chapter is structured along the two climate-related challenges emphasised previously: it first reviews the literature that examines the relationship between cities spatial patterns and greenhouse gas (GHG) emissions; it then reviews available investigations on the relationship between cities' geographical patterns and climate vulnerability or, to be more specific, that have assessed how cities land cover composition can help reducing the impact of extreme weather events.

Two major takeaways arise from this literature review. For some of the largest cities in the most developed countries, there is robust evidence that a more compact urban development is associated with lower CO₂ emissions. However, little is known about the CO₂ impacts of compactness and higher density in Latin America, where urban planning capacities tend to be more limited and cities already display important congestion effects. Importantly, beyond the somewhat banal and static observation that higher density can be associated to lower emissions, a dynamic analysis considering the full spectrum of cities and potential relocation effects is still required to provide a prospective view of the CO₂ effects that future urbanization could bring. Secondly, an important literature relying on case-study analysis and hydrological modelling has shown that a greener land cover can improve the hydraulic response of cities. However, to the best of my knowledge, there is no empirical evidence that determines the extent to which a greener land cover can alter the relationship between extreme rainfall and urban economic activity. This limits our ability to provide evidence-based estimates of the benefits associated to a greener city land cover and inform on the potential role that green infrastructure can play to adapt to a changing climate where extreme rainfall events are expected to be more frequent.

3.1 City spatial extent and CO2 emissions

While higher urbanization rates are unambiguously associated with higher GHG emissions per capita (see Figure 5 in Chapter 1), a growing body of literature has examined the relationship between city spatial expansion and GHG emissions. These studies use diverse approaches and geographical scope but generally underscore that density and “compactness” are defining feature for GHG emissions at the city level. A now famous comparison between Atlanta and Barcelona provides a visually compelling illustration of what a compact urban development implies compared to a more sprawled urban development (Figure 10). While both cities had a similar population in 1990 (approximately 2.5 million people), the built-up area of Atlanta is more than 26 times larger than the one of Barcelona (Bertaud and Richardson 2005).¹⁴ Presumably, these differentiated spatial patterns could lead to differentiated levels of GHG emissions in each city even, *everything else being equal*.

Figure 10. The spatial extent of Barcelona VS Atlanta, 1990



Extracted from: Bertaud and Richardson (2005).

As an analogy to agglomeration economies, higher density could be instrumental to deliver climate mitigation benefits at the city-level. The mechanisms at play and different transmissions channels found in the literature are detailed below. They can be broadly grouped in two categories: (i) denser cities streamline energy consumption in the housing and building sectors as dense residential buildings tend to be more energy efficient than private dwellings; (ii) high-density cities favour a transport-oriented urban development that promotes public transport and alternative low carbon transport systems (e.g. biking, walking...), while

¹⁴ This spatial extent is measured in terms of built-up areas and both cities are here defined based on the administrative limits of their respective metropolitan areas. I dig deeper into these aspects in Chapter 4 when discussing the methodology of this thesis.

requiring less materials, concrete, roads and network infrastructure to service the same amount of persons.

However, the climate benefits intuitively associated to higher density might differ across countries and cities. In Latin American contexts, where urban planning capacities tend to be more limited and fast-growing cities already display important congestion effects, higher density might bring about more negative congestion effects than agglomeration benefits (Ferreyra and Roberts, 2018). In this setting, increasing further the density levels of some cities could result in uncertain impacts on CO₂ emissions. Additionally, as highlighted by Gaigné, Riou, and Thisse (2012), compactness and higher-density policies generate changes in prices, wages and land rents, which in turn incentivize firms and households to move locations -either to a new city or to suburban areas. These relocations effects might eventually dominate the benefits of higher density. In fact, when these general equilibrium effects are considered, the effects of higher density policies in urban centers could raise the overall CO₂ emissions of a city and/or boost the total emissions of the broader urban system.

To better understand the relationship between cities' spatial expansion and CO₂ emissions, I start by presenting relevant studies from the literature. These studies can be classified under three different geographic scopes, which are directly linked to the data source they rely upon.

3.1.1 Detailed case studies of single major metropolitan areas

Case studies of large metropolitan areas have been pioneers in identifying the channels through which the spatial expansion of cities can reduce GHG emissions. These investigations leverage highly granular data on households' energy consumption or transport-related surveys to derive CO₂ emissions estimates.

Liu and Sweeney (2012) have for example investigated the relationship between heating energy use and urban form for the Greater Dublin Region. Using building thermal balance model at the district level, they found that compact dwellings characterized by smaller floor areas are a significant factor to streamline overall heating energy demand and individual dwelling energy consumption. On this basis, two urban development scenarios were compared, suggesting that a "compact city" scenario could reduce domestic heating energy consumption per household by 16.2% compared with a "dispersed city" scenario. This compact city scenario could therefore have a direct impact to significantly reduce energy-related CO₂ emissions.

Another relevant case study has been provided by Ma, Liu, and Chai (2015). Their investigation has focused on the relationship between urban form and transport behaviour and

resulting carbon emissions in Beijing. Using an activity diary survey, they show that residents living in neighbourhoods with higher job density, close to an employment sub-center and greater subway accessibility tend to travel shorter distance or choose low-carbon travel modes, which in return reduces CO₂ emissions from work-related trips. Likewise, people living in neighbourhoods with higher retail density or mixed land use tend to travel shorter distance and have less CO₂ emission from non-work trips.

3.1.2 Samples including some of the largest urban areas within a country

Beyond single-city analyses, investigations pooling different cities have highlighted similar effects between urban forms and CO₂ emissions. These investigations have been mainly conducted in developed countries (i.e. United States, Japan, Italy) and rely upon CO₂ emissions data at the city level or energy consumption surveys.

Lee and Lee (2014) have examined CO₂ emissions in the 125 largest urbanized areas in the United States using data on household's energy consumption. Their results indicate that doubling the population density would lead to a 35 % and 48 % reduction in household residential and transportation energy consumption, respectively. These reductions would produce a notable effect since residential and transport energy consumption account for 42% of total CO₂ emissions in the United States. Makido, Dhakal, and Yamagata (2012) have focused their study on a sample of 50 Japanese cities and leveraged available CO₂ emissions data at the municipality level that dated from 2005. Using landscape metrics to describe compactness and complexity¹⁵ of urban settlement patches, they found that that compact cities emit less CO₂ from the passenger transportation sector than the sprawled cities. Interestingly, their study suggest that complexity has less significant impacts than compactness on CO₂ emissions. Following a similar approach, Cirilli and Veneri (2014) provide a European perspective and focus on CO₂ emissions due to commuting in the 111 largest Italian urban areas. They found that smaller, more compact and less monocentric areas are associated with lower CO₂ emissions per commuter.

3.1.3 Samples proxying CO₂ emissions to include the totality of the cities within a country

More recently, a new strand of the literature has used night-time light (NTL) satellite imagery to spatially disaggregate CO₂ emissions. This new methodology has allowed to proxy CO₂

¹⁵ Complexity in this study refers to the shape index. I describe more in-depth this shape index in the first case study of this thesis.

emissions for all urban areas within a country, regardless of their size or the availability of GHG inventories. This has revealed critical to capture small and intermediate cities, which were not considered in previous studies.

Methodologies to spatially distribute CO₂ emissions through NTL satellite imagery usually rely on national level estimates of GHG emissions and allocate emissions that can be associated to specific locations and/or activity. Therefore, they generally focus on fossil fuels energy-related emissions (see Chapter 4 in section 4.2.1 for a more in-depth discussion of the scope of different GHG accounting methodologies). It is nonetheless important to clarify here that these methodologies generally rely on a common hypothesis: night-light intensity as captured by satellite imagery correlates strongly with energy consumption and therefore with CO₂ emissions.

Leveraging this new approach, two recent studies have been conducted in China to assess the relationship between cities form and CO₂ emissions. Ou et al. (2019) have estimated CO₂ emissions in each Chinese city using NTL satellite imagery to spatially disaggregate provincial energy statistics. They then used socio-economic indicators to classify cities into different tiers and evaluate the relationship between urban forms and CO₂ emissions at different development stages. Their overall results confirm that urban land expansion increases CO₂ emissions, while a more irregular or fragmented urban form could result in more CO₂ emissions due to the increase in potential transportation requirements. However, their study depicts a more nuanced relationship: the benefits of higher density in terms of CO₂ emissions are found to progressively decline as cities become increasingly developed and are even reversed for the richest cities. Such results highlight the importance of considering both a city's development level and its spatial development patterns to accurately anticipate CO₂ emissions impacts of a given spatial or urban planning policy.

Zhou and Wang (2018) use a similar approach to obtain city-level energy-related CO₂ emissions estimates for all Chinese cities through NTL. Nonetheless, their study highlights new effects: they found evidence of spatial dependence in the geography of city-level CO₂ emissions, with high emissions cities geographically close to each other. This underlines the influence cities exert on their neighbours and the need to go beyond single city analysis to consider urban systems dynamics. In addition, this analysis found that road density (including railway) and the traffic coupling factor (a proxy to describe the extent of the coupling relation between a city's spatial structure and traffic) exert strong negative influence on city-level CO₂ emissions. Consequently, authors point out to the need to improve the coupling degree between the urban spatial structure of a city and its traffic organization to reduce CO₂ emissions.

3.1.4 Remaining knowledge gap

From the review above, it appears that the scope of existing literature is restricted by a twofold issue linked to: (i) scant GHG emissions inventories or energy-related statistics at the city or metropolitan area level; and (ii) methodological problems in delimiting urban areas in an internationally consistent way.

Globally, only a few cities have GHG emissions inventories and these are usually outdated, inconsistent and of differing scope and coverage, hindering comparability across cities, regions and countries (see Mia, Hazelton, and Guthrie (2019) for a description of the caveats limiting GHG emissions inventories comparability and Box 4 in Chapter 4 for a discussion of the three different scopes of GHG inventories that exist). This is even truer in Latin America, where Baltar de Souza Leão et al. (2020) reviewed available city-level inventories in Brazil and identify two major reporting gaps (i.e. incompleteness and lack of transparency gaps) that affected almost all available inventories. A conventional practice to address this data limitation and cover more cities in a systematic way is to rely on emissions parameters from engineering studies, applied to survey-based activity measures for energy production, manufacturing and transport. While this methodology is useful to get harmonized CO₂ emissions estimates across cities, it still requires energy statistics at the city level, which are often only available for large cities in developing countries. This explains why most of the abovementioned studies drawing upon available inventories or city-level energy statistics have focused on a small set of cities displaying relatively homogeneous spatial patterns and development levels.

On the other hand, recent studies using satellite imagery to spatially distribute carbon emissions have been mainly conducted in China, limiting the scope of their investigations to single-country analyses. In fact, comparing cities or urban areas across countries is a long-standing issue traditionally faced by economic geography and urban economics analysis. Urban areas are defined on a national basis and criteria vary significantly (UN Statistical Commission, 2020). Until recently, there were no harmonized definition of what constitutes a “city” and computing statistics at the city-level across different countries represented a challenging task -not only for CO₂ emissions. This is one of the main issues that this thesis is addressing from a methodological perspective (see chapter 4).

As a result of this twofold limitation, existing studies are heavily biased towards developed countries, characterized by mature urban systems and effective urban management. By contrast, little is known about the GHG impacts of compactness and higher density in Latin America, where urban planning capacities tend to be more limited and cities already display

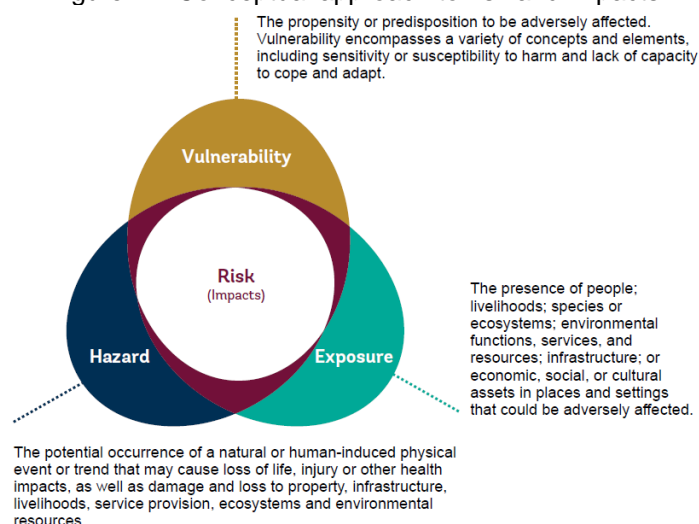
important congestion effects (Ferreyra and Roberts, 2018). Against this background, more empirical analysis is required to improve our understanding of the relationship between cities spatial expansion patterns and CO2 emissions in Latin American urban contexts. More importantly, beyond the somewhat banal and static observation that higher density can be associated to lower emissions, a dynamic analysis considering the full spectrum of cities that compose the urban system is still required to provide a prospective view of the CO2 effects that future urbanization could bring.

Knowledge gap: The absence of large-scale, international analyses of the relationship between city spatial expansion and CO2 emissions greatly restricts our ability to provide evidence-based advice that could contribute to the development of sustainable urban systems in Latin America. More importantly, a thorough analysis of the dynamics characterizing the spatial expansion of cities in Latin America is still required to provide a forward-looking view of the potential CO2 effects attached to different urban spatial development scenarios.

3.2 City land cover and climate vulnerability

Under the effects of climate change, extreme weather events are expected to become more frequent, prompting the need to better understand how geographical patterns can drive climate vulnerability at the city-level. From a conceptual point of view, it is important to distinguish hazards from exposure and vulnerability (see Figure 11). Following the IPCC (2012), hazards refer to “the occurrence of a value of a weather or climate variable above (or below) a threshold value near the upper (or lower) ends (‘tails’) of the range of observed values of the variable”. Exposure relates to what could be affected by the weather event in that location, such as the number and type of buildings, or the assets and people residing in that location. Vulnerability is defined as “the propensity of exposed elements such as human beings, their livelihoods, and assets to suffer adverse effects when impacted by hazard events”. Under the effects of climate change, it is expected that the frequency and intensity of some hazards will be altered, increasing the probability of rare extreme weather events. However, the ultimate impacts associated with more frequent extreme events will be the result of a complex set of interactions between hazard, vulnerability and exposure conditions. This review of literature therefore focuses on geographical patterns that have been identified to help reducing vulnerability to two weather-related hazards, namely heat waves and extreme rainfall.¹⁶

Figure 11. Conceptual approach to risk and impacts



Source: Extracted from IPCC (2012).

¹⁶ Cyclones or drought are two other weather-related hazards that are expected to be altered under the effects of climate change but they will only affect selected cities (those exposed to cyclones) and, in the case of drought, will more directly impact rural areas. They are therefore not the focus on this review of literature.

3.2.1 City land cover and temperature

An important strand of literature has already looked at how the land cover composition of a city can reduce local temperatures. In fact, at least since the 1990's urbanization itself, through the conversion of natural landscapes into impermeable surfaces and built-up areas, has been identified as one of the factors exacerbating the impacts of heat waves through the so-called "urban heat islands" (UHI, see Oke 1995). From a physical point of view, the phenomenon is well understood. Concrete and impervious surfaces absorb and trap more solar radiation than natural landscapes, leading to higher temperatures within cities than in surrounding areas, particularly during the nights (K. Lee et al. 2020). The negative effects of UHI and high temperatures have also been thoroughly studied and are primarily linked to human health. They include children's mortality and hospital admissions (Xu et al. 2012), cardiorespiratory morbidity (Turner et al. 2012) and premature mortality in general (Guo et al. 2014; Gasparrini et al. 2015; Ye et al. 2012). Strategies aimed at reducing UHIs have been well identified and fundamentally seek to turn city's land cover "greener". These strategies include the replacement of impervious surfaces with permeable or vegetated areas (Avissar 1996; Onishi et al. 2010), increasing tree coverage (Ziter et al. 2019; Schwaab et al. 2021) or even the introduction of green roofs or facades (Rosenfeld et al. 1998; Virk et al. 2015).

More importantly, recent studies using satellite imagery to map urban tree coverage have provided robust empirical evidence that a greener land cover can reduce the impacts of heatwaves and mitigate the mortality burden associated with UHI effects. Examining a sample of 93 European cities, lungman et al. (2023) have for example conducted a quantitative health impact assessment and found that increasing tree coverage to 30% would cool cities by a mean of 0.4°C, which could prevent 2,644 premature deaths, corresponding to 1,84% of all summer deaths. Likewise, Marando et al. (2022) estimated the cooling capacity of trees in more than 600 European cities and evidenced that urban vegetation cooled European cities by an average of 1.1°C and up to 2.9°C, which allows to significantly mitigate UHIs adverse effects. In a nutshell, there is already ample and robust evidence that urban green areas and tree coverage are key geographical patterns to reduce the adverse effects of heat waves and UHIs. In consequence, I consider that examining further this issue would not fundamentally add value to the existing literature nor help addressing a significant knowledge gap.

3.2.2 City land cover and extreme rainfall events

On the other hand, hydrological literature has long established that deforestation can exacerbate flood risk (Clark 1987). Here again, the physical mechanisms through which vegetation cover can improve hydraulic properties of soils have been painstakingly

documented (Lunka and Patil 2016; Chandler et al. 2018; Shuttleworth et al. 2018, among others). A densely vegetated cover improves the hydraulic properties of soils through two major channels. First, trees and vegetation cover enable water infiltration and increase water retention in the soil, which reduces superficial water run-off. Second, tree roots, mushrooms and organic soil associated with forest or vegetated ecosystems reduce soil erosion, which in return facilitates water absorption and avoids riverbanks sedimentation.

Building upon these findings, various studies have evidenced how in urban areas the expansion of impervious surfaces alters the rainfall-runoff process and increase urban flood risk (Yao, Wei, and Chen 2016; Jacobson 2011; Mejía and Moglen 2010; Arnold Jr. and Gibbons 1996). Impervious surfaces refer to any human-made structures or materials that prevent or significantly reduce the infiltration of water into the underlying soil. These surfaces include paved roads, parking lots, sidewalks, rooftops, and other hardened surfaces. The mechanisms are very similar to those described in the previous paragraph. In short, impervious soil interferes with the natural process of water infiltration and increases both the velocity and volume of surface run off, potentially exacerbating the magnitude of urban floods for a given level of heavy precipitation.

Despite this evidence, to mitigate the negative impacts implied by the expansion of impervious surfaces, cities have primarily relied upon traditional flood control infrastructure. Traditional urban flood control infrastructure such as dikes, drainage networks or channels can efficiently drain stormwaters out of the city. However, they entail important upfront capital costs and are complex to maintain in urban contexts characterized by poor solid waste management capacities (Lamond, Bhattacharya, and Bloch 2012), such as those found in most Latin American cities. They also display a finite water transport capacity, requiring costly upgrades in case of fast-paced urban growth and/or changes to precipitation patterns to avoid quick saturation in case of storm events (Schmitt, Thomas, and Ettrich 2004). These elements explain why in most Latin American cities, urban drainage and traditional flood control infrastructure remain insufficient and/or poorly calibrated.

Against this background, more recent investigations have been looking at the potential to confront urban flood risk through a greener city land cover. These solutions have been labelled as green infrastructures (GI). Green Infrastructures are part of Nature-based Solutions, which can be defined as measures that seek to leverage ecosystem services provided by the Earth system to address climate change challenges (Brink et al. 2016). In essence, GI for flood protection constitute a set of alternative interventions that seek to bring hydrological response closer to pre-urbanized conditions by enhancing water infiltration

capacity.¹⁷ GI to address urban pluvial flooding typically include rain gardens, infiltration trench, bio-swales or permeable pavements. Some of these GI are shown in Illustration 1. Likewise, interventions to reduce the impact of fluvial flooding can range from localized streambed re-naturalisation to more ambitious re-meandering and restoring upstream floodplains or wetlands. Interventions to address fluvial flood risk usually imply important coordination works but deliver high flood protection benefits (EEA 2017; Gourevitch et al. 2020). Importantly, all GI provide additional co-benefits ranging from recreational opportunities to biodiversity conservation and carbon sequestration. Importantly, all GI deliver additional co-benefits by providing multiple ecosystems services ranging from aesthetic value and recreational opportunities to biodiversity conservation, temperature regulation and carbon sequestration (Brink et al. 2016).

Illustration 1. Examples of GI to address urban pluvial flood risk



These investigations have shown that GI are capable to significantly reduce and postpone peak runoff, thus limiting downstream flooded area for a given extreme rainfall event. Using a comprehensive hydrologic model for a small urban catchment on the eastern fringe of Melbourne, Australia, Schubert et al. (2017) have found that for storm durations equal or less than 3 h, a full implementation of GI would reduce downstream flooded area on average by 91% and lower maximum flow intensities by 83%. However, for storm durations longer than 3 h, GI start saturating and cannot retain the resulting rainfall depths, resulting in a reduction of flooded area and flow intensity of only 8% and 5.5% respectively.

¹⁷ Green infrastructures go beyond flood protection measures but for the sake of conciseness, it has been decided to restrict it to flood. A broader definition of green infrastructure is provided by EEA (2017): “Green Infrastructure is a strategically planned network of high quality natural and semi-natural areas with other environmental features, which is designed and managed to deliver a wide range of ecosystem services and protect biodiversity in both rural and urban settings”.

Similarly, Liang et al. (2020) have applied the Storm Water Management Model (SWMM) to examine the concept of “sponge city” for the city of Xining in China. Authors found that the reduction in imperviousness was positively correlated with the hydrological performance of the city and that the peak flow was most sensitive to this reduction in impervious surfaces, followed by runoff volume and peak time. Interestingly, they also noted that as rainfall intensity increased, the contribution of imperviousness reduction was less significant to improve the hydrological performance of the city.

Along the same lines, Yao, Wei, and Chen (2016) conducted a comprehensive assessment of the impact associated to imperviousness surfaces using a model-based analysis in an urban residential catchment in Beijing, China. Synthetic input storms were selected to match several typical flood-induced rainfall events with varying amounts and locations of rainfall peak, and durations. Imperviousness-derived metrics are found to be a powerful predictor for predicting runoff variables under various storm cases. As in previous investigations, the results indicate that at a very fine spatial scale (<1 ha) the performances of imperviousness related metrics are very heterogeneous and may vary markedly depending on storm conditions. Hossain Anni, Cohen, and Praskievicz (2020) simulate flood events on the University of Alabama campus, USA, using different soil imperviousness hypothesis. Using a 2D hydrodynamic model they find consistent results: while traditional flood control infrastructure significantly decreases flooding volume, flood simulation predictions are sensitive to soil input data, with pervious soil leading to less severe flooding though with decreasing relative impact for larger events. Eventually, detailed flood risk simulations for Shanghai have highlighted that GI can play a critical role, although on their own, they cannot maintain future flood risk at a low level (Du et al. 2020).

In a nutshell, hydrological modelling studies suggest that GI deliver non-linear effects in terms of flood protection, with highly heterogeneous relationship between imperviousness changes and rainfall-runoff alterations at small scale. Likewise, saturation effects seem to materialize once the infiltration capacity of the existing GI is exceeded. However, evidences provided by these approaches relies on hydrological modelling approaches and computer simulation limited by many uncertainties (Li et al. 2017). More generally, flood risk reduction measures, including GI schemes, are rarely monitored and available assessments have predominately focused on high-income countries (Poussin 2015; EEA 2017). Empirical evidence of the effectiveness of GI is very scarce and are inexistent or anecdotal for most of small and intermediate cities in Latin America. In fact, despite this growing interest, properly quantifying the value of GI remains a challenging task notably because little is known about the benefits of GI in terms of protecting assets and reducing economic disruption triggered by extreme rainfall events.

3.2.3 Remaining knowledge gap

The comparison with the existing literature examining heatwaves and UHI is instructive to clarify the knowledge gap that remains regarding extreme rainfall effects. The literature on UHI has identified that impervious surfaces are exacerbating the adverse impacts associated with heatwaves in terms of increasing premature death. Consequently, this literature has empirically estimated the benefits of a greener city land cover in terms of avoided premature death (Lungman et al. 2023). I did not find similar studies for the case of extreme rainfall. The hydrological literature has evidenced that the expansion of impervious surfaces exacerbates water run-off, potentially resulting in larger or more severe floods. However, to date, there is no empirical valuation of the benefits that a greener city land cover could bring in terms of avoided impacts associated with extreme rainfall at the city-level. These avoided impacts could be quantified in terms of avoided human impacts (e.g. death, displaced persons) or in terms of avoided economic impacts (e.g. damages to assets or disruptions to economic activity).

Two significant knowledge gaps are thus identified from the above review literature: (i) very scarce empirical evidence exists on the effectiveness of GI to reduce the impacts of extreme rainfall in different geographical and development contexts; (ii) in return, this has restricted the ability to provide an estimate of the benefits that a greener city land cover can bring in terms of avoided impacts associated with extreme rainfall events.

The hydrological literature presented above is, per essence, focused on a limited geographic area (i.e. one or few watersheds) to be able to unveil the detailed physical mechanisms and hydrological factors that trigger local flooding. Developing a broader set of empirical evidence would require capturing extreme rainfall events over a much larger geographical area and during a longer time-period. In this setting, we could use counterfactual analysis to test whether the presence or absence of green areas within a city alter the impacts associated with observed extreme rainfall events (as opposed to synthetic flood catalogue). Empirical studies of this nature would be crucial to increase the confidence of policy makers on the feasibility and benefits of GI to reduce the impacts of extreme rainfall events. Obviously, such settings imply the ability to collect information on rainfall patterns and greenness of the land cover over large geographic areas. The approach proposed in the next chapter is precisely seeking to address this methodological issue.

In more general terms, relatively little is known about the impacts of extreme rainfall on urban economic activity. From a conceptual point of view, extreme rainfall damage assets and disrupt economic activity, which could refrain local economic activity -at least in the short-term. Agglomeration economies, one of the main sources of productivity growth in urban

settings, require efficient supply chains and logistics networks to facilitate the movement of goods and services within and outside the urban area. Extreme rainfall can significantly disrupt these logistics networks, leading to increasing transportation costs and times, and ultimately negatively impacting the productivity and competitiveness of businesses operating within the city. Extreme rainfall can also force businesses to temporarily suspend operations, disrupting the concentration of firms in a particular area and weakening the potential synergies and knowledge spillovers that occur within clusters of related industries. Although there is emerging evidence that urban economic activity is adversely impacted by floods and that firms and agents do not relocate from areas that are at high risk of recurring floods (Kocornik-Mina et al. 2020), the nature and dynamics of urban economic responses to extreme rainfall is still poorly understood, restricting the possibility to quantify the benefits of GI in terms of avoided economic impacts from extreme rainfall.

As a result, for most intermediate and small cities in Latin American countries, there is very little empirical evidence that determine the extent to which GI can alter the relationship between extreme rainfall events and its impacts on local economic activity.

Although GI could be particularly attractive to Latin American cities, which often display insufficient traditional flood control infrastructure and face complex maintenance challenges, the absence of a clear valuation of the economic benefits that GI can bring in terms of avoided losses or reduced economic disruptions is an important missing element to conduct cost-efficiency analysis at scale.

Knowledge gap: For most intermediate and small cities in Latin America, there is very little empirical evidence that determines the extent to which a greener city land cover can alter the relationship between extreme rainfall and its impacts on urban economic activity. This limits our ability to provide a sound valuation of the benefits associated with urban green areas in terms of economic losses associated with extreme rainfall events.

4 METHODOLOGY AND DATA SOURCES

One of the main contributions that this thesis is seeking to make is the development of a methodology that enables the empirical examination of different hypothesis about the human-environment relationship. To do so, it leverages Earth Observations (EO) as its main source of empirical observations. Earth Observations can be defined as the gathering of information about the physical and biological systems of the planet via satellite imagery and remote-sensing technologies. Over the last 30 years, the ever-increasing number of satellites operating around our planet has prompted a sharp increase of EO. In return, this has facilitated a whole range of new applications ranging from the detection of forest fires in remote areas to the acquisition of information about local economic activity in zones where traditional statistics are missing.

This new source of information has proven particularly useful to capture the status and changes of land-use and land-cover. In fact, through recurrent and georeferenced measurements, EO provide new empirical evidence to evaluate cities' geographical patterns and apprehend their dynamics over time and space. EO display unique spatial features both in terms of resolution (some dataset used in this thesis have a 30-meter spatial resolution) and geographical coverage (potentially the entire globe). In addition, observations are collected at regular time interval, enhancing timeseries analysis. The spatiotemporal granularity of this new source of information is crucial to shed lights on the two guiding questions of this thesis, namely: (1) Whether and to what extent cities' geographical patterns enable a shift towards low-carbon urban systems? (2) Whether and to what extent do geographical patterns reduce vulnerability to extreme weather events and influence cities' capacity to adapt to climate change?

To harness the full potential of EO, the methodology developed in the framework of this thesis entails three major steps:

- First, I delineate cities in a harmonized way across countries relying on the *Degree of Urbanization* concept, a population-based approach.
- Second, I conduct spatial analysis of earth observations datasets to produce the relevant variables at the required spatial level (e.g. CO₂ emissions at the city-level, urban economic activity, greenness of city land cover, precipitations -among others).
- Thirdly, once those datasets are compiled, I use statistical analysis and econometric techniques that replicate quasi-experimental designs to unveil causal relationships for the two guiding questions above.

The remaining of this chapter is structured around three sections that detail each of these steps. It is worth noting that all the EO used for this thesis are freely available on internet in an open-data format. Similarly all the data processing of this thesis -both the spatial and statistical analysis- has been conducted using the R software, which is a free software environment. As such, beyond the climate change challenges here addressed, the methodology developed in the framework of this thesis could easily be replicated in different regions and/or employed to examine other dimensions of the human-environment nexus.

4.1 An internationally harmonized approach to delineate “cities” across 7 Latin American countries

4.1.1 What is an urban area?

What constitutes a city and how to spatially delineate it? To this question there is probably as much responses as cities across the world. In Latin America, the concept of urban areas (as opposed to city see Box 3) is generally defined at the national level. Different concepts, approaches and thresholds values are used, making it a very heterogeneous object to study. Based on a review of the definition of “urban areas” used in various Latin American countries, three main approaches have been found¹⁸:

- *Population thresholds*: this approach defines urban areas as human settlements exceeding a given population threshold. However the thresholds vary strongly from one country to the other. Nicaragua defines urban areas as settlements exceeding 1,000 persons, Argentina and Bolivia use a threshold of 2,000, while México considers that settlements that gather more than 15,000 persons are urban areas. This dispersion in thresholds does not seem to follow a clear rationale whereby for example more populated or more “urbanized” countries would display higher thresholds. When looking at these population thresholds at the global level, there is even more dispersion: countries like Japan or China defining urban areas as settlement exceeding 50,000 person or 100,000 persons respectively.
- *Administrative limits*: countries like Brazil, Colombia, Costa Rica, Ecuador, Paraguay or Dominican Republic all define urban areas on an administrative basis, meaning that the area covered by an urban area is arbitrarily classified as urban or rural without looking at its population.

¹⁸ This classification and the numbers provided here is based on CEPAL (2001).

- *Structural features*: a third set of countries look at structural features that differentiates living in urban and rural areas. Cuba and Panama consider for example that urban areas are these where the access to infrastructure or basic services (such as health and education) is above a given level. Chile on the other hand considers that urban areas are areas where most of the population is involved in non-agricultural activities and therefore defines urban areas as those settlements where more than 50% of the population is working in the secondary and tertiary sectors.

Obviously, these differentiated approaches relate to the specific context of every country and are not merely an accounting issue. Political economy factors are a major element to consider when analysing these aspects. The reclassification of a settlement from rural to urban can have strong implications in terms of fiscal transfers or obligations to provide public services. I am not seeking to tackle these aspects in this thesis. However, a major issue arises with international comparisons of urbanisation trends that rely on data collected using these national definitions: they entail big differences on what actually is an urban area. The famous sentence according to which “*more than 50% of the world population now lives in urban areas*”, for example, relies on a compilation of population living in urban areas according to each country’s national definition. To address this long-standing issue in geography and urban economics, my thesis resorts to the concept of “Degree of Urbanization”.

4.1.2 The Degree of Urbanization

In March 2020, the United Nation Statistical Commission endorsed the Degree of Urbanization (DoU) as the recommended methodology to facilitate international comparability of urban and rural areas. This approach was developed by a consortium of six international organisations and agencies.¹⁹ It allows to delineate cities in a consistent and internationally harmonized way. Importantly, it has been designed to better capture the urban-rural continuum and provides a more nuanced view on human settlements than the “urban” VS “rural” binary categories used by many national statistical offices. Dijkstra et al. (2020) detail the approach and describe the results of applying this concept at the global level and UN-Habitat (2022) provides a policy-oriented application of the DoU. I invite interested readers to refer to these two investigations for a detailed presentation of the DoU. In the remaining of this section I am simply describing how the DoU has been used in my thesis.

¹⁹ The European Commission, the Food and Agriculture Organization of the United Nations (FAO), the United Nations Human Settlements Programme (UN –Habitat), the International Labour Organisation (ILO), the Organisation for Economic Co-operation and Development (OECD) and The World Bank. See United Nation Statistical Commission (2020).

The DoU is a population-based approach that clusters population based on specific criteria. More precisely, the DoU classifies a territory into three classes: 1) urban centers, 2) towns and semi-dense area, and 3) rural areas. Each class is defined as follows:

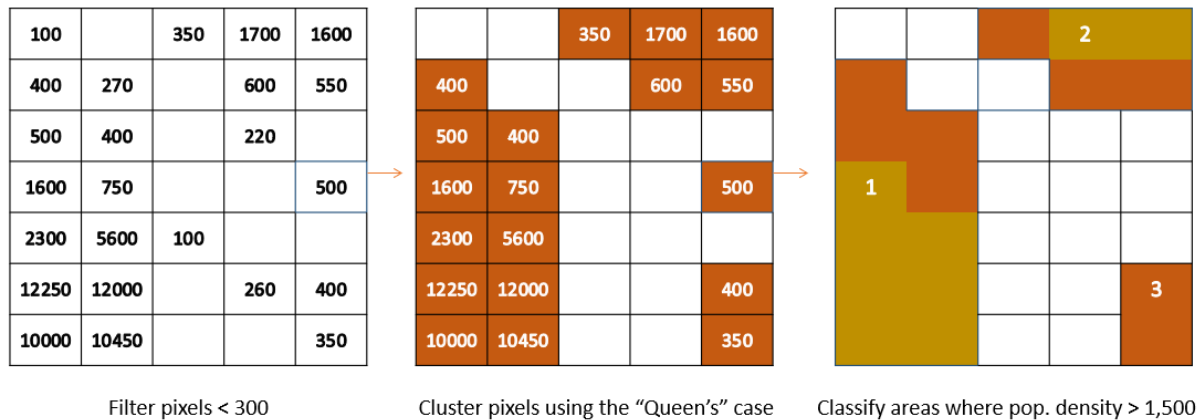
- **Urban centers** consist of contiguous grid cells that have a density of at least 1,500 inhabitants per km². The contiguous cells should have a total population of at least 50,000.
- **Towns and semi-dense areas** consist of contiguous grid cells with a density of at least 300 inhabitants per km². The contiguous cells should have a total population of at least 5,000 and less than 50,000. When these semi-dense areas are contiguous to an urban center, this thesis consider them as “suburban areas”.²⁰
- **Rural areas** consist of low-density grid cells (<300 personas/km²) that do not meet the previous criteria.

Based on this definition, I have developed an algorithm that follows this classification rules. I have applied this algorithm to the gridded population raster from the Global Human Settlement Layer provided by the European Commission (GHS-POP). This raster is freely available online and I have used the version R2019A with a spatial resolution of 1km and a World Mollweide projection (EPSG:54009).²¹ Although this population grid is also available in geographic format, this projected coordinate system (PCS) has been selected to preserve the spatial properties related to area, which will be crucial to accurately compute the spatial extent of different cities. As our area of interest goes from the northern Mexican border to the Patagonia in southern Argentina and Chile, national or local PCS were not deemed appropriate and this global equal-area PCS was preferred. For illustrative purposes, the following diagram summarizes the main steps of the algorithm developed for this thesis. My algorithm considers the queen's case when defining adjacent pixels.

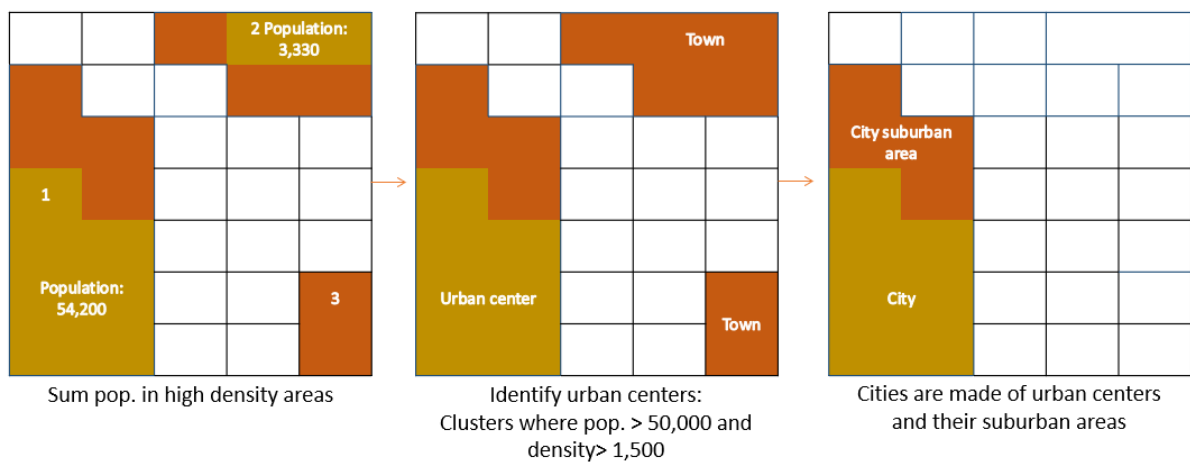
²⁰ This is what is proposed in the second level of the Degree of Urbanization, which splits towns and semi-dense areas into towns and suburban areas.

²¹ The underlying raster is available [here](#).

Illustration 2. Diagram illustrating the Degree of Urbanization application for a population grid.
Step 1



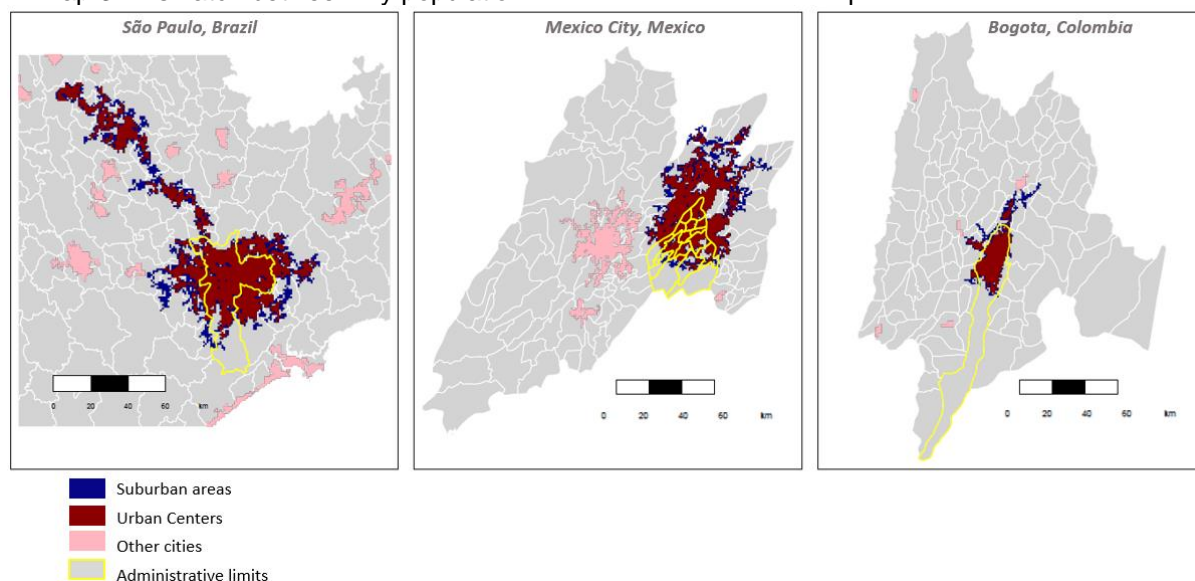
Step 2



Source: own elaboration based on the criteria of the Degree of Urbanization.

In this thesis, cities are therefore considered to be population clusters meeting the double criteria of at least 50,000 persons and a density of minimum 1,500 habitant/km². These objective criteria are independent from the administrative boundaries of a city. Instead, this definition of "cities" is seeking to capture the spatial distribution of population, which is more likely to depict the socio-economic reality and functional interrelationships of the urban system than are administrative boundaries. To highlight this, Map 3 depicts 3 cities in three different countries identified using the algorithm developed for this thesis. This figure reveals the mismatch between a city's administrative boundaries and its population distribution: cities as I have defined them in this thesis (i.e. the red and blue areas) do not overlap with their corresponding administrative areas (highlighted in yellow).

Map 3. Mismatch between my population-based “cities” and their respective administrative areas



Note: For each city, the corresponding administrative boundaries are highlighted in yellow. The grey area is the corresponding administrative 1 area.

Source: own elaboration based on GHS-POP. Base map: GADM.

As a result of applying this algorithm to Mexico, Colombia, Ecuador, Peru, Chile, Argentina and Brazil, 635 cities are identified, ranging from small urban areas (i.e. 50,000 people, as per the definition of the degree of urbanization) to giant megalopolises (20+ million people for Sao Paulo and Mexico City).²² Case study 1 and 2 provide descriptive statistics and more details on the features of this dataset but it is already worth mentioning that small and intermediary cities make up the bulk of the urban system. In 2015, half of the cities had a population below 130,000 and only 44 cities had a population over 1 million.

²² The seven countries of interest of this thesis represent approximately 60% of the 1042 cities identified through the DoU across all the Latin American and Caribbean region.

Box 3. Glossary of the terms used to refer to human settlements in this thesis

The different terms used to refer to and classify urban settlements throughout this thesis are defined as follows:

Cities: They are delineated using the Degree of Urbanization concept and are based on the spatial distribution of persons. Their extent does not match traditional administrative or metropolitan areas boundaries. By definition, cities have a minimum population of 50,000 persons and a minimum density of 1,500 persons/km². Cities can comprise an urban center and suburban areas. Except in illustration 2, towns are a subcategory of cities with a population above 50,000 persons but below the median population of the sample of cities. The term cities and human settlements are used interchangeably.

Urban areas: They correspond to the areas officially defined as “urban” at the national level using a variety of population thresholds, administrative boundaries or other structural features. The thresholds or features that define urban areas are different in each country and international comparisons relying on the concept of “urban areas” might be inappropriate.

Urbanization: The process through which the proportion of people living in areas defined as urban areas rise. Sometimes, this term also refers to the proportion of persons living in cities (as defined by the DoU) but then the text clearly specifies it. Importantly, this thesis emphasises that the urbanization process encompasses both a demographic and land change process.

Urban systems: A set of cities considered interconnected by various forms of social, economic or environmental interactions. The geographic scope of urban system may be national or regional.

4.2 Overlaying the “city layer” on Earth Observations

In addition to facilitating the comparison of cities across countries, the DoU approach described in the previous section allows me to spatially delineate the extent of each of the 635 cities. Indeed, after applying my algorithm to the gridded population raster for the seven countries of interest, I have created a “city layer” which can be used to determine the location and spatial extents of cities. In practice, this “city layer” is a binary raster that can be used to mask other rasters and collect observations within city borders. The cell-shaped “cities polygons” derived from the DoU can also be used to extract values that fall within city borders. This overlay between city extents and other variables of interest constitutes the second step of my methodology.

As mentioned earlier, my thesis largely relies on Earth Observations (EO), which can be defined as the gathering of information about the physical and biological systems of the planet via satellite imagery and remote-sensing technologies. To collect the required data at the city-level, I am therefore performing an overlay between the city layer and the relevant EO dataset. The process is fairly intuitive and I will illustrate it through the description of the main data used in the two case studies of this thesis. For case study 1, I will describe the process used to estimate CO₂ emissions at the city-level and briefly touch upon the main advantages and limitations of the approach selected. For case study 2, I will detail the data sources used to proxy urban green areas, local economic activity and precipitation patterns.

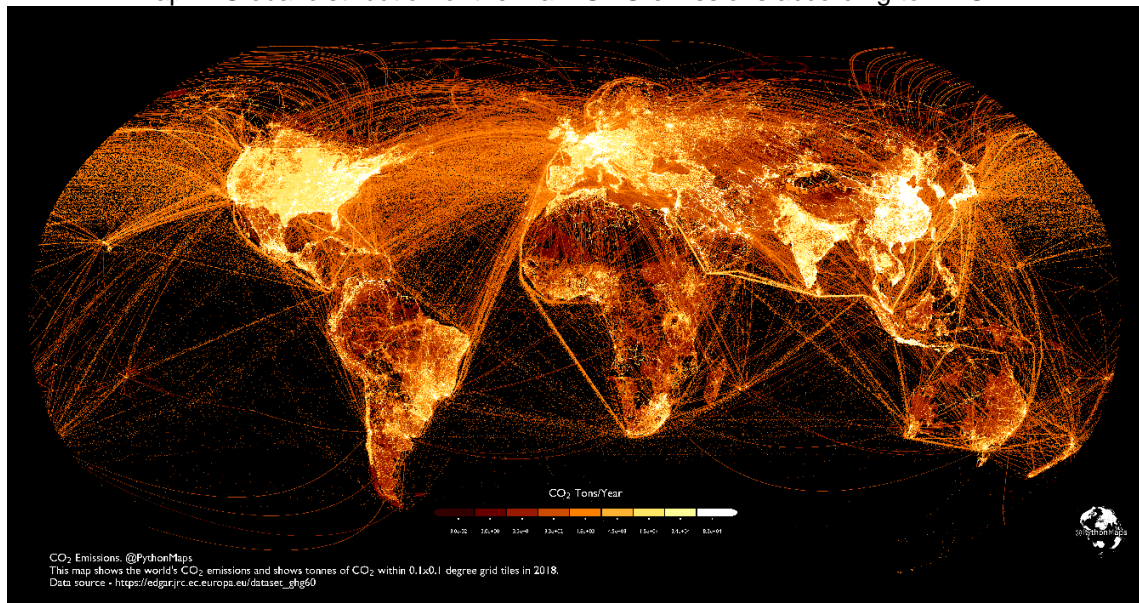
4.2.1 Case study 1: CO₂ emissions at the city-level

As mentioned in the literature review chapter, at the global level, information provided through GHG emissions inventories at the city level is discontinuous, of different scopes and sometimes inconsistent (Mia, Hazelton, and Guthrie 2019). More importantly, the estimation of GHG emissions at the city level is dependent on how the city in question is defined. Many cities’ GHG emissions inventories are compiled based on the administrative boundaries of the cities and/or metropolitan regions that delimit these urban areas. As illustrated in the previous subsection, these administrative boundaries rarely correspond to the socio-economic realities and functional interrelationships of cities. Using inventories for the seven Latin American countries of interest would thus significantly limit the scope of my first case study and potentially bias estimates.

As an alternative methodology, various authors have made use of NTL satellite imagery to spatially disaggregate national emissions inventories. For more than 20 years, NTL satellite imagery has been identified as an excellent proxy for spatially distributing human settlements and the intensity of certain human activities (Elvidge et al., 1999). As of 2023, two major open

datasets relying on these NTL (among other sources of information) provide spatially disaggregated emissions at the global level: the Open-source Data Inventory for Anthropogenic CO₂ (ODIAC) and the Emissions Database for Global Atmospheric Research (EDGAR).

Map 4. Global distribution of the main GHG emissions according to EDGAR



Source: Extracted from [Visual Capitalist](#). Consulted on January 13th, 2023.

EDGAR maps (available [here](#)) are provided by the European Commission at a 0.1° resolution (approximately 11km at the equator; see Map 4). EDGARv8.0 offers estimates for emissions of the three main greenhouse gases (i.e. CO₂, Methane and Nitrous Oxide) and a sectoral breakdown of emissions using the IPCC sectoral codes (i.e. Power Industry, Combustion for manufacturing, Energy for Buildings, Road Transportation...). On the other hand, the ODIAC dataset (available [here](#)) is provided by the National Institute for Environmental Studies (NIES) from Japan and has a 1x1km spatial resolution. The ODIAC dataset estimates emissions by fuel type and covers CO₂ emissions from fossil fuel combustion, cement production and gas flaring, which is referred to as anthropogenic CO₂. Although it does not account for Methane and Nitrous Oxide, its finer spatial resolution is deemed more appropriate to perform city-level analysis. For this and the reasons detailed below, I have decided to rely on the ODIAC dataset for case study 1.

To better understand the nature of our CO₂ estimates at the city level, it is important to clarify the scope and coverage of the ODIAC data product in comparison to the entire universe of GHG emissions. In 2019, global GHG emissions stood at 49,8 GtCO₂e. CO₂ accounted for 74% of the total, while Methane (CH₄) and Nitrous Oxide (N₂O) together represented less than 24%. Using the IPCC sectoral codes definition,

Illustration 3 shows how each sector and end-use activity relates to these gases. CO₂ emissions result almost exclusively from activities in the energy and industrial processes sectors. On the other hand, CH₄ and N₂O emissions are largely driven by activities in the agricultural and waste sectors. This means that emissions captured by the ODIAC dataset are the result of activities in the electricity and heat production, transportation, buildings, manufacturing and construction sectors as well as a large proportion of industrial processes. However, emissions linked to land use change and forestry or agriculture and waste, which release mostly non-CO₂ gases (i.e. CH₄, N₂O and F-Gases), are excluded from ODIAC estimates and thus from city-level emissions estimates used for this thesis.

Illustration 3. ODIAC Coverage compared to Global Greenhouse Gas Emissions in 2019 by Sector, End Use and Gases

Source: Adapted from Climate Watch with raw data from International Energy Agency.

combination of satellite observations of nightlights and geographical locations of specific emissions source such as power plants, cement production, industrial facilities and gas flares. Interest readers are encouraged to read Oda, Maksyutov, and Andres (2018) for a full description of the methodology. I just want to underscore that the inclusion of point sources for specific emission source is particularly relevant to produce consistent city-level emissions estimates. Point sources emissions such as power plants, cement production, industrial facilities and gas flares are less spatially correlated with population and affluence (and hence nighttime lights). By pinpointing emissions associated to power plants or other point sources and subtracting them to the total emissions to be spatially distributed through nighttime light, the ODIAC product ensure that city-level emissions estimates produced in this thesis more accurately capture emissions associated with activities located within city boundaries. Unfortunately, information on the geolocation and power plant profiles is not available for every country. In the Latin American region, information on power plant locations was available for seven countries, which have therefore been selected as the area of interest for this thesis. For the seven countries of interest, the share of national emissions allocated to point sources is significant: Argentina (21.0%), Brazil (6.4%), Chile (35.3%), Colombia (15.1%), Ecuador (11.5%), Mexico (25.0%), Peru (18.2%). I do not consider other Latin American countries that do not have point source estimates because this would have resulted in less precise CO₂ emissions estimates at the city level.

Using the boundaries of cities delineated according to the degree of urbanization approach, city-level emissions for this thesis are computed through overlaying and zonal statistics on the ODIAC data product. Before performing these spatial operations, I have reprojected the original geographic ODIAC raster to the World Mollweide projection used to delineate my city layers using the bilinear method, which is more appropriate for numeric rasters. The bilinear method computes the output cell value based on the four nearest cells in the original raster. The new values in the projected raster correspond to the distance-weighted average of the values from these four cells: the closer the input cell is to the center of the output cell, the greater its weight.

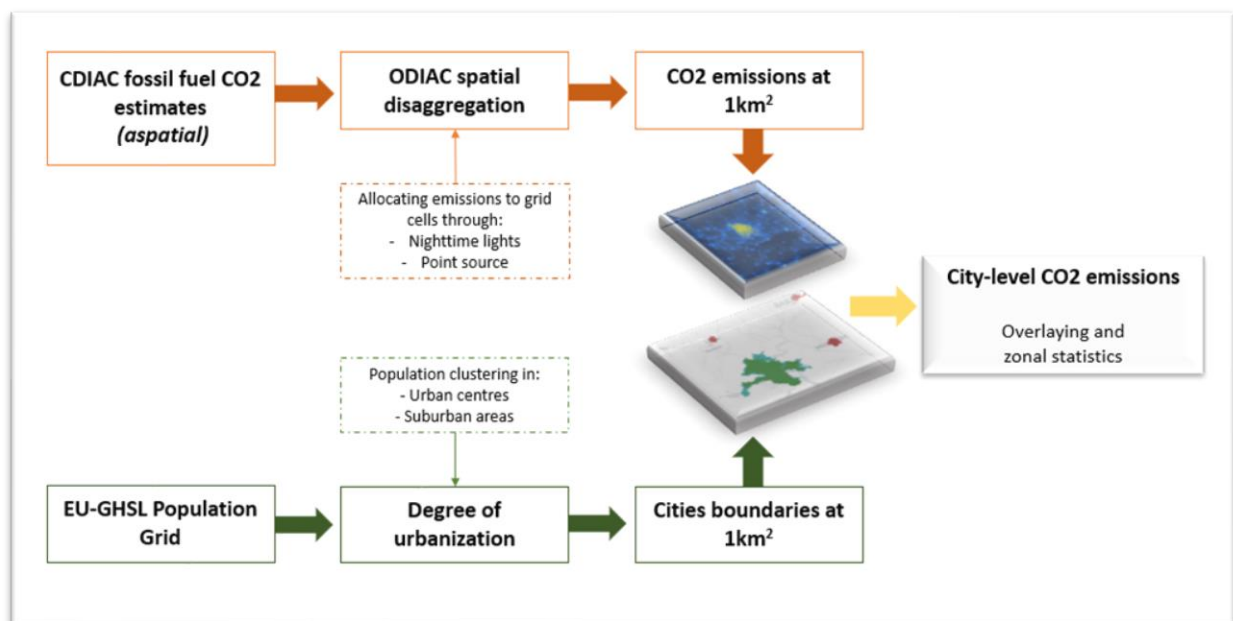
With this methodology city-level emissions correspond to the share of fossil fuel CO₂ emissions allocated to pixels that fall within the boundaries of my cities. CO₂ emissions estimates at the city level are thus a function three major components: (i) national fossil fuel CO₂ estimates, which largely depend on the total population of the country, its affluence and the CO₂ content of its energy matrix; (ii) nighttime lights value of pixels located within city boundaries, which represent the prosperity of a city relative to other cities; and (iii) city spatial

extent, which, as we detail in case study 1, reflects the dynamic patterns of spatial expansion specific to each city.

In a nutshell, the proposed approach combines the Degree of Urbanization with ODIAC and a schematic view of the process followed is summarized in

Illustration 4. Descriptive statistics on CO₂ emissions estimates at the city level are provided and discussed through the first case study of this thesis. It is nonetheless important to keep in mind that the proposed methodology does not seek to provide the most comprehensive CO₂ estimate for a given city, which is by essence a complex exercise (see Box 4). Instead, I have designed this methodology with the ultimate objective to capture city-level emissions that are likely to be influenced by activities in the building, transportation and electricity and heat sector, which are the ones most likely to be influenced by city geographical patterns. In addition, the proposed methodology seeks to use a systematic definition of cities and a consistent measurement of CO₂ emissions to be able to replicate this approach and compile information across a large sample of cities.

Illustration 4. Schematic outline of the methodology used to estimate city-level CO₂ emissions



Source: own elaboration.

While the methodology detailed above offers the advantage to provide a systematic and consistent assessment of CO₂ emissions at the city-level, three limitations must be highlighted.

First, although three major approaches exist to account for city-level GHG emissions (see EEA, 2013 and Box 4), none fully corresponds to the one presented in this thesis. The methodology proposed follows a territorial-based approach, whereby emissions produced by

activities within city borders are accounted for. Emissions produced by activities located outside the city are not imputed to the city -even if the output of these activities are consumed within the city. However, the proposed territorial-based approach relies on population distribution -as opposed to administrative boundaries employed to conduct GHG inventories. Therefore, CO₂ emissions estimates obtained through this methodology differ from estimates obtained through on-the-ground GHG inventories. This also renders an upfront comparison of the proposed estimates against the very few city-level GHG inventories available in Latin American challenging.²³

Second, estimates of city emissions provided here do not offer sectoral breakdown, which limits our ability to inform city climate action through detailed sectoral measures related to the transportation or energy sectors. Likewise, actions related to solid waste management, which usually fall under the responsibility of cities or municipal governments, would typically alter non-CO₂ emissions (such as methane) and are usually included in climate action plan at the local level. Nonetheless, emissions from the waste sector are not covered in the estimates presented in this thesis and the conclusions I will draw from the analysis do not apply to this sector.

Eventually, the spatial disaggregation of national emissions used in this thesis follows a top-down approach that relies heavily on night light imagery, which can be subject to measurement error. A well-identified issue of the Defense Meteorological Satellite Program (DMSP) satellite suite is, for example, the saturation for high-level luminosity pixels in urban areas (Gibson et al. 2021). Although the ODIAC dataset uses a special DMSP product to address this “saturation bias”, nighttime values only represent a proxy of the actual activity producing CO₂ emissions. I acknowledge that they can result in imprecise estimates in some areas.

²³ Even if for some selected cities and selected years GHG emissions inventories exist, a validation of the proposed estimates against on-the-ground inventories would require a substantial work to (i) harmonize the different scopes and dates of these GHG inventories and (ii) account for the differences between inventories and our methodology. Any straightforward comparison would be misleading. It must also be noted that the lack of GHG inventory is precisely what motivated the proposed approach and makes it particularly relevant.

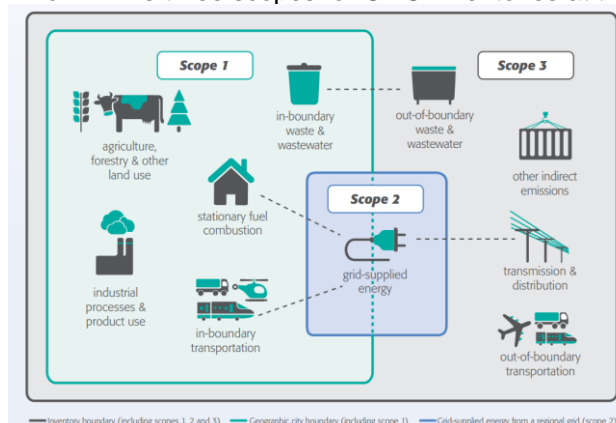
Box 4. How to account for Greenhouse Gas at city level?

Following EEA (2013), three major GHG accounting perspectives can be distinguished: territorial, production and consumption.

- The territorial based approach accounts for emissions released to the atmosphere from within a city jurisdiction. This perspective is the one followed by countries and the only method accepted by international environmental law to account for a country's emissions and mitigation efforts.
- The production-based accounting (PBA) covers emissions related to companies and households whose economic interest lie within the city boundaries irrespective of the geographic location where their activities take place.
- The consumption-based accounting (CBA) considers that city emissions correspond to the emissions that result from the consumption of all products and services consumed within city borders, regardless of the location where production of these goods and services result in emission. This perspective complements the two above by linking GHG emissions to demand for goods and services by cities citizens. The consumption-based perspective is not considered in international conventions.

To offer guidance and enhance accounting and reporting standards, the [Greenhouse Gas protocol](#) has detailed the content and activities included under each of the three scopes of city-level GHG inventories (see illustration below for a summary). It must be noted that there is an increasing degree of complexity, data requirements and uncertainty as the scope of the GHG inventory increases. Whilst territorial and production-based methods rely on standardised methods, the computation of consumption-based emissions does not and the assumptions to be made lead to higher uncertainty in emission estimates. CBA are for example dependent on the availability of data on the supply, use and trade of goods and services consumed within city borders, which are rarely available.

Illustration Box 4. The three scopes for GHG inventories at the city-level



Extracted from Greenhouse Gas Protocol (2014).

In the European Union (EU) a comparison between the traditional PBA and the CBA perspective was conducted for 10 cities. It unveiled a notable disparity between the two methods (Harris et al. 2020). In general, CBA emissions show a trend of rising emissions over time, whereas the production and territorial based perspectives show a downward trend. This issue is not specific to city-level GHG accounting. It is for example often argued that the reduction in GHG emissions reported by the EU using the territorial-based approach only reflects the relocation of most of its high-emitting activities outside the EU.

4.2.2 Case study 2: proxying local economic activity, greenness and extreme precipitation events at the city level

For case study 2, the same approach is replicated: the “city layer” is overlaid on earth observations to collect data that relates to our three variables of interest: (i) local urban economic activity, (ii) weather patterns and extreme rainfall events (iii) greenness of city land cover. This subsection details the data source and the process performed to collect the data.²⁴ Case study 2 provides descriptive statistics and stylized facts based on these data.

Nighttime lights and local urban economic activity: Since the work of Chen and Nordhaus (2011), night-time lights have been increasingly used by economist and geographers to proxy economic activity. This alternative source of data has proven particularly useful to quantify the impacts of climate-related shocks in small geographic areas. Cities affected by extreme rainfall may for example experience power outages, damage to streetlights infrastructure or even evacuation that lead to reduced or altered city night-light patterns. These changes in light intensity and distribution provide quantitative insights into the severity and duration of extreme rainfall impacts that can be used to proxy variations in local economic activity. These effects are more clearly illustrated in Map 12 of the second case study of this thesis.

The Defense Meteorological Satellite Program (DMSP) satellites, with a spatial resolution of approximately 1km and an annual temporal coverage over the period 1992-2013, have been extensively used to assess the impacts of weather anomalies at sub-national levels (Felbermayr et al. 2022) or to quantify the impacts of extreme precipitations, floods and typhoons (del Valle, de Janvry, and Sadoulet 2020; Kocornik-Mina et al. 2020; Elliott, Strobl, and Sun 2015). More recently, the release of the Visible Infrared Imaging Radiometer Suite (VIIRS) instrument has provided a newer source of NTL data with a finer spatial resolution (approximately 450m at the equator) and a monthly coverage for the period April 2012 until present times. Contemporaneous observations are generally issued with a 4-month lag (see Elvidge et al. 2017 for a comprehensive description). This dataset has also been used to proxy (i) local economic activity (X. Chen and Nordhaus 2015; N. Zhao et al. 2017) or (ii) detect damages and power outages in the aftermath of flood events (X. Zhao et al. 2018; Levin and Phinn 2022) and hurricanes strikes (Mohan and Strobl 2017).

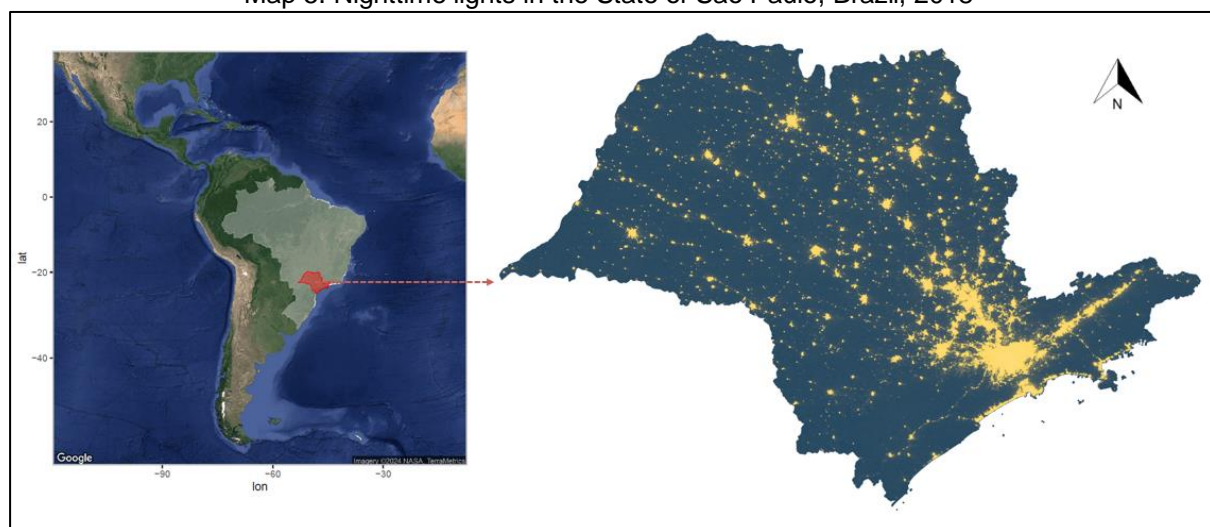
As evidenced by Gibson et al. (2021), the VIIRS dataset is more suitable than the DMSP one to proxy local economic activity at the city-level. This is primarily due to the top-coding feature

²⁴ It is important to highlight that for comparability purposes across case study 1 and case study 2, I have worked on the same sample of cities in both cases although the information recollected for case study 2 is potentially available for all the countries of the region.

of the DMSP, which understates the intensity of lights in brightly lit city centers.²⁵ Additionally, the monthly frequency of this NTL data source is crucial to capture relatively short-term disruptions such as the one triggered by urban floods, which could be averaged out when using annual observations provided by the DMSP product. Previous studies have nonetheless highlighted that important cloud coverage can represent a limitation in using the daily version of the VIIRS dataset (i.e. the “black marble”) and that spatial or temporal aggregation might help to reduce the very high volatility of VIIRS NTL in some areas (X. Zhao et al. 2018).

Given the above, this thesis relies on the monthly VIIRS NTL dataset to provide a proxy of local urban economic activity at the city-level. To provide an illustration of this product, Map 5 depicts these nighttime lights for the Federal State of Sao Paulo in Brazil as an average of the months of March and April 2018. These NTL clearly correlate with the cities identified through the DoU as observed in Map 3, illustrating their ability to provide insights about human settlement patterns. This dataset is freely available in the Google Earth Engine (GEE).²⁶ As such, for every city identified through the DoU approach, I have performed a zonal sum of all NTL pixels located within city extents. This zonal sum is performed each month over the period 2013-2021.

Map 5. Nighttime lights in the State of Sao Paulo, Brazil, 2018



Source: own elaboration based on VIIRS NTL; basemap GADM and NASA Terrametrics (left panel).

²⁵ The DMSP measures NTL intensity using a Digital Number ranging from 0 to 63. While city centers pixels typically register the maximum value of 63, other regions like suburbs or smaller towns also saturate DMSP sensors, resulting in the same number and lessening distinctions in light intensity among areas. VIIRS sensors offer a broader range and do not show saturation problems.

²⁶ Data available at: https://developers.google.com/earth-engine/datasets/catalog/NOAA_VIIRS_DNB_MONTHLY_V1_VCMCFG

Weather patterns and extreme rainfall events. Precipitation data is extracted from the CHIRPS pentad product (Funk et al. 2015) at a spatial resolution of 0.05°. ²⁷ CHIRPS is a 30+ year quasi-global rainfall dataset that incorporates satellite imagery with in-situ station data to create gridded rainfall time series for trend analysis and seasonal drought monitoring. City-level precipitations are computed based on a zonal sum of the CHIRPS pixels intersecting with city extents. Following standard climatological practices that use a minimum of 30 years to define “climate normal”, the 5-days precipitation data is aggregated on a monthly basis over the period 1991-2021 (WMO, 2023). To be able to accurately capture extreme rainfall events across different climatological areas, I then normalize precipitations on a city-monthly basis using the traditional Z-score formula described in equation 1.

$$Z_{m,j} = \frac{X_{m,j} - \bar{X}_{m,j}}{\sqrt{\frac{1}{M} \sum_M (X_{m,j} - \bar{X}_{m,j})^2}} \quad (1)$$

$$Extreme\ rainfall_{m,j} = \begin{cases} Z_{m,j}, & \text{if } Z > 2 \text{ and } \bar{X}_{m,j} > 30 \\ 0, & \text{otherwise} \end{cases} \quad (2)$$

With $X_{m,j}$ the monthly precipitation in month m in city j and $Z_{m,j}$ the Z-score of this precipitation relative to its mean and standard deviation over the period 1991-2021. By normalizing precipitation data, we obtain a measure that is comparable across Latin American geographies and that is independent of the absolute amount of rain. Our extreme rainfall index is then computed flowing a double condition: first Z-score should be above 2 (i.e. monthly precipitation two standard deviations above the mean precipitation); second absolute monthly precipitation must exceed 30 mm to ensure that only extreme rainfall events occurring during a rainy month are retained (see equation 2). This double condition is employed to focus on months where soil infiltration capacity is more likely to be saturated and where extreme rainfalls are therefore more likely to trigger damaging floods. With this definition, extreme rainfall events constitute less than 3% of total precipitation observations over the period, which is consistent with WMO recommendations that consider extreme rainfall events as those events whose “*occurrence tends to take the form of the upper 90th, 95th and 99th percentile of precipitation*” (WMO, 2023). To test the robustness of our approach, two alternative precipitation indexes are also used across this thesis: the first one is based on the full range of precipitation Z-score values;

²⁷ Data available through GEE library at: https://developers.google.com/earth-engine/datasets/catalog/UCSB-CHG_CHIRPS_PENTAD

the second one is based exclusively on positive Z-score and accounts for a month where a city experiences precipitation above its mean value.

We repeat the same process for temperature data, which is potentially correlated with precipitations. To be more precise, the Clausius-Clapeyron relation suggest that, for every 1°C of increased air temperature, the water-holding capacity of the atmosphere rises by about 7%. More moisture is therefore available in a warmer atmosphere than in a colder one, creating heavier rainfall when precipitation forms. As temperature and precipitation can both affect economic activity, the exclusion of temperatures could bias our estimates. Temperature data is extracted from the ERA-5-Land product provided by the Copernicus Climate Change Service (C3S) at a 0.1° resolution (i.e. approximately 11km at the equator).²⁸ The value of pixels intersecting with city extents is extracted and averaged by area before being normalized using the same Z-score formula than for precipitation.

City land cover and greenness index: The number of satellite-derived land cover products has been rapidly growing during the last decade, although these products differ significantly in terms of spatiotemporal resolution and scale. Among the existing products, Landsat surface reflectance imagery has proven to be one of the most optimal data sources to accurately capture land cover features at the global level (Sun et al. 2022). The Normalized Difference Vegetation Index (NDVI) derived from Landsat imagery is largely used in this thesis to depict the greenness of city land cover (see Box 5). This approach has been used by many researchers. Corbane et al. (2020) have for example extracted NDVI values from the Landsat annual Top-of-Atmosphere (TOA) reflectance composites to proxy the quantity of vegetation cover within urban centers extent.

Consequently, to proxy vegetation cover this thesis leverages annual NDVI composites from the Landsat 8 Collection 1 Tier 1 orthorectified scenes, using the computed top-of-atmosphere (TOA) reflectance.²⁹ These composites are created from all the scenes in each annual period beginning from the first day of the year and continuing to the last day of the year. In this case, I perform a zonal operation to extract the NDVI values of all pixels intersecting with city borders. NDVI pixels have a 30-meter resolution and, following usual practice in land cover analysis, I consider that pixels with a value above 0.5 are associated with dense vegetation, such as trees, urban gardens or parks or even urban forests. I therefore computed the annual share of pixels with a value above 0.5 for each city in our sample over the period 2013-2021. To mitigate potential seasonal trends and inter-annual variability, the greenness index used in

²⁸ Dataset available here: <https://cds.climate.copernicus.eu/cdsapp#!/dataset/reanalysis-era5-land-monthly-means?tab=overview>

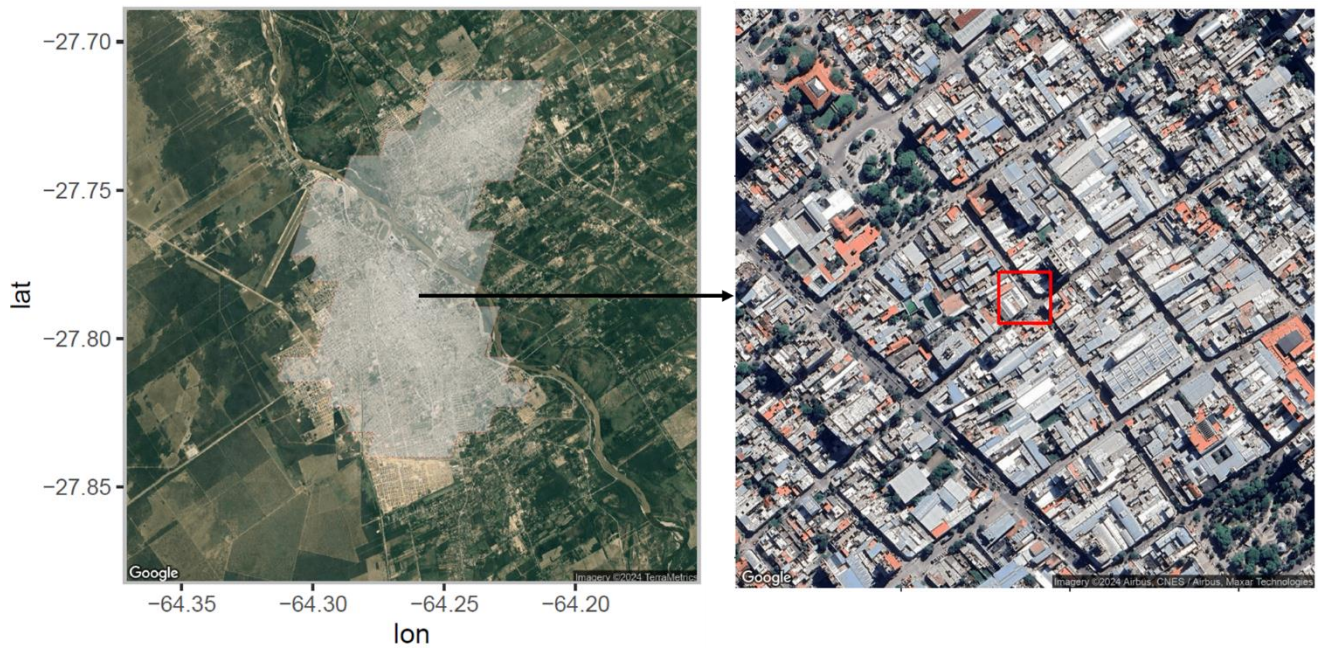
²⁹ Dataset courtesy of the U.S. Geological Survey and available through GEE here: https://developers.google.com/earth-engine/datasets/catalog/LANDSAT_LC08_C01_T1_ANNUAL_NDVI#bands

case study 2 of this thesis correspond to the average of this annual value over the period 2013 to 2021, depicting the presence of stable dense vegetation throughout the period of analysis. My benchmark greenness index is expressed through the ratio of dense vegetation areas within the city relative to the total city area, as shown in equation 3.

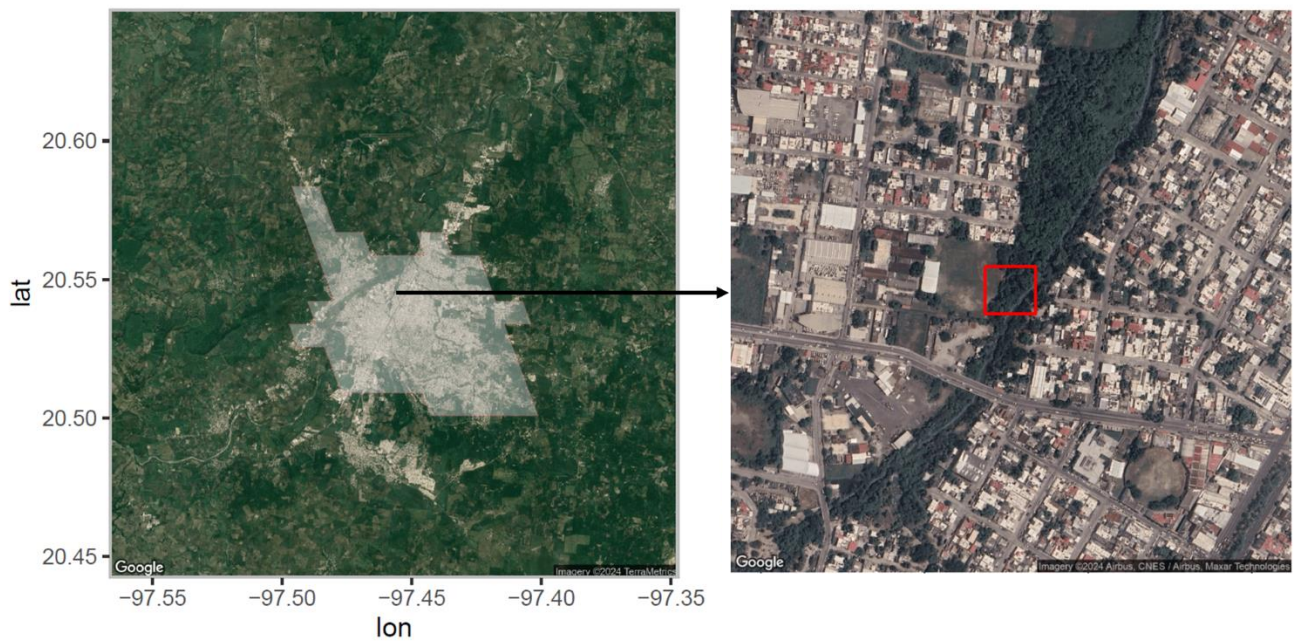
$$Greenness\ index_j = \frac{Dense\ vegetation\ areas\ (NDVI>0.5)_j}{Total\ city\ area_j} \quad (3)$$

I conducted a quick visual comparison of different cities through Google maps satellite imagery (i.e. a different data source than the one used to compute NDVIs). Map 6 shows the cities of Poza Rica, Mexico and Santiago del Estero, Argentina, which display a greenness index of 27.8 and 6.5, respectively. Randomly zooming within city borders confirmed a prominent presence of dense vegetation in Poza Rica, which is consistent with a higher value of the greenness index. To test the sensitivity of our results to different greenness measurement, we computed a more restrictive greenness index based on the share of NDVI pixels above 0.6 and used an alternative source of data to derive the greenness index. These alternatives greenness indexes are used to perform the different robustness tests presented as part of the case study 2 of this thesis (see Appendix to case study 2).

Map 6. Visual comparison of two cities displaying differentiated greenness indexes
Santiago del Estero, Argentina



Poza Rica, Mexico

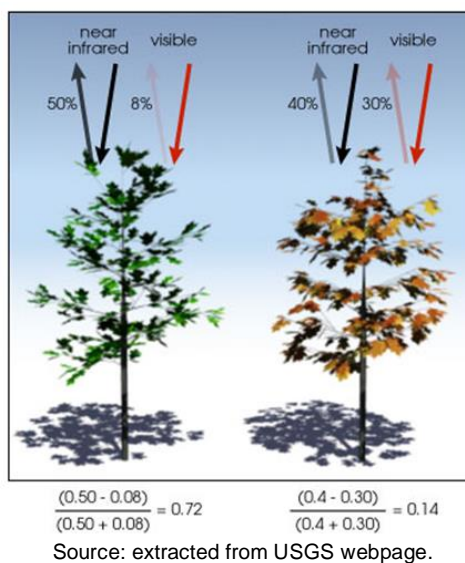


Note: The left panel maps the extent of each city in grey -according to the UCDB definition. The right panel zoom-in on the centre of each map to provide an illustration of vegetation cover. The red squares represent a 30meters pixel.

Source: own elaboration. Basemap: Google Maps.

Box 5. The NDVI: a quantitative measure of the amount of vegetation in a given area

The Normalized Difference Vegetation Index or NDVI, is a widely used metric in remote sensing to quantify vegetation greenness. It has been successfully used to depict vegetation density, assess land cover changes, deforestation or changes in plant health -among other applications. It relies upon the physical response of vegetation to different wavelengths of light. Typically, chlorophyll in plants strongly absorbs light energy during photosynthesis, in particular in the red parts of the electromagnetic spectrum. Likewise, chlorophyll reflects a high proportion of the near-infrared light. An illustrative example is provided below where a “green tree” (i.e. with abundant chlorophyll) would absorb a higher percentage of red light and reflect a higher percentage of near infrared light than the same “brown tree” (i.e. with less chlorophyll) would do.



The NDVI is typically calculated as a ratio between the red (R) and near infrared (NIR) values, as follows:

$$NDVI = \frac{NIR - RED}{NIR + RED}$$

where NIR is the reflectance in the near-infrared spectrum, and RED is the reflectance in the red spectrum. Both values are extracted from the same pixel in the imagery. The resulting NDVI values range from -1 to 1, with specific interpretations for different ranges:

- High Positive Values (e.g., 0.5 to 1): Represents healthy and dense vegetation.
- Low to Moderate Values (e.g., 0 to 0.5): Corresponds to less dense or stressed vegetation, bare soil, or non-vegetated surfaces. It can also indicate the presence of built-up areas.
- Negative Values: Typically represent water bodies or features that absorb more in the red spectrum than in the near infrared.

4.3 Identifying causal relationships across a large sample of cities

An important feature of the proposed methodology is that it seeks to test and quantify causal relationships between cities geographical patterns and climate change challenges. To this end, this thesis harnesses the large amount of observations gathered in the previous step of the methodology to develop a quasi-experimental setting. The basic idea of this quasi-experimental design is that the variations of cities geographical patterns constitute a “treatment effect”. Concretely, two treatments are “assigned” through my sample of cities: the spatial extent of city and the greenness of its land cover. I then compare outcomes of interest at the city-level (i.e. CO2 emissions or impacts of extreme rainfall) conditional upon this “treatment effect” to get an estimate of the average treatment effect associated to each geographical pattern. My thesis is thus testing whether and to what extent specific cities’ geographical patterns influence climate change challenges, *holding all other factors fixed*.

This approach directly draws from the recent advances in what has been labelled the “climate-economy” literature. It mainly relies upon fixed effect econometrics to strengthen the identification of causal effects. This subsection gives a brief overview of the econometric challenges addressed in the specific context of this thesis. Interested readers are nonetheless encouraged to consult Hsiang (2016) and Wooldridge (2002) for a more comprehensive discussion of these aspects.

To fix ideas, let’s imagine that we are interested in identifying the effects of extreme rainfall events on local economic activity at the city level, *ceteris paribus*. In an ideal experiment, we would have two perfectly identical cities in terms of population, economic structure, technology and other factors that affect local economic activity (i.e. the outcome of interest). The only difference between these two cities is that one would be exposed to an extreme rainfall event (or a set of extreme rainfalls), whereas the other would remain unaffected. In this setting, we could compare local economic activity in each city and attribute the difference in this outcome to the extreme rainfall event. To put it differently, we would compare local economic activity in a city conditional on the occurrence of an extreme rainfall event. Formally, this average treatment effect β could be expressed as:

$$\beta = E(Y_{it} | Xtrm_{it}, X_{it}) - E(Y_{it} | No\ xtrm_{it}, X_{it}) \quad (4)$$

Where Y_{it} is the outcome variable for city i in time t , X_{it} denotes a vector of observable non-climatic factors that affect the outcome and $Xtrm_{it}$ captures the materialization of an extreme rainfall event. Obviously, in practice, this ideal experimental setting does not exist. Every city is unique and it is impossible to control for all factors that influence local economic activity, notably because some of them are difficult to observe (e.g. institutional quality, cultural and

historical factors, quality of urban infrastructure). More fundamentally, inference is challenging because β can never be observed directly, as the city i can never be exposed to both counterfactuals X_{trm} and $No\ x_{trm}$ for the exact same interval of time t . This is the primary problem of causal inference (Holland 1986).

To address this issue, two research design delivering an approximation of Equation 4 have been found in the literature (Hsiang 2016). Cross-sectional approaches traditionally seek to add numerous observable variables to condition distinct city and assume that they are comparable after these variables are accounted for. However, this approach is subject to the well-identified Omitted Variable Bias: when variables that affect Y_i are not included in either X_{trm_i} or X_i but are correlated with one of their elements, the resulting estimates will be biased (Wooldridge 2002). To illustrate this through my example, comparing output across different cities is likely to deliver confounded estimates of β if we cannot reasonably assume that we are accounting for all factors that determine local economic activity at the city-level. This is referred to as the *unit homogeneity assumption*. This assumption is very unlikely to hold in the setting of this thesis: I am examining a very heterogeneous set of cities, distributed across different countries, geographies and development levels and with many unobservable sources of heterogeneity.

The second option to approximate the conditions of an ideal experiment is the use of fixed-effects econometrics. Fixed-effects econometrics compare a city to itself when it is exposed to extreme rainfall events versus moments where it is unaffected by extreme rainfalls due to randomly occurring weather variations. As such, a city observed during a “normal” episode is the ‘control’ for that same city observed during an extreme rainfall ‘treatment’ episode. This process is repeated for each city in the sample and individual “treatment effects” are then averaged over the sample. This estimation process is known as the “within” estimator and it has been increasingly used to deliver an unbiased estimate of the average treatment effect associated with weather patterns (Dell, Jones, and Olken 2014).

This second research design is the one I will use in my thesis. Obviously, this research design has been selected because the datasets assembled through the process described in the previous subsections are panel observations: they provide observation of a specific city over regular time intervals. This kind of dataset are perfectly suited for fixed-effect econometrics as they allow to control for both unobservable heterogeneity at the city-level as well as time trends potentially affecting our outcome and independent variables. More details are provided on these aspects when discussing the specific models developed for case study 1 and case study 2 of this thesis.

To summarize, the methodology detailed in this chapter permits a quasi-experimental design to examine the two relationships of interest, namely (i) spatial expansion VS CO2 emissions and (ii) greenness of the land cover VS vulnerability to extreme rainfall. This methodology follows a three-step approach. The first step relies on the Degree of Urbanization to consistently define cities across different countries. This method is key to work across a large dataset of cities with potentially important variations in terms of geographical patterns. The second step of the methodology leverages earth observations to objectively measure these geographical patterns (i.e. spatial expansion and greenness of the land cover) as well as the variables of interest of each case study (i.e. CO2 emissions and local economic activity). These observations are gathered at regular time intervals and allow me to put together large panel data. Thirdly, I use fixed-effect econometrics on these large panel data to robustly test and quantify the causal relationships of interest.

The three-steps of this methodology are therefore fully complementary and can be viewed as a holistic approach to enhance causal analysis at the city-level. The large amount of observations together with the rigorous statistical techniques employed give me confidence that the approach designed is robust enough to provide empirical evidence that can inform the elaboration of urban public policies. However, I acknowledge that this approach does not offer the same level of granularity than an in-depth case-study analysis focusing on a single city. While my approach is well suited to quantify *average treatment effects*, single city analysis would probably be richer in detail and “on the ground” accuracy. In addition, it would facilitate the identification of the specific and unique features that a given city displays in relation to climate change challenges as opposed to average effects. Insights derived from this thesis should therefore be used to inform how and to what extent geographical patterns can shape climate change challenges for a large set of cities and towns -as opposed to single city analysis.

The two case studies presented in the following chapters apply this methodology to seven Latin American countries and constitute the core analysis of this thesis. Following the conceptual approach laid out in Chapter 1, the first case study looks at how the spatial expansion of cities influence CO2 emissions i.e. how cities’ geographical patterns can mediate the impact of human on the Earth system; the second case study delves into how the greenness of the land cover reduce vulnerability to extreme rainfall events i.e. how geographical patterns can moderate the impacts of the Earth system onto our well-being.

5 CASE STUDY 1: CITIES SPATIAL EXPANSION AND CO2 EMISSIONS IN SEVEN LATIN AMERICAN COUNTRIES

A streamlined version of this case study has been published as an article in the Journal [Cities](#) (Cite score: 11.2; IF: 6.7). The abstract of this paper is provided in the box below and the text is [available online here](#). Sections 5.1 and 5.5 of this case study are not part of the published paper as they have been developed after the article was submitted to the Journal.

Abstract: The way urban development will be shaped during the next decade will have a decisive impact on our ability to limit global temperature increase. The goal of this paper is to develop a better understanding of the relationship between carbon dioxide (CO₂) emissions and the spatial expansion of Latin American cities to inform how urban planning can help shaping low-carbon urban systems. To this end, a new methodology is proposed: cities are delineated based on a population-based clustering approach; and spatially disaggregated fossil fuel CO₂ emissions are used to systematically evaluate the CO₂ emissions of 635 cities across seven Latin American countries for the years 2000 and 2015. City spatial expansion is then characterized through the evolution of two indicators: population density, which is used to proxy city compactness; and the suburban ratio, which captures suburban sprawl and potential relocation effects. Using a spatial panel model, results unveil that a 1 % increase in density reduces CO₂ emissions by 0.58 %, while a 1 % growth in the suburban ratio boosts emissions by 0.41 % ceteris paribus. These coefficients imply opposite CO₂ effects for most Latin-American cities, which have experienced a concomitant increase in density and suburban ratio. Finally, city-level emissions are projected until 2030 using these elasticities and the growth rates associated with the three major spatial expansion patterns identified during the period 2000–2015. The findings are important for future planning purposes given that the ‘compact expansion’ model generates a 12 percentage points smaller increase in emissions than its passive counterpart. However, even under this compact scenario, city-level emissions grow faster than city population.

Full article reference:

Van der Borcht, Rafael, and Montserrat Pallares Barbera. 2023. ‘How Urban Spatial Expansion Influences CO₂ Emissions in Latin American Countries’. *Cities* 139 (August):104389. <https://doi.org/10.1016/j.cities.2023.104389>

At the global level, urban areas are estimated to be responsible for about 75 % of primary energy consumption (UN-Habitat, 2016). However, the individual carbon performance of cities varies greatly. As an analogy to agglomeration economies, numerous authors have hypothesized that higher density could streamline energy consumption and transportation needs, resulting in lower GHG emissions at the city-level *everything else being equal*. In fact, as referenced in Chapter 3 (*Cities Geographical Patterns in a changing climate: a review of literature*), for some of the largest cities in the most developed countries, there is robust evidence that a more compact urban development is associated with lower CO2 emissions at the city-level. By contrast, little is known about the CO2 impacts of higher density in developing countries, where urban planning capacities tend to be more limited and fast-growing cities already display important congestion effects. This is particularly true in Latin America where higher density might bring about more negative congestion effects than agglomeration benefits (Ferreyra and Roberts, 2018; Monkkonen et al. 2019), with uncertain impacts on city-level emissions. More importantly, beyond the somewhat banal and static observation that higher density can lead to lower emissions, a dynamic analysis considering the differentiated patterns of spatial expansion observed over the full spectrum of cities that compose the Latin American urban system is still missing. Developing a broader knowledge basis on these aspects is required to provide a prospective view of the CO2 effects attached to different urban development scenarios. This forward-looking approach is also crucial to quantify the potential contribution that a more compact urban development could deliver.

The proposed case-study seeks to fill this gap by assessing whether and how differentiated spatial expansion patterns result in diverging carbon dioxide (CO2) emissions pathways at the city level. In doing so, it intends to shed lights on the role that urban planning policies, which provide the tools to shape the spatial expansion of cities, can play in enhancing low-carbon urban systems in Latin America. The proposed approach relies on the methodology detailed in Chapter 4 (*Methodology and data source*) and allow to address the shortcoming of previous studies. As such, this case study makes three significant contributions to the literature that are worth highlighting before delving into the analysis.

First, the methodological approach allows city-level metrics to be compiled systematically across different Latin American countries. The resulting data set covers the spectrum of small and intermediate cities that make up the bulk of the urban system, providing a more comprehensive view of human settlements than previous studies focused exclusively on large urban areas.

A second important contribution of this case study is to go beyond city compactness defined through traditional density measurements (i.e. people/area ratio). Instead, this study

apprehends the spatial expansion of cities through the joint evolution of two indicators: adjusted density (i.e. people/built-up surface ratio) and suburban ratio. The suburban ratio is defined as the ratio of people living in adjacent suburban areas to people in the urban centre. Including the evolution of the suburban ratio is critical to gain a refined understanding of the dynamics driving new settlements at the city level. As underscored by recent urban analysis, cities are part of a broader urban system characterized by complex interdependencies with their immediate surroundings (Ribeiro et al. 2021; Altmann 2020; Keuschnigg, Mutgan, and Hedström 2019). Gagné, Riou, and Thisse (2012) have also highlighted that compactness policies generate changes in prices, wages and land rents, which in turn incentivize firms and households to move towards the outskirts of the city. By incorporating suburban areas adjacent to urban centres, it is possible to capture these networks and relocation effects -at least partially. In fact, the data compiled for this case study unveils that, for most cities in the region, higher density has come along with an increase of the suburban ratio.

Thirdly, based on the IPAT identity and its stochastic application (York, Rosa, and Dietz 2003), I build a spatial panel model to estimate CO₂ elasticities at the city level and their spatial diffusion across cities. The use of fixed-effects allows to isolate the impacts of spatial expansion factors from those associated to population, affluence and all other time-invariant unobserved heterogeneity. The spatial nature of my analysis also confirms that city-level emissions are affected by a spatial diffusion process, evidencing that CO₂ emissions are not only the product of activities occurring at the city level, but also the result of interactions with a broader system of cities.

This case study is organized as follows: section 5.1 provides some background information on GHG emissions in Latin America and 2030 emissions reduction targets; section 5.2 leverages the richness of the dataset assembled to gain a refined understanding of the patterns of spatial expansion and CO₂ emissions of the cities in my sample. Section 5.3 presents the empirical framework and the results of the statistical analysis for the relationship between spatial expansion and CO₂ emissions at the city-level. In section 5.4, city-level emissions pathways are projected to evidence how distinct spatial expansion patterns generate diverging CO₂ emissions pathways for an average city, while the heterogeneous impact of higher density on CO₂ emissions are further explored; Section 5.5 projects regional urban emissions up to 2030 for the seven countries considered under different spatial expansion scenarios. The last section summarizes the main findings and concludes this case study.

5.1 GHG emissions in Latin America: context and 2030 targets

At the global level, the pathway to meet the long-term temperature goal of the Paris Agreement is clearly identified. Limiting global temperature increase to 1.5°C above preindustrial levels, a threshold which represents the scientific consensus to avoid the worst impacts of climate change (IPCC 2018), requires that greenhouse gas (GHG) emissions fall by about 45 % by 2030 compared with 2010 levels and reach net zero by the middle of the century (See Chapter 1, section 1.3). These estimates are based on the concept of remaining carbon budget (RCB), which is commonly used to evaluate political action against the goals of the Paris Agreement. The RCB is defined as the net amount of CO₂ humans can still emit without exceeding a chosen global warming limit. For a 50% chance of keeping warming to 1.5°C, the RCB is estimated at about 250 GtCO₂ as of January 2023 (Lamboll et al. 2023). With annual global GHG emissions above 50 GtCO₂e, this RCB will be exhausted in approximately six years if current CO₂ emissions are not drastically reduced. In other words, if current CO₂ emissions levels are maintained until 2030, we will face a higher than 50% chance to exceed a global warming of 1.5°C.

Distributing the RCB across different regions, countries and citizens of the world is a complex task with intricate distributional and ethical implications. Since the international climate negotiations in the early 1990s, the concept of a “*common but differentiated responsibility*” has been pivotal. This concept fundamentally means that there is a “shared” moral responsibility between different groups of countries to address global climate change, nevertheless the proportions of such responsibility are differentiated. However, until now, climate diplomacy has failed to translate this concept into an actionable and clear governance mechanism. Instead, in 2015, the Paris Agreement has marked the transition to a different approach that relies on *Nationally Determined Contributions* (NDCs), which are a bottom-up approach in which each party determines its own national climate targets and commits to self-respect and self-report these differentiated responsibilities. While different rounds of negotiations were supposed to gradually increase the level of ambition of climate actions, the climate targets contained in the NDCs submitted by countries ahead of COP28 are still not compatible with global temperature increase limited to 1.5°C. Estimates indicate that, if left unaltered, by 2030, current commitments will produce an emission gap that has been estimated at 14 GtCO₂e, for a 2°C goal and at 22 GtCO₂e for the 1.5°C goal (UNEP, 2023, see Chapter 1, section 1.3). If current goals expressed in the NDCs and binding long-term targets are met, they are estimated to produce an aggregate 2.5°C temperature increase by the end of the century (CAT, 2023). In other words, international negotiations have not yet

found a way to distribute in an effective and fair manner the RCB and align it with the long-term Paris Agreement goals.

According to Gore (2021), considering a RCB compatible with a warming of 1.5°C, every person on Earth would need to emit no more than 2.3 tonnes by 2030. This average target does not mean a *fair target* since a significant part of the total carbon budget was consumed by few rich industrialised countries before the 1990s, with limited “*historical responsibility*” of most of the countries in the world. The citizens of these emerging and developing countries can therefore legitimately claim that a large share of the RCB should be reserved to their own development needs. In other words, an emission target in per capita terms would also have to account for the “*differentiated responsibilities*” of each country. These discussions are beyond the scope of this thesis but are important to keep in mind. For example, I will use the 2.3 tonnes per capita limit to provide contextual information and references to the RCB but this target is not to be viewed as a *fair target* for the Latin American region.

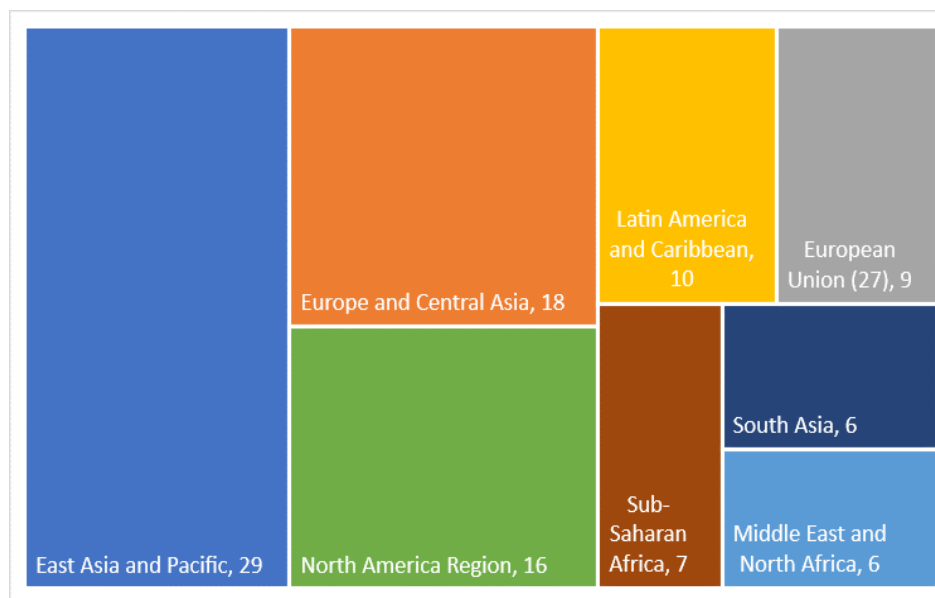
Historically, cumulative GHG emissions released from the LAC region remain limited.

Although long-term analysis of CO₂ emissions entails significant uncertainty, a reanalysis of CO₂ emissions from fossil fuels, cement, land use and forestry over the period 1850-2021 suggests that within the LAC region only large countries such as Brazil, Mexico and Argentina have a distinguishable impact on cumulative emissions at the global level. CO₂ emissions in these 3 countries are mainly driven by deforestation and land use changes (notably in Brazil) and collectively account for 7.1% of the total CO₂ emissions pumped into the atmosphere during 1850-2021 (Evans 2021, see Figure A.1 in appendix). Data on overall GHG emissions for the period 1990-2020 confirm this order of magnitude: LAC GHG emissions have represented less than 10% of the global emissions during the last 30 years (see Figure 12). In per capita terms, except for small countries rich in oil or other fossil fuels resources (e.g. some Caribbean islands, Suriname, Guyana), most of the countries of the region display emissions below the North American region or the European Union (respectively NAR and EUU in Figure 13). With an average estimated at 7.6 tonnes per capita, the LAC region is nonetheless emitting three times more than the target compatible with a 1.5C warming, suggesting that emissions should be curbed as soon as possible (Figure 13).

Collectively, the LAC region has committed to reduce GHG emissions by 22% in 2030 compared to a BaU scenario (Samaniego et al. 2022). From a sectoral point of view, the bulk of expected GHG emissions reduction will be driven by measures in the energy sector and reforms aimed at curbing deforestation. Interestingly, carbon savings (i.e. the CO₂ reduction that a policy action could deliver compared to a baseline scenario without this policy) that could be obtained through a more compact urban development are mentioned and

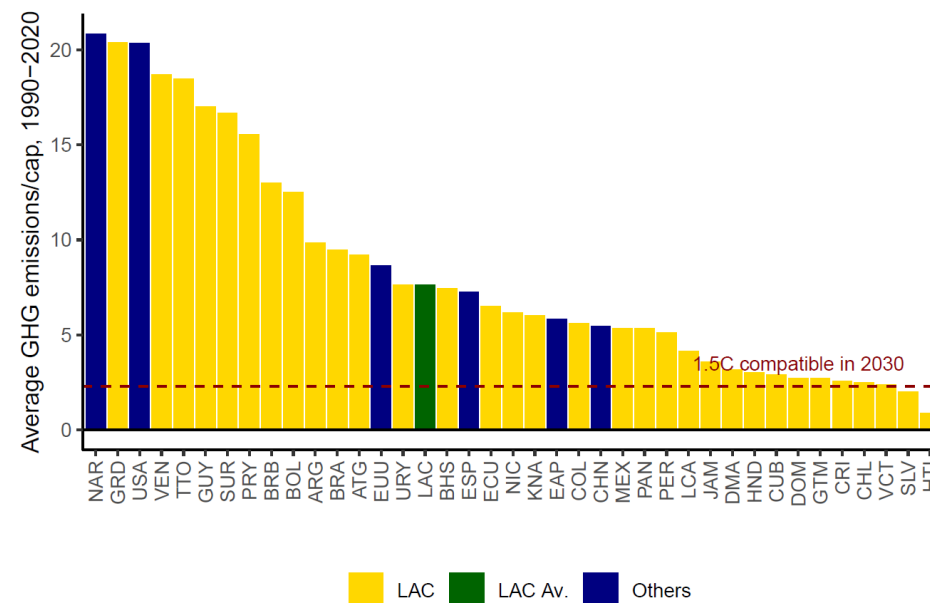
qualitatively discussed in some of these NDCs but are nowhere quantified. The case study developed in the framework of this thesis is therefore of direct practical interest for the countries of the region that will have to regularly update their NDCs. It provides evidence-based answers to the following questions: Can a more compact urban development help meeting GHG emissions reduction target set out in the NDCs? If yes, how much carbon savings can be obtained from these efforts? How to design the most effective spatial and urban planning policy actions in terms of potential CO₂ reductions and which cities/regions are to be prioritized?

Figure 12. Distribution of global GHG emissions by regions, 1990-2020 average



Note: this data comes from diverse sources and might be different from the one reported in national inventories.
Source: Author based on Climate Watch, total emissions.

Figure 13. Average emissions per capita in LAC countries and selected comparators, 1990-2020



Note: Belize has been removed to improve legibility of this graph.
Source: Author based on Climate Watch, total emissions.

5.2 The patterns of spatial expansion and CO₂ emissions across Latin American cities

As detailed in Chapter 4, this thesis relies upon a new methodology aimed at systematically evaluating cities' emissions and apply it to seven Latin American countries (Mexico, Brazil, Argentina, Chile, Peru, Ecuador and Colombia), which collectively account for 76 % of the Latin American region's GHG emissions. Interested readers are invited to refer to this Chapter 4 for a full description of the methodology and data sources but it is useful to repeat that 'cities' in this case study are defined using the spatial distribution of population, which is more likely to depict the socio-economic reality and functional interrelationships of the urban system than are administrative boundaries. Building on Oda et al.'s (2018) work providing spatially disaggregated CO₂ emissions at a 1km² resolution, I then estimate CO₂ emissions at the city level as emissions resulting from fossil fuel activities occurring within the boundaries of cities. Consequently, I assembled a unique data set providing systematic information for 635 cities across Mexico, Colombia, Ecuador, Peru, Chile, Argentina and Brazil for the years 2000 and 2015. All city-level estimates included in the remaining of this case study are based on this sample of cities. This includes a very heterogeneous set of cities, ranging from small urban areas (i.e. 50,000 people, as per the definition of the degree of urbanization) to giant megalopolises (20+ million people for Sao Paulo and Mexico City). Small and intermediary cities make up the bulk of the urban system: in 2015, half of the cities had a population below 130,000 and only 44 cities had a population over 1 million.³⁰

5.2.1 The patterns of spatial expansion of Latin American cities

One important contribution of this first case study is to consider both suburban areas and urban centres to delineate cities. The algorithm described in Chapter 3 is applied to the GHS-POP population grid with a spatial resolution of 1km and a World Mollweide projection (EPSG:54009). Although I acknowledge that this equal-area projection might not perfectly preserve the accuracy of angles and shapes, I have chosen it to ensure that features related to the "area" covered by each grid cell is as accurate as possible. This allows me to directly compute the spatial extent of a city as a count of 1km² pixels located within city borders.³¹ Since, by definition, city borders reflect population distribution, they are dynamics and are delineated using the population grids for 2000 and 2015 respectively. An illustration of what is meant by the spatial expansion of cities is provided in Map 7, which depicts the

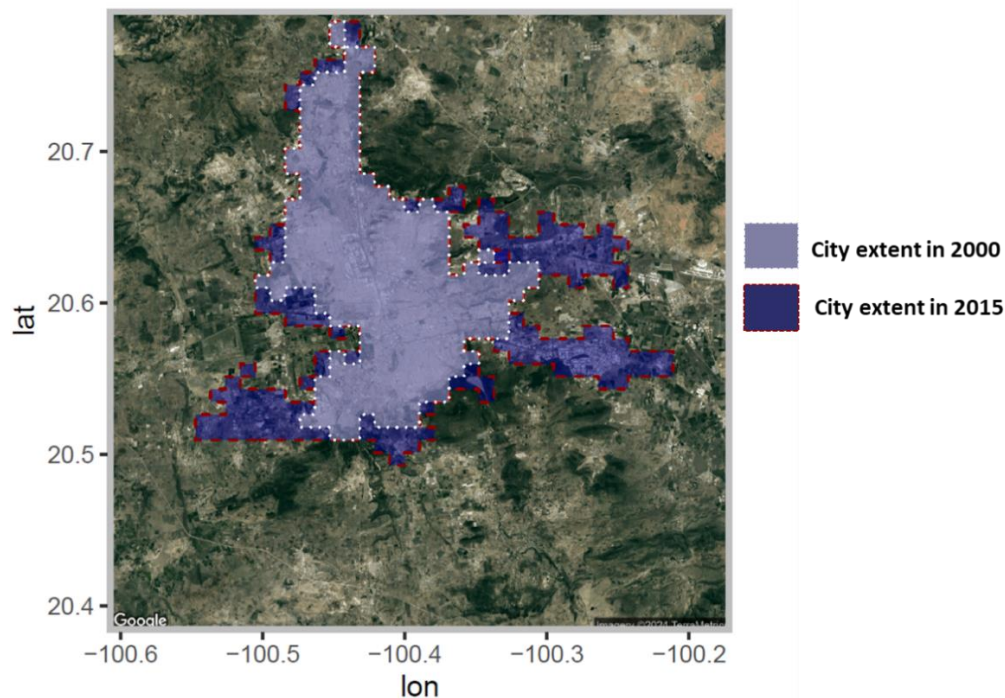
³⁰ To avoid measurement errors, after applying the algorithm described in Chapter 4, we manually removed from our data set the following observations: a city with 0 emissions in Brazil; another city with extremely high emissions per capita in Argentina (37 t of CO₂e/cap); and 10 cities with abnormally small built-up areas (below 2km²).

³¹ Although population grids with a finer spatial resolution are freely available, I purposely use the 1km² resolution because the underlying DoU definition entails a density threshold defined in terms of person/km². See Chapter 4 for more details.

spatial extent of the city of Queretaro in Mexico in 2000 (white borders) and in 2015 (red borders) according to my algorithm. This spatial extent covers both urban centres and suburban areas of Querétaro. The areas in dark blue correspond to the spatial expansion that the city has experienced between 2000 and 2015 and, in numeric terms, represent an expansion of 35%.

Map 7. The spatial expansion Santiago de Querétaro in Mexico, 2000 VS 2015.

Santiago de Querétaro, Mexico



Source: Own elaboration with GHS-POP. Basemap: Google Maps.

To get a better understanding of the dynamics of spatial expansion of Latin American cities, I have computed two complementary indicators for each city: (i) an “adjusted density” index; (ii) a suburban sprawl ratio. The joint evolution of the suburban ratio and the adjusted density indicator is then used to identify differentiated spatial expansion patterns. Two additional variables are computed and described at the end of this subsection as they are likely to influence the level of CO2 emissions at the city level: an indicator related to city geometric form and a proxy of GDP at the city-level.

Adjusted density: City density is usually measured as the ratio between the population and the total urban area. Most of the studies referenced in the review of literature of Chapter 3 actually use this density measurement as a proxy of “compactness”: denser cities are viewed as more “compact” cities. However, in this case-study, we follow Jedwab, Loungani, and Yezer (2021) and use the built-up surface rather than the total urban area to assess density and proxy compactness. Built-up data are extracted from the GHS-BUILT product, providing a measurement of the built-up surface in each cell (as a percentage of the total surface; the

technical description can be found in Florczyk et al., 2019). This raster is freely available online and I have used the version R2018A with a spatial resolution of 1km and a World Mollweide projection (EPSG:54009) to ensure consistency in the overlay with the city layer previously produced.³² Since every pixel of the GHS-BUILT product has a resolution of 1km², I simply perform a zonal sum of the values of every pixels within city borders to get an estimate of the built-up surface in km² associated to each city.

This case study selects the built-up surface as I believe that it represents a better proxy than the total city area for measuring the ‘liveability’ associated with a given level of density. This is especially important in Latin America where higher density can exacerbate congestion effects and produce unclear effects on productivity or emissions. Liveable density requires adequate floor space per person, which in turn implies high levels of infrastructure and built-up area. In Latin American contexts, cities with a high people/area ratio may be reflecting two realities depending on the amount of built-up structure in this same area: a first, where high population density is associated with numerous buildings and infrastructure that potentially provide more floor space per person and presumably produce more liveable density levels; and a second, where high population density is combined with low levels of infrastructure and poor-quality built structures, such as in the case of shantytowns, suggesting an overcrowded area with less liveable density levels. Using the traditional people/area ratio would prevent me from differentiating between these two kinds of density and could biased the density measurement, which ultimately seeks to proxy “compactness” and positive agglomeration benefits usually associated to higher “liveable” density.

The benchmark density measurement of this case study is therefore computed using the built-up surface and I will refer to it as the “adjusted density” or simply density measurement. For the sake of completeness, a “traditional density” indicator is also estimated using the total city area expressed in kilometres (see below). In both cases, an increasing density over time reflects a spatial expansion model where population growth is accommodated within a city’s boundaries and/or is faster than the city’s built-up or the city’s area expansion.

$$\begin{aligned} \text{Adjusted - density}_{i,j} &= \frac{\sum \text{Population}_{i,t}}{\sum \text{Built - up}_{i,t}} \\ \text{Traditional density}_{i,j} &= \frac{\sum \text{Population}_{i,t}}{\text{Total area}_{i,t}} \end{aligned}$$

With i indexing cities and t indexing years (either 2000 or 2015).

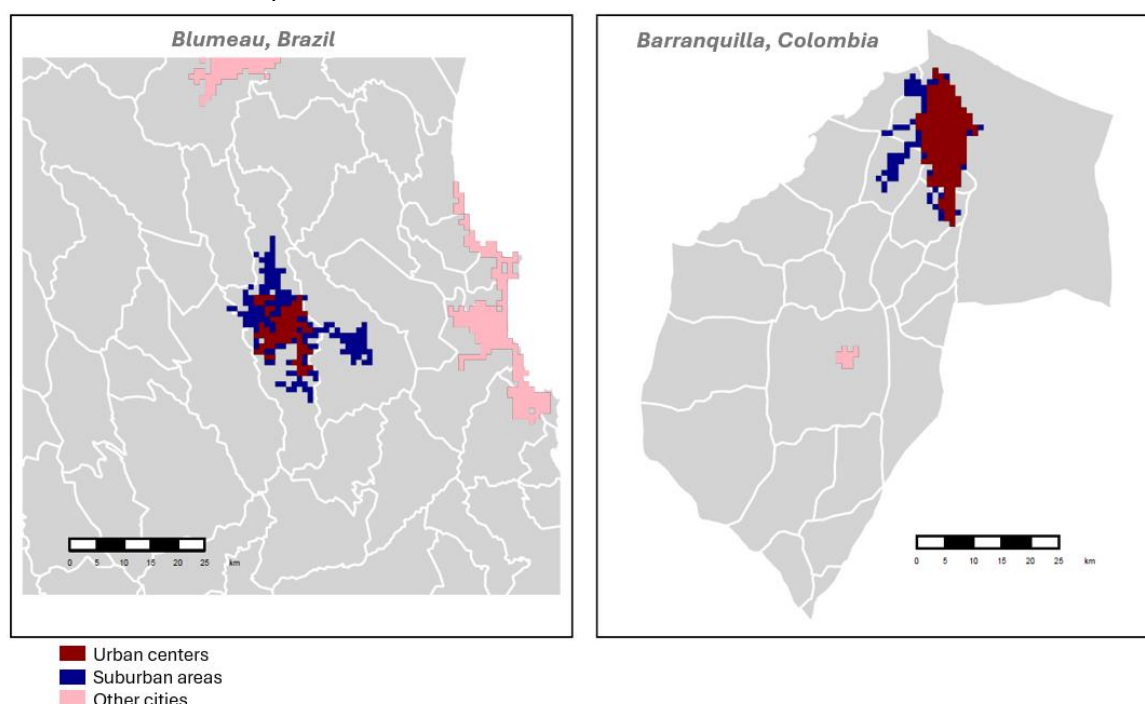
³² Data is available [here](#) although more recent GHS Built-up datasets have been released since the moment this analysis was undertaken. The use of more recent dataset is warranted for future analysis.

Suburban sprawl: To better understand the underlying dynamics driving the spatial expansion of cities and capture potential relocation effects at the city-level, this case study develops a second indicator focused on suburban sprawl. Suburban expansion has become a defining feature of contemporaneous urbanization (Guastella, Oueslati, and Pareglio 2019). From a theoretical point of view, suburban sprawl can be driven by two relocation effects: from (i) urban centres to suburbs and (ii) from rural areas to suburbs. In the first case, policies aimed at increasing density in urban centres can generate a sharp increase in land and housing prices (Gagné, Riou, and Thisse 2012). Likewise, poorly planned density can engender intense congestion effects and saturate historic urban centres. Irrespective of its driver, densification might incentivize urban populations and firms to move to suburban areas, where congestion effects are less prevailing and land cheaper. In the second case, the economic dynamism of cities can attract rural populations looking for better opportunities. Without proactive urban planning policies to accommodate this influx of people, rural migrants are likely to settle in the immediate surroundings of urban centres, where land and housing tend to be cheaper than more centrally. In practice, both relocation effects could act simultaneously to inflate the suburban population relative to the urban centre population. To characterize suburban sprawl and capture these dynamics I thus compute the ratio between the population living in semi-dense areas in the immediate surroundings of urban centres (areas in blue in Map 8) and the population living in urban centres (areas in red in Map 8). This ratio, labelled the ‘suburban ratio’, is computed according to the formula below. In dynamic terms, this ratio will increase over time if the population in semi-dense areas grows at a faster rate than the population in urban centres. By contrast, if population growth is mostly accommodated within urban centres, the population will grow more rapidly here than in semi-dense areas, leading to a decrease in the suburban ratio. A decrease of the suburban ratio is therefore more likely to depict a compact spatial expansion model.

$$Suburban\ ratio_{i,t} = \frac{\sum Pop.\ in\ semi - dense\ areas_{i,t}}{\sum Pop.\ in\ urban\ centres_{i,t}}$$

To illustrate how heterogeneous cities are, Map 8 compares the city of Blumeau in Brazil, to Barranquilla in Colombia. In 2015, Blumeau had a total population of 380,171 habitants but only 59.6% of its population was living in the urban center (i.e. 226,693 persons), resulting in a suburban ratio of 0.67. Contrastingly, the same year, Barranquilla had a total population just above 2 million habitants, of which almost 95% was living in the urban centers (i.e. 1.9million), leading to a suburban ratio of 0.05. Consequently, as can be seen in the corresponding map, which uses a similar scale to facilitate comparison, although Barranquilla was more than 5 times more populated than Blumeau, the two cities had a relatively similar spatial extent.

Map 8. Urban centers and suburban areas in selected cities



Note: For each city, the grey area is the corresponding administrative 1 area; Administrative boundaries corresponding to the admin 2 level are in white.

Source: own elaboration with GHS-POP. Base map: GADM.

I now use these two indicators to characterize the spatial expansion of cities in my sample or, in other words, assess how these indicators relate to the evolution of the total area of a city (in km) between 2000 and 2015.

The data confirms that demographic trends constitute a major driver of urban spatial expansion. Between 2000 and 2015, 609 out of 635 cities in my sample increased their population, for an overall increase in cities' population of +21%. The rate of population growth tends to be differentiated based on the initial level of population. Small towns and cities with a population below 1 million in 2000 experienced the most dynamic evolution, with an average growth rate of almost 26% during the period. By contrast, large cities with more than 1 million people exhibited an average growth rate of approximately 21% (Figure 14. A). A similar pattern is found when looking at spatial expansion growth rates: in relative terms, small and intermediate cities experienced faster spatial expansion than cities with more than 1 million inhabitants. In fact, the evolution of population and spatial extent of a city are positively correlated with a Pearson coefficient estimated at 0.39. This pattern is consistent with previous investigations showing that demographic trends constitute the primary driver of urban spatial expansion and that, without addressing urban market failures, a fast-growing population will exacerbate urban spatial expansion (Brueckner 2000). Indicators related to density and suburban sprawl are now mobilized to get a better sense of how city population growth is spatially accommodated within city borders.

While density evolution strongly correlates with population growth, it only marginally explains cities spatial expansion dynamics. With a Pearson coefficient of 0.82, population growth and adjusted-density growth were strongly and positively correlated. On average, a 1% increase in city population was accompanied by a 0.71% increase in city density (Figure 14. B). Contrastingly, during the period, not a single city increased its density without increasing its population.³³ However, with a Pearson coefficient estimated at 0.09, the evolution of density constitutes poorly explains the speed at which spatial expansion materializes. Cities that densified in the same magnitude displayed very different speeds of spatial expansion (Figure 14. C). For example, between 2000 and 2015, the city of Itapoã in Brazil (75K habitants and area of 16km² in 2000) has experienced a reduction of its density levels by -3.2%, while its spatial extent increased by almost 19%. During the same period, the city of Pitalito in Colombia, comparable in terms of population and extent (84K habitants and an area of 14km² in 2000) has expanded in the same magnitude (i.e. 21%) but has seen an increase in density levels of 23.1%. This underscores the need to go beyond density indicators to understand the underlying dynamics driving urban spatial expansion.

The suburban ratio provides a finer understanding of the dynamics driving the spatial expansion of cities. Between 2000 and 2015, more than 85% of the cities experienced an increase in their suburban ratio, implying that for most of the cities in my sample, the population in suburban areas was growing faster than that in urban centres. This provides evidence that for most cities in Latin America, relocation effects are playing out in the immediate surroundings of urban centres, with important implications for the dynamics of spatial expansion. This also confirms the relevance of going beyond urban centers and consider the suburban ratio to accurately proxy the compactness of a city.

Looking simultaneously at the evolution of the suburban ratio and the density indicator unveils different spatial expansion patterns at the city-level (Figure 14. D). Cities in quadrant 1 in Figure 14. D increased their density, while reducing their suburban ratio (approximately 10% of Latin American cities appear in this quadrant). This points to a situation where urban centre population growth has been driving densification, suggesting that densification has principally occurred within urban centres. This spatial expansion is potentially linked to proactive urban management and public policies seeking to reinvigorate urban centres to accommodate population growth without further exacerbating suburban sprawl. Cities in this quadrant might also have experienced such a strong dynamism in some of the areas classified as suburban in 2000 that these areas were considered urban centers

³³ Figure 3 displays this relationship for the benchmark density indicator, but a very similar figure is obtained with 'traditional density'. By construction, when using the adjusted-density measurement, increasing density while keeping population constant would require reducing the built-up surface of the city, which is very unlikely to happen in practice.

in 2015, further boosting population growth in urban centers and consequently reducing the suburban ratio. This suggest a similar “compact” spatial expansion: some suburban areas have considerably densified and have integrated to the city -as opposed to continued suburban sprawl without changes or only marginal increases in density in these areas.³⁴ On the opposite side, the spatial expansion of cities in quadrant 3 of Figure 14. D materialized through urban sprawl, as revealed by a decrease in density simultaneously with an increase in the suburban ratio (i.e. a faster increase in the suburban population than in the urban centre population). Eventually, 64% of cities appear in quadrant 2 of Figure 14. D, having experienced increases in both density and the suburban ratio. This situation potentially reflects passive land use management or weak urban planning capacities, which failed or did not seek to accommodate population growth within urban centres. In other words, for most Latin American cities during this period, spatial expansion was driven by a consolidation of suburban areas, with population growth in these areas outpacing that occurring in urban centres.

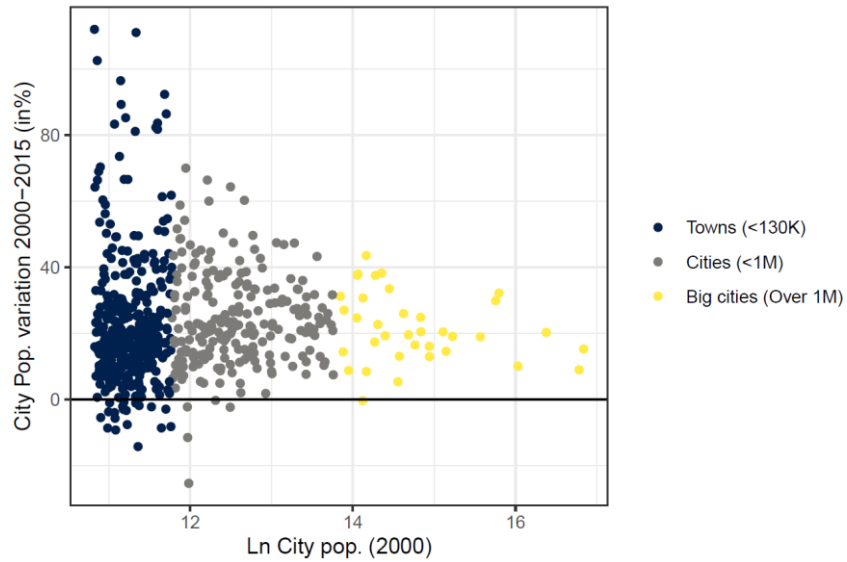
Three spatial expansion patterns emerge from these stylized facts and will be used in the remaining of this case study: (i) compact expansion, whereby increasing density is combined with a decreasing suburban ratio (quadrant 1 in Figure 14. D); (ii) passive expansion, whereby rising density occurs in conjunction with an increase in the suburban ratio (quadrant 2); and (iii) sprawl, whereby density follows a downward trend and the suburban ratio increases (quadrant 3). Classifying Latin American cities according to these features effectively unveils distinctive patterns: urban land expansion is more effectively harnessed under the compact expansion model, with a mean spatial expansion rate two percentage points smaller than that under the passive model (Figure 14. E). A t-test comparing the means of the cities contained in each of these two groups confirmed that this difference in means is statistically significant.³⁵

³⁴ To be reclassified as part of the urban centers, adjacent suburban pixels must have a minimum density of 1,500 habitants/ km² VS 300habitant/ km² to be considered suburban areas. See the DoU definition in Chapter 4 for more details.

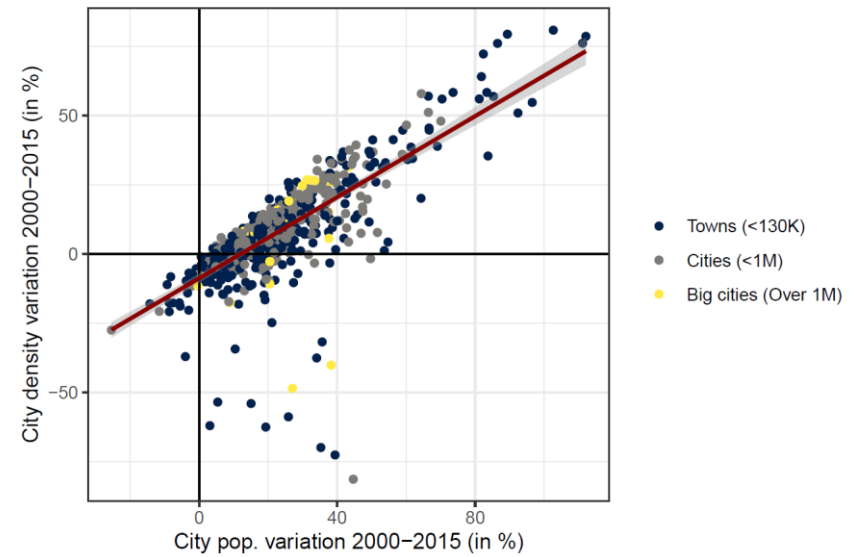
³⁵ I have used an equal variance t-test since I was not able to reject the null hypothesis of equality of variance under the F-Test performed on these two distributions.

Figure 14. The patterns of spatial expansion in Latin America cities, 2000–2015

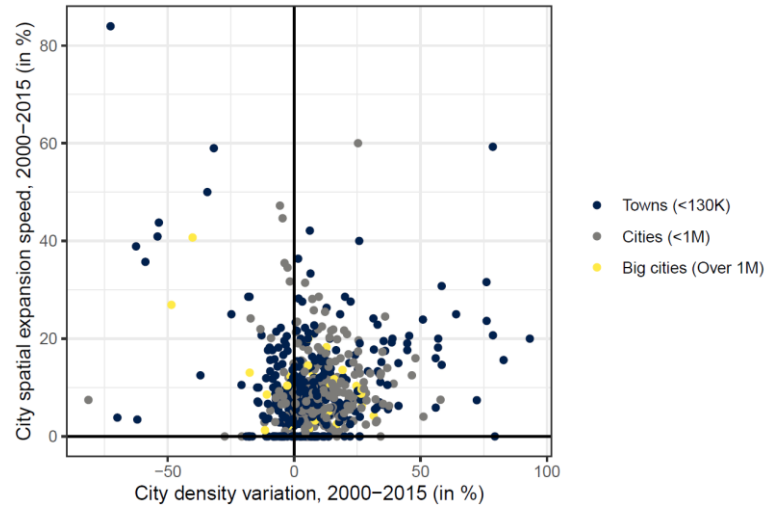
A. City population growth is differentiated by level of population



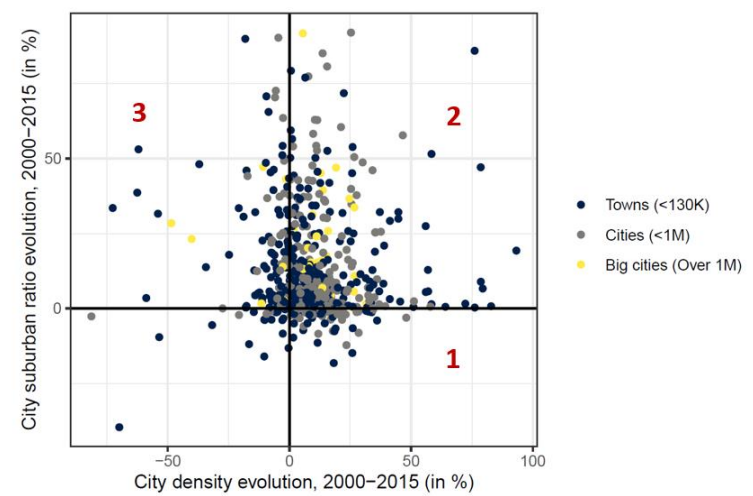
B. Population and density growth are strongly associated in almost all cities.



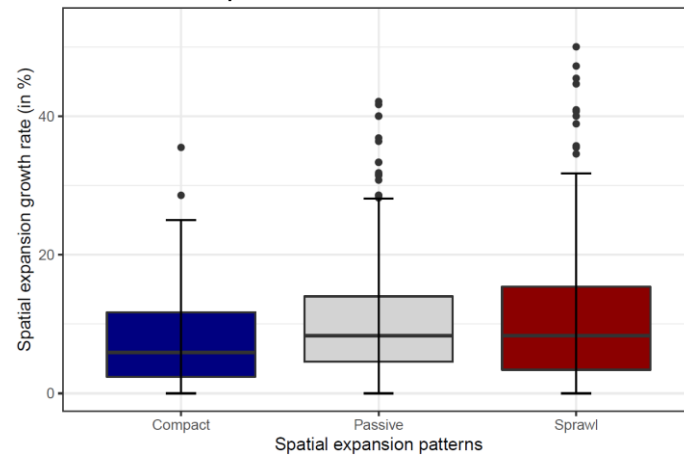
C. The evolution of density is not a good predictor of the speed at which a city expands I



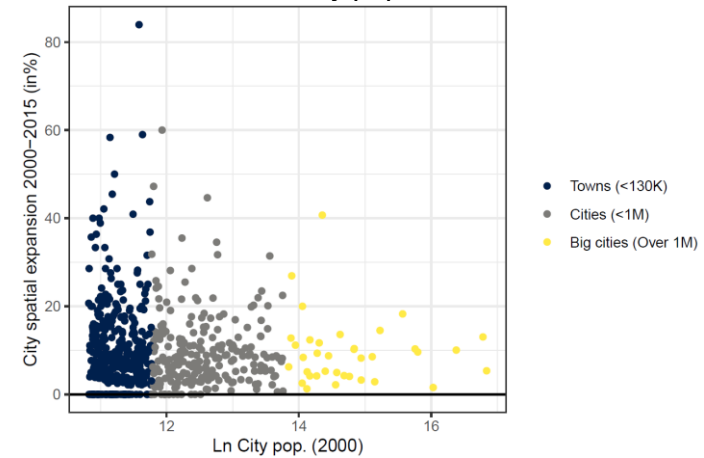
D. The joint evolution of density and suburban ratios unveils different spatial expansion patterns



E. Expansion growth rates of cities under each spatial expansion pattern, 2000–2015



F. The growth rates of spatial expansion are differentiated based on initial city population



Notes: Each point represents a city. In 2000, the median value of city population in our sample is 130,818, while the 90th decile value is 801,284.

In Graph A, 6 cities displaying population growth rates above 125 have been manually removed to improved legibility.

In Graph B, the red line depicts a lineal regression between our two variables of interest.

In Graph E, 4 cities with spatial expansion growth rates above 55% have been removed (3 under the sprawled and 1 under the passive expansion models).

Source: own elaboration.

Two additional indicators related to cities structural patterns are compiled before conducting the statistical analysis of the next section. First, the shape index is computed to provide information regarding the geometric form of cities.³⁶ Urban form is traditionally analysed through landscape metrics and refers to the geometric shape of a city. From a conceptual viewpoint, complex urban forms may complicate urban transportation, as urban journeys tend to be concentrated around relatively few nodes, potentially increasing congestion effects and ultimately CO2 emissions as well. Nonetheless, when complex urban forms are associated with polycentric urban areas, less individual transportation across large areas is required, potentially resulting in lower urban emissions. To test for the impact of urban form on CO2 emissions, we compute the shape index of each city in the sample. The shape index is the normalized ratio of the city perimeter in which the complexity of the city shape is compared to a standard shape (square) of the same size (see below). It is interpreted as follows: the index is equal to one for square cities of any size and increases without limits with more geometrically complex (i.e. less square) city shapes. This index is intended to be used as a variable controlling for the effect of geometric compactness in the subsequent econometric analysis. However, I acknowledge that the gridded nature of the population rasters used to delineate cities boundaries constrain the ability to accurately depict the geometric features of cities. This metric is likely to add more value in settings where refined polygons of cities are available, which was not the case in this study.

$$Shape\ index_{i,t} = \frac{Perimeter_{i,t}}{Min.\ perimeter_{i,t}}$$

$Perimeter_{i,t}$ refers to the perimeter of city i in year t , while $Min.\ Perimeter_{i,t}$ is the minimum perimeter derived from a square city of the same size (both in metres).

A last key feature that is likely to shape urban spatial expansion is the ability to successfully implement urban planning policies. As there are no comparable data on this dimension across the full sample of our cities, we compute city-level GDP per capita as an imperfect proxy for dimensions such as regulatory and institutional capacity and urban planning quality. To this end, we use the spatially disaggregated estimation of GDP at a 1km² resolution provided by Kummu, Taka, and Guillaume (2018) and overlay it with the layer of cities described in chapter 4.³⁷ Before performing spatial operations, I have reprojected the original geographic raster provided by these authors to the World Mollweide projection using the bilinear method, which computes the output cell value based on the four nearest cells in the original raster. The new values in the projected raster correspond to the distance-weighted average of the values from

³⁶ This index is computed using the R package “landscapemetrics”.

³⁷ Kummu et al. (2018) spatially allocated national and subnational GDP statistics using various population datasets. Although the raster they provide remains representative of the official statistics, it is not based on administrative boundaries. Instead, it relies on the spatial distribution of the population, which is fully consistent with our definition of cities and the different metrics employed in this thesis.

these four cells: the closer the input cell is to the center of the output cell, the greater its weight. City-level GDP is then obtained through zonal statistics, summing GDP pixels within each city borders. We repeat this exercise for the years 2000 and 2015.

5.2.2 The patterns of CO2 emissions of Latina American cities

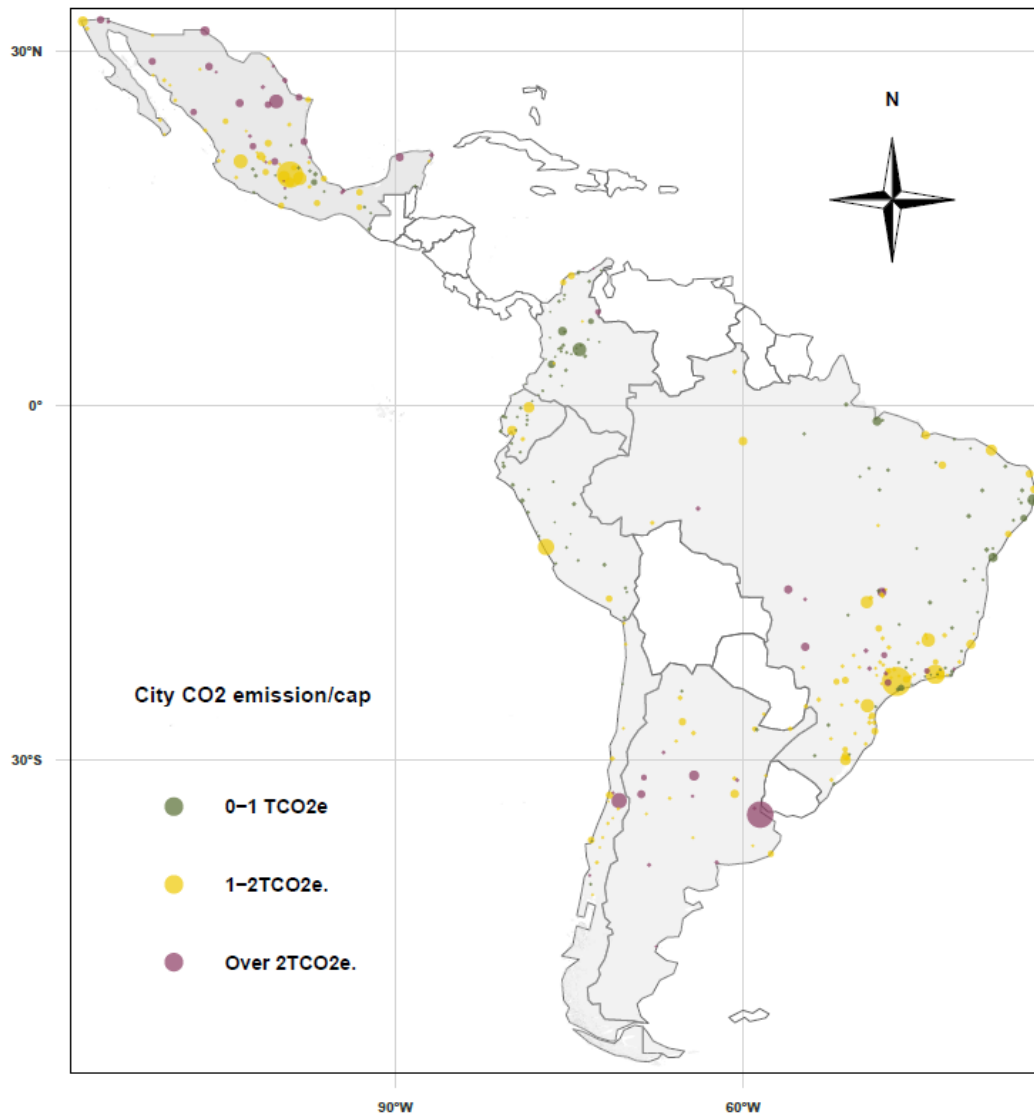
Based on the methodology described in Chapter 4, I have gathered CO2 emissions estimates at the city-level for all the cities in my sample. Map 9 illustrates some of the city-level CO2 per capita estimates produced through this methodology and the geographical coverage of this case study. The remaining of this subsection discusses the main patterns of CO2 emissions at the city level between 2000 and 2015 and explores how these relate to the usual drivers of emissions, namely population and affluence. A third driver is examined: geography, here understood as location and distance to neighbouring cities. The descriptive statistics presented here are not meant to explain CO2 variations at the city-level, which is the objective of the statistical analysis conducted in the next section.

In 2015, CO2 emissions produced within cities boundaries represent almost 61% of total fossil fuel CO2 estimates for our seven countries of interest. This share of CO2 emissions attributed to cities differs by countries and reaches a maximum of 90% of total emissions in Chile or a minimum of 39% in Colombia. Although this latter level might come across as low, results are consistent with the methodology used. This methodology follows a territorial-based approach, whereby city-level emissions are defined as emissions produced by activities located within city borders. This implies, for example, that emissions associated to a power plant located outside of a city will not be imputed as “city-level emissions”, even if the power plants services exclusively this city. Beyond the absolute level of emissions attributed to each city, it is important to keep in mind that the proposed methodology does not seek to provide the most comprehensive CO2 coverage for a given city, which is by essence a complex exercise requiring a lot of assumptions (see Chapter 4 for more details). Instead, I have designed this methodology with the ultimate objective to capture city-level emissions that are likely to be influenced by activities in the building, transportation and electricity and heat sector, which are the ones most likely to be influenced by city spatial patterns.

Estimates of CO2 emissions per capita at the city level display relatively low levels. More than 50% of the cities in my sample are estimated to have CO2e emissions below 1ton/capita and the 90th decile value is 2.06 tonnes/capita. Interestingly, towns and intermediate cities display a large dispersion of CO2 emissions/capita, while for big cities, with a population over 1 million habitants, most values range between 1 and 2 tonnes/ capita. For most cities, CO2 emissions per capita are generally well below what is reported nation-wide (see Figure 15). This is consistent with the differences in methodology and scopes (national estimates include more

sectors and more gases than fossil fuel CO₂ estimates) and the numbers obtained through both approached should not be compared upfront. Eventually, as happened for most statistics related to urban systems, CO₂ emissions are heavily concentrated in a few cities: the 5% largest cities account for approximately 57% of total city emissions, a pattern that has remained almost unchanged between 2000 and 2015 (Figure 16).

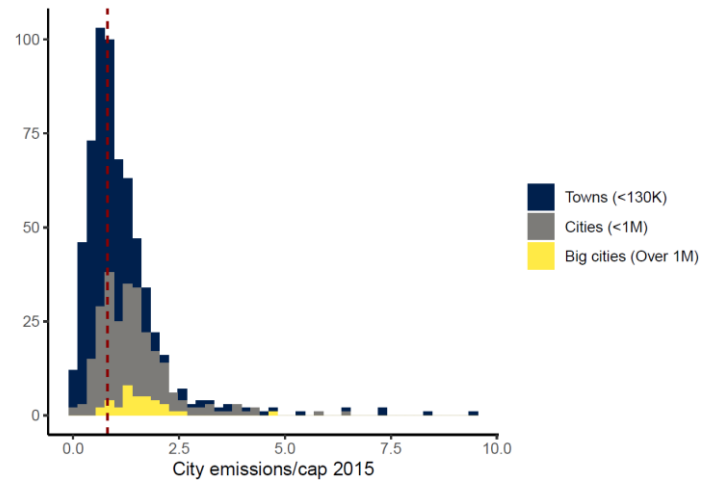
Map 9. Estimated CO₂ emissions per capita and spatial extent of selected cities in 7 Latin American countries



Note: The size of the bubble is proportional to the spatial extent of urban centres. To improve legibility, only cities above 120,000 inhabitants -i.e. 55% of total cities in my sample- are mapped.

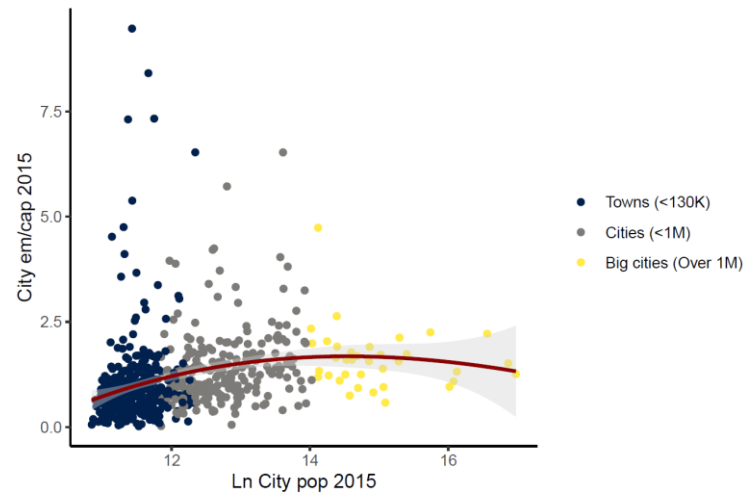
Source: own elaboration. Basemap: Natural Earth.

Figure 15. Distribution of estimated fossil fuel CO2 emissions per capita in 2015



Note: the dotted red line depict the median of the distribution

Figure 17. City population VS estimated fossil fuel CO2 emissions per capita in 2015



Note: the redlines correspond to (i) a non-parametric regression using splines, which divides dataset in 3 bins and fit separately each bins using polynomial fit (left figure) and (ii) a linear trend (right figure). 4 cities outliers with emissions per capita above 10 have been manually removed to improve legibility.

Source: own elaboration.

Figure 16. Concentration of estimated fossil fuel CO2e emissions by cities category

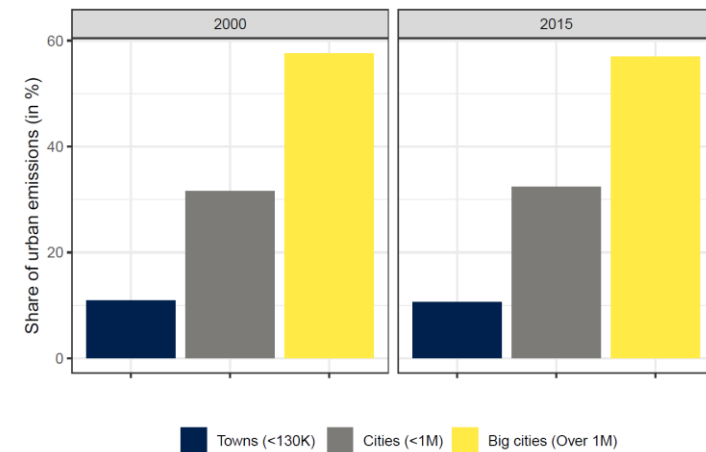
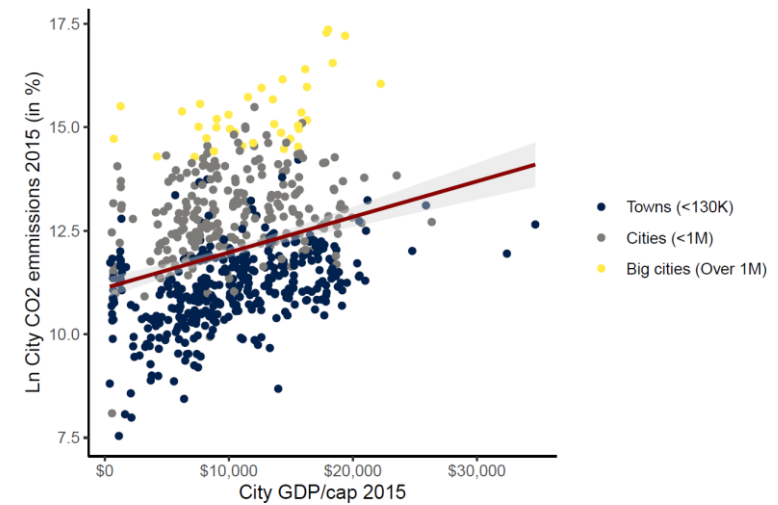


Figure 18. City GDP/cap VS estimated fossil fuel CO2 emissions in 2015



At the regional level, between 2000 and 2015, CO2 emissions produced within all the cities of my sample have increased by 68%. This growth rate is far exceeding the growth rate of population living in these cities (+21%), unveiling how most cities in my sample have increased not only their overall level of emissions but also their level of emissions per capita during the period. When looking at city-level patterns, on average, the higher the population of a city, the higher its level of emissions per capita (see Figure 17). Interestingly, this figure suggests a non-lineal relationship between total city population and carbon efficiency (as proxied by the emissions/cap ratio): as a city increases its population, emissions/capita start rising but *plateau* or even slightly decrease when the overall city population reaches approximately 1 million persons. In other words, there might be a “size effect” that allow cities above 1 million habitants to be more carbon efficient and keep increasing their population without increasing their emissions per capita. Of course, this effect could be confounded with other factors as more populated cities also tend to be denser and richer. Disentangling the causal impact of the different drivers of emission will require a more detailed statistical analysis that I will conduct in the next subsection.

A higher GDP at the city-level is unambiguously and almost linearly associated with more important CO2 emissions at the city-level. At the aggregated regional level, the GDP of the cities in my sample has been boosted by +55% between 2000 and 2015, an increase of a magnitude close to the one registered for CO2 emissions (+68%). At the city-level, when looking at affluence (measured in terms of GDP/capita) and CO2 emissions, there is not strong evidence of an inverted U-shaped relationship -which would be consistent with the environmental Kuznets curve (EKC) hypothesis (Figure 18).³⁸ When examining the relationship between GDP/capita and emissions/capita (as opposed to city emissions), an even more lineal relationship is detected, further suggesting the absence of an EKC (see Figure A.2 in Appendix to this case study). Of course these are only preliminary observations requiring a more detailed investigation before conclusions can be drawn. As this thematic is not the core focus of my thesis, I leave it as an avenue for future research.

Finally, the spatial nature of my dataset allows me to explore the spatial correlation among cities' CO2 emissions. Of course, I am not referring to a spatial diffusion process of the CO2 in the atmosphere which is a physical process. I examine here spatial spillovers effects linked to the diffusion of economic progress, technology and specialization in a specific activity that tend to be spatial clustered. To test for this spatial dependence effect, I compute a matrix of neighbours that includes for each city in the sample the three nearest cities geographically.

³⁸ The EKC is named for Simon Kuznets, who hypothesized that income inequality first rises and then falls as economic development proceeds. According to the EKC hypothesis, environmental pressures increase as income level increases at the initial stage of economic development, but later these pressures diminish along with the income levels.

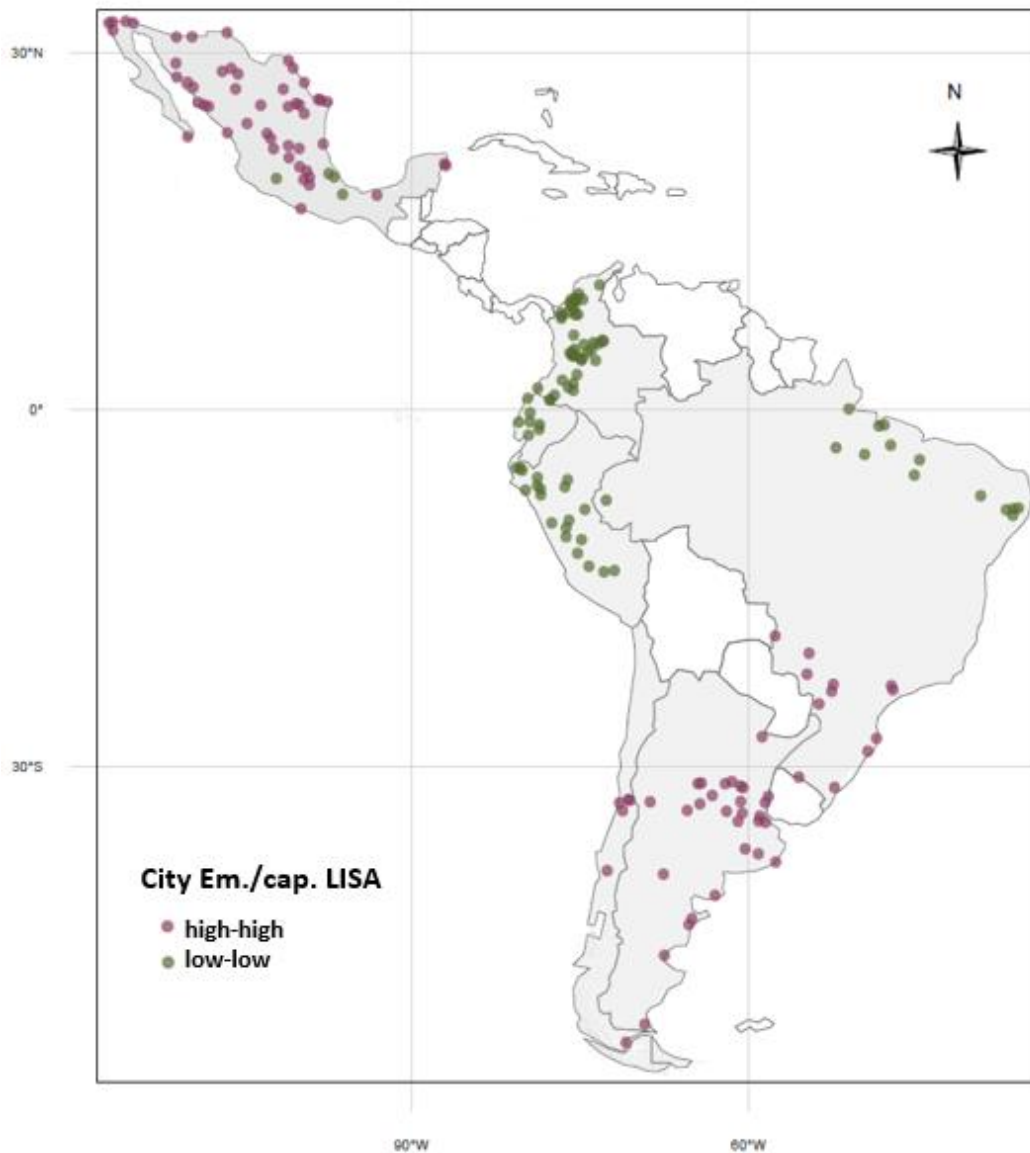
The global Moran's I spatial autocorrelation statistic is then used to assess the correlation among neighbouring cities and to identify patterns and levels of spatial clustering.

I am interested in assessing spatial autocorrelation of Log-transformed CO₂ emissions at the city level, which is the dependant variable in my subsequent statistical analysis. Log-transformed CO₂ emissions at the city level display spatial correlation, with a global Moran's I estimated at 0.14 in 2015 and significant at the 1% confidence level (Figure 19). The spatial autocorrelation of city emissions was slightly higher in 2000, with a significant global Moran's I estimated at 0.17. To ensure these findings are not overly sensitive to the choice of neighbours, alternative matrices of neighbours were built based on the five and ten nearest geographical neighbours, confirming the significance of spatial autocorrelation. Accordingly, when controlling for population, the global Moran's I of the log-transformed CO₂ emissions per capita displays a much higher correlation coefficient of 0.43, significant at the 1% level. In other words, cities with similar levels of CO₂ emissions are located relatively close to each other.

In addition, I conducted a local indicators of spatial association (LISA) analysis, revealing a double pattern of local spatial autocorrelation: the clustering of cities with higher-than-average emissions per capita is mainly distributed along the valleys and grasslands of southern Brazil, Argentina and northern Mexico. On the other side, cities with lower-than-average levels of emissions per capita are clustered in the Andean region along the Pacific coast and in northern Brazil. These findings are a reminder of Tobler's first law of geography, which states that "everything is related to everything else, but near things are more related than distant things". Another important implication of the presence of spatial autocorrelation is that it is crucial to properly account for these effects in order to disentangle the causal impacts of urban spatial patterns on CO₂ emissions and ensure unbiased estimations (Anselin 2013).

In summary, it appears that city-level emissions are influenced by three major drivers: population, affluence and geography (understood as location and distance). All these drivers will be considered to design an identification strategy that allow to isolate and make a causal claim on the effects of cities spatial patterns in the subsequent statistical analysis.

Map 10. Cities emissions/cap local indicators of spatial association (LISA)



Note: Only cities displaying statistically significant LISA indicators have been plotted.
Source: own elaboration. Basemap: Natural Earth

Figure 19. Moran's plot of Ln city emissions, 2015. Moran's I: 0.14***

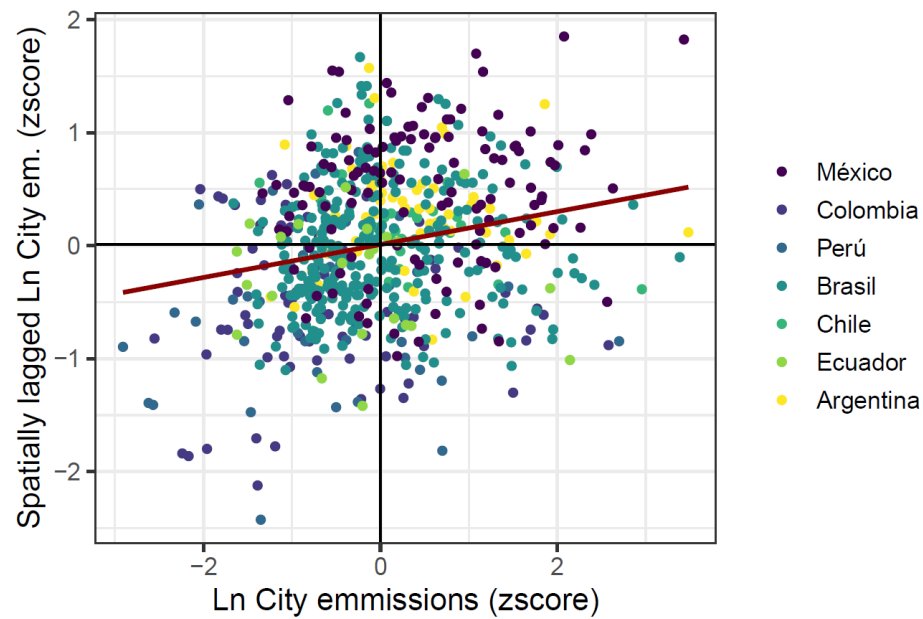
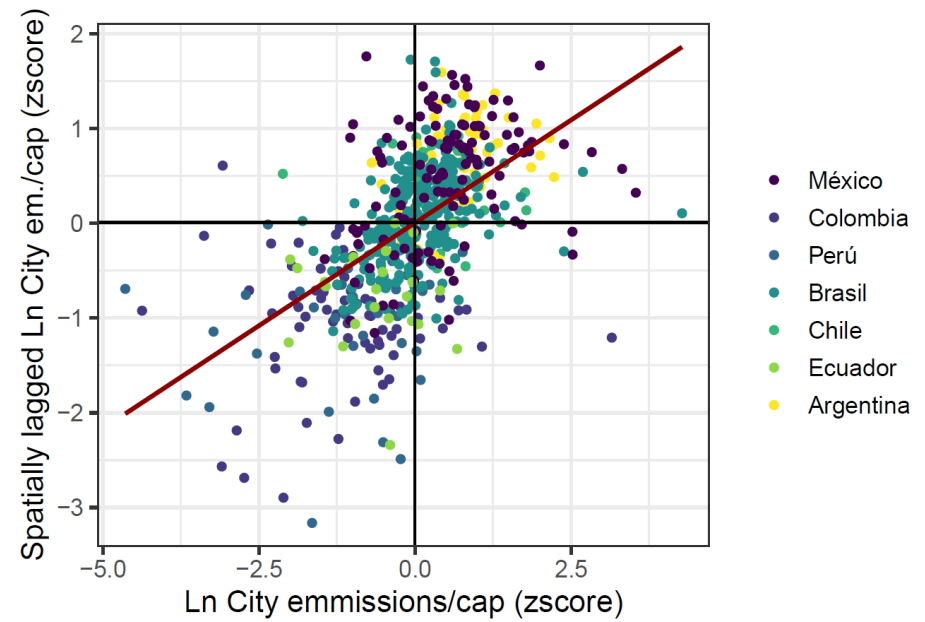


Figure 20. Moran's plot of Ln city emissions/cap, 2015. Moran's I: 0.43***



Source: own elaboration

5.3 A revamped STIRPAT model: The impact of spatial expansion dynamics on CO2 emissions

To robustly assess the impact that the spatial expansion of a city can produce on its CO2 emissions and isolate this effect from other factors, I will rely on the famous Kaya identity (Kaya 1989). The traditional IPAT specification states that environmental impacts are the multiplicative product of three key driving forces: population, affluence and technology, as shown in the following equation.

$$I_{it} = P_{it} \cdot A_{it} \cdot T_{it}$$

This mathematical identity has typically been used as an accounting equation, in which known values of I, P and A are used to solve T. Affluence is typically operationalized as per capita gross domestic product (GDP/P), so that $P \cdot A = P \cdot (GDP / P) = GDP$. Thus, by construction, $T = I / (PA)$ or $T = I / GDP$, so that T is the impact per unit of economic activity. However, the key limitation of IPAT is that, as an accounting equation (i.e. mathematical identity), it does not permit hypothesis testing since the known values of some terms determine the value of the missing term. Furthermore, proportionality in the functional relationship between factors is assumed *a priori* and not tested.

As discussed in York, Rosa, and Dietz (2003) in full length, the IPAT identity can be adapted and transformed into a stochastic model that can be used to empirically test hypotheses and different functional relationships. The framework developed by York and colleagues is known as Stochastic Impacts by Regression on Population, Affluence and Technology (STIRPAT). In the typical application of the basic STIRPAT model, T is included as part of the error term, rather than estimated separately, making it consistent with the IPAT model. Indeed, in a conventional statistical model, the residual term captures ‘everything else’ not explicitly included as regression predictors. In the traditional IPAT equation, T represents everything that is not population and affluence. To be able to interpret parameters as elasticities, the STIRPAT model is generally expressed in additive terms with all variables in logarithmic form. Consequently, the traditional STIRPAT model is as follows:

$$\ln Impact_i = \alpha_i + \beta_1 \ln Pop_i + \beta_2 \ln Affluence_i + \epsilon_i$$

It must be noted that simply solving for T in the IPAT formula ($T = I / (PA)$) and using this value in the STIRPAT regression model does not facilitate hypothesis testing since it makes the model tautologically true, invariably resulting in an R2 value of 1.0.

To robustly assess the impact of urban spatial expansion on CO2 emissions at the city level, this case study builds upon this framework and develop an expanded version of the STIRPAT. Specifically, it adds a set of variables related to the spatial expansion of cities. While previous studies have relied on the traditional density ratio to capture the “compactness” of a city, I will use the unique features of my dataset to provide a more refined view on this dimension. As shown in the previous section, the adjusted density indicator together with the suburban ratio are useful to distinguish between the three main patterns of spatial expansion that have prevailed during the period, namely the compact (increasing density combined with a decreasing suburban ratio), passive (both density and suburban ratios rise) and sprawled (both ratios decrease) expansion. Importantly, the expanded STIRPAT version proposed in this case study seeks to isolate the influence of spatial expansion on CO2 emissions from affluence, population, level of emissions in neighbouring cities and other time-invariant unobserved city heterogeneity. To this end I will use fixed effects panel models. Such models are well-suited to this kind of analysis as they allow one to control for unobserved individual heterogeneity (Wooldridge, 2002).

Here, I seek to explain city-level CO2 emissions through city population, city affluence, level of emissions in neighbouring cities and the set of indicators on spatial patterns detailed previously. The model is expressed in additive terms with all variables in logarithmic form. It thus has the following generic form:

$$\ln Y_{i,t} = \lambda \sum_{j \neq i} W_{ij} Y_{j,t} + \beta_1 \ln population_{i,t} + \beta_2 \ln GDPPC_{i,t} + \beta_3 Spatial\ Patterns_{i,t} + \omega_i + \varepsilon_{i,t}$$

With $\ln Y_{i,t}$ denoting the natural logarithm of CO2 emissions of city i in year t , W_{ij} the row-standardized neighbours matrix used to compute the spatial lag of cities' emissions and λ the spatial lag parameter, which reflects the strength and direction of spatial autocorrelation between one city and its geographical neighbours. $\ln population_{i,t}$ is the log-transformed population of city i in year t , while $\ln GDPPC_{i,t}$ accounts for the log-transformed city gross domestic product (GDP) per capita in year t . *Spatial patterns* is a vector containing the two features discussed in the previous section, namely city density and the suburban ratio, all log-transformed. As discussed below, the shape index of cities is also included under this vector despite its limited ability to accurately translate the complexity of the shape of a city (see previous subsection). Finally, ω_i refers to the city fixed effects that control for time-invariant unobserved heterogeneity, such as a city's geographic characteristics, prevailing climatic conditions and cultural specificities. City fixed effects limit potential omitted variable bias and

are crucial to making a causality claim on the parameters to be estimated.³⁹ Given that all our variables are log-transformed, the estimated parameters are to be interpreted as city-level CO2 emissions elasticities.

Before estimating multiple regression models, it is important to ensure that independent variables are not too highly correlated with each other. In our setting, this issue may arise as variables describing city spatial patterns can potentially be strongly linked. To check for multicollinearity among our independent variables, a correlation matrix is built and presented in Table 1. Although density is somehow correlated with the suburban ratio and GDP per capita, the correlation coefficients are lower than 0.4. More worrying is the high correlation between the shape index and the population index, suggesting that these two indicators may deliver redundant information in the statistical analysis. However, all the variance inflation factor (VIF) values are below the threshold of 5 traditionally used, which confirms that we do not have severe multicollinearity issues in the independent variables and that the two spatial pattern indicators can be used simultaneously. When using the traditional density measurement instead of the benchmark density indicator, the suburban ratio and traditional density display higher correlation, although the VIF values remain below 5, allowing us to disregard multicollinearity concerns.

Table 1. Pearson correlation coefficient and VIF of the independent variables

	In Dens	In Shape	In Sub_ratio	In Pop	In GDP/cap	In Dens tradi.	VIF
In Dens	1	-0.11 ***	-0.39 ***	-0.02	-0.39 ***	0.68 ***	3.73
In Shape	-0.11 ***	1	0.34 ***	0.75 ***	0.18 ***	-0.06 **	1.37
In Sub_ratio	-0.39 ***	0.34 ***	1	-0.12 ***	0.2 ***	-0.75 ***	4.12
In Pop	-0.02	0.75 ***	-0.12 ***	1	0.15 ***	0.35 ***	1.22
In GDP/cap	-0.39 ***	0.18 ***	0.2 ***	0.15 ***	1	-0.28 ***	2.99
In Dens tradi.	0.68 ***	-0.06 **	-0.75 ***	0.35 ***	-0.28 ***	1	2.16

Additional specification tests are conducted, including a Hausman test for both the static and the spatial panel model that rejected the null hypothesis of an absence of correlation between individual effects and explanatory variables. Regarding the spatial panel model specification, although robust versions of the Lagrange multiplier tests are not fully conclusive when using a neighbour matrix based on the three closest cities, the test statistic is far higher for a spatial lag alternative than for a spatial error model. Test results are included at the bottom of Table 2. In addition, when using a neighbour matrix based on the five nearest cities geographically, we do not reject the hypothesis of an absence of spatial error dependence in the robust version of the Lagrange multiplier test. We therefore opt for a spatial lag model estimated using a

³⁹ We do not include a time trend as we only have two distant years (i.e. 2000 and 2015). In addition, as our main variables are likely to drive the potential time trend between these two years including a time trend would strongly reduce the variance in our data and obscure the statistical effects of our variables of interest. Given the micro-panel nature of the data ($N \gg T$), I consider that potential serial and cross-sectional correlation in residuals is not a big concern.

maximum likelihood strategy. Standard errors are computed using the Lee and Yu orthonormal transformation of the data (L.-F. Lee and Yu 2010).

5.3.1 Estimation results

Column 1 of Table 2 presents the estimation results for a static panel model that includes adjusted density (people/built-up ratio), city shape index and the suburban ratio as the main features defining city spatial patterns but does not consider the spatial dependence between cities' CO₂ emissions. City GDP per capita is introduced along with its squared terms to better capture non-linearities.⁴⁰ Columns 2–5 are spatial panel models accounting for the spatial dependence of emissions across cities. The results reported here are based on a matrix that includes the three closest neighbours but are qualitatively similar when using five or ten neighbours. Column 2 uses the same independent variables as the static panel but includes city GDP per capita in a linear fashion, while column 3, the benchmark model, uses GDP per capita along with its squared term. Columns 4 and 5 are used as robustness tests where the traditional definition of density (i.e. people per total area) is used instead of the people/built-up ratio (column 4); moreover, a reduced model form is employed to check whether the coefficient of the benchmark density measurement (people/built-up ratio, column 5) is affected by the absence of other spatial patterns indicators.

⁴⁰ Introducing the *Squared Ln City GDP* per capita term as an additional regressor improves the statistical fit of our model, with an increase of more than 0.06 points in the adjusted R-squared.

Table 2. Estimation results

	Static Panel Model	Spatial Panel Model	Spatial Panel Model 2	Spatial Panel Model (Trad.)	Spatial Panel Model (reduced)
Ln City CO2 emissions					
Spatial Factor λ		0.568 *** (0.025)	0.540 *** (0.027)	0.545 *** (0.026)	0.587 *** (0.024)
Ln City Density	-0.566 *** (0.162)	-0.253 *** (0.065)	-0.267 *** (0.065)		-0.270 *** (0.065)
Ln Trad. Density				-0.816 *** (0.168)	
Ln City Shape index	-0.071 (0.133)	-0.145 (0.095)	-0.143 (0.095)	-0.309 *** (0.102)	
Ln City Suburban ratio	0.381 *** (0.086)	0.189 *** (0.047)	0.189 *** (0.047)	0.095 (0.052)	
Ln City Pop.	1.951 *** (0.131)	0.972 *** (0.073)	0.951 *** (0.075)	1.412 *** (0.146)	1.005 *** (0.070)
Ln City GDPPC	-2.171 *** (0.301)	0.001 (0.018)	-0.685 *** (0.228)	-0.582 ** (0.226)	0.012 (0.018)
Sq. LnCity GDPPC	0.136 *** (0.017)		0.042 *** (0.014)	0.035 ** (0.013)	
City Dummy	YES	YES	YES	YES	YES
Observations	1,270	1,270	1,270	1,270	1,270
Individuals	635	635	635	635	635
Adj. R-Squared	0.39				
AIC	-832.0	-1435.7	-1436.9	-1452.9	-1416.0
Hausman Test	99.90 ***	67.3 ***			
LM panel test for spatial lag dep.		603.7 ***			
LM panel test for spatial error dep.		220.8 ***			
Robust LM panel test for spatial lag dep.		364.1 ***			
Robust LM panel test for spatial error dep.		28.4 ***			
Note	* p<0.1; ** p<0.05; *** p<0.01				

5.3.2 CO2 emissions elasticities at the city level

Across all models and specifications, the coefficient of density is negative and highly significant, indicating that, on average, higher density reduces CO2 emissions at the city level, even when considering the spatial dependence across cities' emissions. In addition, the CO2 density elasticity is of a similar magnitude across all spatial panel specifications. I have also tested whether the impact of density follows a U-inverted shape by introducing density in its quadratic form but found no evidence of such an impact. The coefficient of the suburban ratio is positive and significant, implying that a higher suburban ratio (i.e. more suburban inhabitants relative to urban centre inhabitants) results in higher CO2 emissions at the city level. The coefficient associated with the shape index is negative but insignificant, except when using the traditional definition of density (i.e. column 4). In this case, the negative coefficient would suggest that more geometrically complex shapes (i.e. less square) lower CO2 emissions. However, this result is not robust across the different models tested and we suspect that in column 4 the shape index might in fact absorb part of the effects associated with compact cities -which are not properly accounted for by traditional density measures. By contrast, the suburban ratio is no longer significant in column 4, possibly owing to the strong correlation between the traditional density measurement and the suburban ratio. Overall, this suggests that effects associated with the shape index and the suburban ratio are less significant than the benchmark density indicator in statistical terms. Furthermore, the coefficient λ of the spatial lag factor is positive and highly significant, implying that the level of CO2 emissions of neighbouring cities has a positive impact on the level of emissions of a given city. The spatial lag models also display an Akaike information criterion (AIC) that is markedly lower than that of the static panel model, indicating that this specification provides a better fit to the data. More importantly, it confirms that city-level CO2 emissions are affected by a spatial diffusion process, implying that CO2 emissions are not only the product of standalone activities at the city level but also the result of interactions with a broader system of cities.

Based on the model specification expressed in column 3, the quantitative impact of each explanatory variable in terms of CO2 emissions at the city level is derived. To this end, the spatial interaction process between neighbouring cities is considered through the coefficient λ . This implies that we estimate the direct effect that a change in an explanatory variable can produce on emissions for a given city as well as the indirect effect that this variation creates for neighbouring cities. The total effect presented in Table 3 corresponds to the average of the direct and feedback effects produced across all cities by a change in an explanatory variable. Except for the shape index, these effects are all significant at the 1% confidence level.

Table 3. Direct, indirect and total city-level CO2 emissions elasticities

	Direct	Indirect	Total
Ln Density	-0.29	-0.28	-0.58
Ln Shape	-0.16	-0.15	-0.31
Ln Suburban	0.21	0.20	0.41
Ln City Pop.	1.05	1.02	2.07
Ln City GDPPC	-0.76	-0.73	-1.49
Sq. LnCity GDPPC	0.05	0.05	0.09

Note: Elasticities estimated from the model in column 3 of Table 2. Simulated standard errors indicate that all variables are significant at the 1% threshold, except *Ln Shape*.

The results indicate that, on average, when a city population increases by 1%, its CO2 emissions soar by +2.07%. Of course, the net impact of this population growth on CO2 emissions will depend on the evolution of other variables and notably on the spatial expansion patterns prevailing at the city level. As highlighted in the previous section, cities are only able to increase their density when population raises, with on average a 1% increase in city population translated into a 0.71% increase in city density (Figure 14. B). As such, when population growth is conducive to a 1% increase in density levels, CO2 emissions are reduced by 0.58%. In addition, when this densification occurs in urban centres as opposed to suburban areas, CO2 emissions are further reduced: a 1% decrease in the suburban ratio lowers emissions by 0.41%. Eventually, the effect of GDP per capita on CO2 emissions at the city level becomes non-linear and follows a U-shaped relationship, suggesting that the marginal impact of city GDP per capita on CO2 emissions is first conducive to a reduction in city emissions, although this effect is quickly reversed and, for more than 90% of the cities in our sample, a higher GDP per capita implies higher CO2 emissions at the city level.⁴¹ At the median value, a 1% increase in city GDP per capita drives emissions 0.13% higher; at the maximum value, a 1% increase in city GDP per capita results in emissions 0.40% higher *ceteris paribus*.

⁴¹ Based on columns 1 and 2, the vertex of the marginal impact of city GDP per capita is estimated to be located at US \$2,794 or US \$3,321 respectively. Only 9% of the cities in our sample exhibit a GDP per capita below US \$3,321.

5.4 CO2 emissions pathways at the city-level and heterogeneity across cities

5.4.1 CO2 emissions pathways for an average city

What do these parameters mean for spatial planning and CO2 emissions in Latin American cities? Human settlements are the result of long-term processes in which history, geography and culture, among other major drivers, constantly interact to consolidate specific urban spatial patterns. From a policy perspective, substantially modifying cities' spatial patterns *ex-post* (i.e. once cities have emerged and are consolidated) is a challenging task. This thesis acknowledges it and is rather focusing on future urban expansion. Looking forwards, urban population is expected to continue increasing in the region (UNDESA, 2019). Similarly to what has been observed between 2000-2015, small and intermediate cities are likely to display the most dynamic growth rates over the next decade. The spatial configuration of these new urban settlements will thus contribute to reshape Latin American urban systems, with potential impacts in terms of CO2 emissions. To illustrate how future urbanization could lead to diverging CO2 emissions pathways, we use the elasticities estimated in the previous section to project CO2 emissions at the city level up to 2030 under each of the three spatial expansion patterns identified in this case study.

It is important to underscore that these projections are not seeking to predict CO2 emissions for a specific city. Instead, they intend to shed lights on the CO2 pathways that differentiated spatial expansion patterns would produce for an average city. As such, we assume that the population and GDP/cap growth rates are the same across all spatial expansion scenarios.⁴² We acknowledge that differentiated spatial expansion patterns are likely to be associated with different economic and population growth rates at the city-level. However, the projections below do not account for this effect as they seek to illustrate CO2 emissions pathways under differentiated urban spatial expansion scenarios, "*everything else being equal*". In other words, differences in CO2 emissions across scenarios are exclusively linked to the features of each spatial expansion model i.e. on how city population growth translates into differentiated density and suburban ratio evolutions.

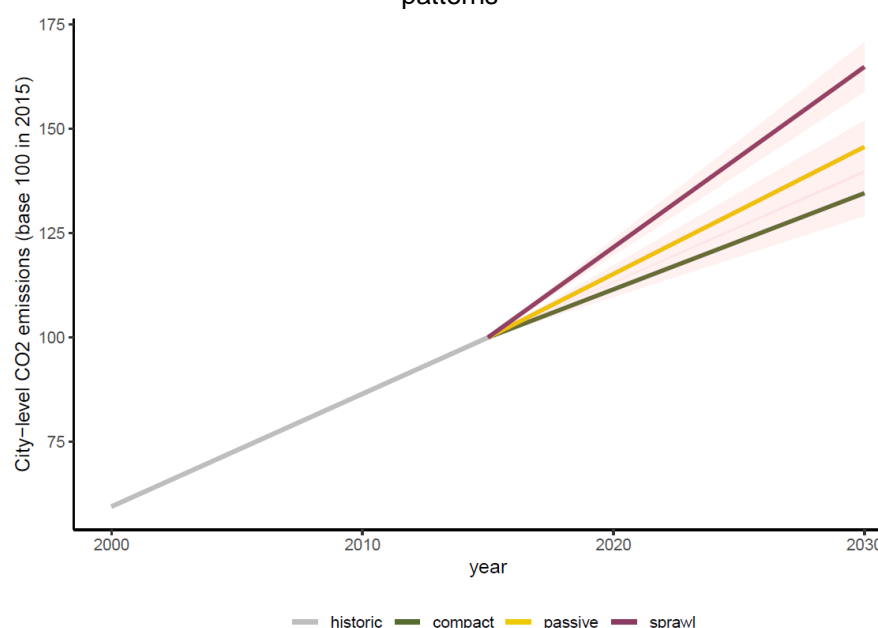
As detailed above, cities spatial expansion in Latin America has historically followed three patterns: under the compact scenario, new settlements will occur mainly within the urban centre -decreasing the suburban ratio- and city density will increase over time. Under the passive expansion model, although city density will increase, population growth will be faster

⁴² Population growth is assumed to converge to 21% over 2015–2030, which is in line with historic trends. GDP/capita is assumed to increase by 38% over the same period, which is close to the average growth rate in our sample during 2015-2030. Altering these growth rates would modify the absolute values of projected CO2 emissions but it would not change the differences across scenarios, as we employ the same growth rates under each scenario.

in suburban areas vis-à-vis the urban centre. Eventually, under the sprawled expansion model, new urban populations will primarily settle in areas adjacent to the urban centre, lowering the density level of the city and further intensifying its spatial expansion. The evolution of density and suburban ratios under each model is calibrated using average historic values over the period 2000-2015. Table A.2. of Appendix reports these average values.

Projections are plotted in Figure 21 and confirm that distinct spatial expansion models would result in diverging CO2 emissions pathways *ceteris paribus*. For a given average city assumed to experience a 21% population growth and a 38% increase in GDP/capita between 2015 and 2030, the compact expansion model would result in an increase of CO2 emissions of 34%, whereas it would boost CO2 emissions by 45% and 64% under the passive and sprawled scenarios, respectively. Policies aimed at increasing density and accommodating population growth within urban centres can therefore significantly slow emissions growth, with a difference of almost 12 percentage points between the compact and passive models. However, it is important to note that even under the compact expansion scenario, the CO2 emissions growth rate exceeds city population growth by thirteen percentage points, implying a rising level of emissions per capita. Shaping the spatial expansion of cities will therefore produce significant impacts on emissions pathways, but without complementary measures to decarbonize the energy matrix or alter mobility patterns, these actions will not be enough to produce an absolute reduction in CO2 emissions per capita at the city level.

Figure 21. Projected CO2 emissions pathways for an average city under three spatial expansion patterns



Note: Projections using the coefficients in Table 2 and the average density and suburban ratio evolutions under each spatial expansion model during the period 2000–2015. Shaded areas correspond to the statistical uncertainty associated to the parameter of interest. “Historic” values correspond to the average evolution of city-level emissions.

5.4.2 Heterogeneity of CO2 elasticities across the sample of cities

The projections presented above use the mean CO2 density effect to project emission pathways at the city level. However, the cities in our sample are very heterogeneous in terms of both population and affluence. A detailed assessment of the differentiated impacts of density and suburban ratios across the full sample of cities is thus undertaken to attain a more nuanced understanding of CO2 impacts depending on the specificities of each city. To this end, two interaction terms are successively introduced to assess whether and how the density and suburban CO2 elasticities vary according to different structural factors at the city level. Specifically, we estimate the following model:

$$\ln Y_{i,t} = \alpha + \beta_1 \ln population_{i,t} + \beta_2 \ln GDPPC_{i,t} + \beta_3 \ln Density_{i,t} + \beta_4 \ln Suburb_{i,t} + \beta_5 (\ln Density_{i,t} \cdot Mod. fact_{i,t}) + \beta_6 (\ln Suburb_{i,t} \cdot Mod. fact_{i,t}) + \omega_i + \varepsilon_{i,t}$$

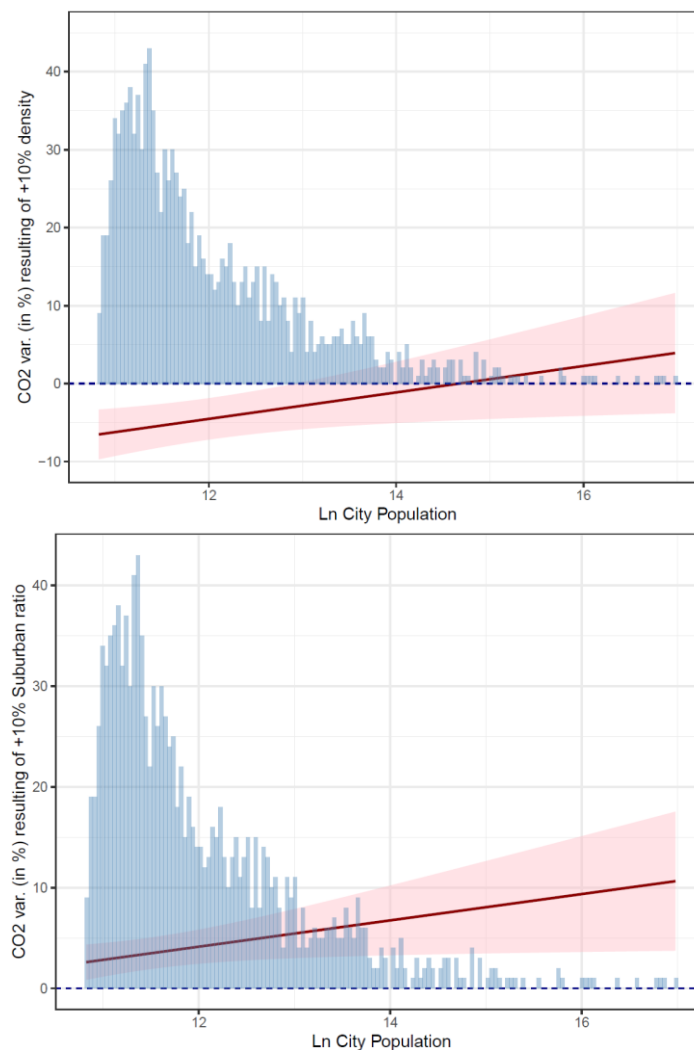
The two moderating factors considered are: (i) city population and (ii) city GDP per capita. To facilitate interpretation, we report the estimation of the marginal effects resulting from the sum $\beta_3 + \beta_5$ and $\beta_4 + \beta_6$ in Figure 22 and Figure 23 below as well as the distribution of our cities along the moderating variables considered. In these figures, the red line is to be interpreted as the CO2 effect of a 10% increase in city density or in city suburban ratio for a given level of the moderating variables. Full numerical results of these regressions are presented in Table A.3 of the Appendix of this case study.

When interacted with city population, the CO2 density effects reveal a nuanced impact. For the 50% smallest cities in 2015, whose populations were between 50,000 and 105,000 people (i.e. below $\ln population$ 11.56), a 10% increase in city density would result in a reduction in the range of 8% to 5% in city level CO2 emissions. However, as city population increases, the CO2 reduction obtained through higher density are progressively reduced and become statistically insignificant as city population reaches 1 million (i.e. close to $\ln population$ 13.81). This indicates that for large Latin American cities, which are potentially already overcrowded, an increase in density exacerbates congestion effects, resulting in non-significant effects in terms of CO2 emissions. By contrast, in small and intermediate cities, the benefits of higher density remain clear and harnessing future urban land expansion will produce decisive impacts on the CO2 emissions pathway of these cities.

Regarding the carbon elasticity attached to suburban ratio, the analysis reveals how this elasticity is amplified when city population gets larger, indicating that a higher suburban ratio produce more severe CO2 increases in large cities than in small towns. Specifically, for small towns below 105,000 persons, emissions will grow by less than 5% for a 10% increase of the suburban ratio. Contrastingly, for large megalopolis with population above 1 million, a 10%

increase of the suburban ratio could lead to an almost 10% surge of CO2 emissions at the city-level. Although estimates are less precise for these large cities, they remain statistically significant across the entire sample of cities. This heterogeneity can potentially reflect the compounding CO2 effects associated with large suburban areas surrounding big cities. For these big cities, expanding an already large suburban area can trigger cascade effects on transportation and other congestion externalities that, ultimately, will produce a stronger increase in CO2 emissions compared to small towns with incipient suburban sprawl.

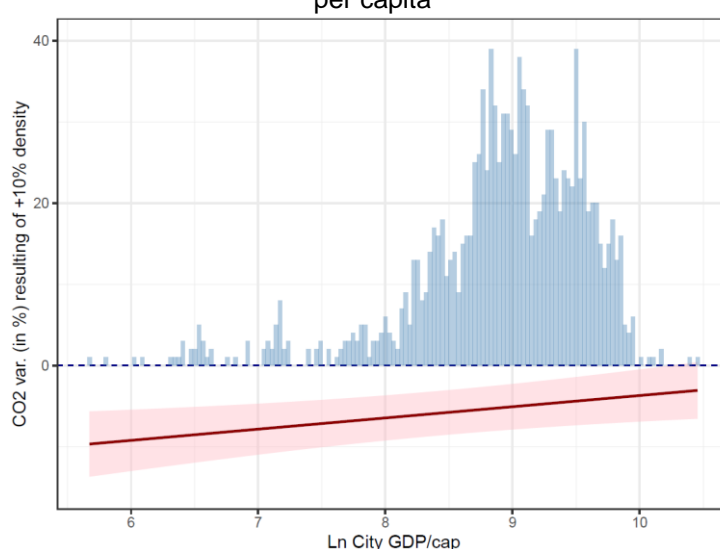
Figure 22. The heterogeneous effects of density and suburban ratios on CO2 emissions as a function of city population



Note: These plots are based on Column 2 of Table A.3. of the Appendix. Blue histograms depict the distribution of city population across the sample

When interacted with city GDP per capita, the magnitude of the reduction in CO2 emissions delivered through higher density is also moderated, indicating that higher density has a relatively less powerful effect on CO2 emissions for cities with higher levels of GDP per capita. For cities displaying the lowest values of GDP per capita in our sample, the impact of a 10% increase in density can be as considerable as a 10% reduction and reaches close to 3% for the cities with the highest GDP per capita. This differentiated impact may be linked to the fact that spatial patterns become relatively less powerful in reducing emissions when cities become richer, as consumption and affluence develop into major drivers of CO2 emissions. Nonetheless, the CO2 density effect remains negative and statistically significant for almost the entire sample of cities, highlighting the importance of spatial patterns across the full spectrum of development levels. Regarding the suburban ratio, interaction with the GDP per capita turns insignificant from a statistical point of view, suggesting that the CO2 elasticities attached to suburban ratios are not strongly differentiated by city GDP per capita.

Figure 23. The heterogeneous effects of density on CO2 emissions as a function of city GDP per capita



Note: This plot is based on column 3 of Table A.3. of the Appendix
The blue histogram depicts the distribution of the GDP/cap across the sample.

5.5 Projecting regional urban emissions under different spatial expansion scenarios

The projections of CO₂ emissions presented previously unveil how differentiated spatial expansion model could lead to diverging CO₂ emissions pathway for a given city. For a given average city, the compact spatial expansion model can reduce emissions by 12 percentage points compared to the passive spatial expansion model. However, during the period 2000-2015 only 10% of the cities in my sample followed a compact spatial expansion. This suggest that a profound shift to prevailing urbanization patterns is required to meaningfully alter future urban emissions aggregated at the regional level.⁴³ This is all the more true than subsection 5.4.2 (*Heterogeneity of CO₂ elasticities across the sample of cities*) has evidenced that the benefits of a compact expansion are heterogeneous across the sample of cities, with higher density producing non-significant effects for cities exceeding 1 million persons. Since cities with a population above 1 million persons concentrate approximately 57% of regional urban emissions, a large share of regional urban emissions is likely to remain unaffected by changes to density and the aggregated regional benefits that could be obtained from shaping cities spatial expansion remain unclear.

To provide a prospective view of regional urban emissions, in this last section, I conduct a back of the envelope calculation to project CO₂ emissions for the entire sample of cities. In the same spirit than the city-level projection performed in the previous section, these aggregated projections are not intended to be a forecast of regional urban emissions in 2030. These projections rather seek to illustrate how regional urban emissions could evolve under different spatial expansion scenarios. To this end, I contrast a Business-as-Usual (BaU) scenario with a “compact expansion” one. Under the BaU, cities prolong urbanization dynamics prevailing over the period 2000-2015 until 2030. Under the compact expansion scenario, I assume that approximately half of the cities in my sample harness their spatial expansion more efficiently and follow a dynamic close to the one observed under the compact expansion model (as opposed to only 10% of the cities following this model of expansion during 2000-2015).

The compact expansion scenario represents a marked departure from historical urbanization patterns and illustrates how altering the spatial distribution of future urban population can facilitate a transition towards a low carbon pathway. Assumptions and

⁴³ In this subsection, the term “regional urban emissions” is employed to refer to the sum of city-level emissions for the seven countries of interest.

details of the two scenarios are provided in the next subsection. The last subsection discusses more in-depth the results of these projections.

5.5.1 The Business-as-Usual VS the compact scenario

To project urban emissions up to 2030, I use the STIRPAT modelling framework presented under the previous section. I assume that regional urban emissions will be mainly driven by three factors: (i) population growth, (ii) GDP/cap evolution and the (iii) joint evolution of density and suburban ratios. Projecting this set of variables for each individual city of my sample is a complex modelling task that is way beyond the scope of this thesis.⁴⁴ Instead, I conducted projections at an aggregated level by distinguishing three group of cities displaying relatively homogeneous patterns of spatial expansion. The potential evolution of CO2 emissions up to 2030 is therefore computed for each group of cities and imputed to the total emissions of each group in 2015, as shown below:

$$Em\ 2030 = \sum_{i=1}^3 Em\ 2015_i \cdot (1 + \Delta Em_i)$$

With: $\Delta Em_i = \beta_1 \Delta Population_i + \beta_2 \Delta GDPPC_i + \beta_{3i} \Delta Density_i + \beta_{4i} \Delta Suburban_i$

Where $Em\ 2030$ is the projected sum of CO2 emissions for all the cities over the seven countries of interest (i.e. *regional urban emissions*); $Em\ 2015_i$ the sum of CO2 emissions for the group of cities i the year 2015; and ΔEm_i the variation of CO2 emissions for this same group of cities between 2015-2030. ΔEm_i is obtained by summing the variations attached to each of the above-mentioned drivers.

CO2 elasticities are tailored to three groups of cities to account for the heterogeneous effects associated with suburban and density ratios. These three groups are as follows: “towns” correspond to urban settlements with a population below the median (i.e. below 105K); “intermediary cities” are settlements above the median but with less than 1 million persons; “big cities” are cities with a population exceeding 1 million habitants.⁴⁵ Each group of cities is representative of a “CO2 typology” at the city-level, meaning that for cities within the same group higher density or suburban ratios will produce relatively homogeneous effects. The previous section has evidenced, for example, that a 10% increase in density leads to almost a 7% emission reduction in small towns but produces non-significant effects for cities

⁴⁴ Recent studies such as Gao and O'Neill (2020); Schiavina et al. (2022) have projected the future expansion of urban land using assumptions about urban population and urban GDP as the main drivers of this expansion. This case study relies on a different research design and assumes that all these three dimensions (population, GDP and urban expansion) constitute drivers of CO2 emissions.

⁴⁵ Since the BaU scenario uses historical growth rates over 2000-2015, the 2000 median value is used to classify cities in 2015 and ensure that the growth rates are consistently applied to each group of cities. Due to the important urban growth experienced during the period 2000-2015, in 2015, approximately 62% of the cities are above the 2000 median value.

exceeding 1 million persons (see Figure 22). To account for statistical uncertainty, for each group of cities, elasticities are drawn from a normal distribution with a mean equal to the average of the coefficients attached to each group of cities and a standard deviation equivalent to the standard deviation of these same coefficients. That is, for towns, I randomly draw CO2 elasticities from a normal distribution with a mean equal to the mean of all coefficients displayed by cities between 50k and 105k and a standard deviation corresponding to the standard deviation of this set of coefficients. I repeat the process 5,000 times for each group of cities and the average elasticity along with its standard error for each group of cities is presented in Table 4. This procedure is useful to provide a range of likely variability in future CO2 emissions rather than coming up with a single point estimate. The elasticities for population and GDP/cap are held constant across the three groups of cities and set to 1.23 and 0.23, respectively. These elasticities are retrieved from column 2 of Table A.3. in Appendix of this case study.

Table 4. Tailored elasticities for each group of cities

<i>CITY CATEGORY</i>	<i>DENSITY ELASTICITIES</i>	<i>SUBURBAN ELASTICITIES</i>
TOWNS	-0.605 (0.032)	0.310 (0.0252)
INTERMED. CITIES	-0.414 (0.101)	0.461 (0.0798)
BIG CITIES	0.020 (0.133)	0.771 (0.107)

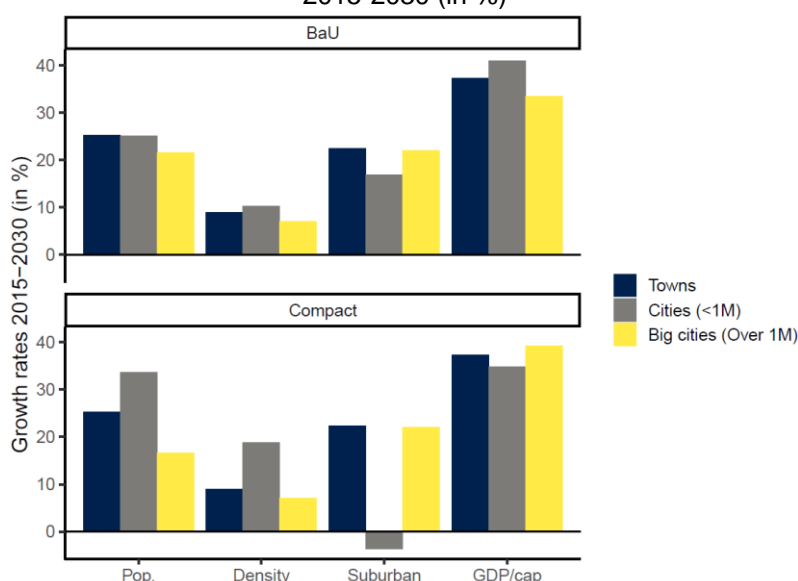
Note: Elasticities correspond to city-level CO2 responses to a 1% increase in density or suburban ratio. To account for statistical uncertainty, 5,000 elasticities are used for each group of cities. This table displays the mean elasticities used for each group along with the standard deviation of this elasticity indicated in brackets.

At the aggregated regional level, the evolution of cities' population and GDP/capita is assumed to be the same under both scenarios. Specifically, during 2015-2030, approximately 56 million new urban dwellers will settle in the cities of our seven countries of interest, implying an +21% increase -in line with trends observed during 2000-2015. Likewise, GDP/capita is expected to rise by 32% at the regional level, an evolution aligned to the rise observed over 2000-2015. The evolution of GDP and population at the aggregated regional level is the same across the two scenarios. As such, altering the growth rates for population and GDP at the regional level would change the absolute level of projected CO2 emissions but would leave unaltered the differences amongst the two scenarios. In fact, the differences of CO2 emissions are exclusively produced by a differentiated spatial distribution of the population within the cities (urban centres VS suburban areas) and across the urban system (big cities VS intermediary cities). This modelling choice implies that, at the aggregated level, the drivers of CO2 emissions are assumed to be independent. To put it differently, I consider that altering the spatial distribution of the population within and across the urban system will

not influence the aggregated evolution of urban GDP or population for the seven countries of interest. Of course, this hypothesis is very unlikely to hold for each individual city in the sample but, at the regional level, relocation and spillover effects can potentially compensate and average-out differences observed at the city-level. More importantly, this modelling framework was chosen to better illustrate the regional differences implied by changes to spatial expansion patterns *everything else being equal*. Because the sample of cities I am using is large enough (635 individual cities), I deem this framework adequate for regional projections, although I acknowledge that it should better incorporate the interrelationships between these drivers if results were needed at a finer level of spatial aggregation (e.g. cities, provincial or country level).

Under a scenario where everything remains the same, I used the 2000-2015 average growth rates of each group of cities to project the evolution of CO2 emissions up to 2030. To ensure the adequacy of the proposed approach, before projecting CO2 emissions until 2030, I have projected CO2 emissions from 2000 up to 2015 using these average historic growth rates for each group of cities. I found that projected emissions in 2015 are in the same order of magnitude than observed emissions (see Appendix for more details). In this BaU scenario, the increase of urban population has therefore been calibrated according to the average of historic growth rates for each group: 25% for towns and intermediary cities and 21% for big cities (upper panel of Figure 24). Likewise, density and suburban ratios as well as the evolution of GDP/cap converge to the average growth rates observed under each group during 2000-2015 (upper panel of Figure 24). It is important to underscore that, under the BaU, none of the group of cities displays a decrease of the suburban ratio concomitant to a rise of density -a pattern that would define a compact expansion. This is consistent with the fact that, over the period 2000-2015, only a limited number of cities has displayed a pattern of compact expansion.

Figure 24. Evolution of the main drivers of CO2 emissions under the BaU VS the compact scenario, 2015-2030 (in %)



Note: The absolute increase in population and GDP/cap at the aggregated regional level is the same in the two scenarios, although it is differently distributed across the three group of cities in each scenario. Rates used for the BaU correspond to the historic average for each group of cities while rates under the compact scenario assume that intermediary cities (<1M) follow a compact expansion model.

Under the compact expansion scenario, the spatial distribution of new urban dwellers is modified, both at the city-level (city centres VS suburban areas) and across the urban system (between the three group of cities). Under the compact expansion scenario, I assume that “intermediary cities” (i.e. urban settlement between 105K and 1millions persons) follow a compact expansion model. Consequently, it is assumed that this pool of intermediary cities will experience the population, density and suburban growth rates associated with the compact expansion model during 2000-2015 (see appendix for the growth rates associated to each spatial expansion model).

The compact expansion scenario entails two profound changes in comparison to the BaU. First, intermediary cities will receive a larger influx of new urban dwellers (+33% VS +25% under the BaU), which implies a redistribution of the new urban population across the group of cities since the overall urban population rise is maintained equal in the two scenarios. This stronger increase for intermediary cities was calibrated by assuming a lower increase for the group of “big cities”.⁴⁶ This redistribution of the population across the urban system is therefore meant to illustrate what would happen if people and firms relocate out of the overcrowded megalopolises and move into intermediary cities potentially less congested and more liveable. The second important difference under the compact scenario relates to city-level features: in this scenario, intermediary cities are expected to expand in a compact

⁴⁶ In practice, the number of additional persons needed to produce a +33% increase in this group of intermediary cities was retrenched from the influx of new population allocated to the group of “big cities” under the BaU.

fashion, which means that new urban dwellers settle principally within urban centres, producing a dramatic increase in density (+18,8%) accompanied by a reduction of the suburban ratio (-3.6%). It is important to note that neither a reduction of the suburban ratio nor an increase in density of this magnitude have been observed for such a large group of cities during the period 2000-2015.

5.5.2 Projected regional urban emissions and contribution of each driver

Results unveil how aggregated urban emissions could be significantly shifted if the distribution of the urban population within the city and across the urban system is altered. Under the BaU, the mean of the 5,000 projections indicates that regional urban emissions soar by 51%, increasing from 446 million of tonnes (Mt) in 2015 to 674Mt CO₂ in 2030. Under the compact expansion scenario, regional urban emissions are also expected to rise but are consistently projected at a lower level, with the mean projection reaching 656Mt CO₂ in 2030, or an increase of approximately 47% compared to 2015 levels. On average, the compact expansion scenario could thus deliver a “carbon saving” of almost 19Mt CO₂ in relation to the BaU (see Figure 25). Additionally, a t-test confirms that the difference in means between the two distributions is not equal to 0. In relative terms, the compact expansion scenario would lead to a 2.7% reduction of CO₂ emissions relative to the BaU. This potential reduction is to be compared to the collective objective set out by the countries of the region through their NDCs: a 22% unconditional reduction of GHG emissions relative to the BaU. These results therefore evidence that altering the spatial distribution of future urban population can facilitate a transition towards a low carbon pathway. However, in both scenarios, the increase of CO₂ emissions is higher than the increase of cities’ population, notably because GDP/capita continues rising and everything else is maintained constant. This implies again that complementary measures to decarbonize the energy matrix or alter mobility patterns will be required. The last chapter discuss the complementarity between a compact expansion and low-carbon urban mobility more in detail.

Figure 25. Projected regional urban emissions in 2030 under a BaU VS a compact expansion scenario

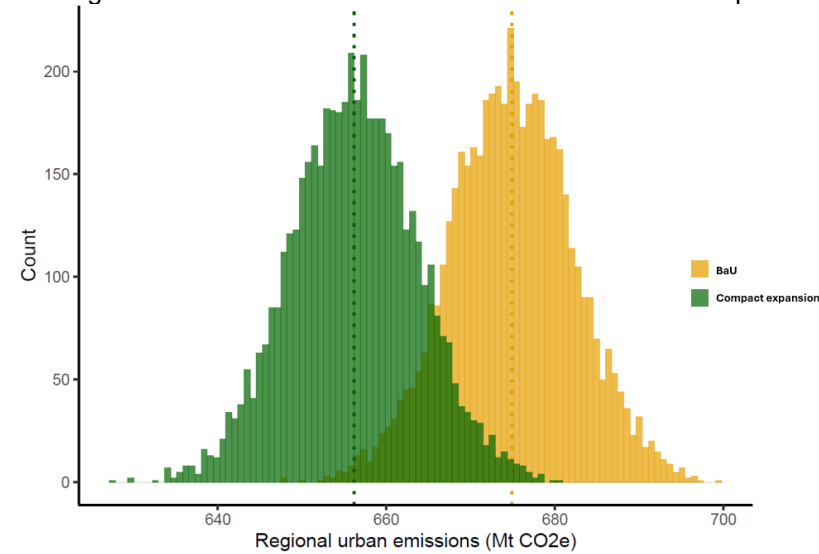
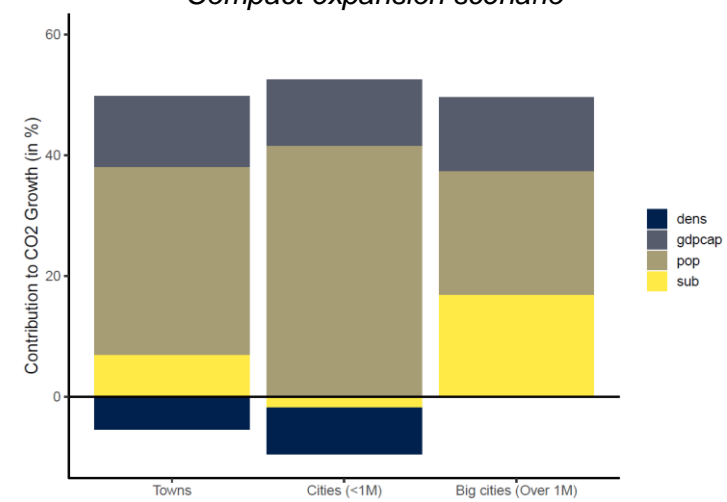
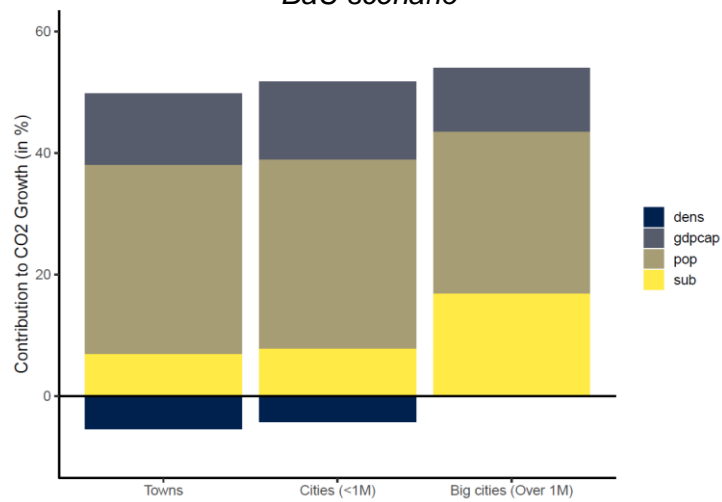


Figure 26. Contribution of each driver to the evolution of CO₂ emissions, by group of cities, 2015-2030 (in %)
BaU scenario *Compact expansion scenario*



Breaking down results by group of cities reveals insightful differences between the two scenarios. Figure 26 plots the contribution of each driver of CO₂ emissions for each group of cities. To ease interpretation, I only plot the mean contribution of each driver over the 5000 scenarios. Under the BaU, for the three group of cities, population and GDP per capita represent powerful drivers of CO₂ emissions, jointly accounting for 67% to 76% of emissions variations. Consistent with the heterogeneous density effects highlighted above, higher density only contributes to reducing CO₂ emissions for towns and intermediary cities. Big cities are projected to increase their density levels by 7.1% on average, although this evolution will produce indiscernible effects in terms of CO₂ evolution. Eventually, suburban expansion contributes to further escalate CO₂ emissions for each group of cities, although effects are considerably more pronounced for big cities where this driver boosts emissions by almost 17%. It must also be underscored that, for the three group of cities, the rise of emissions associated with the increase of the suburban ratio (i.e. a faster increase of the population in suburban areas relative to urban center) is never fully compensated by the reduction of emissions obtained through higher density. Again, these contradictory effects evidence the complex interrelationship between density and suburban expansion and the need to consider both dimensions to properly account for city-level emissions.

Under the compact scenario, the contribution of each driver is modified for intermediary and big cities. By construction, for towns, this contribution remains unaltered. On the other hand, intermediary cities are projected to receive a larger influx of new urban dwellers, exacerbating the contribution of population growth to CO₂ emissions. In this alternative scenario, population becomes by far the most important driver of emissions for intermediary cities, representing more than 60% of the variations of emissions in this group. Interestingly, since intermediary cities are assumed to better harness their spatial expansion, they experience a reduction of their suburban ratio (i.e. population in urban centres grows faster than in the suburbs), which in turn produces a negative contribution of the suburban ratio to CO₂ emissions. Likewise, under compact expansion, intermediary cities raise their density, which contributes to further reduce CO₂ emissions. The exacerbated contribution of population growth to CO₂ emissions is therefore more than compensated by the notable reductions associated with higher density and lower suburban ratio. As a result the net increase of CO₂ emissions for intermediary cities in the compact scenario is slightly below the one observed under the BaU (42% VS 47%, respectively). Finally, for big cities, population growth is less important than in the BaU, which is consistent with the calibration described above. This results in a lower contribution of population growth and a slightly higher one for GDP/cap, with each driver boosting emissions by 21% and 11% respectively. Since the spatial expansion patterns of big cities is assumed to remain unchanged, the contribution of the

suburban ratio is equal than under the BaU. Overall, under this scenario big cities are projected to increase their emissions by approximately 52%, whereas this increase was projected at around 54% in the BaU. Although this might seem to be a minor alteration, this lower growth has a powerful impact on the overall evolution of regional urban emissions since big cities account for 59% of total urban emissions in 2015.

To conclude this prospective exercise, it is useful to clarify that the projections proposed are unlikely to materialize in practice. The BaU is probably overestimating CO₂ growth because urban population growth rates are likely to be lower in the future than during the period 2000-2015. This slower urban population growth is likely to happen because of (i) a less dynamic demographic expansion for some of the countries in the region, (ii) lower growth rates of urban population as countries get more urbanized. This slower urban population growth will mechanically reduce the growth of urban emissions. Similarly, the compact scenario implies a dramatic change to historical urbanization patterns, which are, by essence, processes hard to change quickly. As noted previously, the compact expansion model assumes that more than 300 cities will adopt this spatial expansion model, whereas in practice less than 70 have followed it during 2000-2015. More importantly, I have purposely left out of these projections the impacts linked to technological changes (the “T” component of the IPAT framework). In other words, the carbon intensity of the production process is assumed to remain constant until 2030 in all projections. This is an assumption that will not hold, as already evidenced by the fast reduction of the carbon intensity of GDP observed in recent years. In a nutshell, the level of CO₂ emissions projected under both scenarios is unlikely to be met in practice. These scenarios are to be viewed as useful tools to illustrate how regional urban emissions can evolve under different spatial expansion patterns.

5.6 Conclusion

This case study has developed a methodology to systematically assess city-level CO₂ emissions in seven Latin American countries. The proposed population-clustering approach has been used to define cities as a combination of urban centres and immediately adjacent suburban areas. Spatially distributed CO₂ emissions have been used to estimate city-level emissions resulting from fossil fuel activities occurring within cities' boundaries. The assembled data set shows that under the significant increase in urban population during the period 2000–2015, almost all cities have spatially expanded. However, three differentiated expansion patterns can be distinguished: (i) compact expansion, whereby new settlements occur mainly within the urban centre and city density increases over time; (ii) passive expansion, whereby increasing density is combined with faster suburban population growth vis-à-vis the urban centre population; and (iii) sprawled expansion, whereby the new urban population primarily settles in areas adjacent to the city and spatial expansion is intensified.

The STIRPAT framework was then used to build a spatial panel model and estimate CO₂ elasticities at the city level. City fixed effects were used to mitigate omitted variable bias concerns and isolate the effect of urban spatial expansion from population and GDP/capita. The inclusion of a spatial lag factor reveals that city-level CO₂ emissions are not only the product of standalone activities at the city level but also the result of interactions with a broader system of cities. Numerical findings indicate that a 1% increase in density, reduces CO₂ emissions by 0.58%, while a 1% increase in the suburban ratio increment emissions by 0.41%. These coefficients imply opposite CO₂ effects for most Latin-American cities, which have experienced a concomitant increase in density and suburban ratio. The net CO₂ impact of higher density at the city-level is thus uncertain and depends on the magnitude of these two opposite and interrelated effects.

Using these elasticities, regional urban emissions were then projected up to 2030 under a BaU and a compact scenario. Although the compact expansion scenario represents a marked departure from historical urbanization patterns, it evidences how altering the spatial distribution of future urban population can reduce aggregated CO₂ emissions by approximately 3%. Beyond these impacts, a more compact expansion of cities will be key to induce changes in urban mobility patterns or to limit the destruction of carbon sinks in the surroundings areas of cities. Although quantifying these second-round effects at the regional level entails more uncertainty, they illustrate how shaping structural features such as the spatial extent of cities can help triggering system-level changes.

5.7 Appendix

5.7.1 Additional Statistics

Table A.1 Summary statistic for the sample of city

	Mean	Standard deviation
Population	469,082	1,633,124
Density (Pers./built up area)	200	426
Density tradi. (pers/km2)	4,041	2,297
City-level emissions (1,000 tones CO2e)	703	2,560
GDP/cap (US\$ 2011)	10,246	5,314
Shape Index	2.07	0.92
Suburban Ratio	0.15	0.18

Note: This table reports values for year 2015

Table A.2 Mean growth rates over 2000-2015 under each urban spatial expansion model.

Scenario	Spatial expansion Growth Rate	Density Growth Rate	Suburban Ratio Growth Rate	Population Growth Rate	GDP/cap Growth Rate
Compact	8.0%	18.8%	-3.6%	33.7%	34.9%
Passive	10.5%	15.6%	20.8%	29.3%	36.9%
Sprawl	12.0%	-9.6%	34.0%	9.6%	46.9%

Note: These rates are used to project CO2 emissions for the corresponding scenario.

As noted in the main body of text, long-term analysis of CO₂ emissions entails significant uncertainty. A reanalysis of CO₂ emissions from fossil fuels, cement, land use and forestry over the period 1850-2021 was nonetheless conducted in Evans (2021) at the global level. Results are reported below to better apprehend the complexity of operationalizing the concept of “*common but shared responsibility*” in climate change.

Figure A.1. Cumulative CO₂ emissions from fossil fuels, cement, land use and forestry, 1850-2021.
Billions of tonnes of CO₂ (Gt)

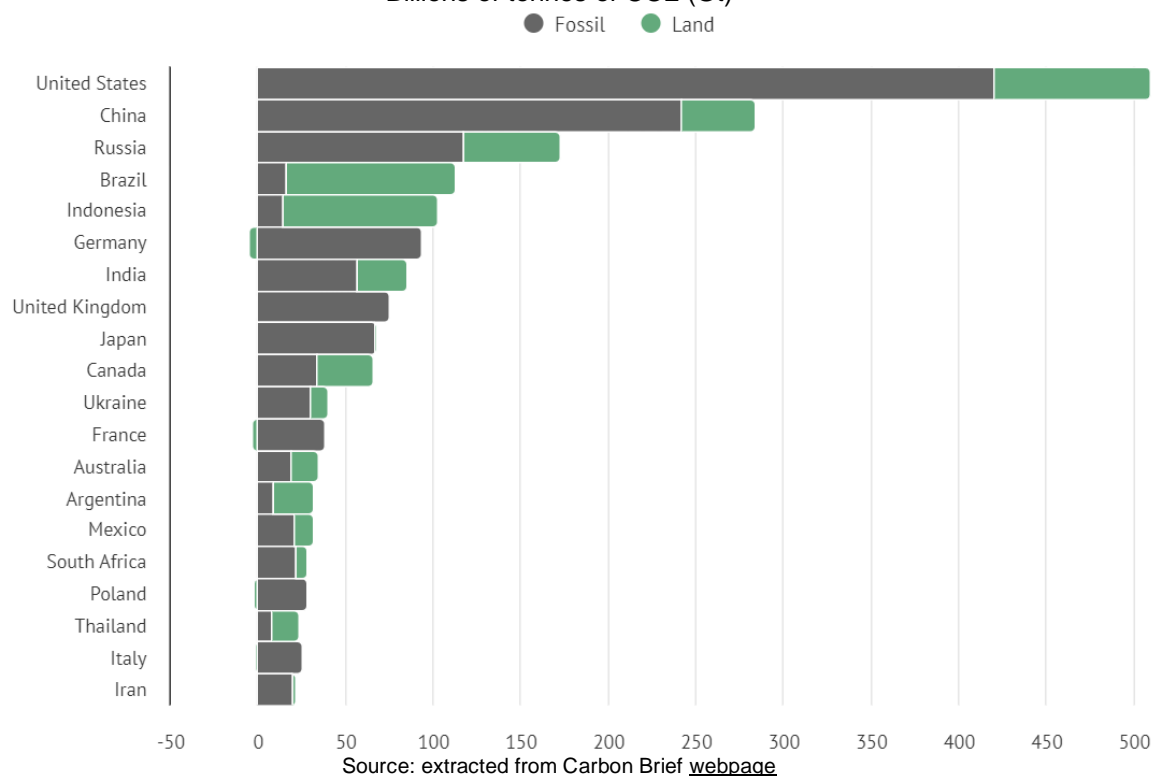


Figure A.2. The relationship between city GDP/cap and City CO₂/cap is also hinting at the absence of an EKC for CO₂ at the city-level.

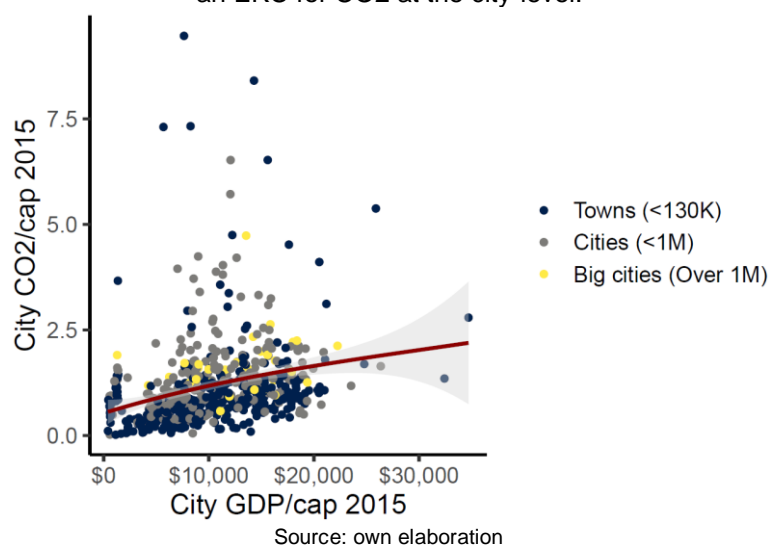


Table A.3. Econometric results of the regressions underpinning Figure 22 (column 2) and Figure 23 (column 3)

	<i>Dependent variable:</i>		
	Ln City Emissions		
	(1)	(2)	(3)
Ln Density	-2.49*** (0.91)	-2.46*** (0.89)	-1.75*** (0.48)
Ln Suburban	-1.85** (0.76)	-1.15 (0.72)	0.13 (0.37)
Ln City Pop	1.55*** (0.37)	1.23*** (0.36)	1.91*** (0.12)
Ln City GDPPC	0.04 (0.03)	-1.98*** (0.28)	-0.53** (0.22)
Sq. ln City GDPPC		0.12*** (0.02)	
Ln Dens: Ln Pop	0.17** (0.07)	0.17** (0.07)	
Ln Sub: Ln Pop	0.19*** (0.07)	0.13** (0.06)	
Ln Dens: Ln CGDPPC			0.14** (0.05)
Ln Sub: Ln CGDPPC			0.03 (0.04)
Observations	1,270	1,270	1,270
R ²	0.69	0.71	0.68
Adjusted R ²	0.37	0.41	0.36
F Statistic	228.29*** (df = 6; 629)	218.82*** (df = 7; 628)	223.09*** (df = 6; 629)
<i>Note:</i> *p<0.1; **p<0.05; ***p<0.01			

Note: For Section 5.5 we project regional urban emissions using the marginal effect associated to the mean GDP/cap in 2015 (i.e. US\$10,200). This marginal effect is estimated at 0.23.

5.7.2 Projection of regional urban emissions between 2000 and 2015

Although my objective is not to predict regional urban emissions in 2030, I test whether the proposed approach provides a fairly accurate estimate of the rise of urban regional emissions between 2000 and 2015 by projecting the level of emissions from 2000 to 2015 with the approach described in the main text and comparing this projection to the observed emissions in 2015. To this end, I use the parameters described in the main text and the average of the growth rates of each city comprised in each group of cities.⁴⁷ I then impute the estimated increase for each group of cities to the 2000 emissions of each group of cities. Following this approach, I obtained regional urban emissions in the range 397-403 (P25-P75) for the year 2015. In practice, regional urban emissions went up from 265Mt CO₂ in 2000 to 446Mt CO₂ in 2015. This implies that the median estimate of my projections stands at around 90% of the

⁴⁷ I have also tried to project emissions using the growth rates associated with each group of cities when all cities are pooled in their respective group (as opposed to the average of the growth rates of each city under a given group) but find a higher discrepancy with observed emissions in 2015.

actual level of regional urban emissions in 2015, which in the absence of additional data can be viewed as a fairly accurate projection.

Discrepancies between observed and projected CO₂ in 2015 can potentially come from three major sources: (i) I use the mean evolution of the drivers for each group of city as opposed to the actual growth rate experienced by each individual city; (ii) cities are classified in three groups and elasticities are calibrated to be relatively homogeneous across the set of cities, but further “typologies of cities” are probably required if we want to improve the accuracy of forecasts; and (iii) cities move across these “typologies of cities” between the 15 years that separate 2000-2015 and parameters should be adjusted in more dynamic way to improve accuracy of forecasts. As this is not the objective of this case study I rather focus on contrasting different policy scenarios and assessing the relative importance of each driver of emissions.

6 CASE STUDY 2: CITIES LAND COVER AND VULNERABILITY TO EXTREME RAINFALL EVENTS IN SEVEN LATIN AMERICAN COUNTRIES

A streamlined version of this case study has been published in the Journal [Global Environmental Change](#) (Cite score: 18.2; IF:8.9): The abstract of this paper is provided in the box below and the text is [available in open access here](#). Sections 6.1 of this case study and various elements in section 6.2 and 6.3 are not part of the published paper.

Abstract: Latin American cities are increasingly impacted by floods and this trend is likely to be further exacerbated under the combined effects of climate change and urbanisation. To reduce urban flood risk, green infrastructure and the ability to preserve and rehabilitate green spaces is often mentioned as an option to improve the hydraulic response of cities. Yet, little empirical evidence exists about the degree to which a greener city land cover can reduce the impacts of extreme rainfall on urban economic activity. Using earth observations from 630 cities across Latin America, this paper shows that extreme rainfall has a negative impact on urban economic activity, as proxied by cities' night lights. Importantly, it finds that this negative impact diminishes as city's land cover becomes greener: for cities where dense vegetation represents more than 20% of total city area, the marginal impact of extreme rainfall is broadly halved vis-a-vis cities below this threshold. A counterfactual analysis for the year 2015 suggests that increasing the greenness of 25% of the cities in our sample could have reduced losses by US\$ 6,500 million -equivalent to a 19% reduction of total estimated losses. These results evidence the benefits that a greener city land cover that makes room for green infrastructure can provide to adapt to more erratic rainfall patterns.

Full article reference:

Van der Borcht, Rafael, and Montserrat Pallares-Barbera. 2024. 'Greening to Shield: The Impacts of Extreme Rainfall on Economic Activity in Latin American Cities'. *Global Environmental Change* 87 (July):102857. <https://doi.org/10.1016/j.gloenvcha.2024.102857>

In Latin America, both the frequency and damages associated to floods have been on an upward trend. While, on average, 4 floods per year were reported during the 1960's, this number has been steeply rising to reach 13.8 floods per year during the decade of the 2010's and more than 22 per year during the first years of the 2020's (CRED, see Figure 35). Likewise, flood damages have been multiplied by almost seven to reach an average of US\$ 1,726 million per year during the decade of the 2010's (US\$ 2022 adjusted, see Figure 35).⁴⁸ Although these trends have been mainly driven by a steady expansion of population and assets into flood-prone areas (Jongman, Ward, and Aerts 2012), local flood impacts display considerable variations across locations. Flood risk is in fact to be viewed as the product of a complex set of interaction between hazard (i.e. extreme rainfall events), exposure (i.e. the presence of assets and persons in flood prone areas) and vulnerability (i.e. soil infiltration capacity, topography, flood protection infrastructure and other factors that influence the capacity to deal with extreme rainfall) (see Figure 11. Conceptual approach to risk and impacts).

In most cities of the region, this rising exposure to flooding has combined with a dramatic expansion of impervious soil surfaces, magnifying the impacts of extreme rainfall events. Over the period 2015-2018, South America is estimated to have experienced the fastest expansion of impervious surfaces among all continents (Sun et al. 2022). Looking forward, urbanisation is anticipated to continue across central and south America and could increase the extent of urban areas located in flood-prone areas by a factor 3.2 by 2030 (Güneralp, Güneralp, and Liu 2015). Thus, the future expansion of cities could not only increase the extent of persons and assets exposed to flood but also deepen the soil-sealing process already observed and further alter the rainfall-runoff process (see the literature review in Chapter 3).

Simultaneously, the hydrological cycle is expected to continue intensifying as climate warms, resulting in more frequent and/or severe extreme precipitation events in particular in wet regions (Tabari 2020). Projections from 33 models included under the CMIP-6 converge to the conclusions that maximum 5-day precipitations will increase for all Latin American subregions except South-Western America (see section 6.1 and IPCC, 2023). Under the combined effects of urbanisation and climate trends, flood impacts are likely to be further aggravated, in particular in urban centers and their surrounding areas (Dottori et al. 2018; Steinhausen et al. 2022).

⁴⁸ We acknowledge that this upward trend is likely to be partly driven by an improved capacity to collect data on disasters impacts over the years.

To confront these growing risks, GI have been frequently mentioned as an option to reduce urban flood impacts. An important strand of the literature relying on case-study analysis and hydrological modelling has shown that a greener land cover can improve the hydraulic response of cities (see Chapter 3). However, properly quantifying the value of GI remains a challenging task notably because little is known about the benefits of GI in terms of protecting assets and reducing economic disruption triggered by extreme rainfall events relatively. As a result, for most intermediate and small cities in Latin America, there is very little empirical evidence that determines the extent to which GI can reduce the effects of extreme rainfall on urban economic activity. Yet, GI could be particularly attractive to Latin American cities, which often display insufficient traditional flood control infrastructure and face complex maintenance challenges. The prospects of rising urban flood risk throughout the region only reinforce the urgent need to quantify the potential benefits associated with these interventions.

The proposed case-study seeks to fill this gap by assessing whether and to what extent differentiated land cover patterns can shape vulnerability to extreme rainfall event at the city-level. To fill this knowledge gap, this case study leverages the rapidly increasing literature that uses night-time light (NTL) satellite imagery to evaluate the impacts of adverse natural events on local economic activity (del Valle, de Janvry, and Sadoulet 2020; Kocornik-Mina et al. 2020; Mohan and Strobl 2017, among others). This source of data has proven particularly useful when studying the variations of local economic activity in urban areas (Gibson et al. 2021). In this case study, cities affected by extreme rainfall may presumably experience power outages, damage to streetlights infrastructure or even evacuation that lead to reduced or altered city night-light patterns. These changes in light intensity and distribution provide quantitative insights into the severity and duration of extreme rainfall impacts that can be used to proxy variations in local economic activity. Case study 2 therefore investigates (i) whether and to what extent extreme rainfall impact city NTLs and (ii) how a greener land cover in a city can change this relationship. Intuitively, because greener land covers facilitate rainfall absorption and enhance water infiltration, it is expected that cities with a higher proportion of green areas will suffer less economic impacts in case of an extreme rainfall event than those where land cover is almost exclusively made of impervious surfaces.

To empirically test this hypothesis, the definition of cities detailed in Chapter 4 is employed to delineate 630 cities across seven Latin American countries (i.e. Argentina, Brazil, Colombia, Chile, Ecuador, Mexico and Peru). Earth observations are then leveraged over the period 2013-2021, to gather key information on (i) rainfall patterns, (ii) urban economic activity, proxied through monthly night-time lights and (iii) impervious land cover features using NDVI composites. Eventually, fixed effect econometrics are used to assess the causal relationship

between extreme rainfall and NTL and examine how the greenness of city land cover can act as a mediating factor.

The results of this case study fall into three broad categories. This case study first contributes to the climate economy literature by documenting how extreme rainfall triggers negative and significant impacts on NTL at the city level, with the average extreme rainfall event estimated to reduce NTL/cap by 19.8%. Second, results reveal that this negative impact diminishes as city land cover becomes greener; for cities where dense vegetation represents more than 20% of total city area, the marginal impact of extreme rainfall is broadly halved vis-a-vis cities below this threshold. However, in none of the models the adverse effects associated with extreme precipitation are totally wiped out by a greener land cover alone. Eventually, the most important contribution of this paper relies upon the proposed valuation of the benefits that greener land cover could bring in terms of avoided losses. This valuation is conducted through counter-factual analysis. Specifically, I simulate an increase of the greenness index in 25% of the cities in our sample and compare NTL losses under this scenario with observed NTL losses without altering the greenness of the land cover. Leveraging the correlation between NTL and GDP, avoided NTL losses under this simulated scenario are then translated into monetary values. It is suggested that, in 2015 alone, losses could have been reduced by approximately US\$ 6,500 million (2015 constant), which is roughly equivalent to a 19% reduction of observed losses.

This case study is structured as follows: Section 6.1. discusses the evolution of the weather in the Latin American region over the past decades and analyse available climate projections for extreme rainfall events; Section 6.2. provides insights into my measurement of urban economic activity and discuss more in detail how extreme rainfall events are expected to alter this proxy. Section 6.3. provides descriptive statistics about the greenness of the land cover within the cities of my sample, while section 6.4. delves into the empirical estimation of the impacts of extreme rainfall on night-time lights. Eventually section 6.5. presents the simulation conducted to estimate the benefits of a greener land cover and section 6.6. concludes this case study.

6.1 Extreme rainfall in a changing climate: implication for Latin American cities

Under the effects of climate change, it is expected that the frequency and intensity of some hazards will be altered, increasing the probability of extreme weather events. The ultimate impacts of more frequent extreme weather events will be the result of a complex set of interactions between hazard, vulnerability and exposure conditions. To better understand how climate change is shaping flood risk in Latin American cities, this first section delves into historic weather patterns before presenting projected changes to rainfall patterns under different climate change scenarios. In doing so, it is important to underscore that this subsection focuses on the “hazard” component of risk (see Figure 11. Conceptual approach to risk and impacts in Chapter 3). It therefore leaves aside factors associated with exposure (e.g. the expansion of cities in flood prone areas) and vulnerability (i.e. the relationship between a given level of extreme rainfall and its impacts), which are addressed in the following sections.

An analysis of past weather patterns unveils that Latin America is already experiencing a change in climate. Following Dell, Jones, and Olken (2014), in this thesis, “weather” denotes the shorter-run variation of a given variable, while the word “climate” refers to its full distribution over several decades. Consequently, weather events depict a particular realization from a given climate distribution. In our case, the weather variables of interest are temperature and precipitation and would correspond, for example, to the specific temperature and precipitation in each city/month. The word climate is reserved for the corresponding probability distribution function of these variables over a period of 30 years.⁴⁹ Climate change therefore corresponds to a change in the temperature and precipitation probability distribution functions estimated over a period of 30 years. To be able to cover two consecutive periods of 30 years (i.e. a total of 60 years), I have compiled weather data from the Climate Research Unit (CRU) TS-V4.05.⁵⁰ This gridded climate raster gives monthly average temperatures (close to surface) and precipitation with a resolution of 0.5 degrees (approximately 56km × 56km at the Equator). Values are interpolated for each node of the grid based on meteorological stations and are corrected by elevation. To provide a refined view of potential weather impacts on human

⁴⁹ The World Meteorological Organization (WMO) recommends its country members to estimate “climate normal” for periods of 30 years and update these values every 30 years (Arguez and Vose 2011). This implies that climate normal parameters are calculated using a time span of 30 years. Climate normal parameters usually refer to mean and variance but other moments of the probability distribution can be relevant (Hsiang, 2016).

⁵⁰ These data are available at <http://badc.nerc.ac.uk/data/cru/>

systems, we weighted climate variables by population using the GHS-POP population grid for 2015.⁵¹

The underlying data sources used to acquire weather variables during the last 60 years differ from the ones used in the remainders of this case study, illustrating an important trade-off in earth observations analysis. In general terms, the finer the spatial resolution of an earth observation dataset, the shorter the time series. Precipitation data provided by the CHIRPS dataset, for example, have a spatial resolution of 0.05 degrees (approximately 5.6km × 5.6km at the Equator) but starts in 1981. Contrastingly, the data from CRU used in this subsection provides information back to 1900 but has a much coarser resolution (i.e. 0.5 degrees). In other words, the CHIRPS dataset might not be adequate to characterize “climate normal” and estimate the parameters of a given weather distribution because it does not (yet) cover 60 years of historical data; on the other hand, the coarse spatial resolution of the CRU database would not be accurate enough to perform sound city-level analysis. To try to address this tradeoff and provide a more comprehensive view of climate patterns, this subsection uses both datasets, although the remainders of this case study -in particular the statistical analysis- rely exclusively on the CHIRPS dataset.

There is strong evidence that the distribution of temperatures averaged by population has changed between 1961-1990 and 1991-2020. As shown in Figure 27, the more recent temperature distribution has been substantially shifted towards the right, with a regional average increase of 0.5 °C (from 22.7 °C to 23.2 °C). A t-test confirms that the difference in mean temperature between 1961-1990 and 1991-2020 is statistically significant. Interestingly, changes to temperature are spatially differentiated and of a different magnitude across geographies. Figure 28 shows the time evolution of annual average temperature by subregions between 1970-2020. Temperature increases are assessed by regressing yearly temperatures on a yearly dummy.⁵² All coefficients estimated through this linear regression are highly significant and indicate that the average annual temperature increases for Central America and the Caribbean are of 0.018 °C and 0.019°C, respectively, and “only” 0.011°C for South America. This implies that, during the 60-year period of analysis, in the Caribbean and Central America annual temperatures have increased on average by approximately 1.17°C, while this average increase has been limited to 0.67°C in South America. Consistent with global climate patterns, these estimates confirm that temperature increases are very

⁵¹ Data available at: https://ghsl.jrc.ec.europa.eu/ghs_pop2019.php

⁵² Concretely, I estimate the equation $T_{it} = \sigma_i + \varphi_i t + \mu_i$ for each subregion separately, with T_{it} representing the mean population-weighted temperature in subregion i in year t . The increase in the mean temperature is captured in each subregion by φ_i .

heterogeneous across the region, with regions with a warmer “baseline climate” experiencing a faster increase in temperature.

Although this case study does not investigate the effects of temperature evolution, these changes have been included because they are relevant for precipitation patterns and for extreme rainfall events. Indeed, the Clausius-Clapeyron relation suggest that, for every 1°C of increased air temperature, the water-holding capacity of the atmosphere rises by about 7%. More moisture is therefore available in a warmer atmosphere than in a colder one, creating heavier rainfall when precipitation forms. As temperature and precipitation can both affect economic activity, the exclusion of temperatures could bias our estimates. This is why a warmer climate is likely to increase the occurrence of extreme rainfall events. This relationship is also key to understand why, under a changing climate, a projected decrease in total precipitation levels can come along with an increase in heavy rainfalls or extreme rainfall events, potentially reinforcing the “*it never rains but it pours*” pattern already observed in some dry regions (Tabari 2020).

Box 6. Extreme rainfall events according to the World Meteorological Organization

“Extreme precipitation events often result, either directly or through associated floods, landslides and other phenomena, in fatalities, infrastructure damage and major agricultural and socioeconomic losses. [...] Since precipitation patterns differ widely throughout the world, it is not possible to use a single definition of the term “extreme precipitation event” that is suitable for all regions. Extreme precipitation events are also of interest on a wide range of timescales; for example, flash flooding is often driven by rainfall at very short timescales (minutes to hours), while large rivers and reservoirs often respond to rainfall at longer timescales of the order of several days. [...]

Therefore, an extreme precipitation event can be defined as a marked and unusual precipitation event occurring during a period of hours to a longer period of several days, with total precipitation largely exceeding local average conditions of that period. [...]

It is recommended that indices, based on local climatological conditions, be used to objectively characterize an extreme precipitation event. Thresholds can also be defined, departure from which can reflect the abnormal precipitation conditions and extremity of the precipitation event.

While fixed thresholds are more easily applicable for many purposes, percentile-based thresholds are more evenly distributed in space and are arguably more meaningful and applicable when sufficient observational data exist.”

Text extracted from WMO 2023, *Guidelines on the Definition and Characterization of Extreme Weather and Climate Events*, page 6-7

The distribution of historical precipitation does not show a significant shift towards the right and a t-test indicates that we cannot reject the null hypothesis of no difference in means between the two periods (Figure 29 left). Although the tails of the distribution seem to have become a bit fatter in the second period, we were not able to reject the null hypothesis of equality of variance under the Fligner-Killeen's test.⁵³ These statistically insignificant changes do not necessarily mean that precipitation patterns have remained unchanged at the local scale. In fact, these results could reflect some of the geographical features of precipitation data. Temperature is a rather continuous data across space that changes gradually across the territory. On the contrary, precipitations display higher spatiotemporal volatility and can abruptly change from one location to the other, particularly in complex topography and fragmented geographical landscapes. Aggregating these variables on a country/ annual basis is likely to produce limited impacts on temperature data but it can potentially create an "aggregation bias" for precipitation, with changes at the local scale or over shorter time horizon averaged out at higher level of aggregation.

Importantly, this case study investigates the effects of extreme precipitation events, which substantially differ from aggregated precipitations. As suggested by the WMO guidelines (see Box 6), extreme rainfall events can be viewed as a strong departure from mean local precipitations conditions during a period of hours to a longer period of several days. In this setting, as a first approximation to extreme rainfall events using the CRU dataset, I look at changes in precipitations anomalies measured as the differences between precipitation in one specific year and the mean precipitation between 1961-2020. To give a sense of the annual probability of experiencing a given level of anomaly, I have ordered precipitations anomalies by percentile under each sub-period (Figure 29 - right). For Latin America and the Caribbean, during the period 1961-1990, there was a 10% annual probability (i.e. 1-0.9) of exceeding a precipitation anomaly of 40mm (blue line in Figure 29 - right). During the 1991-2020 period, this 10% annual probability was attached to a precipitation anomaly of 55mm, meaning that the same precipitation anomaly in terms of probability of occurrence was associated with a slightly higher level of precipitations (green line in Figure 29 - right). Although the aggregated nature of the data here employed (country/ yearly basis) is not adequate to capture extreme rainfall events, it suggests that rare precipitation anomalies are already being characterized by more abundant rainfall levels.

⁵³ Both the F-test and the Levene's test deliver consistent results. The Fligner-Killeen's test was preferred because precipitation distributions seem to depart from normality.

Figure 27. Temperature distribution in Latin America and the Caribbean: 1961-1990 VS 1991-2020

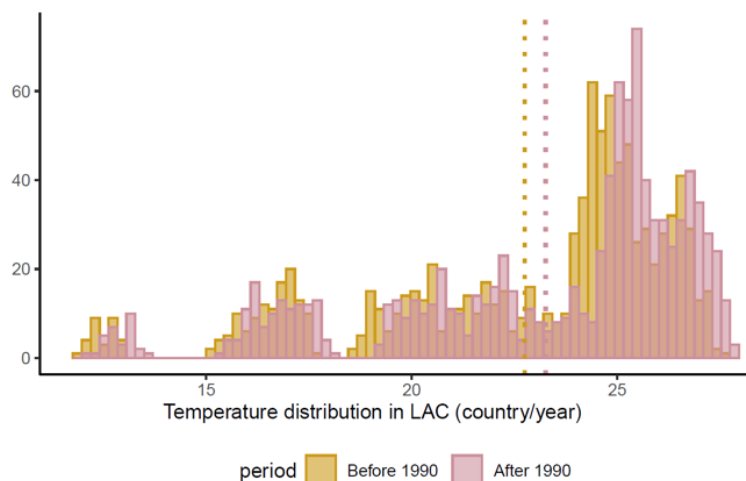


Figure 28. Time evolution of average temperature by subregions, 1961-2020

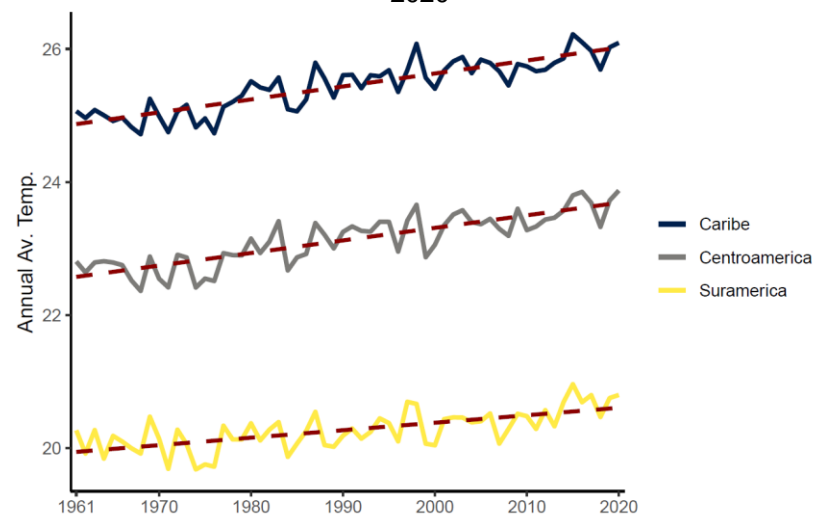
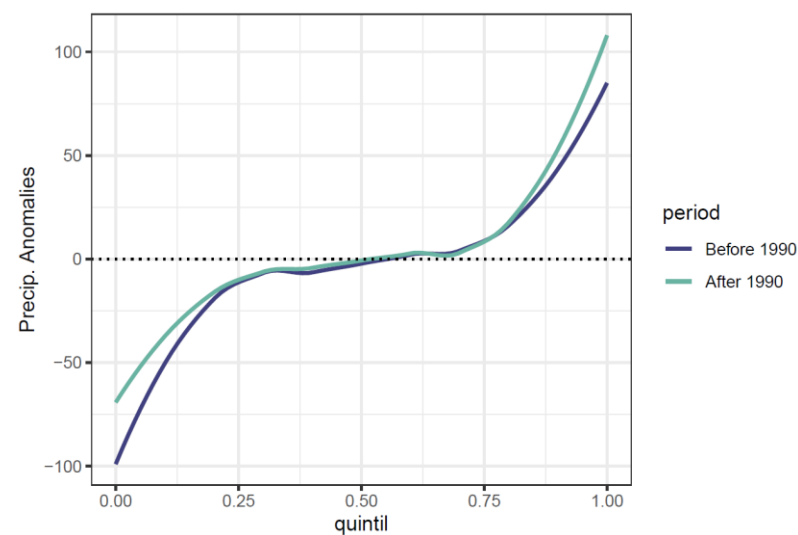
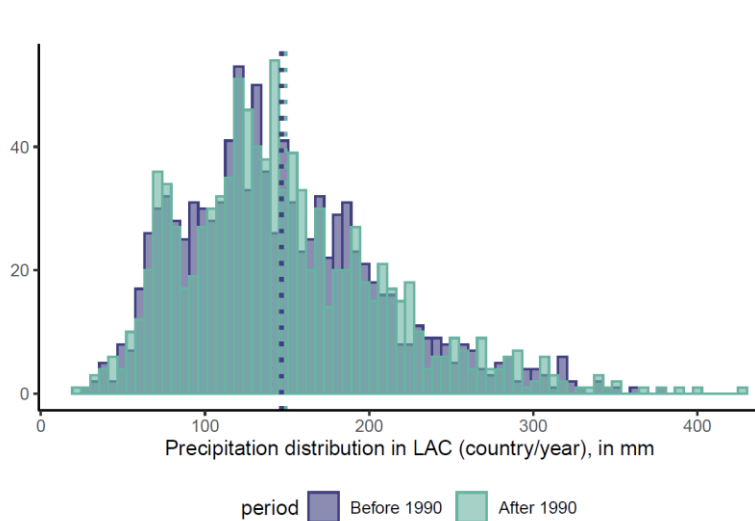


Figure 29. Changes in precipitation distribution (left) and probability of precipitation anomalies (right): 1961-1990 VS 1991-2020

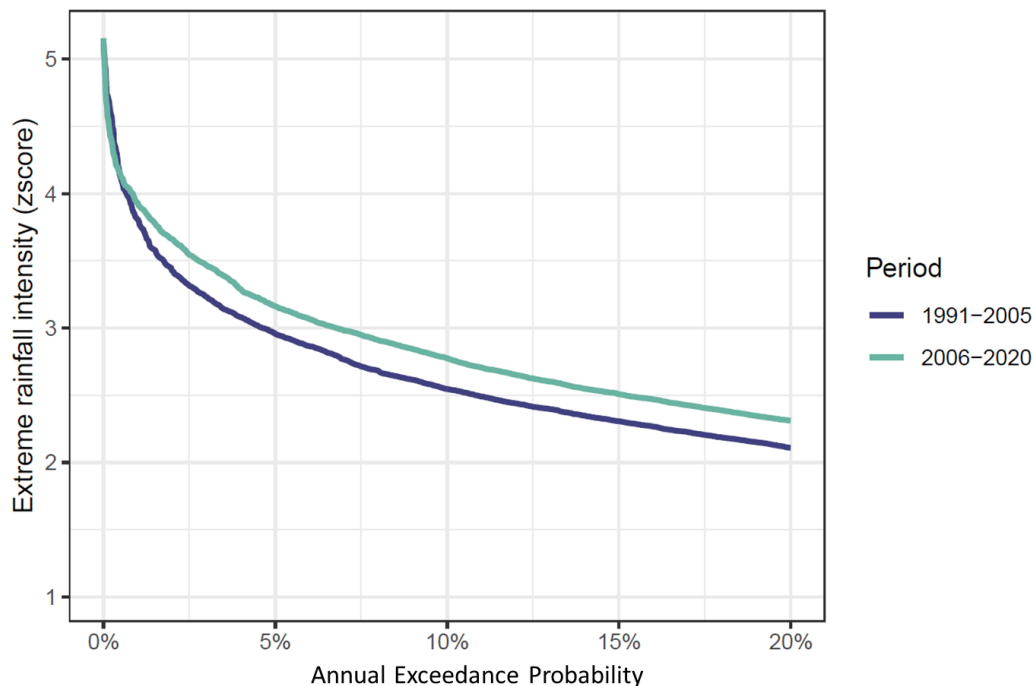


Source: own elaboration based on CRU.

To assess potential changes to the probability of occurrence of extreme rainfall events over the last 30 years, I used the dataset assembled at the city-level for this case study.

As explained in Chapter 4, section 4.2.2, precipitation data from CHIRPS have been normalized through the Z-score formula to enable comparisons across different climatological areas and facilitate the detection of extreme events, irrespective of the absolute precipitation levels recorded. This normalization is very important given the large diversity of climatological regimes covered by the case study. Monthly average precipitations range from 4,077 millimeters in December for the city of Goiania, Brazil, for example, to 26 millimeters in July in Guayaquil, Ecuador. City-level Z-scores were then used to detect extreme rainfall events. Extreme rainfall index corresponds to monthly city-level Z-scores meeting a double condition: a Z-score above two (i.e. local rainfalls are two standard deviations above the mean precipitation for a given month) and an overall monthly precipitation above 30mm. This double condition is employed to focus on tail observations during months where soil infiltration capacity is more likely to be saturated and where extreme rainfalls are therefore more likely to trigger damaging floods or other adverse impacts associated to landslides or other phenomena. Since the deviation from the mean is divided by the standard deviation, implicitly, the Z-score formula assumes that cities located in places with higher precipitation variance are better prepared to cope with extreme rainfall events than cities used to lower precipitation variability.

Figure 30. Intensity-Frequency curves of extreme rainfall events for cities across seven Latin American countries, 1991-2005 VS 2006-2020

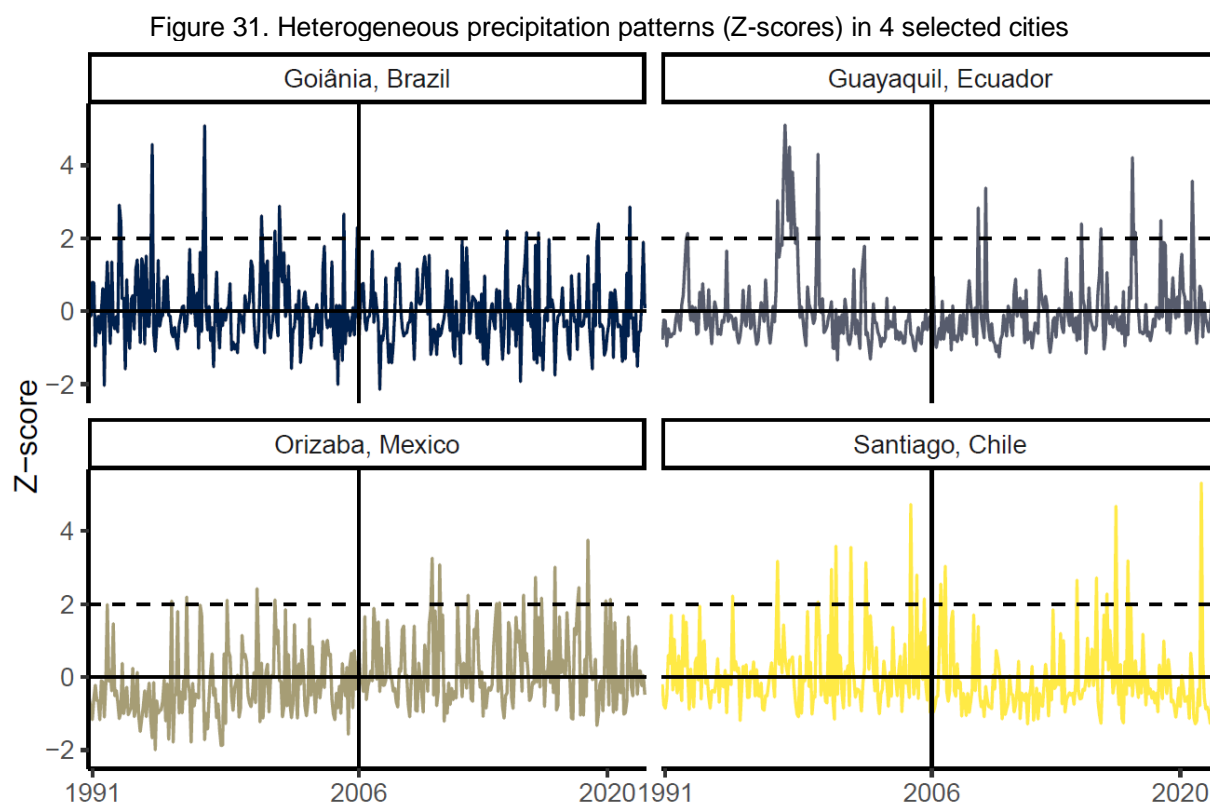


Source: own elaboration based on CHIRPS.

I then split the dataset in two equal periods of 15 years and computed intensity-frequency curves traditionally used in hydrological analysis. Although I acknowledge that these two 15 years subperiods are not long enough to define climate normal and apprehend a change of climate, I want to test whether a change in the annual exceedance probability of extreme rainfall events can be detected over a shorter time horizon. To this end, I estimated an empirical cumulative distribution function by ordering the maximum extreme rainfall events recorded in each city every year. This procedure allowed me to estimate the values of maximum annual extreme rainfall index at different percentiles of the distribution and, consequently, to infer the annual probability of having a city exceeding a given extreme rainfall index. As extreme rainfall events are, by construction, rare events, for most of the city/year observations, no extreme rainfall events were detected. Until approximately the 70th percentile of the distribution, the value of the extreme rainfall index is 0, meaning that, across the seven countries of interest, the annual probability of having at least one city experiencing an extreme rainfall event is less than 30% (1-0.70). Interestingly, as shown in Figure 30, this probability is differentiated between the two subperiods: during the period 2006-2020, there was a 29% annual probability of experiencing at least one extreme rainfall event, whereas this probability was below 23% during the first subperiod. Likewise, extreme rainfall events with a 1% annual probability of occurrence were more intense -in terms of Z-score- during the second subperiod (3.93 in 2006-2020 VS 3.81 in 1991-2005). To put it differently, even if this evolution is only incipient, over the last 15 years the distribution of extreme rainfall events affecting Latin American cities is already departing from precipitation patterns observed in the previous 15 years.

Even if, at the regional level, there is suggestive evidence that Latin American cities are already being impacted by more frequent and/or intense extreme rainfall events, this evolution is very heterogeneous across regions and geographies. The time evolution of precipitation z-score for selected cities clearly shows this heterogeneity (see Figure 31). The cities of Goiania, Brazil, and Guayaquil, Ecuador, have for example experienced Z-scores above 2 more frequently and of a higher magnitude during the first subperiod (1991-2005) than during the second half of the period. On the other hand, Orizaba in Mexico displays more frequent and higher Z-scores above 2 during the period 2006-2020, suggesting that extreme rainfall episodes have become more frequent and/or intense during recent years. Eventually, the city of Santiago de Chile displays a mixed pattern, with more intense extreme rainfall events during the second period but more frequent Z-scores above two during the first subperiod. Altogether, these differentiated patterns underscore how extreme rainfall events at the city-level might differ from aggregated precipitation patterns, highlighting the complexity of climate interactions at the local scale. This complexity is also leading to higher uncertainty in

precipitation projections under different climate change scenarios vis-a-vis the uncertainty of temperature projections.

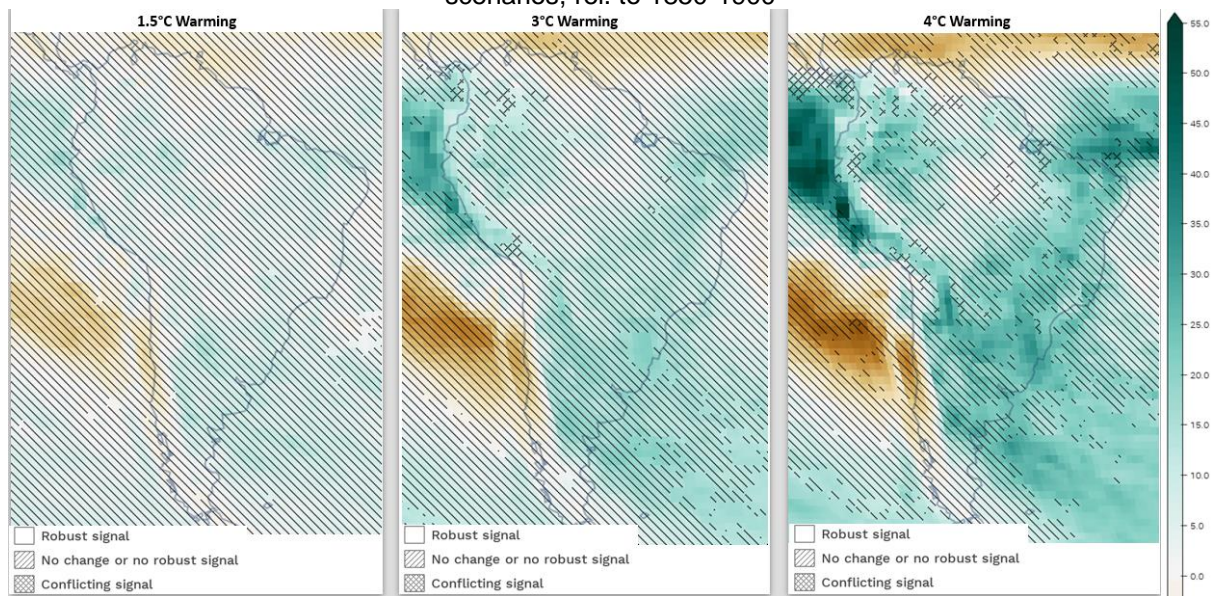


Source: own elaboration based on CHIRPS.

Looking forward, under a warmer climate, extreme rainfall events are projected to become more frequent, although the magnitude of changes is very heterogeneous across geographies. Projections from 33 models included under the Coupled Model Intercomparison Project — phase 6 (CMIP-6) converge to the conclusions that maximum 5-day precipitations as well as the maximum 1-day precipitations -which are commonly used to proxy extreme rainfall events- will increase for all Latin American subregions except South-Western America (IPCC, 2023). The magnitude of this increase is very heterogeneous across climate regions. Median estimates for a level of global warming equivalent to 4°C suggest that maximum 5-day precipitations could experience an increase of almost 24% in the South-Eastern American region or only 4.8% in Southern central America (see panel entitled *4°C warming* in Map 11⁵⁴).

⁵⁴ Map 11 summarize projections simulated through different Representative Concentration Pathways (RCPs) reaching the same level of global warming. RCPs describe different levels of greenhouse gases and other radiative forcings that could occur in the future, ranging from 1.9 to 8.5 W/m².

Map 11. Projected changes to maximum 5-day precipitations (in %) under different warming scenarios, rel. to 1850-1900



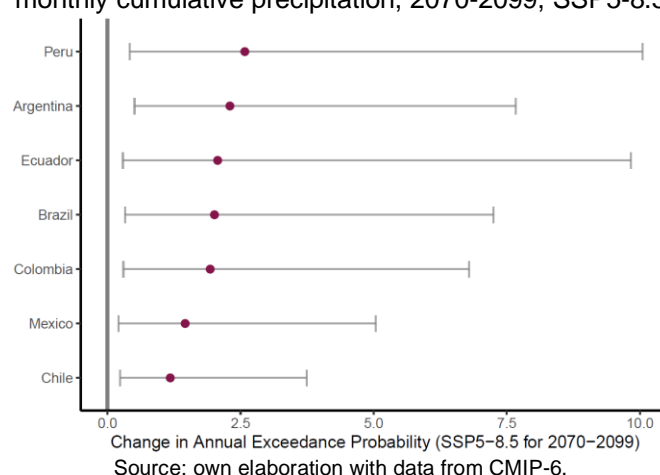
Source: Extracted from IPCC Atlas online.

It is important to stress that, following usual conventions in climatology, this thesis views climate change as a statistically significant deviation from the “natural variability” of a given weather variable. This “natural variability” is assessed in reference to the historical bounds provided by available meteorological records. Consequently, under low-warming scenarios, changes projected to maximum 5-day precipitations are usually within natural variability bounds. This explain why in Map 11 the entire region is classified as “no change or no robust signal” in the left panel entitled *1.5°C warming*. In fact, for South America, even under higher warming scenarios only selected areas along the grasslands of southern Brazil and northern Argentina or coastal areas of Ecuador and Peru strongly depart from this natural variability (areas classified as “robust signal” in Map 11). In other areas, projected changes remain consistent across climate models but are not robustly found to be outside of natural variability bounds. Maps of projected precipitations for the 1-day maximum precipitations or for central America and Mexico are not displayed but suggest a similar pattern: models included under CMIP-6 converge on the fact that maximum precipitations will increase, although they rarely found that this increase will represent a significant departure from historical variability. These results are likely to be linked to the limited historical hydrometeorological information available for large parts of the region. It is nonetheless important to mention it because it highlights the complexity of distinguishing climate change from natural variability, especially in data-constrained regions.

Considering uncertainty and data limitations exposed above, I provide high-level information on potential changes to the probability of occurrence of extreme rainfall events as defined in this thesis. To this end, I rely on projected changes to the Annual

Exceedance Probability of the Largest Monthly Cumulative Precipitation provided under CMIP-6 at the country level. Although I recognise that this metric differs from the extreme rainfall index computed for this case study, projections of monthly maximum precipitation data are used to give a sense of the potential alteration to the exceedance probability of extreme rainfall events.⁵⁵ Figure 32 presents projected changes to the 1% largest monthly cumulative precipitation as a change factor for the period 2070-2099 under SSP5-8.5.⁵⁶ Point estimates correspond to the median estimate and confidence interval span the 10th to 90th percentile estimates included under CMIP-6. These projections are to be interpreted as how much more frequent the 1% largest monthly cumulative precipitation will become. As such, according to the median estimate, the 1% largest monthly cumulative precipitation for Brazil, Ecuador and Colombia could become broadly two times more frequent by 2085 under SSP5-8.5. In statistical terms this implies that maximum monthly cumulative precipitations that, on average, are exceeded once every 100 years could be exceeded once every 50 years.

Figure 32. Change factor for the Annual Exceedance Probability of the 100-year return period largest monthly cumulative precipitation, 2070-2099, SSP5-8.5



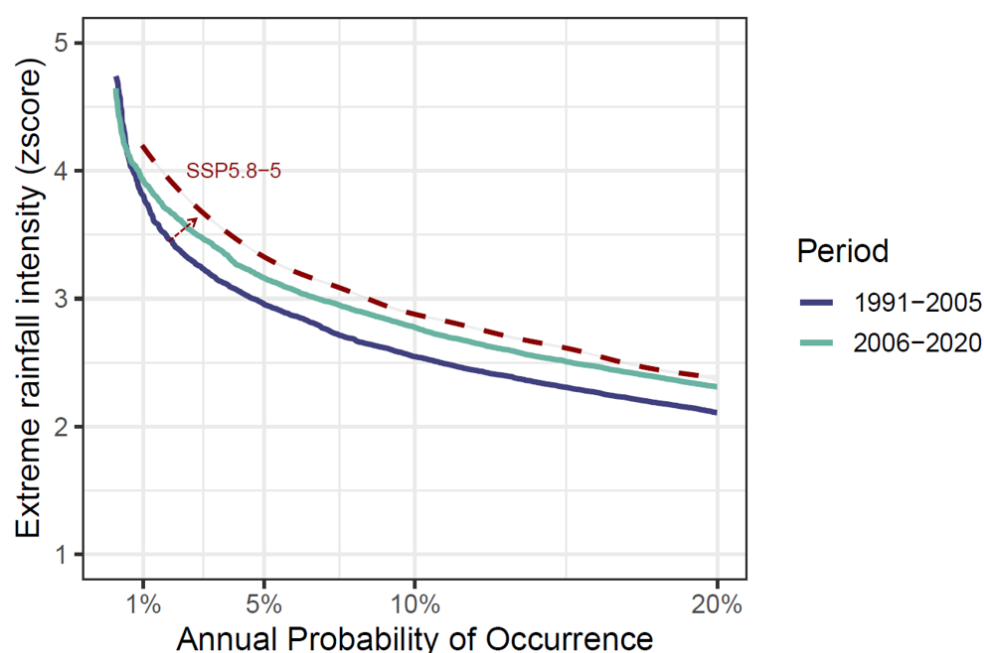
Finally, I performed a back of the envelope calculation to provide an illustration of what these evolutions could entail in relation to the historical intensity-frequency curves of extreme rainfall events. To this end, I used the median estimates of change factors available for selected return periods (i.e. 5, 10, 25, 50 and 100-year return periods) under SSP5.8-5. In the absence of robust estimates of change factors at the city-level, I used the spatial average for the land of each country and averaged these values across the 7 countries of interest. Yet, change factors could be very heterogeneous across different cities within the same country (see Map 11) and I acknowledge that proposed estimates do not capture this. Projected

⁵⁵ A larger monthly cumulative precipitation event will translate into a proportional increase of the extreme rainfall index if monthly precipitation average and standard deviation are not altered. Change factors to Annual Exceedance Probability are considered to be indicative of potential changes to the annual exceedance probability of extreme rainfall events depicted in Figure 30.

⁵⁶ These change factors were retrieved through the World Bank Climate Change knowledge portal, although the underlying source of data is still CMIP-6.

change factors have then been applied to the corresponding return periods empirically estimated over the period 1991-2021. Eventually, based on the new estimated return periods, I fitted an exceedance probability curve that is plotted in red in Figure 33. This new exceedance probability curve has been manually truncated at the 100-year return period (or 1% annual probability) since change factors for events above this return period are not available.

Figure 33. Illustrative shift to the Intensity-Frequency curves for extreme rainfall events under SSP5-8.5



Source: own elaboration with data from CHIRPS and CMIP-6.

These estimates are to be viewed as high-level projection at the regional level. They are directly reflecting estimates of global model output and should not be interpreted as location-specific projections of extreme rainfall event. In addition, since the underlying spatial resolution of climate projections is too coarse to provide robust estimates at the city-level, these estimates rely on median estimates from CMIP-6 and do not explicitly include uncertainty linked to climate projections. Despite these caveats, I believe that Figure 33 unveils an informative pattern. As the average change factors are all above 1, they shorten current return periods or, equivalently, result in a rise of the annual probability attached to a given level of extreme rainfall intensity. Consequently, the new exceedance probability curve is shifted towards the right. Yet this change is not uniform across return periods. For extremely rare events in the tail of the distribution (e.g. those with approximately a 1% annual probability of being exceeded), changes to exceedance probabilities are more pronounced, as denoted by the red arrow in the figure. Conversely, for extreme rainfall events with a 20% annual probability of being exceeded under historic climate patterns, projected changes are less marked -notably when compared to the 2006-2020 period. This exemplifies how, under high-warming climate scenarios, tail events are likely to experience a more notable increase in

frequency. This projected evolution stresses the need to better understand their potential socio-economic impacts to inform the design of climate adaptation policies.

Overall, this subsection has provided evidence that climate is already changing across Latin American cities. It also clarified how extreme rainfall events have been proxied and underscored the complexity to accurately measure and project these events, particularly in data-constrained regions. We now look at patterns of urban economic activity at the city level to better understand how these extreme rainfall events can impact urban economic activity.

6.2 Urban economic activity and extreme rainfall impacts

To assess how differentiated land cover patterns shape economic vulnerability to extreme rainfall, I first need to quantify the impacts of extreme rainfall events on urban economic activity. Properly quantifying the impacts of extreme rainfall on urban economic activity requires overcoming two traditional issues identified in the literature about the economic impacts of natural disasters. Firstly, I need to select strongly exogenous variables to characterize the “shock” associated to extreme rainfalls; secondly, a spatially disaggregated and frequent measurement of economic activity is required to capture impacts that are likely to be rather localized and potentially short-lived. This subsection first delves into these methodological aspects and then provides stylized facts about the night light time (NTL) dataset used in this case study.

Traditionally, the economic impact of natural disasters has been measured through an econometric approach that uses data on the impact of disasters (i.e. number of deaths, economic losses) as the main independent variable and some measure of economic development as the dependent variable. Yet, this approach is problematic from a statistical point of view. Data on the impact of natural disasters -as well as the selection and error measurements affecting these data- is, by essence, an endogenous variable: human and economic damages caused by disasters are functions of vulnerability levels of the affected area, which in turn depend on the level of economic development of these areas (see Felbermayr and Gröschl (2014) for a detailed discussion). A concrete example allows to illustrate this correlation. In January 2010, Haiti was struck by a powerful magnitude 7.0 M_w earthquake that is estimated to have killed about 160,000 persons and generated long-lasting effects on economic development. One month later, Chile experienced an even more powerful 8.8 earthquake but reported “only” 525 deaths and 25 missing, with relatively benign economic impacts. The Chilean earthquake was in fact the sixth strongest earthquake ever measured, approximately 500 times more powerful than Haitian seismic movement, unveiling how the impacts of natural disasters are not only linked to the severity of the natural hazard. Of course

the difference of reported impacts between Haiti and Chile can be explained by a wide range of factors but, in general terms, the level of economic development strongly correlates with data on disaster impacts and an identification strategy relying on data about the impacts of a disaster is likely to deliver biased estimates.

Given the above, in this case study, I have purposely rejected the use of data on flood-related impacts as an explanatory variable. Data on flood-related impacts is not only very scarce for most of the cities in my sample but, more worryingly, it is likely to suffer from endogeneity concerns: poorer cities are less likely to have flood protection infrastructure and could thus suffer more important effects from a given extreme rainfall event because they are poorer -not because of the severity of the extreme rainfall events *per se*. Instead, I built precipitation indexes to proxy extreme rainfall events, which have the advantage of being exogenous to economic development and are preferred in my identification strategy.

My extreme rainfall index seeks to capture potential floods or other hazardous phenomena such as rainfall-triggered landslides that can result in infrastructure damage or economic losses at the city-level. However, my precipitations indexes are not intended to be a perfect predictor of flooding nor to pinpoint the specific areas of a city that were flooded or affected by landslides. In fact, in urban contexts, at a fine spatiotemporal resolution (e.g. city district-daily basis), extreme precipitations events and floods impacts are unlikely to occur at the exact same location and same moment. The location and spatial extent of flooded areas are influenced by local factors such as topography, soil infiltration capacity, and drainage systems capacity -among others- which altogether can channel water runoff away from the location where the rainfall has been poured, generating a “spatial lag” between the location of extreme rainfall events and flooded areas when considering a fine spatial resolution. Likewise flooding materializes only after a significant amount of rainfall has been poured, generating a “temporal lag” between peak precipitations moment and flooding. In this case study, I intentionally worked at a relatively low spatiotemporal resolution to minimize the potential mismatch between extreme rainfall events and floods. I have thus opted for a city-monthly spatiotemporal resolution as opposed to districts /daily level for example. Although geo-referenced data on flood impacts is very scarce in the region, I cross check floods reported by Brakenridge (2023) with precipitation levels and found that out of the 28 urban floods reported in this dataset, precipitation were above normal during the same month for 90% of the cases, increasing my confidence in the use of rainfall-based index.⁵⁷

⁵⁷ As the data from Brakenridge (2023) only provides a set of coordinates for each flood event I arbitrarily created a buffer of 6 km around each point. If this buffer intersects the extent of my cities the event is considered an urban flood.

Regarding the measure of economic activity -the dependant variable- another classical issue found in the literature is linked to the fact that losses arising from floods are inherently local and often short-lived. To avoid “averaging out” flood impacts using highly aggregated data, granular data on local economic activity is required (see Strobl 2011 for a comprehensive discussion of this issue). To address this challenge, an increasing number of authors has resorted to nighttime lights (NTL) data to detect damages and power outages in the aftermath of flood events (Zhao et al. 2018; Levin and Phinn, 2022) or quantify the impacts of hurricanes, typhoons and floods on local economic activity (Elliott et al., 2015; Mohan and Strobl, 2017; del Valle 2020; Kocornik-Mina, 2020). Following this rapidly increasing literature (detailed in Chapter 3), this case study uses the VIIRS dataset to proxy local economic activity at the city-level. The monthly frequency of this NTL data source is crucial to capture relatively short-term disruptions such as the one triggered by urban floods. To reduce the potential spatiotemporal mismatch between extreme rainfall and flood impacts indicated above, I performed a zonal sum of NTL pixels located within city extents. This zonal sum also allows me to mitigate the high volatility displayed by monthly VIIRS NTL dataset at the pixel level.

Beyond these statistical considerations, the VIIRS NTL dataset offers unique insights about extreme rainfall economic impacts. NTL variations are potentially picking up two kinds of impacts triggered by extreme rainfall events: (i) power outages and (ii) direct destruction of city light infrastructure. Although it is impossible to distinguish between these two effects with the data that I have, capturing both effects provides a comprehensive view of the impacts of extreme rainfall on urban economic activity. In fact, these two channels represent very different economic impacts in nature: one denotes a direct destruction of physical and productive assets whereas the other is associated with disruption and indirect losses linked to interrupted activities, foregone revenues or higher costs. As explained in Box 7, I argue that for large extreme rainfall events, urban economic activity could be more strongly impacted through indirect losses and disruptions that undermine agglomeration economies than through damages to assets that reduce the available stock of capital. This position NTL data as an even more relevant source of information to accurately capture the economic impacts of extreme rainfall in urban settings.

This case study is therefore designed to assess economic vulnerability to extreme rainfall understood as the causal relationship between an exogeneous precipitation-based index and a variable proxying economic activity at the city-level. In doing so, I am not examining the specific nature of the disaster associated with extreme rainfalls. In practice, extreme rainfall is more likely to trigger flash floods but they could also result in landslides or even other disasters and this case study does not explicitly discriminate the nature of the disaster. On the other hand, NTL data aggregated at the city-level capture both the direct

impacts of extreme rainfalls (i.e. destruction of city light infrastructure) and indirect impacts associated with power outages. This approach is not adequate to (i) pinpoint the specific area of the city most damaged in the aftermath of a disaster nor to (ii) capture impacts not correlated with NTL variations, such as the loss of natural capital and biodiversity or more indirect and long-term effects linked to e.g. human health or education. However, the identification strategy underpinning this case study is well suited to quantify the relationship between a measure of extreme rainfall and city-level nighttime lights.

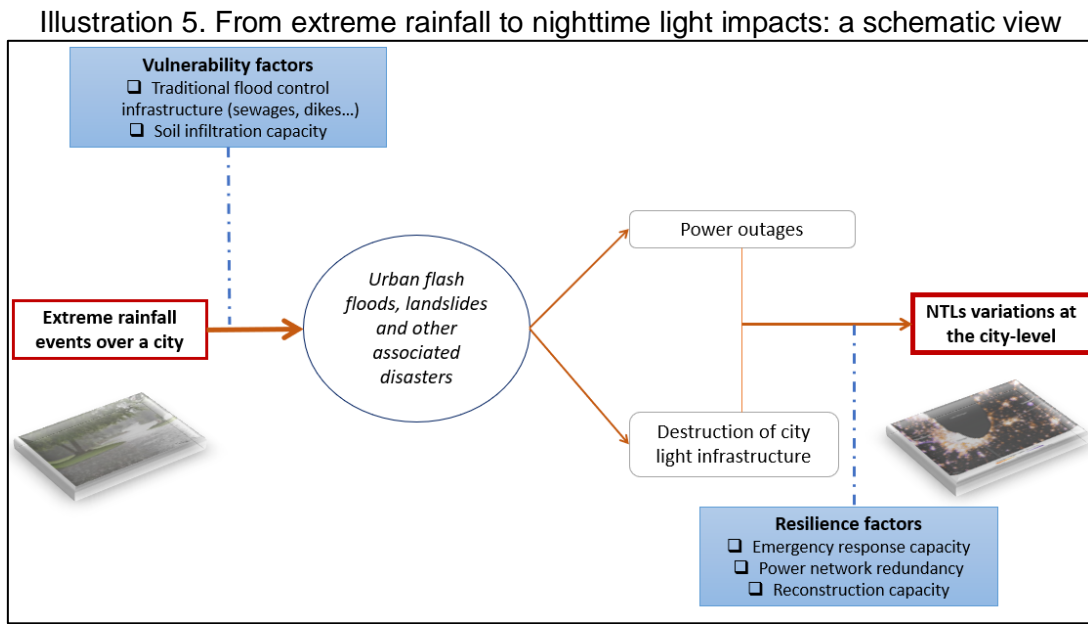
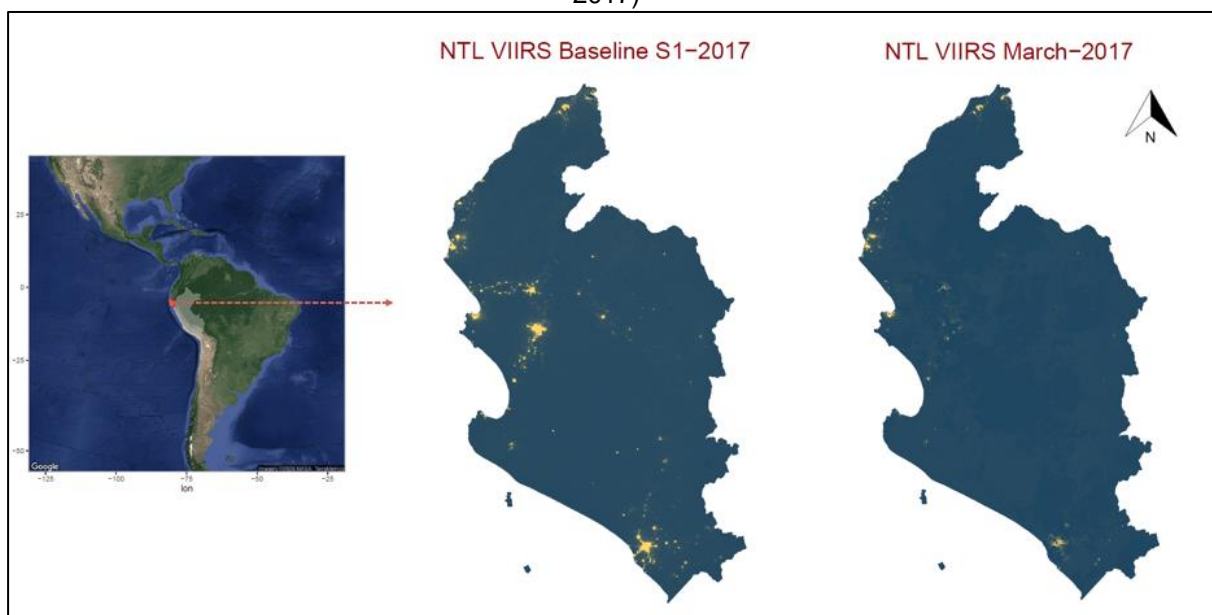


Illustration 5 recap the main channels through which extreme rainfall may affect city NTLs, highlighting how vulnerability and resilience factors mediate this relationship. Conceptually, the model assumes that structural vulnerability factors such as soil infiltration capacity or the presence of flood protection infrastructure will have a direct impact on the magnitude and intensity of a disaster triggered by extreme rainfall events. In turn, once a disaster has struck a city, resilience factors linked to the capacity to respond to the emergency, quickly repair city infrastructure as well as the presence of power network redundancies will determine the magnitude and time during which city-level NTLs deviate from the trend. Both vulnerability and emergency and resilience factors govern the final effect of extreme rainfall on city NTLs. In practice, in this case study, I estimate a reduced form of this model by quantifying the relationship between NTL and extreme rainfall *ceteris paribus* and investigate the heterogeneity in this relationship with respect to vulnerability factors linked to the greenness of the city land cover.

Intuitively, one would expect city-level NTLs to experience a reduction during and/or in the aftermath of an extreme precipitation event. A quick visual examination of different

cities experiencing extreme precipitation events, and for which a flood had been reported, seems to confirm the expected pattern. In March 2017, the northern coastal areas of Peru experienced heavy rainfalls exacerbated by the El Niño conditions prevailing at that moment. Severe floodings and landslides were reported in various locations in the provinces of Piura, Tumbes and Lambayeque. According to EM-DAT (CRED), these disasters left 184 deaths and damages estimated at more than US\$ 3,700 million. To illustrate how nighttime lights fluctuate during this event, Map 12 plots the VIIRS NTL in the three above-mentioned provinces during the March 2017 and contrasts them with baseline NTL in the same provinces. Baseline NTLs were constructed by averaging NTLs during the first semester of 2017 (excluding March 2017). A quick visual examination gives a sense of the magnitude of impacts that these disasters have generated, particularly in cities that appear as the most lit areas in the NTL baseline map. Worryingly, these northern coastal areas of Peru are the one expected to experience the largest increase of extreme rainfall in the region as climate changes (see Map 11), increasing the likelihood of having to face more frequent extreme rainfall events such as this one. The subsequent econometric analysis leverages these variations to estimate the causal impact of extreme rainfall on NTL.

Map 12. Nighttime lights in northern coastal Peru during the March 2017 flooding (baseline VS March 2017)



Source: own elaboration based on VIIRS NTL; basemap GADM and Nasa Terrametrics (left panel).

Figure 36, unveils a similar pattern in two specific cities for which urban flood have been reported. According to Brakenridge (2023), the city of Governador Valadares (in Brazil) experienced flooding from 23rd December 2013 to the first weeks of January 2014. As can be observed in Figure 36, during the following months a significant reduction of NTL/capita has been recorded. In the case of Santiago (in Chile), the flood reported from the 15th to the 18th of April 2016 seemed to have exacerbated a drop in NTLs that started before the flood.

Interestingly, for Santiago, two other extreme precipitation events were detected during the two-year period of this visual analysis and seem to have also been accompanied by a drop of NTLs. Overall, for both cities, NTL/capita reached their lowest level over a two-year period in the aftermath of the reported flood. Although the high volatility of NTL/capita makes it difficult to isolate the effects of extreme precipitation from other variations, this visual examination constitutes suggestive evidence that extreme precipitation could result in a deviation of NTL/cap from baseline trends.

The statistical analysis in section 6.4 of this case study robustly assesses whether NTLs deviate from their trend in the case of an extreme rainfall event and properly quantify this effect by isolating it from other factors. As detailed in Elvidge et al. (2017), VIIRS monthly NTL values correspond to the mean of the values recorded during daily cloud-free observations. My city sample displays an average of 9 days of cloud-free coverage per month, although there is high volatility in the number of cloud-free observations for specific locations (see Appendix to this case study, which provides descriptive statistics regarding the distribution of cloud-free observations). One important concern is therefore linked to the reduction of cloud-free observations during the months where an extreme precipitation event is detected. With a Pearson's coefficient estimated at 0.32, the correlation between the number of cloud-free observations and NTL values warrants a cautious approach. Indeed, the decrease in NTL values during months where cloud-free observations are reduced (i.e. months with numerous days of high cloud-coverage) could confound the estimation of extreme rainfall impacts, as NTL reduction presumably linked to damage or power outages could, in fact, be driven by higher cloud-coverage. While I cannot fully isolate variations in NTL values due to higher cloud-coverage from factors linked to power outages and damage to infrastructure, I argue that if the monthly variation linked to cloud-coverage commonly impacts all cities within a given area, it can be at least partially captured by a country-monthly fixed effect (see Appendix C for more details).

Box 7. The impacts of extreme rainfall on urban economic activity from a conceptual standpoint

To fix ideas, let's assume that economic activity at the city-level can be apprehended through a standard Cobb-Douglas function as follows:

$$Y_t = Z_t K_{t-1}^\alpha L_t^{1-\alpha}$$

Where Y_t is the output in period t , K and L are capital and labor inputs, respectively, and Z_t is the Total Factor Productivity (TFP). To approximate the growth rate of the output in the case of a given shock, we derive the log-transformed equation above. Formally, this corresponds to:

$$\ln Y_t = \ln Z_{y,t} + \alpha \ln K_{t-1} + (1 - \alpha) \ln L_t$$

$$\frac{\Delta Y}{Y} = \frac{\Delta Z}{Z} + \alpha \frac{\Delta K_{t-1}}{K} + (1 - \alpha) \frac{\Delta L}{L}$$

Assuming that labor is maintained constant, we can simplify the above to:

$$\frac{\Delta Y}{Y} = \frac{\Delta Z}{Z} + \alpha \frac{\Delta K}{K}$$

$$\Delta Y = \Delta Z_{y,t} + \alpha (\text{Asset losses}_y)_t$$

Extreme rainfall can thus impact the production function through two channels: (i) asset losses, which corresponds to damaged and destroyed capital in relation to the total stock of capital (i.e., the term “*Asset losses_y*” above); (ii) a decrease in TFP (i.e., the term $\Delta Z_{y,t}$ above), which can arise, for example, from business disruptions and associated foregone revenues or higher operating costs. In other words, extreme rainfall not only reduce the total stock of capital of an urban economy, but also its productivity. This effect is perfectly illustrated through the example of damages to transport and energy infrastructure: if bridges are washed away by torrential rains and power services interrupted, economic impacts will be higher than the value associated to lost bridge or power generation facility. Disruptions to energy and transport networks will reduce the productivity of business and assets relying on this infrastructure -at least until connectivity is restored. Under the proposed framework, this indirect effect can be viewed as a TFP shock. Implicitly, this indirect effect implies that assets affected by extreme rainfall include key TFP-enhancing infrastructure (i.e. airports, roads, power infrastructure).

Importantly, extreme rainfall impacts on urban economic activity can be particularly acute when disruptions triggered by these events undermine agglomeration economies -one of the major sources of productivity increases in urban areas. Indeed, agglomeration economies require efficient supply chains and logistics networks to facilitate the movement of goods and services within and outside the urban area. Empirical observations have shown that extreme rainfall can significantly disrupt these logistics networks, leading to increasing transportation costs and times, ultimately impacting the productivity and competitiveness of businesses operating within the city, even if these businesses are not directly impacted by extreme rainfall. Extreme rainfall can also force firms to temporarily suspend operations, weakening the potential synergies and spillovers that occur within clusters of related industries. Intuitively, one could assume that the more severe the extreme rainfall event, the larger these indirect productivity effects. This is consistent with the non-linear relationship between natural disasters and economic output outlined by Hallegatte and Vogt-Schilb (2019): for extreme events, indirect losses and TFP effects become larger and more pregnant, eventually compounding initial damages and amplifying the overall economic impacts associated to catastrophic disaster.

In summary, not considering indirect impacts that can potentially undermine agglomeration economies and reduce TFP at the city-level could lead to strongly underestimate the overall impacts of extreme rainfall on urban economic activity. This, again, lead me to prefer NTL variations to characterize extreme rainfall economic impacts rather than data on flood-related damages in terms of destroyed assets.

Another concerning feature of NTL observations is the high volatility of monthly values.

Given the underlying process for constructing VIIRS NTL monthly composites, it is frequent that for a given pixel in a given month very low values or even a value of 0 are recorded whereas this same pixel was recorded as intensely lighted in the month before and after. Consequently, at the pixel level, very large monthly variations rates can be frequently displayed. These variations are very case-specific and there is no single explanation that could elucidate them. Some of these variations could be linked to flood, while other could be linked to the varying cloud-coverage mentioned above or other power outages and contextual factors that result in NTL variations (see Elvidge et al. 2017 for a comprehensive discussion). In any case, it is hard to make sense of variations of these magnitudes from an economic point of view. To smooth variations I have therefore used a zonal sum but I acknowledge that this high volatility is concerning and warrants careful considerations when performing analysis at the pixel level.

Given all the above, I processed the NTL VIIRS as detailed in Chapter 4, Section 4.2.2.

Specifically, I performed a zonal sum of all monthly pixels located within urban centres of each city identified through the Degree of Urbanization approach. Importantly, suburban areas that were considered for the first case study of this thesis are here disregarded because they would noise both our NTL and greenness measurements. For NTL, suburban areas introduce very low and highly volatile NTL pixel values; considering these areas in the computation of my greenness index also includes a higher share of bare soils, potentially biasing the NDVI measurements. Following Elvidge et al. (2017), I further cleaned the dataset from very low cloud-free coverage observations, by removing 22 cities that, on average, had less than 3 days of cloud-free observations per month, over the period considered. To further address the airglow issue noted by Uprety et al. (2017), I manually set negative NTL values to '0', which represented 0.1% of total observations.⁵⁸ I then restricted my sample to cities that have experienced at least one extreme rainfall event during the period 2013-2021. The final panel comprised 630 cities observed over 108 months (i.e. 9 full years).

Finally, this case study assumes that urban NTL VIIRS correlate well with overall GDP levels and can be employed to translate a variation of NTL into a monetary variation.

This assumption is in line with previous studies that have used this correlation to proxy economic outcomes in data-constrained regions (X. Chen and Nordhaus 2015) or give a monetary valuation of the impacts associated with natural disasters (del Valle et al. 2020).

⁵⁸ The underlying processes for constructing VIIRS NTL cleans the raw data captured by the satellite to remove noise and direct light from the moon or sun. This process is automated and follow a methodology where an amount is deducted from the raw value of the lights. This process is sometimes affected by airglow and deducts an amount exceeding the value of captured light, resulting in negative NTL values.

Before conducting the analysis proposed in this case study, I have tested this assumption in the context of my seven Latin American countries of interest.

Table 5. The relationship between City NTLs and GDP

	<i>Dependent variable:</i>	
	GDP <i>OLS</i>	Ln GDP <i>panel</i> <i>linear</i>
	(1)	(2)
Yearly NTL	42.99*** (1.55)	
Ln Yearly NTL		0.89*** (0.03)
Observations	63	63
R ²	0.93	0.94
Adjusted R ²	0.92	0.93
F Statistic	764.49*** (df = 1; 61)	806.75*** (df = 1; 53)

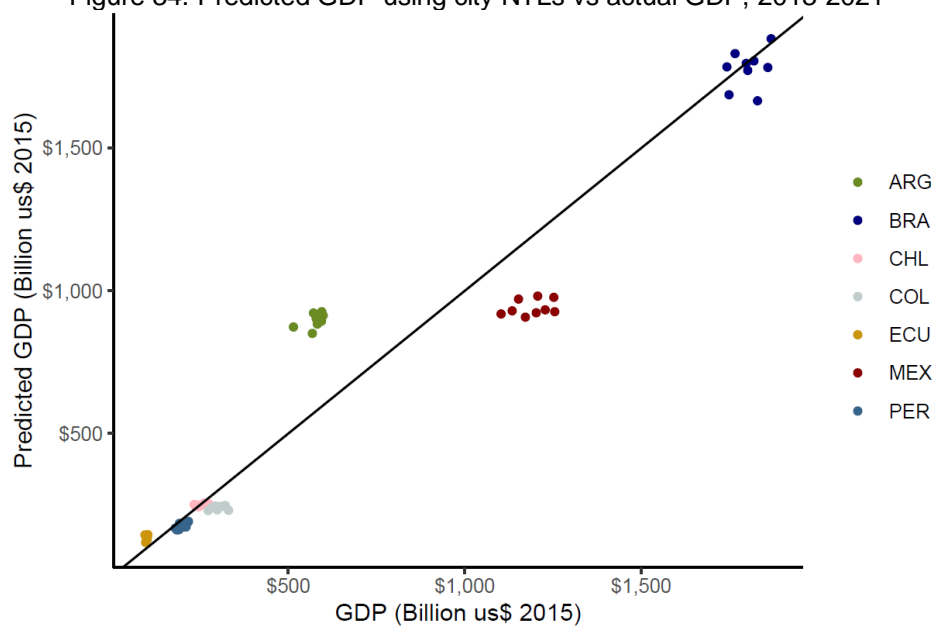
Note: * p<0.1; ** p<0.05; *** p<0.01

Source: own elaboration

To impute GDP variation associated to a given change in city NTL, I had first to aggregate my city-monthly NTL sample at the national-annual level for which the GDP of my seven countries of interest was available. To this end, I computed the mean annual NTL value for each city of my sample by averaging the monthly NTL values of my original sample. I then summed mean annual city NTL values at the national level. These national-annual NTL values over the period 2013-2021 are then regressed against the GDP values of each country expressed in 2015 US\$ constant and extracted from the World Development Indicators of the World Bank. I used both a linear regression (col 1 of Table 5) and a yearly fixed effect with a log-log relationship (col 2 of Table 5). In both cases, the coefficient of interest is highly significant as well as the R-squared. This regression is by no means intended to be interpreted as a causal relationship. It simply seeks to establish a conversion factor between national city NTLs and GDP.

To ensure that this regression is accurate enough to derive monetary values, I use the coefficient of column 1 Table 5 to predict GDP through city-level NTLs. Results are plotted in Figure 34. A perfect prediction of GDP values would deliver a plot where all points are aligned to the 45-degree line. As can be seen, predicted values are quite close to the 45-degree line, indicating that NTL variations are indeed a good predictor of GDP variations in my region of interest. Under the simulation presented in section 6.5.2 of this case study, the results from the regression displayed in column 1 of Table 5 will be used to translate NTL variations into a monetary value.

Figure 34. Predicted GDP using city NTLs vs actual GDP, 2013-2021



Source: own elaboration with data from VIIRS NTL and World Bank.

Figure 35. Evolution of flood frequency and damages in Latin America, 1965-2022 (5 year moving average)

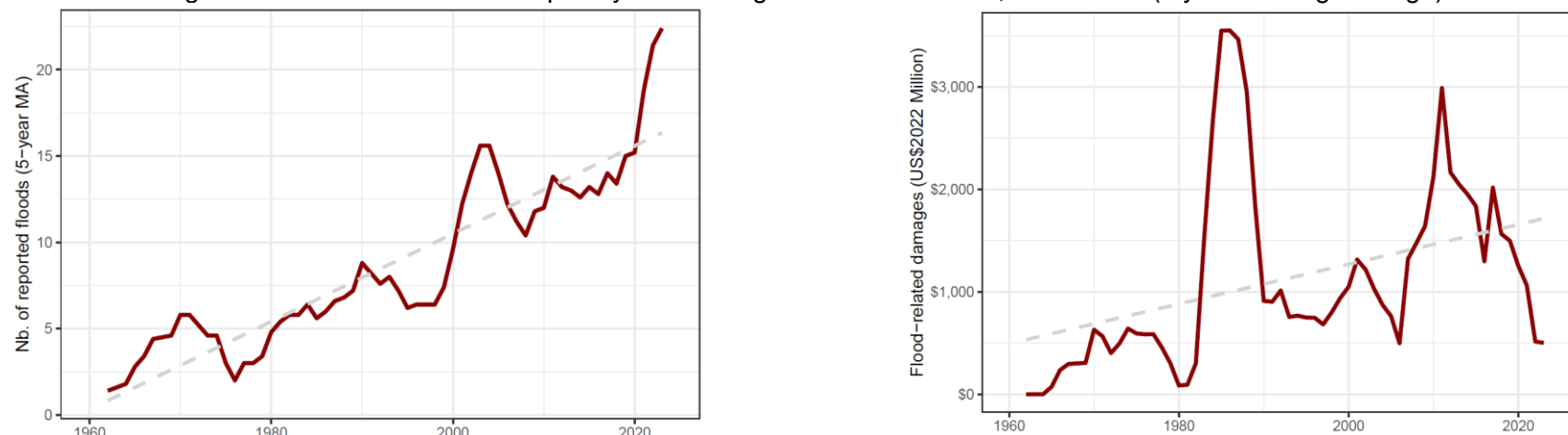
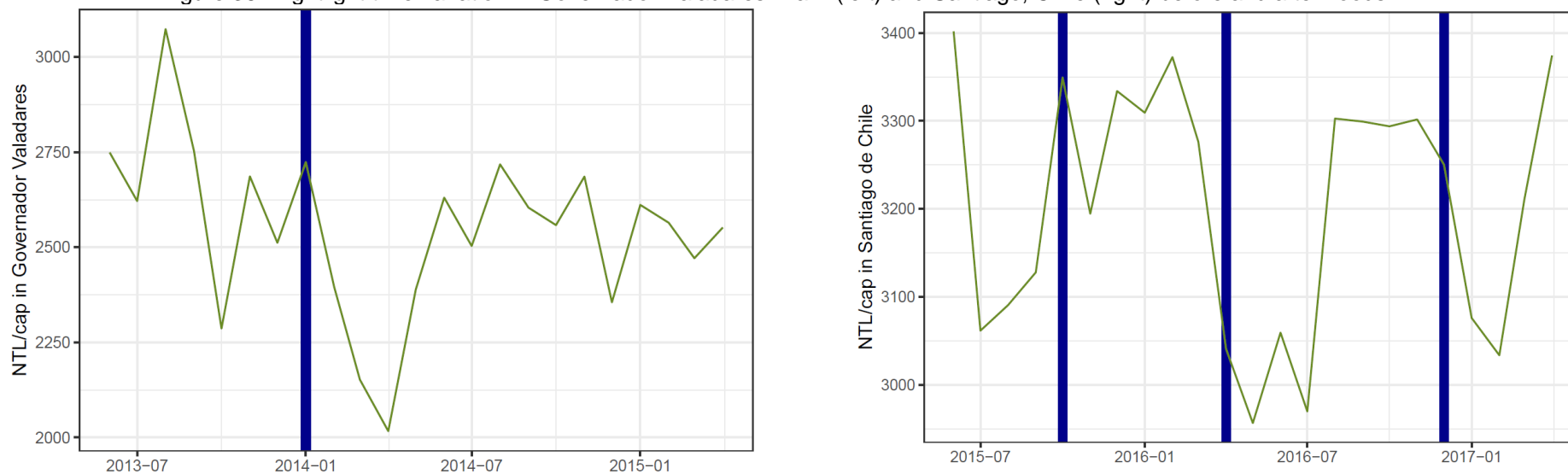


Figure 36. Nightlight time variation in Governador Valadares Brazil (left) and Santiago, Chile (right) before and after floods



Note: the blue bar denotes the occurrence of an extreme rainfall event.
Source: own elaboration based on CRED (above) and VIIRS (below).

6.3 The greenness of the land cover within Latin American cities

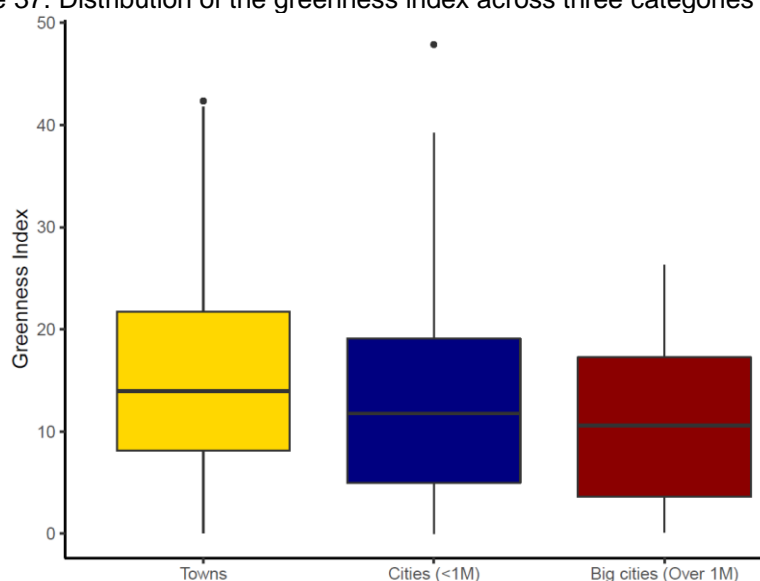
The last important dimension of this case study relates to land cover features, notably the “greenness” of this land cover. In general terms, cities land cover is characterized by high shares of impervious surfaces combined to varying degree with green vegetation and, only marginally, with areas of bare soils.⁵⁹ In fact, within city borders, a strong negative correlation is often detected between the fraction of impervious surfaces and NDVI values, providing the basis for fairly accurate estimates of the evolution of the share of impervious surfaces based on NDVI (see Skougaard Kaspersen et al. 2015, among others). Importantly, as documented in the review of literature (Chapter 3, Section 3.2.2), impervious surfaces which are usually associate with built-up surfaces and the presence of paved areas, roads, or other man-made infrastructure, considerably alter the amount and velocity of run-off during high-intensity precipitation events. On the other hand, hydrological literature has also shown that green infrastructure such as urban parks, rain gardens or densely vegetated areas facilitate water infiltration, thus lessening and postponing peak water runoff and limiting downstream flooding. Before assessing whether a greener land cover can significantly reduce the impacts of extreme rainfall on urban economic activity, I thus present how the “greenness” of the land cover of cities is distributed across my sample. Chapter 4, section 4.2.2 describes more in detail the data source and the methodology used to compute the greenness index described here.

Although the greenness index displays considerable interannual variability, the mean value across our sample is in the range 0.14-0.17 during the period 2013-2021. This confirms that impervious surfaces largely prevail within cities borders with the mean area covered by urban parks, dense vegetation or trees never exceeding 17% of the total area of a city (Figure 38 - left). Nevertheless, the greenness index displays strong temporal variations at the city-level. Although we use annual NDVI composites to try to mitigate these fluctuations, yearly data at the city level still shows strong variations, as evidence for selected cities shown in Figure 38 - right. These variations can be driven by two factors. First, temporal variations reflecting natural variability in the content of chlorophyll of urban vegetation, which are largely determined by hydrometeorological conditions and the water stress endured by the vegetation. In fact, a large scope of the literature has leveraged NDVI temporal variations to detect drought conditions (see Karnieli et al. 2010 for a discussion of the advantages and limitations of this approach). The second source of variations is related to land cover changes within urban areas such as the establishment of new built-up surfaces (or the creation of a

⁵⁹ Because the price of land tends to increase within city borders, bar soils are only marginal. The NDVI value of bar soils is potentially closer to the threshold value employed in this case study to determine “green urban areas” (i.e. $NDVI > 0.5$) but as they are only marginal within urban centres I am not concerned that this would significantly affect the greenness index measurement. In any case, it is another reason that lead me to exclude suburban areas from this case study.

vegetated areas), which would decrease (or boost, respectively), the greenness index used in this case study. Since I have no way to isolate these two drivers with the data available, I averaged the annual greenness index of each city over the period 2013-2021 and used this value to proxy the share of the city area covered by permanent green urban areas or stable dense vegetation.⁶⁰ This is an important caveat to the analysis that must be highlighted. Unfortunately, disentangling the relative importance of these two sources of variations requires local data on water stress episodes and on the creation of new green areas that were not available across the full sample of cities. This work is thus beyond the scope of this thesis but represents a promising avenue to refine the proposed investigation.

Figure 37. Distribution of the greenness index across three categories of cities



Note: Towns are urban settlements whose population was below 107K in 2015. Cities are settlements with a population between 170K and 1 million. Big cities are cities with population exceeding 1 million.

Source: own elaboration.

The greenness index is correlated to city size and rainfall patterns but can be locally shaped. Figure 39 shows the distribution of the mean greenness index over 2013-2021 by country, unveiling how this index is well-distributed in each country and does not seem to be determined by country fixed effects. At the city-level, weather is of course a driver of the greenness index. Figure 40 plots the mean greenness index against the mean monthly precipitation for each city in my sample, clearly showing a trend whereby a higher level of greenness index is associated with more abundant average precipitation -although with person coefficient is 0.48, this association is not to be viewed as deterministic. Besides, city size (in terms of population) also seems to influence the level of the greenness index. Figure 37 refers to the three categories of cities used in case study 1 (based on the distribution of population) and display the distribution of the greenness index in each category. Interestingly,

⁶⁰ This high variability has also led me to opt for a fixed delineation of city borders between 2013-2021 -as opposed to the dynamic delineation employed for case study 1 between 2000 and 2015. This dynamic delineation could have further exacerbated the variations of the share of high NDVI values within city borders.

the greenness index tends to display a lower level in more populated cities with, on average, a decrease of 0.15 points of the greenness index when the population of a city increases by 10%.⁶¹ This trend suggests that, as cities become more populated, land prices rise and the pressure on green spaces is intensified, potentially reducing the share of green areas within large cities. Eventually, with a Pearson correlation coefficient estimated at -0.04, there is no evidence of a strong association between average NTL/cap and greenness index at the city level. Overall, with values ranging from 0 to 50%, the greenness index is a variable that, conditional upon weather variables and city size, displays strong variability. This suggests that there is enough leeway to locally shape the final value of this greenness index, confirming the potential that urban public policy can play in shaping the value of this greenness index.

⁶¹ This effect is estimated through a linear regression of the average greenness index on the 2015 log-transformed population of a city. The coefficient attached to log-population is highly significant. This association could nonetheless suffer from omitted variable bias and further work is required to conduct a more robust analysis. I leave this topic for future research.

Figure 38. Yearly variations of the greenness index across the full sample of cities (left) and selected cities (right), 2013-2021

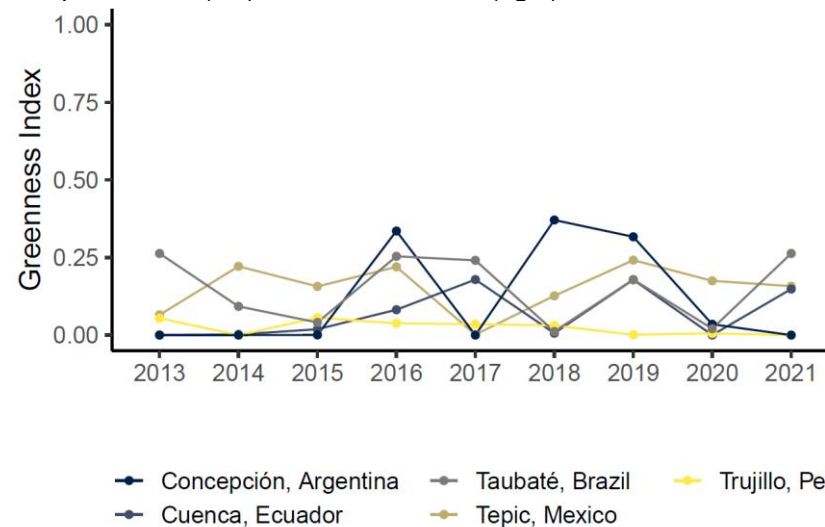
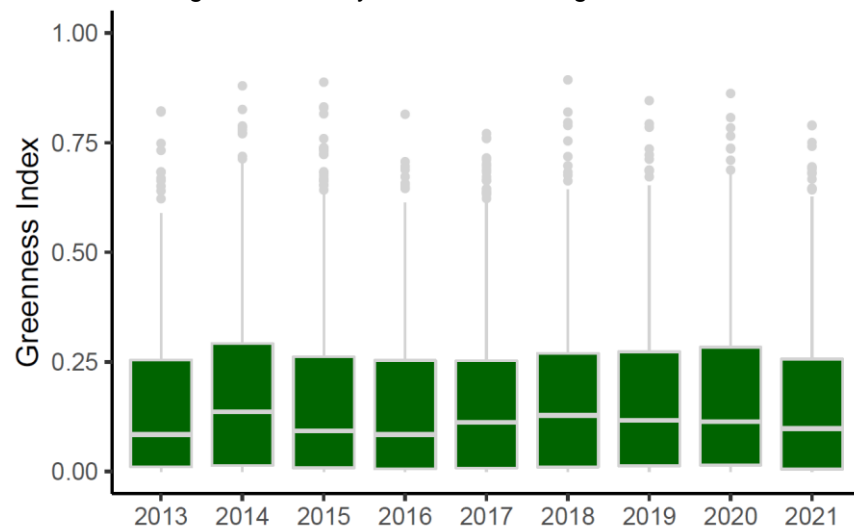


Figure 39. Distribution of the mean greenness index by country

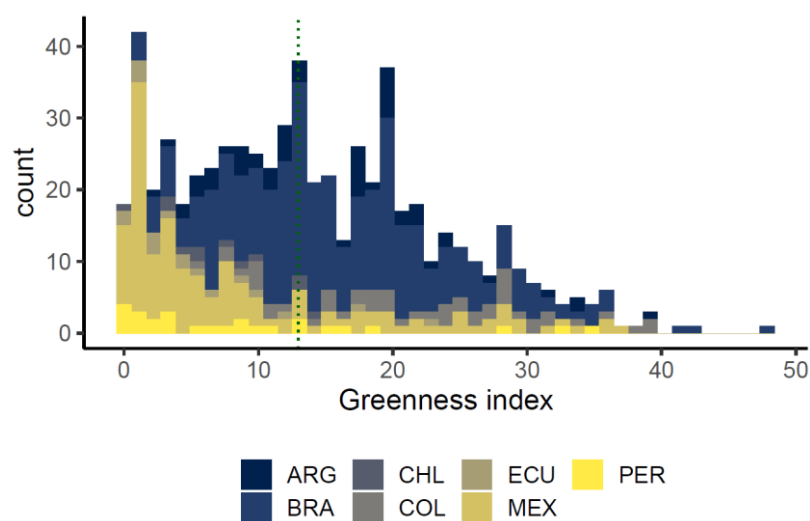
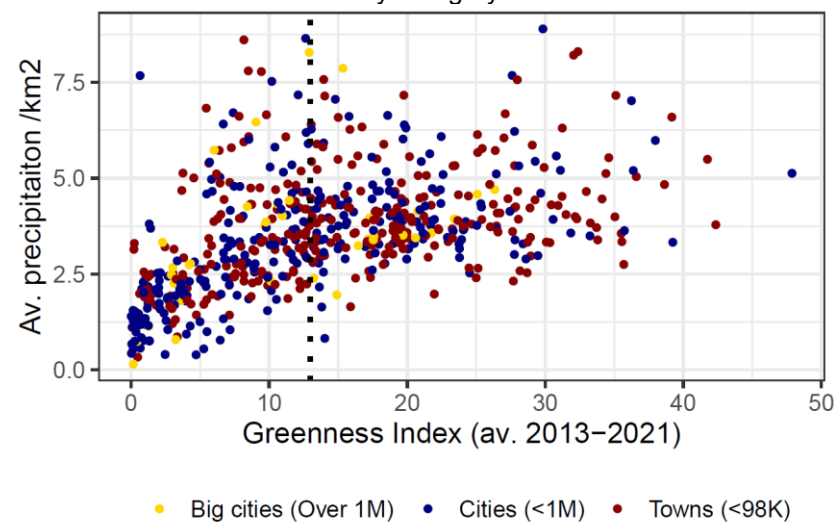


Figure 40. Mean greenness index VS mean precipitation at the city-level by city category



Source: own elaboration.

6.4 Empirical estimation of the impacts of extreme rainfall on night-time lights

The empirical analysis proposed in this case study includes a twofold approach. First the relationship between extreme rainfall and NTL at the city level is investigated; then the heterogeneity of effects associated to extreme rainfall is explored by interacting the extreme rainfall index with the greenness index.

To investigate the effects of extreme rainfall on night-time lights at the city-level, the empirical framework proposed in this paper directly draws from the approach proposed by the new climate-economy literature (see Dell, Jones, and Olken 2014 for a review). The assumption underpinning our identifying strategy is that extreme rainfall events are exogenous conditional on city and country-month fixed effects. Consequently, our benchmark model takes the following form:

$$\ln Y_{i,c,m} = \alpha + \beta_1(Xtrm_{i,c,m}) + \beta_2(Tmp_{i,c,m}) + \omega_i + \theta_{cm} + \varepsilon_{i,c,m} \quad (\text{Eq. 1})$$

Where $\ln Y_{i,c,m}$ represents the log-transformed value of NTL per-capita of city i , in country c , month m .⁶² $Xtrm_{i,c,m}$ is the extreme rainfall index as described in the previous section, $Tmp_{i,c,m}$ is a vector of monthly temperature z-scores, ω_i are city fixed effects and θ_{cm} month-by-country fixed effects (i.e. monthly fixed-effect interacted with country dummies). As precipitation and temperature are potentially correlated, the exclusion of temperatures variables could imply a potential misspecification bias, although in our setting this variable is to be viewed as a control variable. $\varepsilon_{i,c,m}$ is the robust error term clustered by city. In essence, we analyze whether city-specific NTL deviations are related to city-specific deviations from precipitation trends, after accounting for unobserved time-invariant heterogeneity as well as monthly shock common to all cities in the country of interest. This framework is well-suited to isolate the causal effect of extreme rainfall on NTLs and provide a robust estimate of the parameter β_1 of interest, which I presume to be negative.

As noted by Hsiang (2016), the selected approach could still be vulnerable to omitted variables bias. Here we have assumed that variations in weather data over time are exogeneous to socioeconomic process and are driven by stochastic meteorological process. However, many weather variations are in fact correlated over time because they are -at least partially- driven by a similar underlying process. This is for example the case of precipitations over the pacific

⁶² City NTL per-capita are estimated using the 2015 city population estimates provided in the UCDB. Using absolute city NTL values delivers consistent results. We add 0.001 to all city NTL values before log-transforming them to avoid removing observations where monthly NTL values are 0. We further test and reject the null hypothesis of the presence of a unit root in our dependant variable (see appendix).

coast of Peru and Ecuador, which are strongly intensified during periods of El Niño–Southern Oscillation (ENSO). Over a longer time horizon, temperature data might also be considered as a trended variable because of the upward trend associated to increasing concentration of ppm in the atmosphere. The extent to which this issue could bias our estimates remains broadly unknown in the literature and I leave this issue for future research.

A separate concern affecting my identification strategy might be linked to the absence of time-varying controls related to other socioeconomic factors such as, for example, the level of education and risk awareness of a city or its economic structure. These controls have been excluded from our identification approach because, to the extent that they are endogenous and affected by weather variables, they might introduce new biases. This situation is referred to as overcontrolling or “bad controls” (Angrist and Pischke 2008) and I purposely use a parsimonious model to avoid it.

The main estimations results are presented in Table 6. The major finding of this first step is the systematic negative relationship between extreme rainfall and NTL/capita across Latin America cities. Column 1 shows the result of our benchmark specification and provides evidence that, on average, extreme rainfall has a negative and significant impact on city NTL/capita. To ensure the robustness of this estimation, we considered alternative rainfall proxies and a variety of robustness checks. Column 2 removes all other covariates and reveals similar impacts, corroborating the estimates obtained in column 1. Column 3 replaces the extreme rainfall index by an index based exclusively on monthly precipitation above mean rainfall (i.e. Z score > 0) and find consistent negative effects. Column 5 replaces the extreme rainfall index by the full spectrum of precipitation values (normalized per the Z-score formula) and confirms a negative relationship between rainfall deviations and city NTL/cap. Column 4 explores the presence of non-linearities in the relationship between NTL and precipitation by introducing the quadratic term of precipitation Z scores but find no evidence of it.

Interestingly, temperature deviations show a consistent non-linear U-shaped effect on NTL/cap: positive temperature deviations first raise NTL/cap, although this effect is progressively reduced and, beyond a tipping point, reversed. Based on column 1, the tipping point for temperature Z score is estimated to be at 2.28, which is close to the maximum value recorded over the period (i.e. 2.8) and well above 3rd quarter of our temperature sample, indicating that negative effects of temperature only prevail for a handful of cases.

Diagnosis tests and extensive robustness checks are presented in Appendix. They indicate that these results are robust to the choice of fixed effects and different computation of standards errors. Likewise, including cities that did not experience extreme rainfall events or dropping the largest country of the region did not change the significance of the coefficients.

We further control for potential cloud-coverage variations through more restrictive thresholds for cloud-coverage quality and additional seasonal trends controls without finding evidence that this alters our results.

Table 6. Main estimations results.

	<i>Dependent variable:</i>				
	(1)	(2)	Ln NTL/cap (3)	(4)	(5)
Xtrm Rainfall	-0.069*** (0.014)	-0.076*** (0.014)			
Rainfall Zscore				-0.067*** (0.007)	-0.063*** (0.006)
Sq. Rainfall Zscore				0.004 (0.003)	
Temp. Z	0.058*** (0.007)			0.043*** (0.006)	0.044*** (0.006)
Sq. Temp. Z	-0.011** (0.005)			-0.012*** (0.005)	-0.012*** (0.005)
Abov. mean rainfall			-0.088*** (0.009)		
Observations	68,040	68,040	68,040	68,040	68,040
F Statistic	57.130*** (df = 3; 66652)	73.698*** (df = 1; 66654)	184.654*** (df = 1; 66654)	70.880*** (df = 4; 66651)	93.963*** (df = 3; 66652)

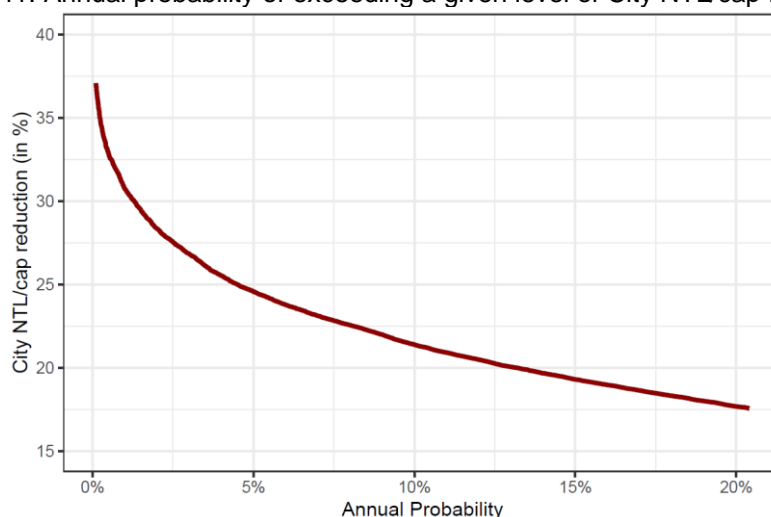
Note:

*p<0.1; **p<0.05; ***p<0.01

Source: own elaboration.

From a quantitative perspective, results in column 1 of Table 6 indicate that, for Latin American cities, when an average extreme rainfall event occurs NTL/cap are reduced by 19.8% (or -0.198 log points). This is obtained by multiplying our coefficient of interest by the average value of the extreme rainfall index (i.e. 2.5). Importantly, since extreme rainfall events are, by construction, rare events, we provide a probabilistic view of our estimates to better reflect the nature of impacts. To do so, we compute an empirical cumulative distribution function of the maximum extreme rainfall index recorded over a year during the period 1991-2021 in each of the 630 cities. This procedure allows us to estimate the values of extreme rainfall index at different percentiles of the distribution and, consequently, to infer the annual probability of having a city exceeding a given extreme rainfall index. As such, until the 73rd percentile of the distribution, the value of the extreme rainfall index is 0, meaning that, across the seven countries of interest, the annual probability of having at least one city experiencing an extreme rainfall event is around 27% (1-0.73).

Figure 41. Annual probability of exceeding a given level of City NTL/cap reduction



Note: This figure is constructed using the empirical cumulative distribution of extreme rainfall events over 1991-2021 and the coefficient in column 1 of Table 6.

Source: own elaboration.

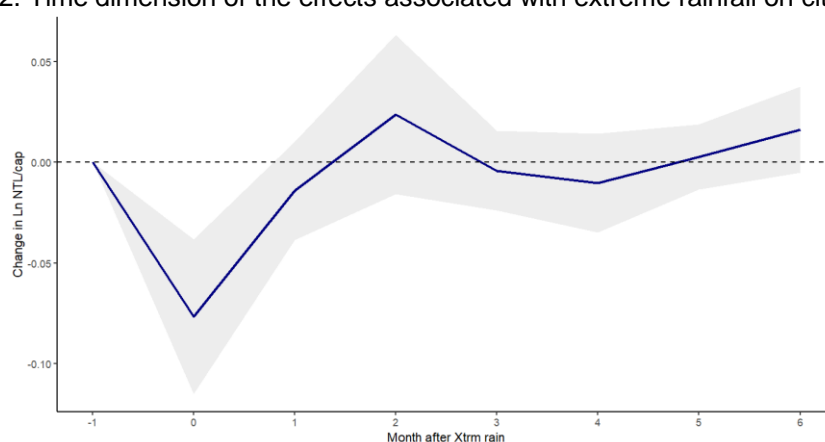
Interestingly this probabilistic view unveils a non-linear relationship between extreme rainfall event realizations and NTL losses. As such, the 80th percentile of the distribution corresponds to a value of 2.23, which implies that, at the regional level, there is a 20% annual probability (1-0.8) of exceeding an extreme rainfall index of 2.23. In other words, the model predicts that, over the long run, Latin American cities face a 20% annual probability to experience an extreme rainfall event that lowers monthly NTL per capita by approximately 17.6% (i.e. 2.23×7.9). For extreme rainfall events displaying a 1% annual probability of being exceeded, city NTL/cap is estimated to be reduced by 30.7%.

Under the effects of climate change, future precipitation patterns are projected to depart from the historical patterns used for this assessment and could shift this exceedance probability curve towards the right. Specifically, extreme precipitation events in the tail of the distribution are expected to become more frequent, thereby increasing the likelihood for the region to have to confront significant losses if no adaptation measures are quickly implemented. Using the outputs of global climate models included under CMIP-6 and the average changes factors described in section 0 of this case study, it is estimated that the 1% probability of facing an NTL/cap reduction of 30.7% could be almost doubled by the end of the century under SSP5.8-5. In other words, if vulnerability to extreme rainfall events is not altered, impacts associated to extreme events that, over the long term, were estimated to be exceeded once every 100 years could be exceeded once every 50 years. Again, this represent a high-level estimate and changes at the city-level will be very heterogeneous.

Finally, a central question is understanding whether negative impacts arising from extreme rainfall events produce (i) permanent effects on city local economic activity (ii) only momentary impact or (iii) are fully offset by a rebound in economic activity in subsequent months.

Following Dell et al. (2014), we assess these effects by including the monthly lagged values of extreme rainfall index in Eq. (1). As can be seen from Figure 42, which plots the results presented in column 1 of Table B.3 in Appendix, the contemporaneous effect of extreme rainfall is significantly negative and the first lag remains negative but no longer statistically different from 0 at the usual 5% threshold value. Subsequent extreme rainfall lags are hovering below and above 0 but are all statistically insignificant. A similar pattern is observed when using the index based only on positive Z score (see Table B.3 in Appendix). This suggests that the adverse economic effects of extreme rainfall are short-lived and, on average, do not persist after the month of impact. Insignificant lagged effects also point to the absence of “economic rebound” in the aftermath extreme rainfall events.

Figure 42. Time dimension of the effects associated with extreme rainfall on city NTL/cap



Source: own elaboration.

6.5 The benefits of greener land cover

6.5.1 Land cover features as a moderating factor

In this section, we investigate the effects of greener urban land cover by testing whether the impact of extreme rainfall on NTL decreases as the level of vegetation cover increases, everything else being equal. To ensure that these effects are not driven by an intrinsically higher vulnerability to extreme rainfall in cities where dense vegetation is inexistent, in this part of the analysis I removed cities that display no or very limited dense vegetation.⁶³ Cities with less than 5% of their total area covered by high greenness pixels (i.e. approximately 20% of our original sample) corresponding to urban centres with almost no trees nor dense vegetation are thus excluded of this analysis.

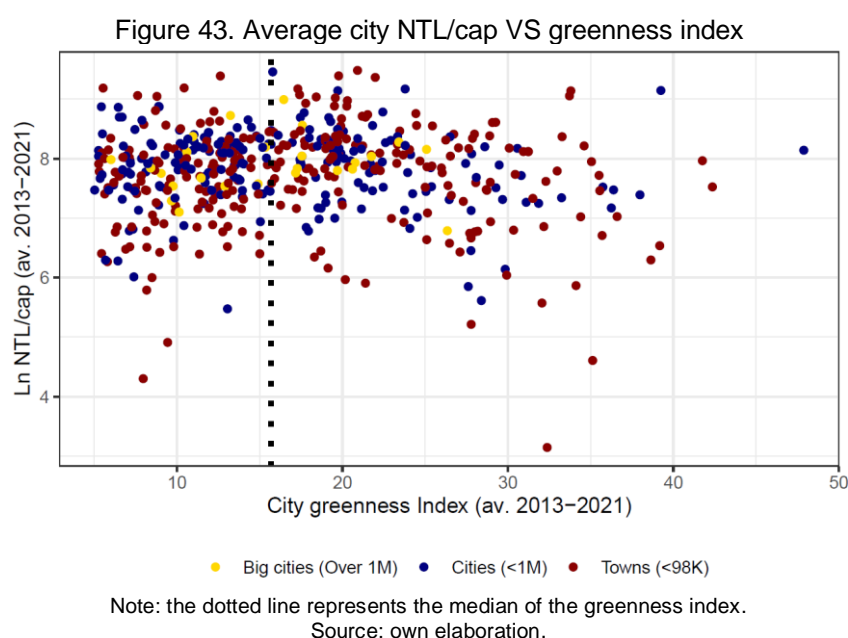
Because the hydrological literature has emphasised that there may be a non-linear relationship between the amount and location of GI and the observed reduction in urban flood extent (Schubert et al. 2017; Yao, Wei, and Chen 2016; Yang, Endreny, and Nowak 2015), we replicated the framework proposed by (del Valle et al. 2020) and explored the heterogeneity of extreme rainfall effects by estimating three different models. For each model, we discretized the city greenness index into various bins, corresponding to its q quantiles. The first model used the median value of the greenness index to create two dummy variables for each equal-sized bin and interact these dummies with the extreme rainfall index. The variable resulting from this interaction was then inserted into our benchmark equation, as shown in Eq. (2).

$$\ln Y_{i,c,m} = \alpha + \beta_1(Xtrm_{i,c,m}) + \beta_2(Xtrm_{i,c,m} \cdot \overline{\text{Green index}}_{i,c}) + \omega_i + \delta_{mc} + \varepsilon_{i,c,m} \quad (\text{Eq. 2})$$

The marginal impact of extreme rainfall in each bin was obtained by summing β_1 and β_2 . This procedure allowed the estimation of effects that vary in a non-linear fashion across bins, potentially capturing non-linearities in the differentiated impacts of extreme rainfall events across levels of greenness. We repeated this assessment using three and four dummies at the tercile and quarter values of the greenness index, respectively.

⁶³ This higher vulnerability could arise for example from the fact these cities are principally located in semi-arid areas with structurally lower soil infiltration rates. Removing cities that do not display abundant vegetation also ensures that the simulation conducted in the following section does not project an increase of the greenness index in cities that cannot accommodate dense vegetation because of strong water availability constraints.

When exploring the effects of the interactions between greenness index and extreme rainfall, we acknowledge that the greenness index could potentially be jointly determined with income per capita (proxied by NTL/cap) and precipitation patterns. To attenuate this issue, we used the average value of greenness over the period and ensured that city NTL/cap and greenness index did not change discontinuously at the threshold values selected, which could have potentially been driving the differentiated effects observed in each bin. As depicted in Figure 43, there does not seem to be a clear relationship between greenness index and NTL/cap at the city level. With a Pearson coefficient of -0.06, the correlation between log-values of NTL/cap and the greenness index remains limited and is unlikely to explain the differentiated impacts of extreme rainfall events. We nonetheless refrained from claiming a causal interpretation of this effect.



Estimated effects are presented in Figure 44 (a) which plots the point estimates and 90% confidence intervals for each of the three models. The city and country-monthly fixed effects are included in the estimations. The coefficients can be interpreted as the marginal reduction in nightlights caused by an extreme rainfall event for each group of cities. In the model with two bins, for cities below the median value of the greenness index (i.e. 15.69), the marginal extreme rainfall effect reduces nightlights by almost 12%. Contrastingly, in cities with greenness indexes above this median value, this marginal effect is reduced to approximately 5%. In addition, the null hypothesis of no differential impact of extreme rainfall events between the two bins was rejected (P value < 0.1). Models with 3 and 4 bins show a consistently decreasing impact of extreme rainfall, as the level of greenness increases. In the case of the model using 4 bins, we were able to reject the null hypotheses of equality between the coefficients associated with the first and the fourth quartile (P value < 0.1). For the model with

3 bins, we were not able to reject it at conventional levels and the reduction of extreme rainfall impact only seems to materializes in the third tercile (i.e. cities with greenness index above 19).⁶⁴ Figure 44 (b) plots the distribution of greenness index in each bin across the three models, unveiling how the impacts of excess rainfall are systematically and significantly lowered for bins displaying a greenness index that exceeds 20 (i.e. bins at the bottom of each figure).

Extensive robustness checks were conducted in Appendix and confirmed that results are not overly sensitive to (i) different NDVI or greenness index thresholds values (i.e. 0.5 or 0.6 to define “green pixels” or varying the minimum greenness index to be included in the sample from 1 to 5 or removing potential outliers) or (ii) alternative spatiotemporal resolution to compute NDVI values. Ultimately, to ensure that results were not driven by other sources of heterogeneity potentially correlated to the greenness index, we perform three additional set of regressions allowing for extreme precipitation effects to vary based on greenness index and (i) total city population, (ii) average precipitation or (iii) city elevation. These regressions confirm that the reduction of impacts associated to a greener land cover remains significant and suggest that more populated cities in higher locations tend to be less vulnerable to extreme rainfall, while average precipitation do not significantly influence extreme rainfall effects.

Altogether, results from these three models suggest that, for cities where dense vegetation represents more than 20% of total city area, the marginal impact of extreme rainfall is broadly halved vis-a-vis cities below this threshold. Consistent with the hydrological literature, in none of the models the adverse effects associated with extreme precipitation are totally wiped out by a greener land cover. This could be linked to limited soil infiltration capacity and saturation effects as well as the impossibility to maintain or expand green areas in some parts of the city. It also insinuates that GI alone might not be able to fully protect against the economic impacts of extreme rainfall. Significant protection benefits are nonetheless associated to a greener city land cover. According to our benchmark model (i.e. greenness index discretized based on its median value), the average extreme rainfall event observed over the period would lead to almost a 30% decrease in urban economic activity in cities where less than 15% of the area is associated with dense vegetation (2.5×-0.119), while this reduction would be limited to approximately 14% in cities where green areas represent more than 15% of total city area (2.5×-0.055).

⁶⁴ Estimating Eq. (2) using the third tercile of the greenness index (i.e. 19.70) to create 2 bins (i.e. above/below third tercile) allowed us to reject the null hypothesis of equality between the two coefficients.

6.5.2 Valuation of the flood protection benefits associated with a greener city land cover

Finally, we leveraged the relationship between city NTLs and GDP to provide an economic valuation of the benefits associated with a higher greenness index, in terms of avoided losses. To this end, a simple calculation was performed using the benchmark model where cities are classified into two bins based on the median value of the greenness index. The computation was conducted for the year 2015 and followed three steps. First, city NTL variations were estimated by multiplying the extreme rainfall index recorded in each city by the coefficient corresponding to the greenness index of the city (either -0.055 or -0.119). Absolute NTL losses were derived by applying this variation to the 2015 mean city NTL/cap value and using the corresponding city population estimate. National NTL losses were obtained by summing all city NTL losses recorded in each country.

A counter-factual scenario was then simulated by computing NTL variations, under the hypothesis that cities displaying a greenness index between 10.52 ($q=25$) and 15.69 ($q=50$) increase their share of green areas. This ‘as-if’ analysis corresponds *de facto* to a scenario where 25% of the cities in our sample increase their average share of green land cover from the actual 13% to close to 23% (i.e. the mean value of greenness index in the “protected bin”). To account for uncertainty in our estimates, this process was repeated 5000 times, drawing the coefficient associated with extreme rainfall from a normal distribution, which had the estimated parameter as its mean value and the estimated standard error as its standard deviation.

In the second step, we investigated the relationship between NTL and GDP to obtain a conversion factor between the two values. To this end, the annual mean city NTL values were summed at the national level and regressed against the value of GDP (in constant US\$ of 2015). This regression did not seek to establish a causal relationship but attempted to provide a conversion factor between national city NTLs and GDP.⁶⁵ This procedure allowed us to translate the national NTL losses estimated in the first step into an equivalent variation of US\$. Thirdly, the benefits of greener city land cover were estimated as the difference between the mean ‘observed’ losses and the mean simulated losses under the ‘as-if’ scenario.

The findings suggest that if 25% of the cities had displayed a higher greenness index, losses from extreme rainfall in 2015 could have been reduced by approximately US\$ 6,500 million

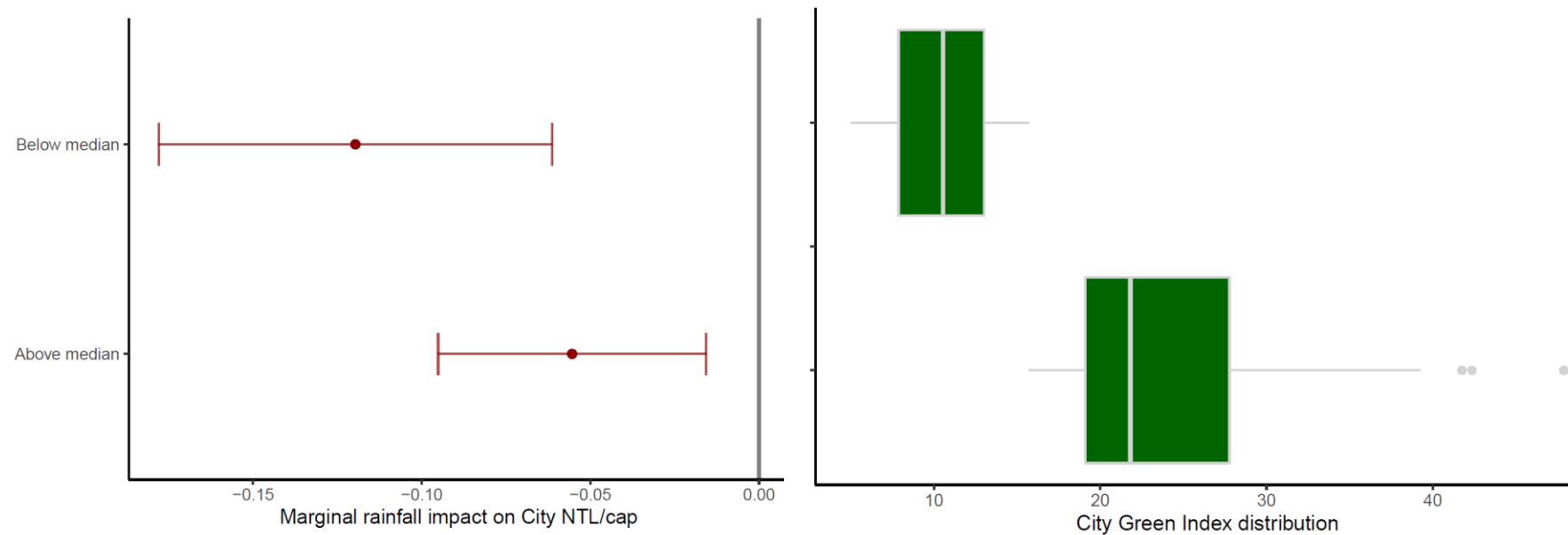
⁶⁵ To account for uncertainty, we used the same procedure as in the first step and repeated the translation of NTL to GDP values 5,000 times, drawing the coefficient of interest from a normal distribution, taking the estimated parameter as its mean value and the estimated standard error as its standard deviation. Parameters and standard errors are extracted from column 1 of Table 5. With a squared R above 0.90, the estimation process is deemed robust enough to provide a conversion factor.

(2015 constant). This reduction accounts for roughly 19% of the total estimated losses that year and a t-test confirms that the difference between the means of the distribution of observed and simulated losses is not equal to 0 (see Figure 45).⁶⁶ This simulated scenario assumes the deployment of green infrastructure in 125 cities already displaying densely vegetated land cover, with a rise of the average greenness index of these cities from 13% to 23%. Moreover, there is no evidence that efforts aimed at increasing the greenness index would lead to reduced affluence in the city (as proxied by city NTLs): city NTL/cap do not change drastically around the median value of the greenness index (see Figure 43).

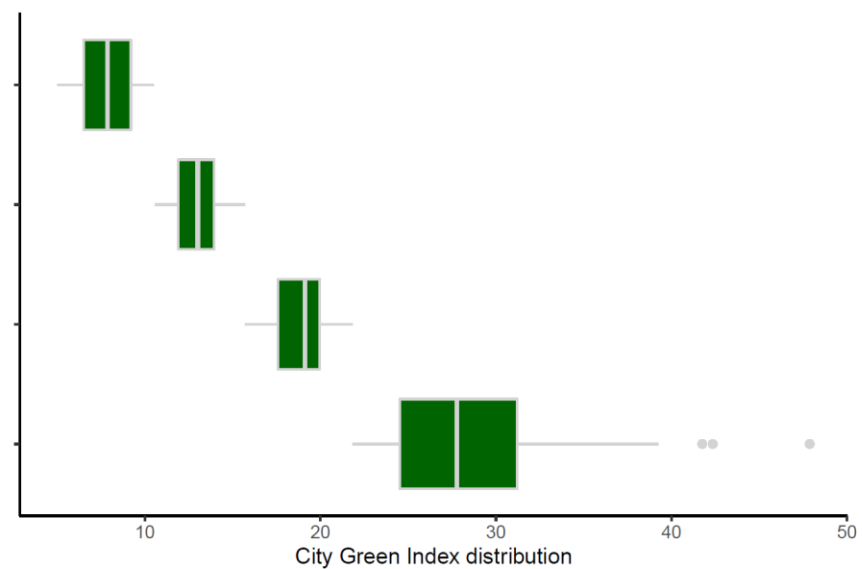
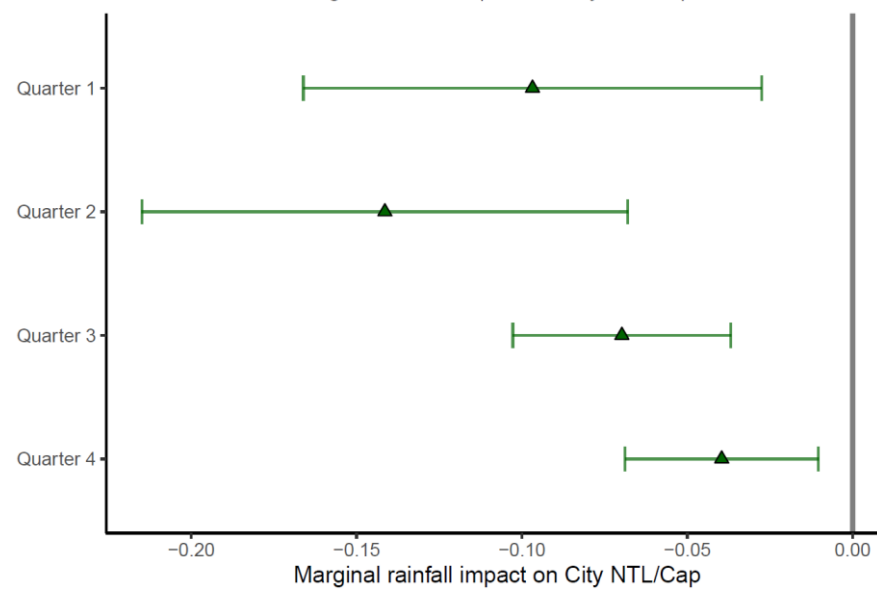
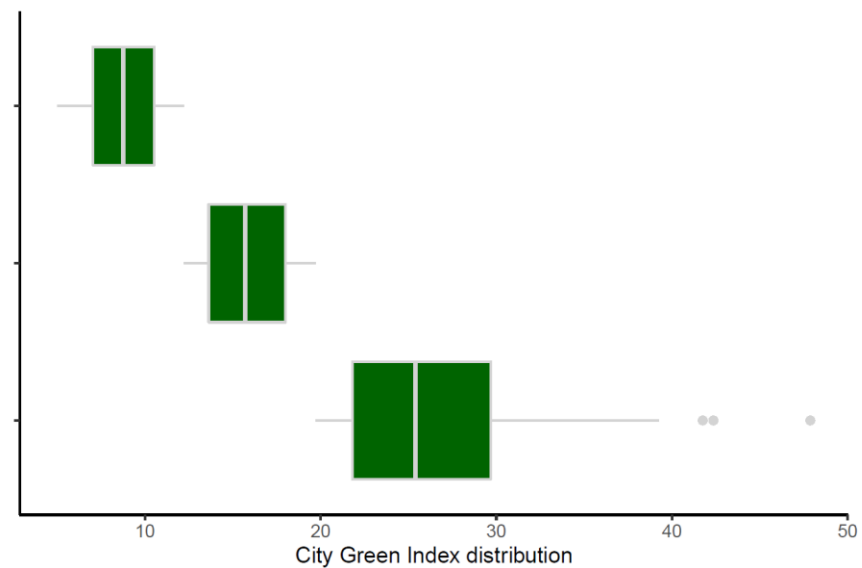
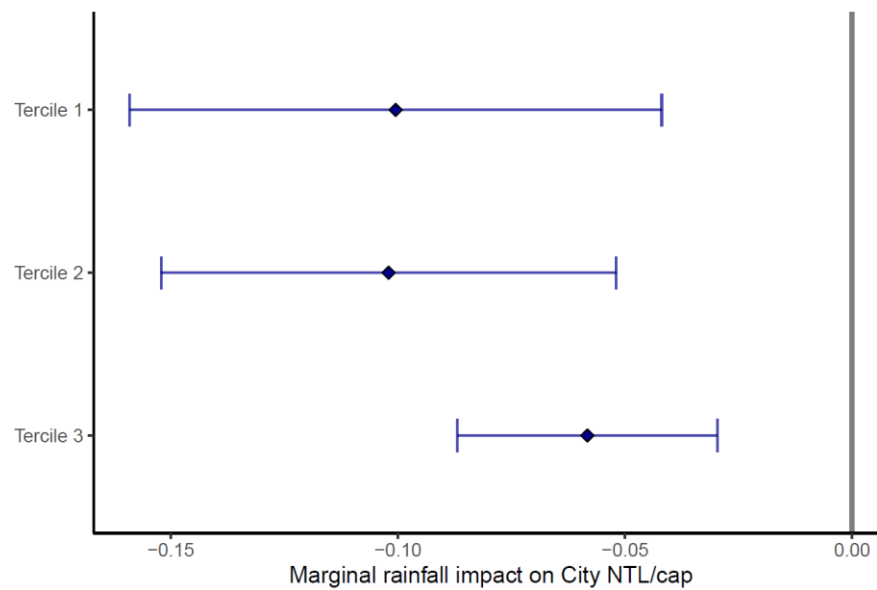
Obviously, these results reflect the specific distribution of extreme rainfall events across cities during the year 2015 and could vary depending on the location, intensity and number of extreme rainfall events recorded over a year. Likewise, these estimates do not consider impacts which are not captured through NTL variations, such as human losses or natural capital degradation. They do, however, provide robust evidence of the benefits that green areas can generate for Latin American cities, in terms of avoided losses and/or reduced economic disruption generated by extreme rainfall.

⁶⁶ Observed losses for 2015 account for roughly 0.77% of the GDP of the 7 countries of interest, with the reduction in impact due to the higher greenness accounting for 0.15% of the aggregated GDP.

Figure 44. Estimated effects of three models of extreme rainfall interacting with q-quantiles of greenness index (q=2, q=3 and q=4; left). (b) Distribution of the greenness index in each group of cities (right)

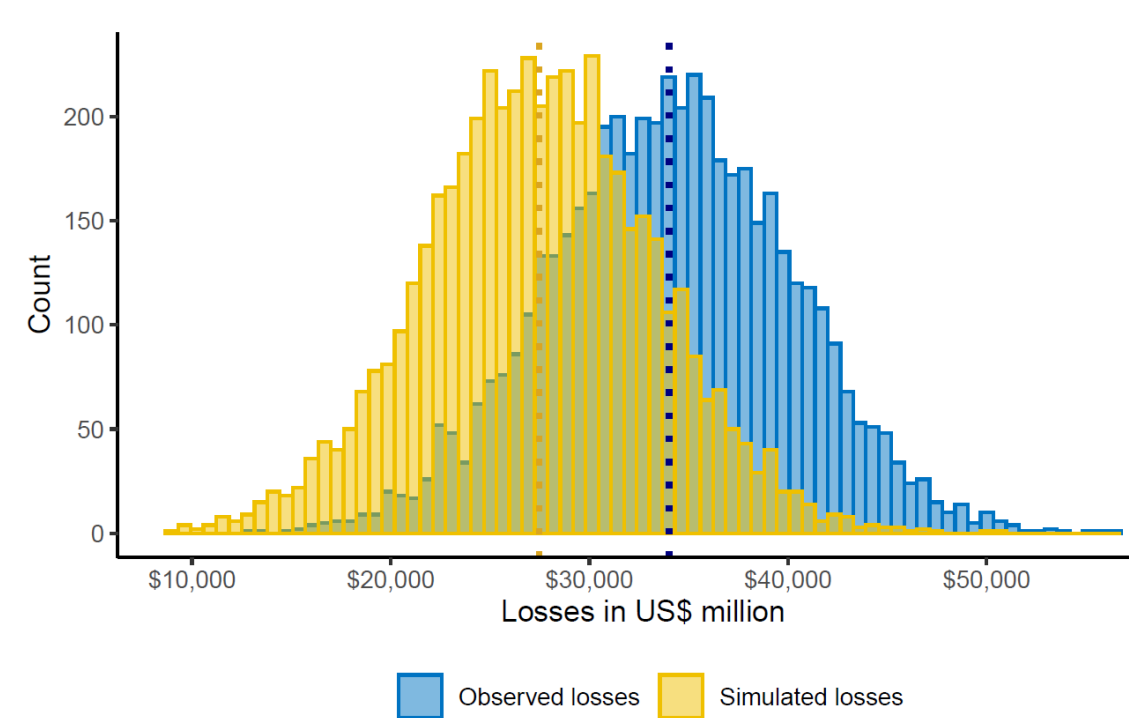


Source: own elaboration.



Source: own elaboration.

Figure 45. Observed vs simulated losses based on the 2015 distribution of extreme rainfall events



Note: The dotted line corresponds to the mean of the observed and simulated losses.
Source: own elaboration.

6.6 Conclusion

This investigation provides empirical evidence that, in Latin America, the negative impact of extreme rainfall on urban economic activity is significantly reduced in cities displaying a greener land cover. These results were obtained using an internationally harmonised definition of cities and leveraging earth observations for the period 2013-2019. Urban economic activity was proxied using monthly night-time lights. Extreme rainfall was detected through an analysis of precipitation patterns over 30 years and the greenness of the land cover was categorised using NDVI composites. To measure the impact of extreme rainfall on urban economic activity, a fixed effects model was employed to control for unobserved city heterogeneity and common monthly changes to all cities in each country. Then, to examine the extent to which the impact of extreme rainfall is differentiated across cities, an interaction term, based on the share of green areas detected within city boundaries, was introduced. Eventually, a counterfactual analysis for the year 2015 was conducted and suggested that if cities 25% of the cities in our sample had increased their average share of green land cover to above 20%, an additional US\$ 6,500 million could have been reaped, in terms of avoided losses and reduced disruption. Taken together, these findings reveal how a more balanced land cover, which makes room for green infrastructure within the city, can contribute to shield economic activity from adverse effects associated with extreme rainfall.

While most of the previous studies assessing the role of GI for flood protection relied on hydrological modelling at the watershed level, the methodology used in this paper innovates in at least two major dimensions: (i) it relies on empirical observations to measure extreme rainfall impacts (as opposed to modelling a set of synthetic flood events); and (ii) it covers a much larger geographical area, spanning nine years of rainfall observations. Consequently, findings differ from those obtained through hydrological modelling studies. They do not offer tailored recommendations at the watershed level about the design and location of urban GI. Instead, the proposed investigation focuses on providing robust evidence that, for most intermediate and small cities in Latin America, a greener land cover can alter the impacts of extreme rainfall.

This framework provides a solid methodology to quantify the benefits that GI could bring in terms of avoided losses or reduced economic disruption in case of extreme rainfall. This adds further evidence on the multiple ecosystemic services provided by GI (e.g. improved air and water quality, temperature regulation, enhanced biodiversity or recreational opportunities, among others) and contributes to expand the methods that can be mobilized to quantify these services. By contributing to a sound quantification of the wide-ranging benefits that GI can

deliver, this study ultimately seeks to inform urban public policies about the strategic value of these interventions.

As cities continue to expand in flood prone areas and climate change further intensifies the hydrological cycle, more frequent and intense extreme rainfall events are expected to affect Latin American cities. This will only make the benefits associated with green infrastructure more relevant and should encourage future research on the efficacy and adequacy of GI for flood protection. Research at a finer spatial resolution will notably be required to examine how GI efficacy can be altered by the type of vegetation used or by different storm intensity and duration parameters under a changing climate. Due to the nature of the data used in this investigation, these factors have not been addressed but remain an important avenue for future investigations.

6.7 Appendix

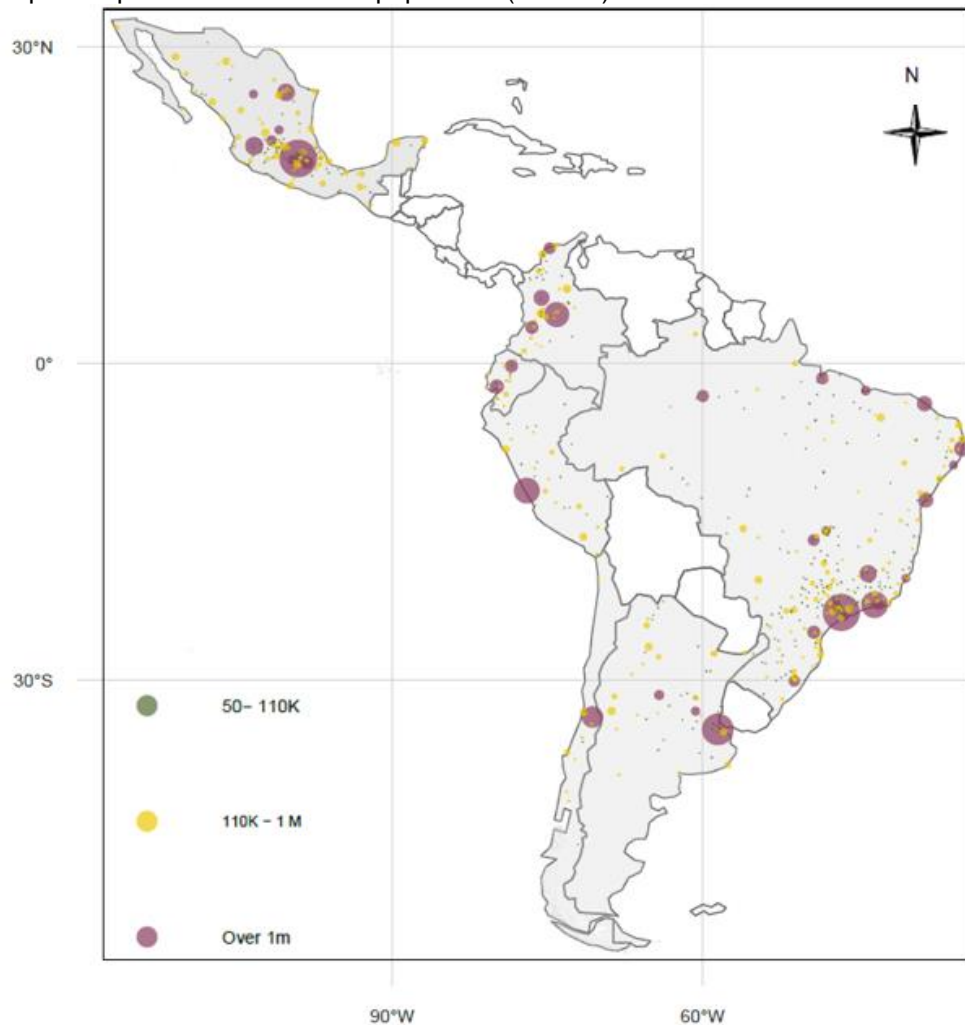
6.7.1 City-level statistics and spatial distribution

Table A.1 Summary statistics

Variable	Mean	Std. Dev.	Min	Max
Ln NTL/cap	7.76	1.33	-6.9	10.71
Extreme Precipitation*	2.59	0.52	2	5.31
Greenness index	0.43	0.19	0.1	1

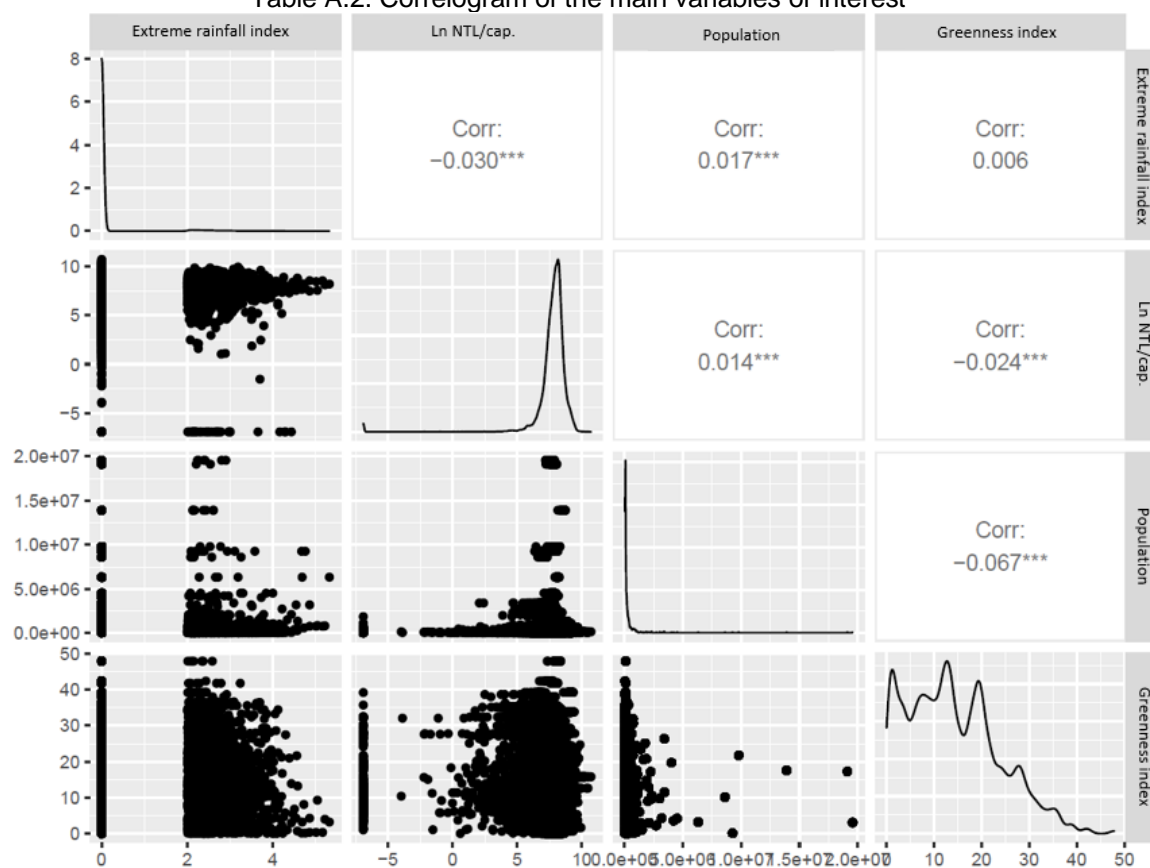
*Extreme precipitation statistics are computed on events realizations only i.e., excluding observations where the index is equal to 0

Map A.1 Spatial distribution and population (in 2015) of the cities included in the study



Note: The size of the bubble is proportional to the population of the city in 2015
Source: own elaboration. Basemap: Natural Earth.

Table A.2. Correlogram of the main variables of interest



6.7.2 Diagnosis tests and robustness checks

From an econometric standpoint, my research design warrants the use of fixed effect within estimator as the preferred estimator. I nonetheless run various diagnosis tests to check whether this approach is unbiased and efficient. Results of these diagnosis tests confirmed that this approach is suitable. They are presented and discussed below.

Table B.0 Results of the main diagnosis tests performed on our benchmark model (i.e. column 1 in Table 6)

Hausman test		
	<i>Statistic value</i>	<i>P-value</i>
Chisq	507.39	0
ADF - Unit Root test		
	<i>Statistic value</i>	<i>P-value</i>
Log NTL/cap (Lag order 2)	-97.353	0
Serial and cross sectional dependance tests		
	<i>Statistic value</i>	<i>P-value</i>
Breusch-Pagan LM test	1416291	0
Pesaran CD test	515.37	0
Breusch-Godfrey Test	5005.5	0

Source: own elaboration.

I first conducted a Hausman test that rejected the null hypothesis of an absence of correlation between unique errors and regressors. This confirms that the use of random models would have been inconsistent and suggests the use of fixed effects. As displayed in Table 6 in the main text of this case study, the F-statistic testing whether all coefficients are different from 0 is also rejected, confirming that the use of fixed effects is appropriate.

I then confirmed the absence of a unit root in the dependant variable. For this I ran an Augmented Dickey-Fuller test for panels and rejected the null hypothesis.

Eventually, I tested for the presence of cross-sectional dependence and serial correlation in residuals. I ran various tests which all consistently indicated the presence of both cross-sectional dependence (see Breusch and Pagan's Lagrange multiplier (LM) test and Pesaran's cross-sectional dependence test) and serial correlation (Breusch-Godfrey's test). Because of the strongly exogeneous nature of my predictors (i.e. extreme rainfall, precipitation z-scores), I assume that this autocorrelation in residuals is caused by the presence of common factors, which are unobserved but uncorrelated with the included regressors. In this setting, the standard fixed-effects estimators are deemed consistent, although not efficient. I therefore computed my standard errors using the two-way clustering approach proposed by Driscoll and

Kraay (1998) to account for this. In any case, as indicated in the following robustness checks, the use of alternative robust covariance matrix and clustering methods at the city level does not alter the significance of the main results.

Besides, extensive robustness checks were conducted to test the sensitivity of the results to different assumptions and specification choices. First, we altered the sample of cities by including all cities detected in the seven countries of interest, i.e. not restricting our sample to cities that have experienced at least one extreme rainfall event over the period of analysis. This raised the number of cities from 630 to 736 but did not substantially modify the results. Table B.1 follows the same approach that the main results displayed in Table 6 of the main text. It shows how the extreme rainfall index (columns 1-2), the above average precipitation value (column 3) and the full scope of Z-score values attached to monthly precipitation (columns 4-5) all have a negative impact on the NTL/cap at the city-level of a similar magnitude to those observed with the restricted sample of cities. When considering this broader sample of cities, the only difference with baseline results appears in column 4, which seems to suggest that there is a U-shaped relationship between precipitation Z scores and the NTL/cap. However, the vertex of this curve is reached with a Z score of 4.78, which is very close to the maximum value of the sample and would imply a potential positive impact on NTL/cap for only a handful of observations. We further tested the sensitivity of our results by removing cities in Brazil, which represented almost half of the cities in our sample, before estimating Eq. (1) with the three aforementioned precipitation indexes. The results remain consistent and suggest a statistically significant negative impact, although a bit noisier and of a lower magnitude (between -0.037 and -0.023).

Table B.1 Sensitivity of results to altering the sample of cities by including cities that did not experience extreme rainfall events over the period (736 cities in total)

	<i>Dependent variable:</i>				
	(1)	(2)	Ln NTL/cap (3)	(4)	(5)
Xtrm Rainfall	-0.076*** (0.014)	-0.085*** (0.014)			
Rainfall Zscore				-0.067*** (0.007)	-0.059*** (0.005)
Sq. Rainfall Zscore				0.007** (0.003)	
Temp. Z	0.059*** (0.005)			0.046*** (0.005)	0.047*** (0.005)
Sq. Temp. Z	-0.016*** (0.004)			-0.017*** (0.004)	-0.016*** (0.004)
Abov. mean rainfall			-0.085*** (0.008)		
Observations	80,352	80,352	80,352	80,352	80,352
F Statistic	60.009*** (df = 3; 79390)	65.545*** (df = 1; 79392)	151.218*** (df = 1; 79392)	67.789*** (df = 4; 79389)	88.436*** (df = 3; 79390)
<i>Note:</i>				*p<0.1; **p<0.05; ***p<0.01	

Source: own elaboration.

Additionally, we changed the structure of our fixed effects by using a subregional-monthly time trend (i.e. a South America-Monthly and Central America-Monthly fixed-effect as opposed to a country-monthly time trend), with little difference in magnitude or significance for the coefficients of interest (Table B.2). Simple monthly fixed effects for the entire continent were also used and delivered consistent results. The use of a month-by-province time trend was not tested as it would dramatically increase the number of fixed-effects (by 23,868 corresponding to 221 provinces* 108 months), strongly reducing the variance in our data and obscuring the statistical effects of our variable of interest. Finally, we computed standard errors using a two-way clustering (i.e. city and country-monthly or subregional-monthly clustering) and confirmed that this did alter the significance of our results.

Table B.2 Sensitivity to changing the structure of the time trend to subregional-monthly fixed-effects

	Dependent variable:				
	Ln NTL/cap				
	(1)	(2)	(3)	(4)	(5)
Xtrm Rainfall	-0.079*** (0.014)			-0.087*** (0.014)	
Rainfall Zscore		-0.065*** (0.006)	-0.070*** (0.007)		
Sq. Rainfall Zscore			0.004 (0.003)		
Temp. Z	0.060*** (0.006)	0.046*** (0.005)	0.045*** (0.005)		
Sq. Temp. Z	-0.013*** (0.004)	-0.013*** (0.004)	-0.014*** (0.004)		
Abov. mean rainfall					-0.093*** (0.009)
Observations	68,040	68,040	68,040	68,040	68,040
F Statistic	75.746*** (df = 3; 67192)	116.469*** (df = 3; 67192)	87.970*** (df = 4; 67191)	96.940*** (df = 1; 67194)	219.199*** (df = 1; 67194)

Note:

*p<0.1; **p<0.05; ***p<0.01

Source: own elaboration

Eventually, we included a lagged extreme rainfall index and confirmed that the contemporaneous effect associated with extreme rainfall remains significantly negative and of a magnitude similar to the one estimated previously (see column 1 in Table B.3). A very similar pattern is observed when using rainfall above the mean (column 2 in Table B.3) or precipitation z-score and their lagged versions.

Table B.3 Time dimension of the extreme rainfall index (col 1) and of Z scores values above 0 (col 2)
(single column fitting image)

	<i>Dependent variable:</i>	
	Ln NTL/cap	
	(1)	(2)
Xtrm Rainfall	-0.09*** (0.02)	
Lag xtrm	-0.02 (0.01)	
Lag2 xtrm	0.01 (0.01)	
Lag3 xtrm	-0.01 (0.01)	
Lag4 xtrm	-0.01 (0.01)	
Lag5 xtrm	0.01 (0.01)	
Lag6 xtrm	0.02** (0.01)	
Above norm.		-0.09*** (0.02)
Lag abv norm		-0.02 (0.01)
Lag2 abv norm		0.01 (0.01)
Lag3 abv norm		-0.02* (0.01)
Observations	64,260	66,150
F Statistic	15.61*** (df = 7; 63420)	59.75*** (df = 4; 65307)
Note:	* p<0.1; ** p<0.05; *** p<0.01	

Source: own elaboration.

6.7.3 Cloud-free coverage

As mentioned in the main text and in Elvidge et al. (2017), varying cloud coverage quality can influence the value of monthly VIIRS NTL. For our sample of NTL values aggregated at the city-level, VIIRS NTL values are based on an average of 9 days of cloud-free coverage per month. Although the distribution of cloud-free observations varies across the seven countries of interest, they all follow a similar pattern and display a limited number of observations with 15 or more cloud-free days (histogram C.1). When looking at the average number of cloud-free observations by month over the period 2013-2021, a seasonal pattern can be detected: Brazil and Peru experienced a notable increase in the number of cloud-free observations during April to September, while it seems to be the inverse in Mexico and, to a lesser extent, in Chile (see histogram C.2). Argentina is the only country where the number of cloud-free observations is flat all year round, at approximately 10 days/month, which is why Argentina is not included in histogram C.2. Importantly, the average value of city NTL/cap seems to follow this seasonal trend but with less pronounced variations: higher (or lower) NTL values are

recorded during the months where more (or less) cloud-free observations are available. Overall, with a Pearson's coefficient estimated at 0.32, the correlation between cloud-free observations and NTL values is quite strong and warrants a cautious approach. In this setting, the observed reduction in NTL values during months of high cloud-coverage (which are also the months where extreme rainfall events tend to occur) could confound the estimation of extreme rainfall impact.

As argued in the main text, the inclusion of a country-monthly fixed effect in Eq. (1) allows the soaking up of all the monthly variations in cloud coverage, that commonly affects the NTL values of cities within a given country. As cloud coverage is more spatially diffuse than extreme rainfall, which are by nature very localized events, we consider that this country-monthly fixed effects at least partially limit this issue. However, to further control the potential impact of cloud coverage variations we used two additional robustness tests. First, we used a more restrictive cloud-coverage quality threshold and removed cities that had less than 6 days of cloud-free observations, on average (i.e. almost a quarter of the sample, or 88 cities, were removed), with the objective of excluding these cities, which are regularly affected by high cloud coverage from the estimation. Second, we added an additional quarter trend fixed effect, to capture a potential cyclical winter/summer variation due to cloud coverage. The results of these two estimations are shown in column 1 and 2 of Table C.1, respectively, and confirm our previous results: extreme rainfall events have a negative impact on city NTL/cap that does not seem to be driven by lower cloud-free observations.

Histogram C.1. Number of cloud-free observations used to compute the monthly NTL values, 2013-2021

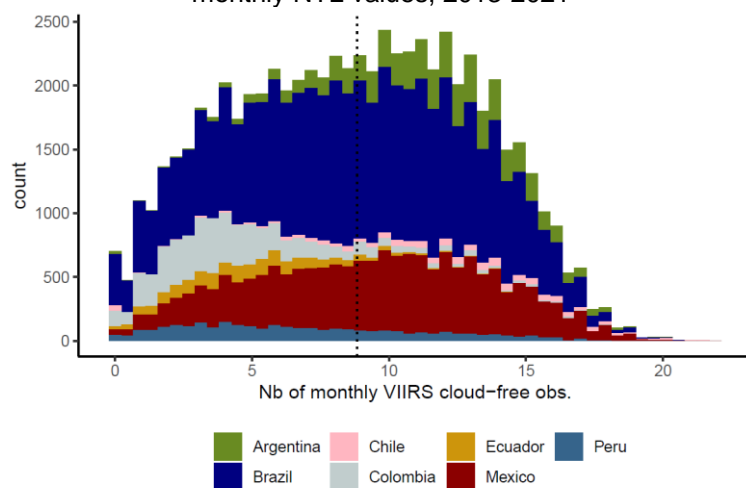
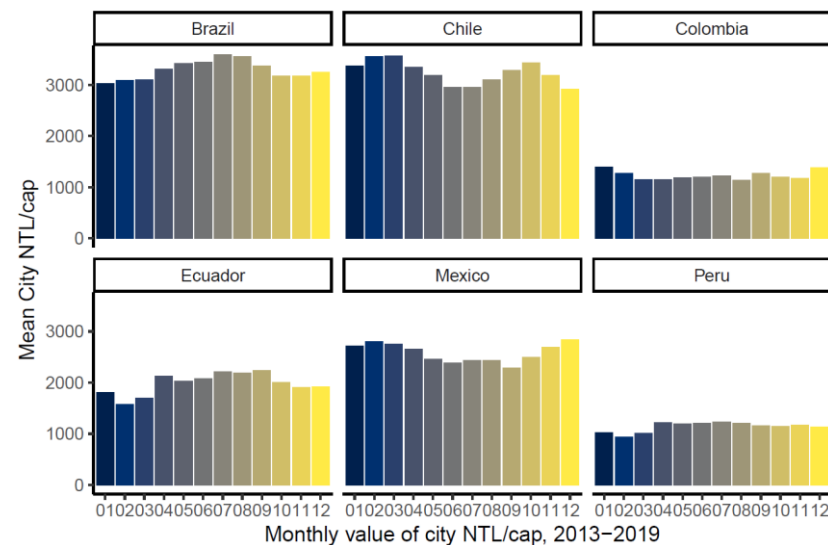
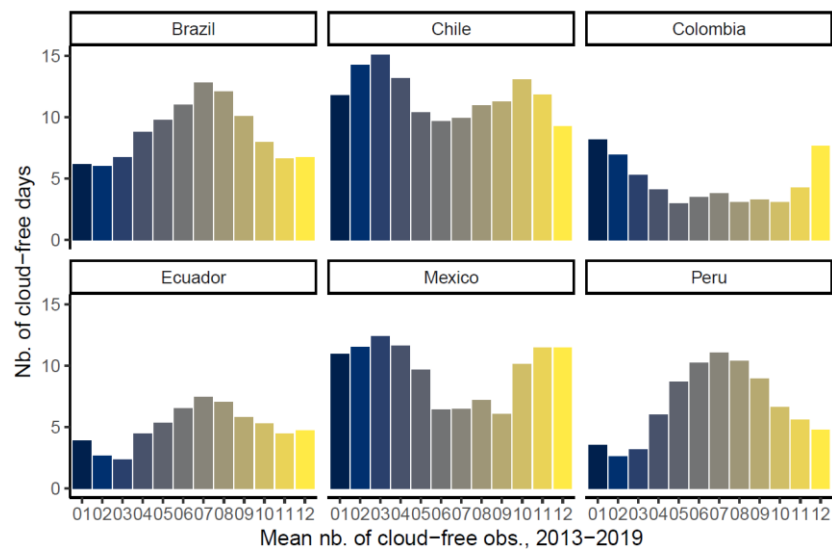


Table C.1. Results for additional cloud coverage quality controls

	Dependent variable:	
	Ln NTL/cap (1)	(2)
Xtrm Rainfall	-0.058*** (0.012)	-0.079*** (0.014)
Temp. Z	0.046*** (0.005)	0.060*** (0.006)
Sq. Temp. Z	-0.014*** (0.003)	-0.013*** (0.004)
Observations	58,536	68,040
F Statistic	56.503*** (df = 3; 57776)	75.746*** (df = 3; 67192)
Restrictive cloud-coverage quality threshold (>6 days)	YES	
Additional Quarter fixed-effect	YES	

Note: *p<0.1; **p<0.05; ***p<0.01

Histogram C.2 Monthly distribution of mean cloud-free observations (left) and NTL values (right), 2013-2021



Source: own elaboration.

6.7.4 Greenness index sensitivity analysis

To test the sensitivity of our results to different greenness index specifications, we conducted extensive robustness checks. First, we altered the different NDVI and greenness index thresholds values used in the main text. Specifically, we started by estimating Eq. (2) including all cities with a greenness index above 1. In doing so, we added 93 cities to the sample used in the main text, which included all cities with a greenness index higher than 5. To ease comparisons, column 1 of in Table D.1 reports the results for our benchmark model using the sample of cities from the main text. Following columns report results splitting the larger alternative sample into two groups at the values corresponding to the median (col. 2) and the 3rd tercile of the greenness index (col. 3). Results confirmed that a higher greenness index reduces the negative effects of extreme rainfall events. Interestingly, the model based on the median value of this new sample (i.e. a greenness index of 13.45) suggests that the difference of impacts between the two bins is not statistically significant, while the model based on the third tercile (i.e. a greenness index of 20.31) evidences a significant difference in impacts, with a reduction of a similar magnitude to what was obtained using the sample in the main text. These estimates suggest that, on average, cities with a greenness index higher than 20 display a lower vulnerability to extreme rainfall events. Results varying the minimum greenness index threshold between 1 and 5 suggested a consistent pattern but are not reported, for the sake of conciseness.

Table D.1 Econometric results for different greenness index threshold

	<i>Dependent variable:</i>		
	Ln NTL/cap		
	(1)	(2)	(3)
Xtrm Rainfall	-0.120*** (0.031)	-0.085*** (0.024)	-0.093*** (0.019)
Xtrm Rainfall: Med. Greenness	0.064* (0.033)	0.009 (0.030)	
Xtrm Rainfall: 3rd Quart. Greenness			0.049** (0.024)
Observations	54,324	64,368	64,368
F Statistic	37.282*** (df = 2; 53064)	36.500*** (df = 2; 63015)	39.185*** (df = 2; 63015)
Minimum greenness index value	5	1	1
<i>Note:</i> *p<0.1; **p<0.05; ***p<0.01			

We then considered a NDVI threshold value of 0.6 to categorize pixels as “dense vegetation pixels” (as opposed to a NDVI threshold value of 0.5 in the main text) and repeated the estimation strategy employed above. Table D.2 reports the results of this more restrictive NDVI threshold value, considering cities displaying a greenness index above 5. Results confirm that previous findings hold, although the difference in effects between the different bins is only statistically different for the model splitting the sample at the 4th quartile of the greenness index (col. 3).

Table D.2 Econometric results using a NDVI threshold of 0.6 to define dense vegetation pixels

	<i>Dependent variable:</i>		
	Ln NTL/cap		
	(1)	(2)	(3)
Xtrm Rainfall	-0.113*** (0.029)	-0.106*** (0.024)	-0.104*** (0.022)
Xtrm Rainfall: Med. Greenness	0.046 (0.033)		
Xtrm Rainfall: 3rd Tercile Greenness		0.045 (0.029)	
Xtrm Rainfall: 4th Quart. Greenness			0.058** (0.028)
Observations	42,660	42,660	42,660
F Statistic (df = 2; 41508)	41.638***	41.277***	41.977***
NDVI Threshold Value	0.6	0.6	0.6
<i>Note:</i> * p<0.1; ** p<0.05; *** p<0.01			

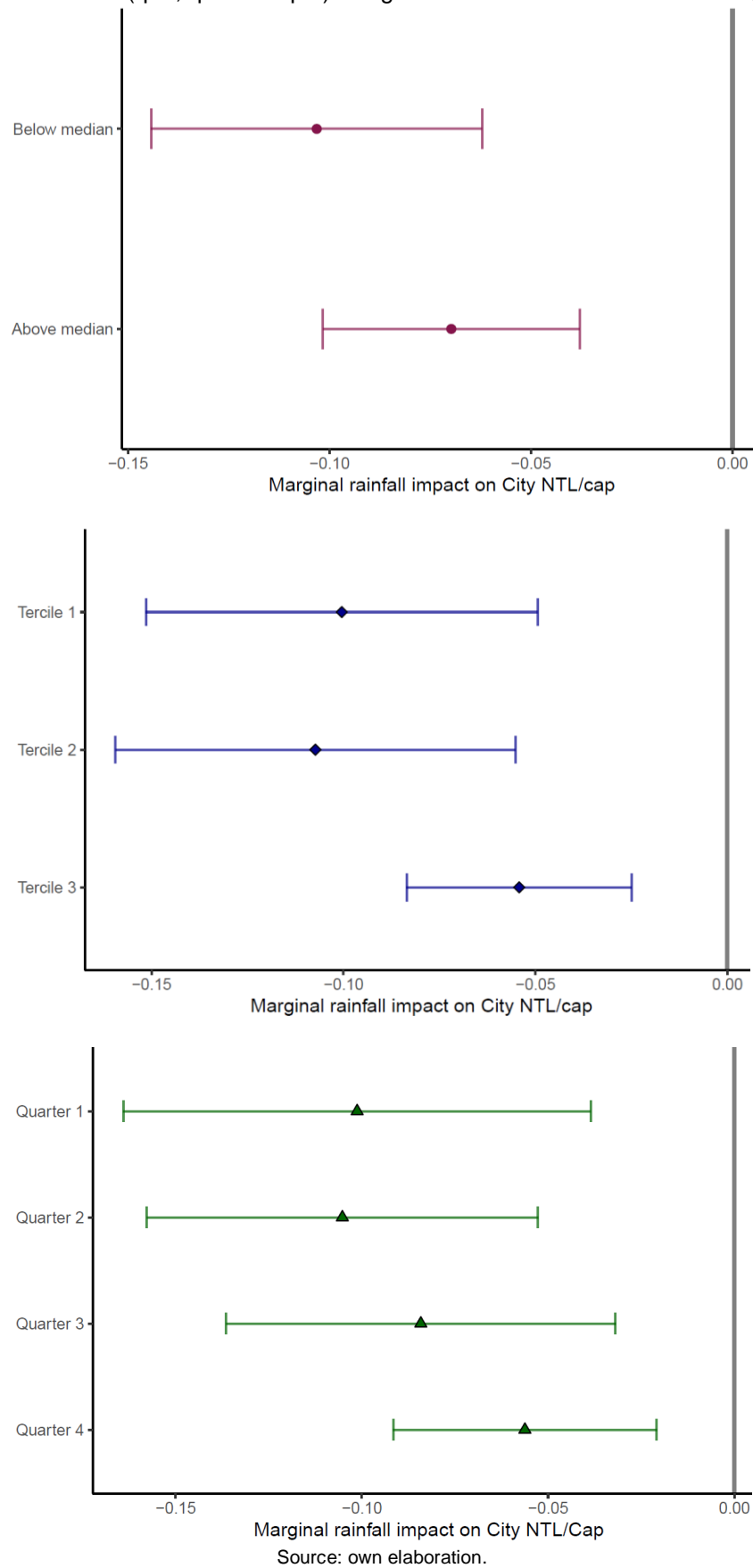
Eventually, we removed cities with a very high greenness index (i.e. cities with a greenness index above 40) to ensure that the estimated effects did not depend on a few cities that could be viewed as outliers, in terms of land cover. Results are almost identical to these displayed in column 1 of Table D.1 and confirm that previous results are not overly sensitive to these high values.

A second set of robustness checks tested an alternative NDVI spatiotemporal resolution. To this end, we leveraged the dataset provided by Corbane et al. (2020), which computed NDVI values within urban centers using the same underlying Landsat annual composites, but working at a 1km resolution on a time interval that spans from 2012-01-01 to 2015-12-30 i.e. only the first part of the period considered in the analysis. Resulting pixel values were classified into one of the three classes as follows: values below 0.1 are associated with

built-up structures, barren rock, sand or snow; pixel values in between 0.2-0.5 are assumed to correspond to shrubs or agriculture areas; pixel values above 0.6 are associated with dense vegetation such as forests, urban garden or parks. I used these categorical values to compute the greenness index as the ratio of pixels above 0.6 over all city pixels, in a similar fashion to our greenness index shown in the main text.

Results are shown in Figure D.1 following the same structure than in the main report: the city greenness index has been discretized into various bins corresponding to the q-quantile values of this alternative greenness index. Again, to exclude any protection benefits that could be derived from the fact that cities without dense vegetation are intrinsically more vulnerable to extreme rainfalls, we excluded cities with a greenness index below 0.1 (approximately 10% of cities from our original sample). We find that differences in impacts are particularly visible when splitting cities into three bins. In this model, for cities below the third tercile of greenness, the marginal extreme rainfall effect reduces nightlights by more than 10%. Contrastingly, in cities with greenness indexes above the third tercile (with an average green index of 0.66), this marginal effect is reduced to approximately -5%. In addition, we tested and rejected the null hypothesis of no differential impact of extreme rainfall events between the second and third bins (P value < 0.1). Models with $q=4$ and $q=2$ show a consistently decreasing impact of extreme rainfall, as the level of greenness increases. In the case of the $q=4$ model, we were able to reject the null hypotheses of equality between the coefficients associated with the last bin and the second bin (P value < 0.1). However, we were not able to reject it for the model with $q=2$ at conventional levels. Overall, when using this alternative source of data, the estimated impacts suggest that adverse effects triggered by extreme rainfall are attenuated in a similar magnitude than previously estimated, although effects seem a bit noisier with this coarser spatial resolution.

Figure D.1 Estimated effects of three models of extreme rainfall interacting with q-quantiles of greenness index (q=2, q=3 and q=4) using NDVI values from Corbane et al. (2020)



Although this investigation has focused on the greenness of the land cover, the effect of extreme rainfall on city NTLs may differ along many dimensions. To ensure that the differentiated impacts reported above are not driven by other sources of heterogeneity potentially correlated to the greenness index, we have performed a final set of robustness checks. Three additional source of heterogeneity that could have potentially confounded our estimation were considered: the population of a city, the mean precipitation level and its elevation. We therefore used Eq (5) in the main text and interacted our extreme rainfall variables with the greenness index as well as a new interaction term based on either (i) 2015 city population, (ii) average rainfall over the period 2013-2021 or (iii) the average elevation of each city.

The population of a city might constitute a very important dimension likely to shape extreme rainfall impacts on city NTLs. We posit that the more populated the city, the lower the marginal impact of extreme rainfall events. In fact, for the largest cities in our sample, due to scale effects, it is unlikely that a given extreme rainfall event affects the entire city population. NTL reductions in one area might thus have a modest impact on overall city NTLs or might even be compensated by positive effects in another area of the city. For very large cities, these spatial spillovers could “averaged out” extreme rainfall effects and produce unclear aggregated effects on city NTLs.

Extreme rainfall effects might also be differentiated in wet and dry regions. We assume that wet regions are used to deal with abundant rainfall and might have more incentives to invest in infrastructure that limit surface run-off and channel water out of the city. In other words, cities in wet regions might be better equipped to cope with extreme rainfall events than cities in dry regions, where rainfall is low and concentrated only over a few months of the year. Although this dimension is partially captured in the z-score formula used to depict extreme rainfall events, we used this second interaction term to test for this effect more explicitly.

Finally, extreme rainfall effects might also be moderated by the elevation of a city. One might expect that impacts of extreme rainfall will be more severe the further downstream a city is located because it is potentially located in areas more prone to flood risk and because pluvial flooding tends to be more intense downstream. Contrastingly, city located upstream or at higher locations could potentially experience less pronounced impacts because extreme rainfall will be more easily channelled out of the city. To test this effect, we have extracted the average elevation estimated within the extent of each city provided by the UCDB. This elevation is expressed in metres above sea level. Cities covered in sample range from almost sea-level altitude for coastal cities, to above 2,500 meters for the highest cities in Peru, Colombia and Ecuador.

Results are shown in Table D.3 and confirm that the marginal effect of extreme rainfall is significantly reduced for cities displaying a higher than median greenness index, even considering these additional sources of heterogeneity. Column 1 indicates that adverse effects are diminished as city population increases, confirming that more populated cities tend to be less vulnerable to extreme rainfall. On the other hand, in column 2, the coefficient associated with average precipitation is not significant, suggesting that cities located in wet or dry regions do not display differentiated responses to extreme rainfall events, everything else being equal.⁶⁷ Finally, column 3 indicates that the higher the elevation of the city, the lower the negative effects associated with the extreme rainfall index, although this does not alter the benefits of a greener land cover.

Table D.3 Other sources of heterogeneity potentially confounding the differentiated impacts of greenness

	<i>Dependent variable:</i>		
	Ln NTL/cap		
	(1)	(2)	(3)
Xtrm Rainfall	-0.568*** (0.202)	-0.123*** (0.032)	-0.150*** (0.038)
Xtrm: Greenness	0.074** (0.035)	0.064* (0.033)	0.067** (0.033)
Xtrm: Ln City Pop	0.037** (0.015)		
Xtrm: Av. Precip.		0.00001 (0.00001)	
Xtrm: Elevation			0.0001*** (0.00002)
Observations	54,324	54,324	54,324
F Statistic (df = 3; 53063)	29.324***	25.047***	29.228***
<i>Note:</i>	* p<0.1; ** p<0.05; *** p<0.01		

Source: own elaboration.

Taken together, these robustness checks confirmed that the results presented in the main text were not driven by other sources of heterogeneity across our sample of cities, nor overly sensitive to the thresholds values employed to characterize city greenness or city outliers in terms of greenness index. Overall they increase our confidence in the estimates used in the main text.

⁶⁷ This is consistent with the results displayed in Column 4 of Table 1 of section 3 in the main text, indicating that relationship between NTL and precipitation is not adequately captured by a U-shaped curve. It

7 SUMMARY OF FINDINGS: SPATIAL AND URBAN PLANNING AS CLIMATE POLICY TOOLS

Human settlements are the result of long-term processes in which history, geography and culture, among other major drivers, constantly interact to consolidate specific spatial and land cover patterns. Substantially modifying these geographical patterns once they have consolidated is a challenging task. However, over the next decades, urban population is expected to continue increasing in the region (UNDESA, 2019), providing a unique opportunity to rearrange the geographical patterns of Latin American cities. As evidenced throughout this thesis, restructuring the spatial configuration and land cover composition of cities is not climate neutral. The two case studies above have examined how these patterns can have important impacts in terms of (i) CO₂ emissions and (i) vulnerability to extreme rainfall events. This chapter summarizes the main findings of these case studies and discuss how urban and spatial planning policies, which provide the tools to reconfigure the geographical patterns of cities, could help addressing climate change challenges.

7.1 Spatial and urban planning policies to enable low-carbon urban systems

This thesis has shown that, in Latin American cities, urbanization has materialized through different spatial expansion patterns, with important implications for CO₂ emissions. Using a population-based approach to consistently delineate cities and spatially distribute CO₂ emissions, case study 1 has indicated that between 2000 and 2015 the population living in a sample of 635 cities has increased by 21%, while the CO₂ emissions of these cities have soared by 68%. Under this influx of new urban dwellers, the spatial extent of cities of the region has been enlarged, although the speed at which each city has expanded has been very heterogeneous. From a spatial perspective, three distinct patterns of expansion have been distinguished: (i) a compact expansion, in which a city densifies over time and new settlements occur mainly within the urban centre -the suburban ratio decreases; (ii) a passive expansion, in which a city densifies but population growth is faster in suburban areas vis-à-vis the urban centre -the suburban ratio rises; (iii) a sprawled expansion, whereby new residents primarily settle in areas adjacent to the urban centre, lowering both the density and suburban ratios. Between 2000 and 2015, approximately 10% of Latin American cities have displayed a compact spatial expansion, while 64% have experienced a passive expansion driven by a consolidation of suburban areas.

These three spatial expansion patterns produce diverging CO2 emissions trajectories. Based on the statistical analysis conducted in case study 1, CO2 elasticities at the city-level indicate that a 1 % increase in density reduces CO2 emissions by 0.58 %, while a 1 % growth in the suburban ratio boosts emissions by 0.41 %. These coefficients thus imply opposite CO2 effects for most Latin-American cities, which have experienced a concomitant increase in density and suburban ratio (i.e. a passive expansion pattern). Using these elasticities and the average historic growth rates associated to each spatial expansion patterns, I showed how, for an average city, the compact expansion model could generate a 12 percentage points smaller increase in CO2 emissions than its passive counterpart, *ceteris paribus*.

Projections of CO2 emissions for all the cities in my sample confirm that a more compact expansion could significantly shift downwards regional urban emissions. Specifically, under the compact expansion scenario, regional urban emissions in 2030 could be almost 3% lower than in the BaU scenario where historical urbanization patterns prevail.⁶⁸ Although this 3% reduction might seem marginal, it is exclusively achieved by altering the spatial distribution of future urban population. It assumes that everything else -i.e. the carbon intensity of the energy matrix or urban mobility patterns- remains unchanged. As such it is not to be interpreted as a forecast of urban emissions but rather as the “carbon savings” that can be obtained by shaping the spatial expansion patterns.⁶⁹ This 3% reduction should therefore be compared to the 2030 collective objective set out by the countries of the region through their NDCs: a 22% reduction of GHG emissions relative to the BaU (or a 28% reduction conditional upon international assistance; Samaniego et al. 2022). This 22% is intended to be achieved primarily by actions in the energy, transport and land use sectors. The GHG impacts of measures related to the spatial expansion of cities have not been quantified in the current NDCs of the region, making them all the more relevant to raise climate ambition.

From a policy perspective, these findings suggest that to maximize carbon savings urban and spatial planning policies should combine (i) actions at the city-level to promote a compact expansion pattern primarily in small and intermediary cities with

⁶⁸ This regional projection incorporates the statistical uncertainty associated to my CO2 elasticities and factors-in the heterogeneous benefits of a compact spatial expansion model across the sample of cities. Notably, for cities with a population above 1 million persons, higher density produces non-significant effects on CO2 estimates. See case study 1 for more details.

⁶⁹ As explained in case study 1, carbon savings are defined as the CO2 difference between projected emissions under a scenario that includes a quantified set of climate policy actions and projected emissions in a baseline scenario without these policies.

(ii) a broader strategic reflexion aimed at rebalancing the population of cities across the urban system of a country/region.

At the city-level, while the literature has generally focused on the effects of higher density, this thesis argues that a more dynamic vision is required to design adequate and relevant policy packages. Beyond increasing-density policies, the dynamics at play between suburban areas and urban centers are a primordial driver of CO₂ emissions at the city-level. For cities that achieve higher density through a consolidation of suburban areas (i.e. faster suburban population growth than urban centers population), carbon savings will be reduced or inexistent. To efficiently reduce CO₂ emissions at the city-level, urban planning policies should seek to achieve higher density levels through a faster population growth in urban centers than in suburban areas. In other words, urban planning policies should seek to reinvigorating historical urban centers to accommodate new urban dwellers within existing boundaries. Simultaneously, these increasing density policies should be controlling for potential relocation effects (either within the city or from surroundings rural areas) that could exacerbate suburban sprawl. In simple terms, it is not so much about density but rather about the spatial expansion dynamics of the entire city (i.e. the urban centre and its suburban areas).

The design of a policy package that can effectively shape spatial expansion dynamics will depend on the specific context of each city but it should incorporate the carbon costs of suburban sprawl. The policy tools that can be mobilized include options ranging from land-use regulations to taxation, building codes, housing programs or transportation incentives. All these tools have been used by urban planners and policymakers around the world to effectively shape spatial expansion dynamics. The design of an appropriate policy package for a particular city is nonetheless a task far beyond the scope of this thesis, notably because it requires intensive participation from all cities stakeholders and should not only focus on climate considerations. In fact, these policy packages will probably be as diverse as the cities analysed in this thesis. However, if they seek to curb CO₂ emissions, these policy reforms will all have to account for the carbon costs of differentiated spatial expansion dynamics.⁷⁰

Accounting for the carbon costs of suburban sprawl implies two major changes. First, from a technical point of view, the CO₂ effects attached to a given spatial expansion

⁷⁰ From a theoretical perspective, Brueckner (2000) already identified two major urban market failures behind urban sprawl: failure to account for the social costs of congestion -which lead to excessive commuting- or failure to make new urban development pay for the infrastructure costs it generates -which lead to fragmented and sprawled cities. Although this is not the core focus of this thesis, from a public economy perspective, the failure to account for the carbon cost of suburban sprawl represents another major urban market failures.

dynamic should be incorporated into traditional urban planning policy tools. In concrete terms, this means that measures related to, for example, land regulation, transportation or public housing should account for their effects on spatial expansion dynamics and the related CO₂ emissions consequences. This thesis has provided elements to measure the CO₂ effects attached to a given spatial expansion pattern. Tailored analysis is now required to quantify the effects of urban planning tools on the expansion dynamics of a given city and derive their potential CO₂ consequences. Second, from a political economy point of view, these technical changes will have to actually impact the core urban decision-making process and influence trade-offs about urban land-use. This second change will probably not happen without a profound redistribution of power that is discussed more in detail in section 7.3.

Beyond city-level measures, my findings also shed light on the role that spatial planning policies can play to promote low-carbon urban systems at the national level.

At the national level, policies aimed at increasing density should prioritize small and intermediary cities with relatively low development levels. As shown in case study 1, these cities are likely to exhibit the fastest population growth rates in the coming years and are those where such policies can deliver the most significant CO₂ reductions. By contrast, increasing density in large and affluent cities is unlikely to have much impact on CO₂ emissions. Higher density could in fact exacerbate congestion effects already observed in some of these large cities and produce unclear effects on CO₂ emissions. In countries where monocentric urban systems are structured around few very large megalopolises, climate policies should focus on rebalancing the population distribution across the urban system. This could be done, for example, through incentives to encourage firms and people to relocate to the urban centres of secondary cities. As Meijers and Burger (2017) pointed out “*agglomeration externalities are not confined to the borders of agglomerations and may instead be shared throughout city networks*”. Identifying and enhancing these positive “city network externalities” can help rebalancing the population between large, congested megalopolises and secondary cities, which in return will reduce the aggregated CO₂ urban emissions that the region would have otherwise produced. Fostering city networks that can facilitate a redistribution of urban population across the cities of a country/ region represents a powerful yet largely unexplored avenue to achieve CO₂ savings.

The set of measures described above will be crucial to enable emission reductions in at least two other sectors. Case study 1 only quantified the direct impacts of spatial expansion on CO₂ emissions. In dynamic terms, two second round effects are likely to play a crucial role for future CO₂ emissions. Firstly, cities that expand in a compact way can

more easily trigger a massive shift in urban mobility patterns. On the one hand, compact cities display shorter travel distance, which facilitates the promotion of alternative transportation modes (e.g. walking cycling). On the other, compact cities have higher density in urban centers, which has been found to be a decisive variable to foster public transport systems (e.g. buses, trams, subways and light rail; see Cooke and Behrens 2017). Secondly, case study 1 has not analysed the impacts of urban land expansion on the ecosystems and potential carbon sinks located in the immediate surroundings of a city. I acknowledge that this could represent an important source of future emissions. Seto, Güneralp, and Hutyra (2012) have for example estimated that, at the global level, the expansion of cities until 2030 could produce irreversible land cover changes that would result in the loss of carbon stored in vegetation biomass for an amount equivalent to approximately 5% of emissions from tropical deforestation and land-use change.

To summarize, shaping the spatial expansion of cities produces direct impacts on CO₂ emissions and enables system-level changes that are required to transition to a low-carbon urban development. Beyond the impacts quantified in case study 1, a more compact expansion of cities could notably foster low-carbon urban mobility patterns and refrain the destruction of carbon sinks in the surroundings of existing urban areas. Although quantifying these second-round effects at the regional level entails more uncertainty, they illustrate how shaping structural features such as the spatial extent of cities can help triggering system-level changes. Without these system-level changes deep and quick emission reductions are unlikely to happen. A better understanding of how actions aimed at shaping cities' spatial expansion interact with policies seeking to alter urban mobility patterns at the local level is now required to maximize synergies and positive spillovers between these sectors. Hopefully, the combined effects of these changes can deliver compounded CO₂ benefits that will produce a reduction of GHG emissions in the magnitude required to preserve global climate stability.

7.2 Urban and spatial planning policies to reduce vulnerability to extreme rainfall

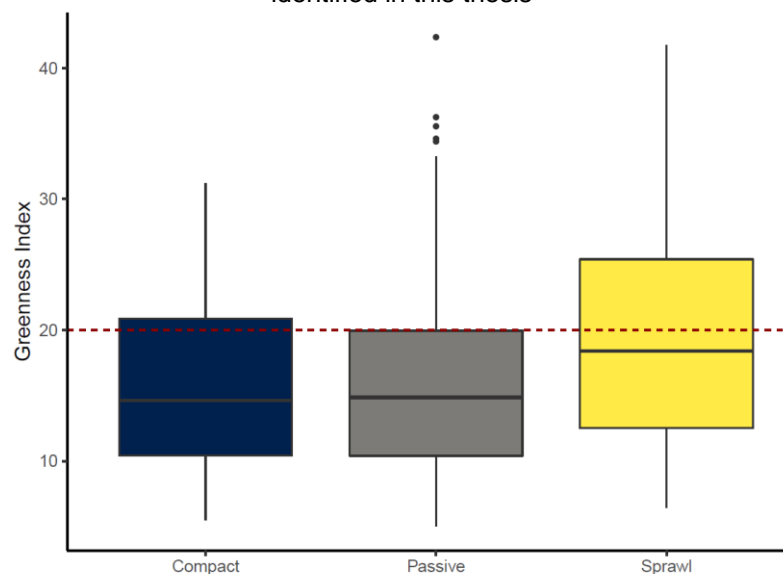
This thesis has shown that in Latin American cities extreme rainfall events trigger negative effects on urban economic activity. To this end, night-time light (NTL) satellite imagery has been used to proxy local economic activity within the borders of my sample of cities. Statistical analysis has shown that extreme rainfall events negatively impact city NTL/cap in the region, with the average extreme rainfall triggering a city NTL/cap reduction of almost 20% *ceteris paribus*. Tail extreme rainfall events -which are expected to become more frequent under high-warming climate scenarios- could further inflate these estimates: rare extreme events with a 1% annual probability of occurring generate losses as high as 30.7%. Interestingly, these negative effects are rather short-term effects that do not persist nor generate a rebound effect in economic activity in the subsequent months.

The second case study of this thesis has also evidenced that these negative effects are substantially reduced in cities that display a greener land cover. To put it differently, cities with considerable urban parks, rain gardens or green areas display a reduced vulnerability to extreme rainfall events, *ceteris paribus*. Specifically, for cities where dense vegetation represents more than 20% of total city area, the marginal impact of extreme rainfall is broadly halved vis-a-vis cities below this threshold. Consistent with the hydrological literature, the adverse effects associated with extreme precipitation are not totally wiped out by a greener land cover, which insinuates this measure alone is not enough to fully protect against the economic impacts of extreme rainfall. Significant protection benefits are nonetheless associated with a greener city land cover and, leveraging the strong correlation between city NTLs and GDP, I provided a monetary valuation of these benefits. A counterfactual analysis for the year 2015 suggests that if a quarter of the cities in our sample had increased their share of green land cover from 13% on average to above 20%, an additional US\$ 6,500 million could have been reaped, in terms of avoided losses or reduced business disruption. These benefits are equivalent to approximately 19% of total estimated losses.

From a policy perspective, these findings imply that greening the land cover of a city can considerably contribute to protecting local economic activity from losses and disruptions caused by extreme rainfall. As cities continue to expand in flood prone areas and climate change further intensifies the hydrological cycle, more frequent and intense extreme rainfall events are expected to impact Latin American cities. Although there is a lot of uncertainty regarding extreme rainfall projections at the city-level, these trends will only

turn the benefits associated with a greener land cover more relevant. It is nonetheless important to underscore that the ability to develop a high share of dense vegetation within the city seems to be differentiated based on the spatial expansion model that a city has followed. Based on the three spatial expansion patterns identified in case study 1, Figure 46 shows how cities under the compact and passive expansion models display a similar distribution of the greenness index. This provides suggestive evidence that the compact spatial expansion pattern is not associated with a lower greenness index than the passive one.⁷¹ However, more than 40% of the cities classified under the sprawled expansion have a greenness index above 20 (i.e. the threshold to start reaping protection benefits in case of extreme rainfall depicted by a red dotted line in Figure 46). This suggests that for sprawled cities, which are characterized by lower density, the preservation of a higher share of green areas is easier.

Figure 46. The distribution of the greenness index in each of the three spatial expansion patterns identified in this thesis



Source: own elaboration.

The set of interventions that can effectively greening the land cover will depend on the specific context of each territory but it requires a fundamental policy reform for all cities: accounting for the climate adaptation benefits associated with a greener land cover. Greening the land cover of a city for flood protection can be done through a wide array of measures including the preservation and restoration of wetlands, or the deployment of rain gardens, infiltration trench and grassed swales that can absorb rainfall

⁷¹Figure 46 is based on the average greenness index over the period 2013-20120. A lineal regression confirms that only the sprawled expansion model has a significant effect on the level of the greenness index. I acknowledge that a dynamic comparison would have been more appropriate but, as explained in case study 2, NDVI values are heavily influenced by climatological factors at the local level. Further data processing would be required to isolate the evolution of green areas from other factors and develop a timeseries that accurately depicts the variation of green areas.

and help managing surface runoff. As for case study 1, identifying the specific combination of interventions for a given city is beyond the scope of this thesis as it requires extensive stakeholder engagement and local agronomic knowledge. Better understanding how rising temperature could impact dense vegetation within the city also remains a crucial issue to adequately calibrate GI interventions to future climate conditions.⁷² From a public policy perspective, fostering such a policy will nonetheless require a common change: ensuring that the benefits associated with a greener land cover in case of extreme rainfall are accounted for and incorporated as a core element of the urban decision-making process.

Properly accounting for the potential benefits associated with a greener land cover requires two important elements. First, from a technical point of view, beyond the evidence provided in this thesis, research at a finer spatial resolution is required to inform the deployment of green infrastructure for flood protection. It is, for example, crucial to evaluate the detailed geographical and hydrological properties of a specific watershed to assess the different locations where green infrastructure can be deployed and evaluate their optimal combination with traditional flood infrastructure already operating. GI efficacy can also be altered by the specific type of vegetation used or by different storm intensity and duration parameters under a changing climate. Due to the nature of the data used in this investigation, these factors have not been addressed. They nonetheless have to be investigated in-depth to inform specific actions for a given city. Secondly, from a political economy point of view, fostering a greening of the land cover of a city often implies confronting vested interest in traditional urban development. As detailed in the next section, strong coordination efforts and a redistribution of power at the city level will probably be required to facilitate the emergence of such a greening policy.

If the two elements above are in place, the benefits associated with a greener land cover could be leveraged through innovative taxation mechanisms based on land cover composition. Grounded in traditional public economy analysis, such mechanisms would seek to address the negative externalities that impervious surfaces generate in terms of urban flood risk. Specifically, given that impervious surfaces exacerbate runoff, a tax proportional to the amount and extent of impervious surfaces could be charged to business and properties located within city boundaries. From a feasibility perspective, aerial imagery could help conducting an objective assessment of the amount of impermeable surfaces attached to each property. This assessment would constitute the base to calculate the

⁷²As climate warms, evapotranspiration will be intensified and the urban heat island effect already observed in cities could further exacerbate the water needs of dense vegetation. In this context, expanding the coverage of urban GI might require strong water availability, which could prove challenging for some cities of the region already experiencing high water stress episodes.

amount to be charged through this tax, which could be levied as part of stormwater charges that agents draining into the city's stormwater management system are usually subject to.⁷³ In return, this tax could serve to (i) fund revamped stormwater infrastructures and enhance climate change adaptation capacities at the city level and/or (ii) to incentivize the greening of the land cover by private agents. Low-income households will probably have to be supported to pay this tax, while business actively implementing green infrastructures and best practices to reduce water runoff could be offered financial incentives and tax rebates. In any case, a careful design is warranted as this tax might have serious distributional impacts and the benefits of green areas can be very heterogeneous across a wide array of dimensions. Similar mechanisms could be envisioned for other climate co-benefits (e.g. reduced UHI effect, groundwater recharge, carbon sequestration...) or ecosystem services (e.g. physical and mental health benefits, recreational, aesthetic and cultural value...) provided by green infrastructures, potentially beefing up the role that this tax can play in shaping the geographical patterns of cities.

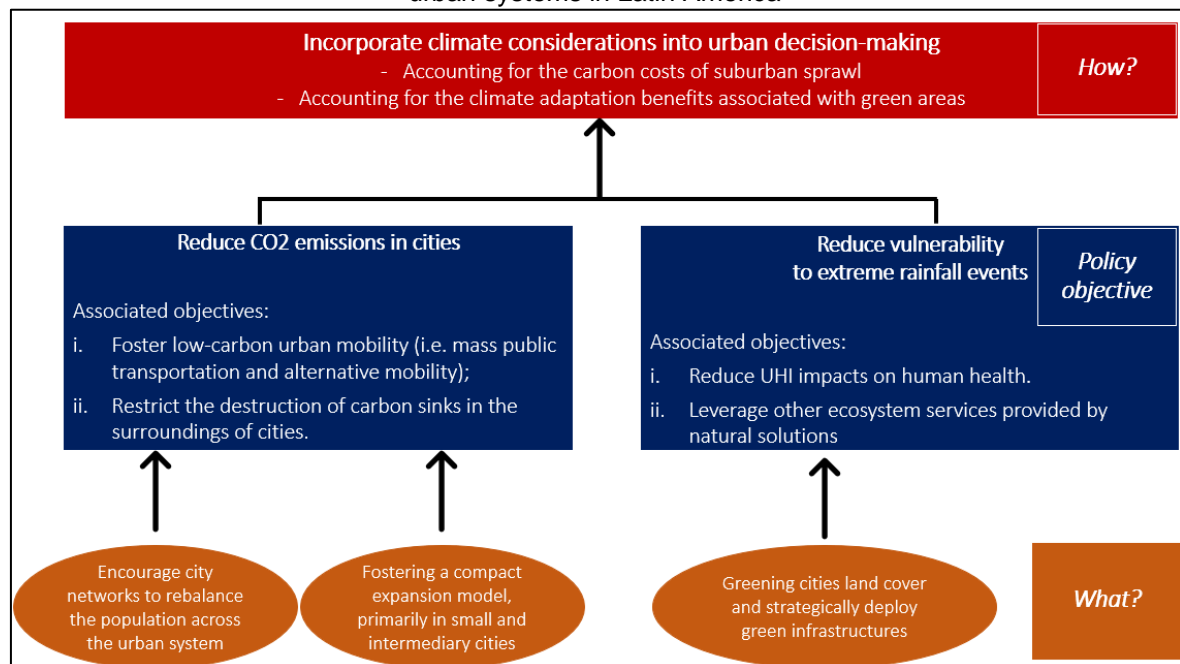
To conclude, it must be underscored that measures seeking to greening cities land cover should be incorporated into a broader set of reforms aiming at strategically manage land-use to reduce urban flood risk and adapt to climate change. Under this broader set of reforms, actions aimed at limiting exposure to flood should be combined with those seeking to reduce vulnerability. Land-use and zoning regulations can for example contain the development of new settlements in flood prone-areas. Similarly, resettlements programs might be the only viable option for low-lying areas that could be permanently flooded under the compounded effects of coastal floods and sea-level rise. On the other hand, the greening of the land cover should be articulated with other measures aimed at managing surface water runoff. The deployment of green infrastructures should for example be incorporated into the broader stormwater management plan of a city to ensure that these interventions efficiently contribute to reduce the burden on drainage systems in case of extreme rainfall events. Ultimately, the integration of this greening policy into a broader land use planning effort will clarify how much and which urban land will have to be greened. In return, these factors will determine the costs and technical feasibility of this greening policy.

⁷³ This kind of mechanisms are already being used in some cities in Canada and it could further inspire Latin American cities. See [more information here](#).

7.3 Towards greener and more compact urban systems?

This thesis has shed light on the role that urban and spatial planning policies could play in enhancing low-carbon and climate-resilient urban systems in Latin America. On the one hand, by harnessing the spatial expansion of cities and redistributing the population across the urban system, significant “carbon savings” can be obtained. A compact expansion is also key to enable system-level changes by fostering complementary actions in the urban transport sector or limiting the destruction of carbon sinks in the immediate surroundings of the cities. On the other hand, by preserving green areas and deploying green infrastructure, cities can lessen economic losses and disruptions triggered by extreme rainfalls. Green infrastructure can also contribute to reduce vulnerability to heatwaves by reducing urban heat islands effects and their associated adverse impacts on human health (see Chapter 3). Figure 47 summarizes these policy options (i.e. the “*what?*” line) and their related policy objectives.

Figure 47. Summary of the policy options proposed to enhance low-carbon and climate-resilient urban systems in Latin America



Source: own elaboration.

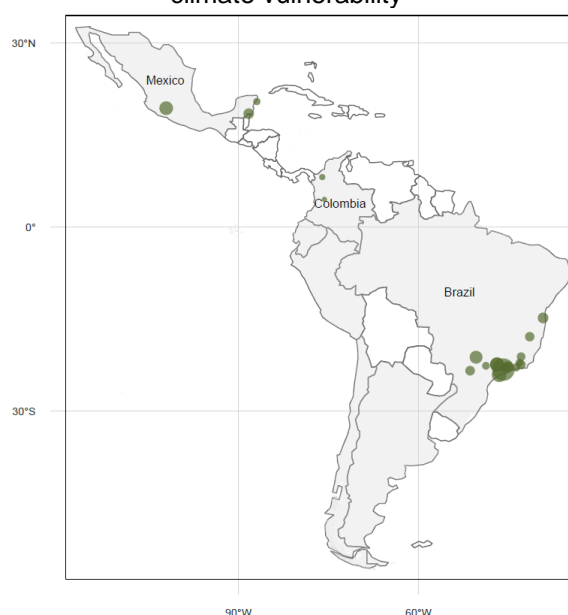
As indicated in the previous section, these policy objectives can be achieved through a wide range of actions that will have to be tailored to the specific context of each territory. They nonetheless require a common systemic change: the incorporation of climate considerations into the core urban decision-making process. Accounting for the carbon costs of suburban sprawl or for the climate adaptation benefits associated with green areas will allow cities to make more informed choices regarding major strategic decisions

on urban land-use. This change to city governance processes will be pivotal to start internalizing the climate externalities associated with different geographical patterns. Without it, urban and spatial planning policies are unlikely to significantly contribute to a low-carbon and climate-resilient future for Latin American urban systems.

The clarity about the changes required to address climate change challenges contrasts with the very limited number of cities actually implementing these changes.

Less than 5% of the cities in my sample display geographical patterns that are simultaneously conducive to a reduction of both CO₂ emissions and climate vulnerability. More precisely, 22 cities, located in 3 countries, have followed a compact expansion while exhibiting a greenness index above the level required to reap protection benefits in case of extreme rainfall. This leaves Argentina, Chile, Ecuador and Peru without any of these cities (see Map 13).⁷⁴ The very few cities that followed a compact expansion while displaying a high greenness index illustrate the magnitude of the challenges that lies ahead: achieving low-carbon and climate-resilient urban systems will require a dramatic departure from the geographical patterns that have historically prevailed in Latin American cities.

Map 13. Cities with geographical patterns conducive to a reduction of both CO₂ emissions and climate vulnerability

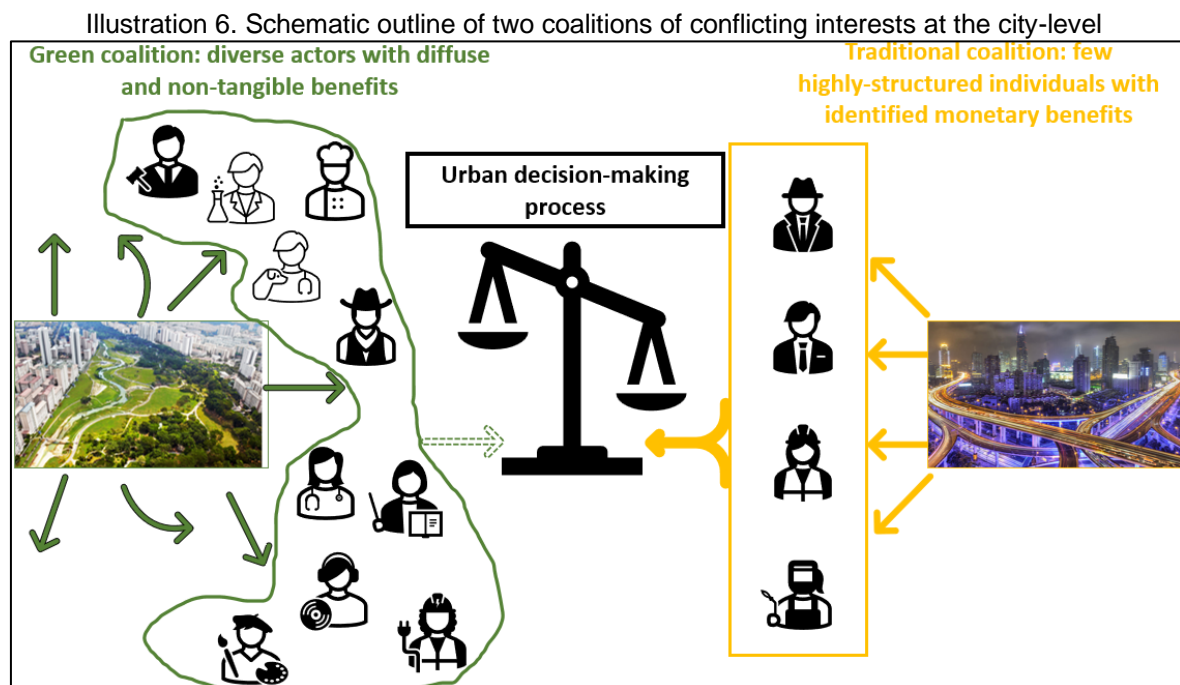


Note: the size of the bubble is proportional to city extents.
Source: own elaboration. Basemap: Natural Earth.

If the benefits associated to these reforms seem so evident, a final question is worth being asked: why 95% of the cities in my sample are not displaying these geographical

⁷⁴ Meeting these two criteria does not necessarily mean that a city is "sustainable". Key dimensions related to environment sustainability (e.g. waste, plastic pollution, air quality) or social dimensions (e.g. inequity, access to education, health, poverty...) are not considered in this analysis.

patterns? This points out to another major issue related to “*how*” to implement the changes required. Although this is not the focus of this thesis, two set of factors have already been mentioned in the previous section. A first one has to do with the strengthening of the technical capacities required to ensure an efficient land-use management. Traditional tools used in urban and spatial planning (e.g. zoning regulations, transport planning, land taxation, housing programs...) will only be efficient if they are adequately used and tailored to the local context. A second set of factors relates to the political economy setting of urban decision-making. In the following paragraphs I provide a schematic outline of the dynamics at play to try to better understand “*how*” these changes could be implemented. Illustration 6 summarizes these dynamics.



Source: own elaboration.

Urban policymakers must address intricate trade-offs on land-use to promote a more compact and greener city. To fix ideas, major strategic decisions on urban land-use can be apprehended as the result of the power relations established between two coalitions of conflicting interests at the city-level. On the one hand, the “traditional coalition” supports priorities such as residential or commercial developments. This coalition is made up of few actors (e.g. business and real-estate developers) with clearly identified monetary benefits that can be individualized (e.g. private profits for entrepreneurs). On the other hand, the “green coalition” is formed by a myriad of actors seeking to develop green urban areas. These actors have very diverse interests associated with the multiple benefits of green areas (e.g. flood protection benefits, biodiversity conservation, temperature regulation, improved physical and mental health to name a few). Moreover, as green areas constitute

urban public goods providing non-excludable and non-rivalrous benefits, the green coalition often perceives diffuse and non-tangible benefits. For example, the protection benefits of a greener land cover quantified in case study 2 of this thesis correspond to avoided losses. Avoided losses are not tangible economic transfers reaped in the form of a direct payment by a private agent. They often go unnoticed. In addition, they favour a large group of persons and the protection benefits received by some do not reduce their availability to others. The same goes for the benefits that green areas produce in terms of reduction of the mortality burden associated with the Urban Heat Island effect. As a result, even when the aggregation of the numerous benefits provided by green areas far exceeds the benefits attached to the measures proposed by the traditional coalition, green areas are not necessarily prioritized by local policymakers.

Prioritizing the greening of city land cover within urban decision-making process requires (i) strong coordination between a wide range of actors and (ii) higher visibility of diffuse interests. Intuitively, because of its reduced number of members and its clearly identified interest, the traditional coalition can easily adopt a well-structured position and efficiently lobby its interest in the urban decision-making process. By contrast, creating a solid green coalition requires strong coordination between the numerous and diverse actors that can benefit from a greener city land cover. Building a strong coordination implies that the benefits associated with green infrastructures are known and understood by a large number of persons. Educating and raising awareness about the benefits of green infrastructure is thus essential to favour their widespread adoption and ease resistance from traditional stakeholders. By quantifying and making more visible the benefits of a greener land cover in case of extreme rainfall, the second case study of this thesis is hoping to contribute to this goal. Only under these conditions the green coalition will be strong enough to confront a well-structured group of vested interests. Unfortunately, the data collected for case study 2 of this thesis suggests that for most of the cities of the region available land for green areas is scarce and tend to be under increasing pressure as cities become more populated (see Figure 37). This insinuates that for larger cities the rising price of land exacerbates trade-offs on urban land-use and tilts the balance towards the traditional coalition.

A similar framework can be used to apprehend urban sprawl. Actors conforming the “traditional coalition” support priorities such as residential or commercial developments for which they have clearly identified monetary benefits that they seek to optimize. One way to optimize these benefits is by acquiring cheaper land, which is usually located at the outskirts of large cities. Because of major urban market failures, the infrastructure costs generated

by new urban developments is generally not supported by this traditional coalition (Brueckner 2000), further increasing the profitability of suburban sprawled for this coalition. On the contrary, a “compact coalition” seeking to harness urban land expansion would have to aggregate a myriad of actors reflecting the diverse and fragmented interests attached to a more compact urban development model (e.g. developing low-carbon urban mobility, preservation of biodiversity and natural landscapes in the surrounding areas, limiting the social costs of congestion attached to excessive commuting...). Although the solutions prioritized by the “compact coalition” are likely to generate a higher aggregated well-being at the city-level, the strong coordination challenges it faces might undermine its ability to lobby and actually influence urban decision-making process.

To recap, this last section has emphasised the magnitude of changes required to address climate change challenges. These changes are of a very high magnitude: 95% of the cities in my sample would have to shift to a more compact expansion pathway and/or considerably greening their land cover. Because the geographical patterns of cities are structural features mirroring the Human-Environment Nexus that has consolidated over the last 200 years, they exhibit strong inertia and path dependency. Consequently, considerably altering them will require more than marginal reforms. Systemic actions are required and these are unlikely to happen without profound changes in the current distribution of power. Essentially, altering cities’ geographical patterns will require the emergence of a new Human-Environment Nexus. As discussed in the last chapter of this thesis, the emergence of a new Human-Environment Nexus is likely to require a shift from the efficiency paradigm towards the robustness paradigm.

8 FUTURE AREAS OF INVESTIGATION

From a theoretical perspective, a major contribution of this thesis is the proposal to mobilize geographical concepts such as space, location and land cover to improve our understanding of climate-related challenges. Traditional investigations of climate change challenges have been driven by energy-related or carbon pricing analysis, which are often *aspatial*. In contrast, this thesis has unveiled the crucial role of geographical features in addressing climate change challenges. This theoretical contribution is directly linked to the development of the methodology detailed in Chapter 4 that leverages Earth Observations (EO) as its main source of empirical observations. As the number of EO will continue increasing in availability and precision, using further spatial and geographical analysis in climate debates remains a promising area for new research. Spatial, locational and land cover features can provide unique insights on dimensions such as: where within a physical space are CO₂ emissions concentrated? How does distance affect carbon performance? Why is carbon performance or climate vulnerability unevenly distributed across space? How do the unique land cover attributes of a place govern its local vulnerability to extreme weather events? How do geographical patterns at the local, regional and national scales interact with one another to produce variations in carbon efficiency and climate vulnerability across space? Guided by this approach, a few areas for potential future investigations have been identified throughout this thesis and are outlined below.

Investigating spatial spillovers and relocation effects induced by climate change challenges

Climate change is likely to induce spatial spillovers and relocation effects that are poorly understood until now. Two major dimensions are worth investigating. First, from a climate adaptation perspective, the negative impacts of extreme weather events (e.g. floods, heatwaves) are likely to trigger spillovers in neighbouring areas. These spillovers could be negative or positive depending on the intensity of the shock considered and the prevailing relationship between the affected and non-affected areas. Climate-related shocks could also trigger relocation of persons from one area to another, although the magnitude and nature of these relocations (e.g. temporary or permanent, local or far-away) have not been investigated in-depth. Better understanding how human systems respond to shocks triggered by adverse natural events is crucial to inform the design of climate adaptation policies. EO can provide new granular insights in this regard. Secondly, relocations and spillovers could also materialize in responses to climate mitigation policies. As an analogy to the rebound effect first proposed by Jevons (1865) and usually used in energy analysis,

the spatial diffusion of a new low-carbon technology through a network of inter-connected cities could end up increasing the overall CO₂ emissions of this city network because of *spatial* rebound effects. Likewise, more stringent carbon regulations in one area could induce relocation effects with unclear aggregate effects on emissions. More empirical evidence on these issues could be obtained by leveraging EO. Elucidating the spatial features of these relocation effects represents a central issue that represent a promising avenue for future investigation in economic geography.

Empirically calibrate vulnerability functions and explore heterogeneity across a range of dimensions to identify effective adaptation measures

While hazards cannot be directly harnessed, exposure and vulnerability can be shaped to reduce the ultimate impacts of a changing climate. When vulnerability is understood as the relationship between the intensity of a given an adverse natural event and its corresponding level of losses, it can be calibrated as a mathematical function. As detailed in this thesis, quantifying this relationship often requires climate exogeneous variables and a spatially disaggregated outcome variable. As EO provides us with both kind of datasets, the number of vulnerability functions that can be empirically calibrated is rapidly increasing. Future research is now needed to empirically calibrate vulnerability functions at the local level. Importantly, exploring how these vulnerability functions are altered by specific spatial or land cover patterns will be crucial to provide empirical evidence on the geographic drivers of vulnerability to extreme weather and climate events and inform the design of climate adaptation policies.

Assess the drivers and distribution patterns of urban green areas

In most developing countries, the geographical patterns of cities are rapidly evolving, with potentially very large impacts for the sustainability of urban development. The critical role that urban green space can play to protect biodiversity and provide a wide range of ecosystemic services to urban citizens is often recognized. Yet there is scarce empirical investigation documenting the changes and distribution patterns of urban green space in developing countries. Consequently, little is known about the drivers of changes in urban green space or the effects that these changes generate for human well-being or biodiversity conservation in cities. EO provide a formidable source of information to capture the greenness of the land cover at a very fine spatiotemporal resolution and could be further leveraged to elucidate these aspects. In particular, while climate patterns are likely to have a strong influence on the ability to preserve and promote urban green areas, anthropogenic factors could also strongly influence these variables. Disentangling the relative strength of

each driver remains a crucial area of research to inform policymakers, urban planners and citizens about the relevance of urban green space. These analyses could also deliver key insights to inform the design of a tax based on the proportion of impervious surfaces such as the one proposed in the previous chapter.

Deepen the political economy analysis of climate change challenges at the city level

There is a major spatiotemporal mismatch between the incentives to act on climate mitigation and climate adaptation at the city-level and the benefits that can be collectively reaped from these actions. For an individual city, the incentives to act on GHG emissions are very low since climate mitigation policies will not bring immediate nor excludable benefits (i.e. specific actions taken by a city to reduce its GHG emissions will contribute to global climate stability for all cities and will only materialize in a very distant future). Additionally, most Latin American cities only marginally contributed to the rise of atmospheric CO₂ concentrations and therefore feel that they have a limited *historic responsibility* in climate change. This further lessens the local incentives to reduce CO₂ emissions at the city-level. On the other hand, an individual city can directly reap the benefits of climate adaptation policies in the form of reduced impacts from extreme climate-related events. However, because of other pressing development needs, the poorest cities in the region might not be able to invest in climate adaptation. This, in turn, could magnify the impacts of climate change in these settlements and generate compounding effects for poor cities that have only marginally contributed to GHG accumulation in the atmosphere. Better understanding how these incentives and relation of power can be shifted to promote collective action and cooperation among cities remains an important area of research to foster collective climate action.

9 FINAL CONSIDERATIONS

“L’eau en poudre : il suffit de rajouter de l’eau pour obtenir de l’eau.” Jean Baudrillard - Cool Memories - 1980-1985.

To conclude this thesis, I take a step back and raise some philosophical considerations about human settlements and climate change challenges. In this thesis I have shown that more compact and greener cities can reduce CO2 emissions and vulnerability to extreme rainfalls across Latin-American urban systems. I have then derived some policy options that could alter the geographical patterns of Latin American cities (i.e. alter their spatial extent and land cover composition), with the ultimate objective of enabling a transition to low-carbon urban systems and facilitate adaptation to a changing climate. However, there is one fundamental issue that this thesis has not addressed: what would be the “non-climate” consequences of altering these geographical patterns? Or to put it differently, can we significantly alter the geographical patterns of cities without a broader change of paradigm?

As discussed in Chapter 1, the geographical patterns of contemporaneous cities are structural features mirroring the current Human-Environment Nexus (HEN). This HEN has been shaped by the scientific revolution initiated in the XVII century that sought to make Humans as *“maitre and possesseur de la Nature”*.⁷⁵ The Industrial Revolution and the Great Acceleration have then harnessed this scientific revolution to totalize human control over “Nature”. From a geographical perspective, these evolutions have been accompanied by the emergence of a new kind of cities. In fact, the geographical patterns of contemporaneous cities are intrinsically linked to modern capitalism. The unprecedented spatial extent of contemporaneous cities together with the predominance of man-made infrastructures and impervious surfaces have driven economic progress and enable agglomeration economies (e.g. labour pooling, spreading of infrastructure costs, reduction of transportation times and costs, sharing suppliers and fostering of innovation....). In short, these patterns have enhanced the efficiency of the economic process and contributed to turn cities into formidable engines of progress.

As such, altering cities’ geographical patterns will not only shape climate change challenges; it will alter the building blocks of the development model that has

⁷⁵ René Descartes in *Discours de la méthode*, 1637. This can be translated as: *«master and possessor of Nature»*.

consolidated during the Anthropocene. Policy reforms seeking to shape more compact and greener cities have to be framed under this holistic approach. They differ from solutions such as carbon dioxide removal (CDR), which implicitly assume that there is no need to alter the current development pathway. Instead, altering cities' geographical patterns is likely to be conducive to system-level changes. And this is precisely why this thesis has focused on this topic: the magnitude of changes required to preserve the stability of the Earth system is so high that marginal and fragmented actions will not be enough. System-level changes are required.

Policy options identified in this thesis should be seen as an entry point to induce domino effects on other dimensions. As touched upon in Chapter 8, fostering a compact expansion of cities can incentivize complementary reforms to decarbonize urban mobility (e.g. alternative mobility and mass public transportation systems). Likewise, greening cities' land cover reduces vulnerability to extreme rainfall but can also be leveraged to reduce the effects of Urban Heat Islands and inspire other nature-based solutions to adapt to a changing climate.

Importantly, if implemented at scale, these reforms could advance broader socio-economic changes. Compact cities could, for example, help promoting social interactions and build more cohesive communities than those living in sprawled urban areas characterized by gated communities or individual housing units. Greener cities that more systematically leverage natural solutions could also have wide-ranging consequences, notably on the way we apprehend the human-nature divide. Contemporaneous cities are largely made of man-made structures totally detached from the "Nature" located in the surrounding rural areas. This contributes to and reinforces the stringent divide between human societies and natural ecosystems that prevails under the Anthropocene. Descola (2015) has for example shown how, for many indigenous societies, the continuum between human settlements and natural landscapes resulted in a more nuanced dichotomy between nature and culture, with non-human entities such as plants and animals considered to have soul, spirit or even a kinship with humans. The famous letter from the Chief Seattle perfectly illustrates this in the following extract: *"We are part of the earth and it is part of us. The perfumed flowers are our sisters. The bear, the deer, the great eagle, these are our brothers. The rocky crests, the dew in the meadow, the body heat of the pony, and man all belong to the same family."*⁷⁶ Conversely, when nature is perceived as something exogeneous to

⁷⁶ Interest readers can find a full [version of this letter here](#).

human settlements, it is more easily reduced to an extractive resource whose use has to be optimized in relation to the economic process.

The examples above essentially reveal that system-level changes will not materialize without a change of paradigm. The current HEN that views humans as *maitre et possesseur de la Nature* is underpinned by what could be labelled the *efficiency paradigm*. This paradigm has proven to be extremely successful at rationalizing and breaking down systemic issues into small problems to which optimal technological solutions can be found. As such, the efficiency paradigm attempts to address the climate-related challenges discussed in this thesis by breaking them down into independent and specific issues for which optimal technological solutions can be found. Options such as electric vehicles, CDR, Artificial Intelligence for energy efficiency (or even satellite imageries used in this thesis) are good examples of the solutions prescribed by this efficiency paradigm. They can help finding an optimal answer to a specific and circumscribed issue; they nonetheless lack a systemic perspective. One major shortcoming of all the above-mentioned solutions is notably that, if implemented at scale, they will trigger vast new demands for energy, rare minerals and natural resources, which would render the potential reduction of CO₂ emissions they promise to deliver ridiculous. In short, these technological solutions are totally ignoring Jevons' Paradox discovered more than 150 years ago (Jevons, 1865) and the rebound effects associated with efficiency gains or new technologies. To give another concrete example, to confront water scarcity issues, the efficiency paradigm might end up providing absurd solutions in the vain of what Baudrillard was ironically proposing: "*L'eau en poudre : il suffit de rajouter de l'eau pour obtenir de l'eau*".⁷⁷ In a nutshell, the efficiency paradigm will be of little help to address climate change challenges because it ontologically inhibits system-level perspective and fails to recognize the interrelationships and feedback loops that exist between the Earth system and human development.

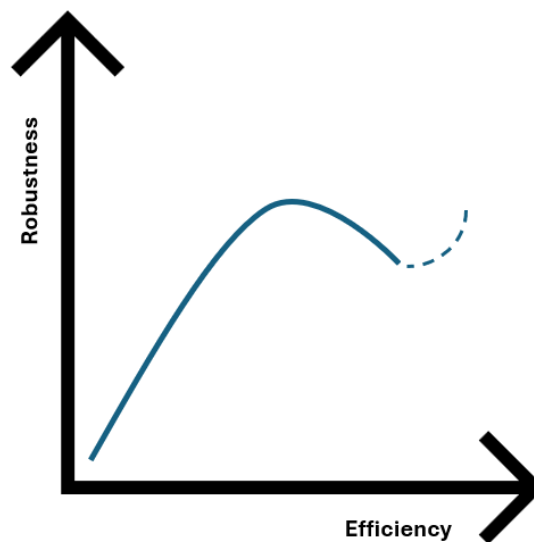
Paradoxically, in its attempt to turn humans in "*maitre et possesseur de la Nature*", the efficiency paradigm has created a Nature that can no longer be predicted -let alone controlled. By now, we have already committed to a level of climate change that will result in more erratic weather patterns, more extreme weather events and weakened life-supporting ecosystems (see Chapter 1). The severity of these changes will depend on future levels of GHG emission and ultimate impacts will be moderated by our collective capacity to reduce vulnerabilities. They will nonetheless create a more fluctuating world. In this fluctuating world, the efficiency paradigm is not only problematic because of its inability

⁷⁷ Which could be translated by: "*Powdered water: simply add water to obtain water*". Baudrillard (1987)

to propose system-level changes; the efficiency paradigm is problematic because it produces systemic vulnerabilities. Essentially, the optimization process entails fragilities. Various examples illustrate this but the 2023 drought in Panama is probably one of the starker examples of the climate vulnerabilities that come along with the efficiency paradigm.

In a globalized world, the Panama Canal is a perfect technological solution to optimize international trade, converting this area in one of most important routes for global marine shipping. However, in 2023, rainfall in Panama was 30% lower than average, making it the third driest year ever recorded (Barnes et al. 2024). As a result, water levels in the rainfall-fed series of lakes that form the canal reached a record low in the second half of 2023. This forced authorities to reduce by more than 20% the daily crossings. Given the central role of the Panama Canal in global trade, shipments of everything from food to Christmas toys or even fuel were delayed. The full economic consequences of this event have not yet been accounted for, but it is easy to perceive the compounding effects that a local drought can generate in a system that has been shaped by the efficiency paradigm. In a fluctuating world, with erratic rainfall patterns, this anecdotal situation is likely to become more frequent.

Figure 48. From efficiency to robustness: a schematic view



Note: the dotted blue line represents one possible pathway for human progress in a fluctuating world
Source: adapted from Hamant (2023).

I thus argue that to navigate in a more fluctuating world, a shift of paradigm away from efficiency and towards robustness is required. The trade-offs between efficiency and robustness have been brilliantly elucidated by Hamant. Grounded in biological research, Hamant's work has shown that plants are robust systems precisely because of their inefficiencies, incoherences or delays (Hamant 2023; 2024a; 2024b). These

inefficiencies have allowed ecosystems to manage highly fluctuating climates during hundreds of thousands of years. These approaches represent a promising source of inspiration to build systemic robustness and give rise to a new HEN. Greening cities to adapt to higher temperatures and more erratic rainfalls are concrete examples that pave the way towards a new HEN where we protect ecosystems to increase our robustness instead of exploiting them to increase efficiency. Figure 48 provides a schematic view of the change of paradigm advocated for in this thesis. Since the industrial revolution, human progress has centred on the x-axis of efficiency. At first, efficiency has come along with an increase in robustness. However, the great acceleration of the past decades has bolstered and consolidated multiple systemic vulnerabilities. We now have to switch to the y-axis. Human progress in the XXI century has to focus on increasing systemic robustness even if this inhibits progress on in terms of efficiency. Increasing robustness is no longer luxury. It is the only viable option to better manage fluctuations and face the threats associated with an unstable Earth system.

For spatial and urban planning policies, this new robustness paradigm would imply a departure from policies that seek to optimize the territory to increase efficiency without considering the vulnerabilities that this entails. Instead, spatial and urban planning policies should pursue systemic robustness and rely on the surrounding ecosystems as a source of inspiration. To put it differently, to develop robust human settlements, we should not only shape the territory but also let the territory shape us.

In this endeavour, Geography as a discipline has a critical role to play. To paraphrase Valéry, we are now living in *the time of the finite world*. Traditional Geography has drawn the map of this *finite world*. Looking forward, geographical analysis should focus on elucidating the interrelationships and interactions between human settlements and the Earth system. Broadly speaking, since there are no unknown territories left to be mapped, Geography can now help (re)arranging different elements on a *finite map*. This represents a promising avenue for the future of the discipline: by facilitating a systemic approach that fundamentally reckons that Humanity is embedded within, intertwined with, and dependent upon the Earth system, Geography can guide a shift away from efficiency and towards robustness. This thesis has attempted to take a first step in this direction.

10 REFERENCES

- Ahamer, Gilbert. 2019. *Mapping Global Dynamics - Geographic Perspectives from Local Pollution to Global Evolution*. Switzerland: Springer Nature.
<https://doi.org/10.1007/978-3-319-51704-9>.
- Altmann, Eduardo G. 2020. 'Spatial Interactions in Urban Scaling Laws'. *PLOS ONE* 15 (12): e0243390. <https://doi.org/10.1371/journal.pone.0243390>.
- Angrist, J. D., and J. S. Pischke. 2008. *Mostly Harmless Econometrics: An Empiricist's Companion*. Princeton, NJ: Princeton Univ. Press.
- Anselin, Luc. 2013. *Spatial Econometrics: Methods and Models*. Springer Science & Business Media.
- Arguez, A., and R. S. Vose. 2011. 'The Definition of the Standard WMO Climate Normal: The Key to Deriving Alternative Climate Normals'. *Bulletin of the American Meteorological Society*, June. <https://doi.org/10.1175/2010BAMS2955.1>.
- Arnold Jr., Chester L., and C. James Gibbons. 1996. 'Impervious Surface Coverage: The Emergence of a Key Environmental Indicator'. *Journal of the American Planning Association* 62 (2): 243–58. <https://doi.org/10.1080/01944369608975688>.
- Avissar, Roni. 1996. 'Potential Effects of Vegetation on the Urban Thermal Environment'. *Atmospheric Environment*, Conference on the Urban Thermal Environment Studies in Tohwa, 30 (3): 437–48. [https://doi.org/10.1016/1352-2310\(95\)00013-5](https://doi.org/10.1016/1352-2310(95)00013-5).
- Baltar de Souza Leão, Eduardo, Luís Felipe Machado do Nascimento, José Célio Silveira de Andrade, and José Antônio Puppim de Oliveira. 2020. 'Carbon Accounting Approaches and Reporting Gaps in Urban Emissions: An Analysis of the Greenhouse Gas Inventories and Climate Action Plans in Brazilian Cities'. *Journal of Cleaner Production* 245 (February):118930. <https://doi.org/10.1016/j.jclepro.2019.118930>.
- Barnes, C., S. Paton, R. F. Stallard, H. De Lima, B. Clarke, M. Vahlberg, S. Sivanu, et al. 2024. 'Low Water Levels in Panama Canal Due to Increasing Demand Exacerbated by El Niño Event'. Report. <https://doi.org/10.25561/111007>.
- Baudrillard, Jean. 1987. *Cool Memories - 1980-1985*. 288 pages. Éditions Galilée. ISBN : 9782718603162
- Bertaud, Alain, and H. Richardson. 2005. 'Chapter 17. Transit and Density : Atlanta , the United States and Western Europe'. In *Urban Sprawl in Western Europe and the United States*, 344. London: Routledge.
<https://www.semanticscholar.org/paper/Chapter-17-Transit-and-Density-%3A-Atlanta-%2C-the-and-Bertaud-Richardson/1f71a32d7713a0219038d642a41417031bde1e6>.
- Bolt, Jutta, and Jan Luiten Van Zanden. 2024. 'Maddison-style Estimates of the Evolution of the World Economy: A New 2023 Update'. *Journal of Economic Surveys*, April, joes.12618. <https://doi.org/10.1111/joes.12618>.
- Brakenridge, G.R. 2023. 'Global Active Archive of Large Flood Events'. Dartmouth Flood Observatory, University of Colorado, USA.
<http://floodobservatory.colorado.edu/Archives/> (Accessed august 21 2023).
- Brink, Ebba, Theodor Aalders, Dóra Ádám, Robert Feller, Yuki Henselek, Alexander Hoffmann, Karin Ibe, et al. 2016. 'Cascades of Green: A Review of Ecosystem-Based Adaptation in Urban Areas'. *Global Environmental Change* 36 (January):111–23. <https://doi.org/10.1016/j.gloenvcha.2015.11.003>.
- Brueckner, Jan K. 2000. 'Urban Sprawl: Diagnosis and Remedies'. *International Regional Science Review* 23 (2): 160–71. <https://doi.org/10.1177/016001700761012710>.

- CAT. 2023. 'Warming Projections Global Update, No change to warming as fossil fuel endgame brings focus onto false solutions'. Climate Action Tracker. Available at: https://climateactiontracker.org/documents/1187/CAT_2023-12-05_GlobalUpdate_COP28.pdf
- Chandler, K. R., C. J. Stevens, A. Binley, and A. M. Keith. 2018. 'Influence of Tree Species and Forest Land Use on Soil Hydraulic Conductivity and Implications for Surface Runoff Generation'. *Geoderma* 310 (January):120–27. <https://doi.org/10.1016/j.geoderma.2017.08.011>.
- Chen, Guangzhao, Xia Li, Xiaoping Liu, Yimin Chen, Xun Liang, Jiye Leng, Xiaocong Xu, et al. 2020. 'Global Projections of Future Urban Land Expansion under Shared Socioeconomic Pathways'. *Nature Communications* 11 (1): 537. <https://doi.org/10.1038/s41467-020-14386-x>.
- Chen, Xi, and William Nordhaus. 2015. 'A Test of the New VIIRS Lights Data Set: Population and Economic Output in Africa'. *Remote Sensing* 7 (4): 4937–47. <https://doi.org/10.3390/rs70404937>.
- Chen, Xi, and William D. Nordhaus. 2011. 'Using Luminosity Data as a Proxy for Economic Statistics'. *Proceedings of the National Academy of Sciences* 108 (21): 8589–94. <https://doi.org/10.1073/pnas.1017031108>.
- Cirilli, Andrea, and Paolo Veneri. 2014. 'Spatial Structure and Carbon Dioxide (CO₂) Emissions Due to Commuting: An Analysis of Italian Urban Areas'. *Regional Studies* 48 (12): 1993–2005. <https://doi.org/10.1080/00343404.2013.827333>.
- Clark, Colin. 1987. 'Deforestation and Floods'. *Environmental Conservation* 14 (1): 67–69.
- Cooke, S., and R. Behrens. 2017. 'Correlation or Cause? The Limitations of Population Density as an Indicator for Public Transport Viability in the Context of a Rapidly Growing Developing City'. *Transportation Research Procedia*, World Conference on Transport Research - WCTR 2016 Shanghai. 10-15 July 2016, 25 (January):3003–16. <https://doi.org/10.1016/j.trpro.2017.05.229>.
- Corbane, Christina, Pesaresi Martino, Politis Panagiotis, Florczyk J. Aneta, Melchiorri Michele, Freire Sergio, Schiavina Marcello, Ehrlich Daniele, Naumann Gustavo, and Kemper Thomas. 2020. 'The Grey-Green Divide: Multi-Temporal Analysis of Greenness across 10,000 Urban Centres Derived from the Global Human Settlement Layer (GHSL)'. *International Journal of Digital Earth* 13 (1): 101–18. <https://doi.org/10.1080/17538947.2018.1530311>.
- Centre for Research on the Epidemiology of Disasters (CRED). (2015) *EM-DAT: The CRED/OFDA International Disaster Database*. Université Catholique de Louvain, Brussels, Belgium. <https://www.emdat.be> (accessed June 16, 2023)
- CEPAL (2001). "Urbanización y evolución de la población urbana de América Latina, 1950-1990". *Boletín demográfico número especial*. Santiago, Chile. División de Población, Comisión Económica para América Latina y el Caribe (CEPAL).
- Crutzen, Paul J. 2002. 'Geology of Mankind'. *Nature* 415 (6867): 23–23. <https://doi.org/10.1038/415023a>.
- Dell, Melissa, Benjamin F. Jones, and Benjamin A. Olken. 2014. 'What Do We Learn from the Weather? The New Climate-Economy Literature'. *Journal of Economic Literature* 52 (3): 740–98. <https://doi.org/10.1257/jel.52.3.740>.
- Descola, Philippe. 2015. *Par-delà nature et culture*. Editorial : Gallimard. 791 Pages. EAN: 9782070465873
- Dijkstra, Lewis, Aneta Florczyk, Sergio Freire, Thomas Kemper, Michele Melchiorri, Martino Pesaresi, and Marcello Schiavina. 2020. 'Applying the Degree of Urbanisation to the Globe: A New Harmonised Definition Reveals a Different Picture of Global

- Urbanisation'. *Journal of Urban Economics* 125 (November).
<https://doi.org/10.1016/j.jue.2020.103312>.
- Dottori, Francesco, Wojciech Szewczyk, Juan-Carlos Ciscar, Fang Zhao, Lorenzo Alfieri, Yukiko Hirabayashi, Alessandra Bianchi, et al. 2018. 'Increased Human and Economic Losses from River Flooding with Anthropogenic Warming'. *Nature Climate Change* 8 (9): 781–86. <https://doi.org/10.1038/s41558-018-0257-z>.
- Du, Shiqiang, Paolo Scussolini, Philip J. Ward, Min Zhang, Jiahong Wen, Luyang Wang, Elco Koks, et al. 2020. 'Hard or Soft Flood Adaptation? Advantages of a Hybrid Strategy for Shanghai'. *Global Environmental Change* 61 (March):102037.
<https://doi.org/10.1016/j.gloenvcha.2020.102037>.
- EEA. 2013. 'European Union CO2 emissions: different accounting perspectives'. Luxembourg: European Environment Agency. Publications Office of the European Union.
- EEA. 2017. 'Green Infrastructure and Flood Management — Promoting Cost-Efficient Flood Risk Reduction via Green Infrastructure Solutions'. Report No 14/2017. Luxembourg: European Environment Agency. <https://www.eea.europa.eu/publications/green-infrastructure-and-flood-management>.
- Elliott, Robert, Eric Strobl, and Puyang Sun. 2015. 'The Local Impact of Typhoons on Economic Activity in China: A View from Outer Space'. *Journal of Urban Economics* 88 (C): 50–66.
- Elvidge, Christopher D, Kimberly Baugh, John Dietz, Theodore Bland, Paul C Sutton, Herbert W Kroehl. 1999. 'Radiance Calibration of DMSP-OLS Low-Light Imaging Data of Human Settlements'. *Remote Sensing of Environment*, 68 (1):, 77-88,
[https://doi.org/10.1016/S0034-4257\(98\)00098-4](https://doi.org/10.1016/S0034-4257(98)00098-4).
- Elvidge, Christopher D, Kimberly Baugh, Mikhail Zhizhin, Feng Chi Hsu, and Tilottama Ghosh. 2017. 'VIIRS Night-Time Lights'. *International Journal of Remote Sensing* 38 (21): 5860–79. <https://doi.org/10.1080/01431161.2017.1342050>.
- Evans, Simon. 2021. 'Which Countries Are Historically Responsible for Climate Change?' Carbon Brief. 5 October 2021. <https://www.carbonbrief.org/analysis-which-countries-are-historically-responsible-for-climate-change/>.
- Felbermayr, Gabriel, and Jasmin Gröschl. 2014. 'Naturally Negative: The Growth Effects of Natural Disasters'. *Journal of Development Economics*, Special Issue: Imbalances in Economic Development, 111 (November):92–106.
<https://doi.org/10.1016/j.jdeveco.2014.07.004>.
- Felbermayr, Gabriel, Jasmin Gröschl, Mark Sanders, Vincent Schippers, and Thomas Steinwachs. 2022. 'The Economic Impact of Weather Anomalies'. *World Development* 151 (March):105745. <https://doi.org/10.1016/j.worlddev.2021.105745>.
- Ferreira, Maria Marta; Roberts, Mark. 2018. *Raising the Bar for Productive Cities in Latin America and the Caribbean*. World Bank Latin American and Caribbean Studies. Washington, DC: World Bank. <http://hdl.handle.net/10986/29279>
- Florczyk, A. J., Corbane, C., Ehrlich, D., Freire, S., Kemper, T., Maffenini, L., et al. 2019. 'Data Package, G. H. S. L.'. Luxembourg: Publications Office of the European Union.
<https://doi.org/10.2760/062975>
- Folke, Carl, Stephen Polasky, Johan Rockström, Victor Galaz, Frances Westley, Michèle Lamont, Marten Scheffer, et al. 2021. 'Our Future in the Anthropocene Biosphere'. *Ambio* 50 (4): 834–69. <https://doi.org/10.1007/s13280-021-01544-8>.
- Funk, Chris, Pete Peterson, Martin Landsfeld, Diego Pedreros, James Verdin, Shraddhanand Shukla, Gregory Husak, et al. 2015. 'The Climate Hazards Infrared Precipitation with Stations—a New Environmental Record for Monitoring Extremes'. *Scientific Data* 2 (1): 150066. <https://doi.org/10.1038/sdata.2015.66>.

- Gaigné, Carl, Stéphane Riou, and Jacques-François Thisse. 2012. 'Are Compact Cities Environmentally Friendly?' *Journal of Urban Economics* 72 (2): 123–36. <https://doi.org/10.1016/j.jue.2012.04.001>.
- Gao, Jing, and Brian C. O'Neill. 2020. 'Mapping Global Urban Land for the 21st Century with Data-Driven Simulations and Shared Socioeconomic Pathways'. *Nature Communications* 11 (1): 2302. <https://doi.org/10.1038/s41467-020-15788-7>.
- Gasparrini, Antonio, Yuming Guo, Masahiro Hashizume, Eric Lavigne, Antonella Zanobetti, Joel Schwartz, Aurelio Tobias, et al. 2015. 'Mortality Risk Attributable to High and Low Ambient Temperature: A Multicountry Observational Study'. *Lancet (London, England)* 386 (9991): 369–75. [https://doi.org/10.1016/S0140-6736\(14\)62114-0](https://doi.org/10.1016/S0140-6736(14)62114-0).
- Gibson, John, Susan Olivia, Geua Boe-Gibson, and Chao Li. 2021. 'Which Night Lights Data Should We Use in Economics, and Where?' *Journal of Development Economics* 149 (March):102602. <https://doi.org/10.1016/j.jdeveco.2020.102602>.
- Gilfillan, Dennis, Gregg Marland, Tom Boden, and Robert Andres. 2020. 'Global, Regional, and National Fossil-Fuel CO2 Emissions: 1751-2017'. <https://data.ess-dive.lbl.gov/view/doi:10.15485/1712447>.
- Giuliano, Genevieve, Sanggyun Kang, and Quan Yuan. 2019. 'Agglomeration Economies and Evolving Urban Form'. *The Annals of Regional Science* 63 (3): 377–98. <https://doi.org/10.1007/s00168-019-00957-4>.
- Glaeser, Edward L., ed. 2010. *Agglomeration Economics*. National Bureau of Economic Research Conference Report. Chicago, IL: University of Chicago Press. <https://press.uchicago.edu/ucp/books/book/chicago/A/bo8143498.html>.
- Gore, Tim. 2021. 'Carbon Inequality in 2030: Per Capita Consumption Emissions and the 1.5°C Goal'. Institute for European Environmental Policy, Oxfam. <https://doi.org/10.21201/2021.8274>.
- Gourevitch, Jesse D., Nitin K. Singh, Josh Minot, Kristin B. Raub, Donna M. Rizzo, Beverley C. Wemple, and Taylor H. Ricketts. 2020. 'Spatial Targeting of Floodplain Restoration to Equitably Mitigate Flood Risk'. *Global Environmental Change* 61 (March):102050. <https://doi.org/10.1016/j.gloenvcha.2020.102050>.
- Greenhouse Gas Protocol (2014). Global Protocol for Community-Scale Greenhouse Gas Inventories. An Accounting and Reporting Standard for Cities Version 1.1. WRI, C40 Cities and ICLEI. Available at: https://ghgprotocol.org/sites/default/files/standards/GPC_Full_MASTER_RW_v7.pdf
- Guastella, Gianni, Walid Oueslati, and Stefano Pareglio. 2019. 'Patterns of Urban Spatial Expansion in European Cities'. *Sustainability* 11 (8): 2247. <https://doi.org/10.3390/su11082247>.
- Güneralp, Burak, İnci Güneralp, and Ying Liu. 2015. 'Changing Global Patterns of Urban Exposure to Flood and Drought Hazards'. *Global Environmental Change* 31 (March):217–25. <https://doi.org/10.1016/j.gloenvcha.2015.01.002>.
- Güneralp, Burak, Meredith Reba, Billy U. Hales, Elizabeth A. Wentz, and Karen C. Seto. 2020. 'Trends in Urban Land Expansion, Density, and Land Transitions from 1970 to 2010: A Global Synthesis'. *Environmental Research Letters* 15 (4): 044015. <https://doi.org/10.1088/1748-9326/ab6669>.
- Guo, Yuming, Antonio Gasparrini, Ben Armstrong, Shanshan Li, Benjawan Tawatsupa, Aurelio Tobias, Eric Lavigne, et al. 2014. 'Global Variation in the Effects of Ambient Temperature on Mortality: A Systematic Evaluation'. *Epidemiology (Cambridge, Mass.)* 25 (6): 781–89. <https://doi.org/10.1097/EDE.0000000000000165>.
- Hamant, Olivier. 2023. *Antidote au culte de la performance. La robustesse du vivant*. Tracts Gallimard, N° 50. 63 pages
- Hamant, Olivier. 2024a. 'Debunking the Idea of Biological Optimisation: Quantitative Biology to the Rescue'. *Quantitative Plant Biology* 5:e3. <https://doi.org/10.1017/qpb.2024.3>.

- . 2024b. 'Is Incoherence Required for Sustainability?' *The Anthropocene Review*, May, 20530196241249680. <https://doi.org/10.1177/20530196241249680>.
- Holland, Paul W. 1986. 'Statistics and Causal Inference'. *Journal of the American Statistical Association* 81 (396): 945–60. <https://doi.org/10.2307/2289064>.
- Hossain Anni, Afrin, Sagy Cohen, and Sarah Praskievicz. 2020. 'Sensitivity of Urban Flood Simulations to Stormwater Infrastructure and Soil Infiltration'. *Journal of Hydrology* 588 (September):125028. <https://doi.org/10.1016/j.jhydrol.2020.125028>.
- Hsiang, Solomon. 2016. 'Climate Econometrics'. *Annual Review of Resource Economics* 8 (Volume 8, 2016): 43–75. <https://doi.org/10.1146/annurev-resource-100815-095343>.
- IPCC. 2012. *Managing the Risks of Extreme Events and Disasters to Advance Climate Change Adaptation*. [Field, C.B., V. Barros, T.F. Stocker, D. Qin, D.J. Dokken, K.L. Ebi, M.D. Mastrandrea, K.J. Mach, G.-K. Plattner, S.K. Allen, M. Tignor, and P.M. Midgley (Eds.)]. Cambridge, UK: Cambridge University Press.
- . 2014. 'Summary for Policymakers. In Climate Change 2014: Mitigation of Climate Change. Contribution of Working Group III to the Fifth Assessment Report of the Intergovernmental Panel on Climate Change.' Cambridge, United Kingdom and New York, NY, USA: Cambridge University Press.
- . 2018. *Global Warming of 1.5°C. An IPCC Special Report on the Impacts of Global Warming of 1.5°C above Pre-Industrial Levels and Related Global Greenhouse Gas Emission Pathways, in the Context of Strengthening the Global Response to the Threat of Climate Change, Sustainable Development, and Efforts to Eradicate Poverty* [Masson-Delmotte, V., P. Zhai, H.-O. Pörtner, D. Roberts, J. Skea, P.R. Shukla, A. Pirani, W. Moufouma-Okia, C. Péan, R. Pidcock, S. Connors, J.B.R. Matthews, Y. Chen, X. Zhou, M.I. Gomis, E. Lonnoy, T. Maycock, M. Tignor, and T. Waterfield (Eds.)]. Cambridge, UK and New York, NY, USA,: Cambridge University Press. <https://doi.org/10.1017/9781009157940.001>.
- . 2021. 'Climate Change 2021: The Physical Science Basis. Contribution of Working Group I to the AR6 [Masson-Delmotte, V., P. Zhai, A. Pirani, S.L. Connors, C. Péan, S. Berger, N. Caud, Y. Chen, L. Goldfarb, M.I. Gomis, M. Huang, K. Leitzell, E. Lonnoy, J.B.R. Matthews, T.K. Maycock, T. Waterfield, O. Yelekçi, R. Yu, and B. Zhou (Eds.)]. In AR6, 1513–1766. Cambridge, United Kingdom and New York, NY, USA: Cambridge University Press. <https://doi.org/10.1017/9781009157896.013>.
- . 2023. 'Climate Change 2023: Synthesis Report. Contribution of Working Groups I, II and III to the Sixth Assessment Report of the Intergovernmental Panel on Climate Change [Core Writing Team, H. Lee and J. Romero (Eds.)]. In *Climate Change 2023*. Geneva, Switzerland.: Cambridge University Press. <https://www.ipcc.ch/report/ar6/syr/>.
- Ilungman, Tamara, Marta Cirach, Federica Marando, Evelise Pereira Barboza, Sasha Khomenko, Pierre Masselot, Marcos Quijal-Zamorano, et al. 2023. 'Cooling Cities through Urban Green Infrastructure: A Health Impact Assessment of European Cities'. *The Lancet* 401 (10376): 577–89. [https://doi.org/10.1016/S0140-6736\(22\)02585-5](https://doi.org/10.1016/S0140-6736(22)02585-5).
- Jacobson, Carol R. 2011. 'Identification and Quantification of the Hydrological Impacts of Imperviousness in Urban Catchments: A Review'. *Journal of Environmental Management* 92 (6): 1438–48. <https://doi.org/10.1016/j.jenvman.2011.01.018>.
- Jedwab, Remi, Prakash Loungani, and Anthony Yezer. 2021. 'Comparing Cities in Developed and Developing Countries: Population, Land Area, Building Height and Crowding'. *Regional Science and Urban Economics* 86 (January):103609. <https://doi.org/10.1016/j.regsciurbeco.2020.103609>.

- Jevons, William Stanley. 1865. *The Coal Question; An Inquiry concerning the Progress of the Nation, and the Probable Exhaustion of our Coal-mines*. London: Macmillan and Co. 2nd edition, revised.
- Jongman, Brenden, Philip J. Ward, and Jeroen C. J. H. Aerts. 2012. 'Global Exposure to River and Coastal Flooding: Long Term Trends and Changes'. *Global Environmental Change* 22 (4): 823–35. <https://doi.org/10.1016/j.gloenvcha.2012.07.004>.
- Karnieli, Arnon, Nurit Agam, Rachel T. Pinker, Martha Anderson, Marc L. Imhoff, Garik G. Gutman, Natalya Panov, and Alexander Goldberg. 2010. 'Use of NDVI and Land Surface Temperature for Drought Assessment: Merits and Limitations', February. <https://doi.org/10.1175/2009JCLI2900.1>.
- Kaya, Y. 1989. 'Impact of Carbon Dioxide Emission Control on GNP Growth: Interpretation of Proposed Scenarios'. In , 76. Paris. <https://www.semanticscholar.org/paper/Impact-of-carbon-dioxide-emission-control-on-GNP-%3A-Kaya/b6bfe4ed86901a81b644062e839ce7485d82d60f>.
- Keuschnigg, Marc, Selcan Mutgan, and Peter Hedström. 2019. 'Urban Scaling and the Regional Divide'. *Science Advances* 5 (1): eaav0042. <https://doi.org/10.1126/sciadv.aav0042>.
- Koch, Alexander, Chris Brierley, Mark M. Maslin, and Simon L. Lewis. 2019. 'Earth System Impacts of the European Arrival and Great Dying in the Americas after 1492'. *Quaternary Science Reviews* 207 (March):13–36. <https://doi.org/10.1016/j.quascirev.2018.12.004>.
- Kocornik-Mina, Adriana, Thomas K. J. McDermott, Guy Michaels, and Ferdinand Rauch. 2020. 'Flooded Cities'. *American Economic Journal: Applied Economics* 12 (2): 35–66. <https://doi.org/10.1257/app.20170066>.
- Kummu, Matti, Maija Taka, and Joseph H. A. Guillaume. 2018. 'Gridded Global Datasets for Gross Domestic Product and Human Development Index over 1990–2015'. *Scientific Data* 5 (1): 180004. <https://doi.org/10.1038/sdata.2018.4>.
- Lamboll, Robin D., Zebedee R. J. Nicholls, Christopher J. Smith, Jarmo S. Kikstra, Edward Byers, and Joeri Rogelj. 2023. 'Assessing the Size and Uncertainty of Remaining Carbon Budgets'. *Nature Climate Change* 13 (12): 1360–67. <https://doi.org/10.1038/s41558-023-01848-5>.
- Lamond, J., N. Bhattacharya, and R. Bloch. 2012. 'The Role of Solid Waste Management as a Response to Urban Flood Risk in Developing Countries, a Case Study Analysis'. In *FRIAR 2012*, 193–204. Dubrovnik, Croatia. <https://doi.org/10.2495/FRIAR120161>.
- Lee, Kyungil, Yoonji Kim, Hyun Chan Sung, Jieun Ryu, and Seong Woo Jeon. 2020. 'Trend Analysis of Urban Heat Island Intensity According to Urban Area Change in Asian Mega Cities'. *Sustainability* 12 (1): 112. <https://doi.org/10.3390/su12010112>.
- Lee, Lung-Fei, and Jihai Yu. 2010. 'Some Recent Developments in Spatial Panel Data Models'. *Regional Science and Urban Economics* 40 (5): 255–71.
- Lee, Sungwon, and Bumsoo Lee. 2014. 'The Influence of Urban Form on GHG Emissions in the U.S. Household Sector'. *Energy Policy* 68 (May):534–49. <https://doi.org/10.1016/j.enpol.2014.01.024>.
- Levin, Noam, and Stuart Phinn. 2022. 'Assessing the 2022 Flood Impacts in Queensland Combining Daytime and Nighttime Optical and Imaging Radar Data'. *Remote Sensing* 14 (19): 5009. <https://doi.org/10.3390/rs14195009>.
- Li, Congying, Tim D. Fletcher, Hugh P. Duncan, and Matthew J. Burns. 2017. 'Can Stormwater Control Measures Restore Altered Urban Flow Regimes at the Catchment Scale?' *Journal of Hydrology* 549 (June):631–53. <https://doi.org/10.1016/j.jhydrol.2017.03.037>.
- Liang, Changmei, Xiang Zhang, Jun Xia, Jing Xu, and Dunxian She. 2020. 'The Effect of Sponge City Construction for Reducing Directly Connected Impervious Areas on Hydrological

- Responses at the Urban Catchment Scale'. *Water* 12 (4): 1163.
<https://doi.org/10.3390/w12041163>.
- Liu, Xiaochen, and John Sweeney. 2012. 'Modelling the Impact of Urban Form on Household Energy Demand and Related CO₂ Emissions in the Greater Dublin Region'. *Energy Policy* 46 (July):359–69. <https://doi.org/10.1016/j.enpol.2012.03.070>.
- López, Saioa, Lucy Van Dorp, and Garrett Hellenthal. 2015. 'Human Dispersal Out of Africa: A Lasting Debate'. *Evolutionary Bioinformatics* 11s2 (January):EBO.S33489.
<https://doi.org/10.4137/EBO.S33489>.
- Lunka, Peter, and Sopan D. Patil. 2016. 'Impact of Tree Planting Configuration and Grazing Restriction on Canopy Interception and Soil Hydrological Properties: Implications for Flood Mitigation in Silvopastoral Systems'. *Hydrological Processes* 30 (6): 945–58.
<https://doi.org/10.1002/hyp.10630>.
- Ma, Jing, Zhilin Liu, and Yanwei Chai. 2015. 'The Impact of Urban Form on CO₂ Emission from Work and Non-Work Trips: The Case of Beijing, China'. *Habitat International* 47 (Complete): 1–10. <https://doi.org/10.1016/j.habitatint.2014.12.007>.
- Makido, Yasuyo, Shobhakar Dhakal, and Yoshiki Yamagata. 2012. 'Relationship between Urban Form and CO₂ Emissions: Evidence from Fifty Japanese Cities'. *Urban Climate* 2 (December):55–67. <https://doi.org/10.1016/j.uclim.2012.10.006>.
- Marando, Federica, Mehdi P. Heris, Grazia Zulian, Angel Udías, Lorenzo Mentaschi, Nektarios Chrysoulakis, David Parastatidis, and Joachim Maes. 2022. 'Urban Heat Island Mitigation by Green Infrastructure in European Functional Urban Areas'. *Sustainable Cities and Society* 77 (February):103564. <https://doi.org/10.1016/j.scs.2021.103564>.
- Marshall, Alfred. 1890. *Principles of Economics*. Macmillan and Company.
- McDonald, Robert I., Pamela Green, Deborah Balk, Balazs M. Fekete, Carmen Revenga, Megan Todd, and Mark Montgomery. 2011. 'Urban Growth, Climate Change, and Freshwater Availability'. *Proceedings of the National Academy of Sciences* 108 (15): 6312–17. <https://doi.org/10.1073/pnas.1011615108>.
- McNeill, J. R. 2001. *Something New Under the Sun: An Environmental History of the Twentieth-Century World (The Global Century Series)*. W. W. Norton & Company.
- Meijers, Evert J, and Martijn J Burger. 2017. 'Stretching the Concept of "Borrowed Size"'. *Urban Studies* 54 (1): 269–91. <https://doi.org/10.1177/0042098015597642>.
- Mejía, Alfonso I., and Glenn E. Moglen. 2010. 'Spatial Distribution of Imperviousness and the Space-Time Variability of Rainfall, Runoff Generation, and Routing'. *Water Resources Research* 46 (7). <https://doi.org/10.1029/2009WR008568>.
- Mia, Parvez, James Hazelton, and James Guthrie. 2019. 'Greenhouse Gas Emissions Disclosure by Cities: The Expectation Gap'. *Sustainability Accounting, Management and Policy Journal* 10 (4): 685–709. <https://doi.org/10.1108/SAMPJ-11-2017-0138>.
- Mohan, Preeya, and Eric Strobl. 2017. 'The Short-Term Economic Impact of Tropical Cyclone Pam: An Analysis Using VIIRS Nightlight Satellite Imagery'. *International Journal of Remote Sensing* 38 (21): 5992–6006.
<https://doi.org/10.1080/01431161.2017.1323288>.
- Monkkonen, Paavo, Jorge Montejano, Erick Guerra, and Caudillo Alberto. 2019. 'Compact Cities and Economic Productivity in Mexico'. *Urban Studies* 57 (November):004209801986982. <https://doi.org/10.1177/0042098019869827>.
- Morice, C. P., J. J. Kennedy, N. A. Rayner, J. P. Winn, E. Hogan, R. E. Killick, R. J. H. Dunn, T. J. Osborn, P. D. Jones, and I. R. Simpson. 2021. 'An Updated Assessment of Near-Surface Temperature Change From 1850: The HadCRUT5 Data Set'. *Journal of Geophysical Research: Atmospheres* 126 (3): e2019JD032361.
<https://doi.org/10.1029/2019JD032361>.
- Oda, Tomohiro, Shamil Maksyutov, and Robert J. Andres. 2018. 'The Open-Source Data Inventory for Anthropogenic CO₂, Version 2016 (ODIAC2016): A Global Monthly Fossil

- Fuel CO₂ Gridded Emissions Data Product for Tracer Transport Simulations and Surface Flux Inversions'. *Earth System Science Data* 10 (1): 87–107. <https://doi.org/10.5194/essd-10-87-2018>.
- Oke, T. R. 1995. 'The Heat Island of the Urban Boundary Layer: Characteristics, Causes and Effects'. In *Wind Climate in Cities*, edited by Jack E. Cermak, Alan G. Davenport, Erich J. Plate, and Domingos X. Viegas, 81–107. Dordrecht: Springer Netherlands. https://doi.org/10.1007/978-94-017-3686-2_5.
- Onishi, Akio, Xin Cao, Takanori Ito, Feng Shi, and Hidefumi Imura. 2010. 'Evaluating the Potential for Urban Heat-Island Mitigation by Greening Parking Lots'. *Urban Forestry & Urban Greening* 9 (4): 323–32. <https://doi.org/10.1016/j.ufug.2010.06.002>.
- Oppenheimer, Stephen. 2003. *Out of Eden: The Peopling of the World*. Constable.
- Osman, Matthew B., Jessica E. Tierney, Jiang Zhu, Robert Tardif, Gregory J. Hakim, Jonathan King, and Christopher J. Poulsen. 2021. 'Globally Resolved Surface Temperatures since the Last Glacial Maximum'. *Nature* 599 (7884): 239–44. <https://doi.org/10.1038/s41586-021-03984-4>.
- Ou, Jinpei, Xiaoping Liu, Shaojian Wang, Rui Xie, and Xia Li. 2019. 'Investigating the Differentiated Impacts of Socioeconomic Factors and Urban Forms on CO₂ Emissions: Empirical Evidence from Chinese Cities of Different Developmental Levels'. *Journal of Cleaner Production* 226 (July):601–14. <https://doi.org/10.1016/j.jclepro.2019.04.123>.
- Pallares-Barbera, Montserrat, Meritxell Gisbert, and Anna Badia. 2021. 'Grid Orientation and Natural Ventilation in Cerdà's 1860 Urban Plan for Barcelona'. *Planning Perspectives* 36 (4): 719–39.
- Poussin, J.K. 2015. 'Effectiveness of Flood Damage Mitigation Measures: Empirical Evidence from French Flood Disasters'. *Global Environmental Change* 31 (March). <https://doi.org/10.1016/j.gloenvcha.2014.12.007>.
- Reyers, Belinda, Carl Folke, Michele-Lee Moore, Reinette Biggs, and Victor Galaz. 2018. 'Social-Ecological Systems Insights for Navigating the Dynamics of the Anthropocene'. *Annual Review of Environment and Resources* 43 (October). <https://doi.org/10.1146/annurev-environ-110615-085349>.
- Ribeiro, Haroldo V., Milena Oehlers, Ana I. Moreno-Monroy, Jürgen P. Kropp, and Diego Rybski. 2021. 'Association between Population Distribution and Urban GDP Scaling'. *PLOS ONE* 16 (1): e0245771. <https://doi.org/10.1371/journal.pone.0245771>.
- Richardson, Katherine, Will Steffen, Wolfgang Lucht, Jørgen Bendtsen, Sarah E. Cornell, Jonathan F. Donges, Markus Drüke, et al. 2023. 'Earth beyond Six of Nine Planetary Boundaries'. *Science Advances* 9 (37): eadh2458. <https://doi.org/10.1126/sciadv.adh2458>.
- Rockström, Johan, Will Steffen, Kevin Noone, Åsa Persson, F. Stuart Chapin, Eric F. Lambin, Timothy M. Lenton, et al. 2009. 'A Safe Operating Space for Humanity'. *Nature* 461 (7263): 472–75. <https://doi.org/10.1038/461472a>.
- Rosenfeld, Arthur H., Hashem Akbari, Joseph J. Romm, and Melvin Pomerantz. 1998. 'Cool Communities: Strategies for Heat Island Mitigation and Smog Reduction'. *Energy and Buildings* 28 (1): 51–62. [https://doi.org/10.1016/S0378-7788\(97\)00063-7](https://doi.org/10.1016/S0378-7788(97)00063-7).
- Samaniego, Jose Luis, Rafael Van der Borgh, José Eduardo Alatorre, and Jimmy Ferrer. 2022. 'Panorama de las actualizaciones de las contribuciones determinadas a nivel nacional de cara a la COP 26'. Santiago, Chile: Comisión Económica para América Latina y el Caribe. <https://www.cepal.org/es/publicaciones/47733-panorama-actualizaciones-contribuciones-determinadas-nivel-nacional-cara-la-cop>.
- Schiavina, Marcello, M. Melchiorri, C. Corbane, S. Freire, and F. Batista e Silva. 2022. 'Built-up Areas Are Expanding Faster than Population Growth: Regional Patterns and

- Trajectories in Europe'. *Journal of Land Use Science* 17 (1): 591–608.
<https://doi.org/10.1080/1747423X.2022.2055184>.
- Schmitt, Theo G., Martin Thomas, and Norman Ettrich. 2004. 'Analysis and Modeling of Flooding in Urban Drainage Systems'. *Journal of Hydrology, Urban Hydrology*, 299 (3): 300–311. <https://doi.org/10.1016/j.jhydrol.2004.08.012>.
- Schubert, Jochen E., Matthew J. Burns, Tim D. Fletcher, and Brett F. Sanders. 2017. 'A Framework for the Case-Specific Assessment of Green Infrastructure in Mitigating Urban Flood Hazards'. *Advances in Water Resources* 108 (October):55–68.
<https://doi.org/10.1016/j.advwatres.2017.07.009>.
- Schwaab, Jonas, Ronny Meier, Gianluca Mussetti, Sonia Seneviratne, Christine Bürgi, and Edouard L. Davin. 2021. 'The Role of Urban Trees in Reducing Land Surface Temperatures in European Cities'. *Nature Communications* 12 (1): 6763.
<https://doi.org/10.1038/s41467-021-26768-w>.
- Seto, Karen C., Burak Güneralp, and Lucy R. Hutya. 2012. 'Global Forecasts of Urban Expansion to 2030 and Direct Impacts on Biodiversity and Carbon Pools'. *Proceedings of the National Academy of Sciences* 109 (40): 16083–88.
<https://doi.org/10.1073/pnas.1211658109>.
- Seto, Karen C., Roberto Sánchez-Rodríguez, and Michail Fragkias. 2010. 'The New Geography of Contemporary Urbanization and the Environment'. *Annual Review of Environment and Resources*. Annual Reviews. <https://doi.org/10.1146/annurev-environ-100809-125336>.
- Shuttleworth, Emma, Martin Evans, Michael Pilkington, Jonathan Walker, David Milledge, and Timothy Allott. 2018. 'Restoration of Blanket Peat Moorland Delays Stormflow from Hillslopes and Reduces Peak Discharge'. *Journal of Hydrology X* 2 (December):100006. <https://doi.org/10.1016/j.hydroa.2018.100006>.
- Skougaard Kaspersen, P., N. Høegh Ravn, K. Arnbjerg-Nielsen, H. Madsen, and M. Drews. 2015. 'Influence of Urban Land Cover Changes and Climate Change for the Exposure of European Cities to Flooding during High-Intensity Precipitation'. *Proceedings of IAHS* 370 (June):21–27. <https://doi.org/10.5194/piahs-370-21-2015>.
- Steffen, Will, Paul J. Crutzen, and John R. McNeill. 2007. 'The Anthropocene: Are Humans Now Overwhelming the Great Forces of Nature?' *Ambio* 36 (8): 614–21.
- Steffen, Will, Katherine Richardson, Johan Rockström, Sarah E. Cornell, Ingo Fetzer, Elena M. Bennett, Reinette Biggs, et al. 2015. 'Planetary Boundaries: Guiding Human Development on a Changing Planet'. *Science* 347 (6223): 1259855.
<https://doi.org/10.1126/science.1259855>.
- Steinhausen, Max, Dominik Paprotny, Francesco Dottori, Nivedita Sairam, Lorenzo Mentaschi, Lorenzo Alfieri, Stefan Lüdtke, Heidi Kreibich, and Kai Schröter. 2022. 'Drivers of Future Fluvial Flood Risk Change for Residential Buildings in Europe'. *Global Environmental Change* 76 (September):102559.
<https://doi.org/10.1016/j.gloenvcha.2022.102559>.
- Strobl, Eric. 2011. 'The Economic Growth Impact of Hurricanes: Evidence from U.S. Coastal Counties'. *The Review of Economics and Statistics* 93 (2): 575–89.
- Sun, Zhongchang, Wenjie Du, Huiping Jiang, Qihao Weng, Huadong Guo, Youmei Han, Qiang Xing, and Yuanxu Ma. 2022. 'Global 10-m Impervious Surface Area Mapping: A Big Earth Data Based Extraction and Updating Approach'. *International Journal of Applied Earth Observation and Geoinformation* 109 (May):102800.
<https://doi.org/10.1016/j.jag.2022.102800>.
- Tabari, Hossein. 2020. 'Climate Change Impact on Flood and Extreme Precipitation Increases with Water Availability'. *Scientific Reports* 10 (1): 13768.
<https://doi.org/10.1038/s41598-020-70816-2>.

- Turner, Lyle R., Adrian G. Barnett, Des Connell, and Shilu Tong. 2012. 'Ambient Temperature and Cardiorespiratory Morbidity: A Systematic Review and Meta-Analysis'. *Epidemiology (Cambridge, Mass.)* 23 (4): 594–606. <https://doi.org/10.1097/EDE.0b013e3182572795>.
- UN Statistical Commission. 2020. "Methodology for delineation of urban and rural areas for international statistical comparison purposes". Available at: <https://unstats.un.org/unsd/statcom/51st-session/documents/>
- UNDESA. 2019. *World Urbanization Prospects: The 2018 Revision*, Online Edition. The Department of Economic and Social Affairs of the United Nations Secretariat, United Nations, New York.
- United Nations Environment Programme (UNEP). 2023. *Emissions Gap Report 2023: Broken Record – Temperatures hit new highs, yet world fails to cut emissions (again)*. Nairobi. <https://doi.org/10.59117/20.500.11822/43922>
- United Nations Human Settlements Programme (UN-Habitat). 2016. *Urbanization and development emerging futures*. United Nations Human Settlements Programme: World Cities Report 2016.
- United Nations Human Settlements Programme (UN-Habitat). 2022. *Envisioning Future Cities: World Cities Report 2022*. United Nations. <https://unhabitat.org/wcr/>
- Upreti, S., Cao, C., Gu, Y., Shao, X. 2017. "Improving the low light radiance calibration of S-NPP VIIRS day/night band in the NOAA operations". IEEE International Geoscience and Remote Sensing Symposium (IGARSS): 4726-4729.
- Valéry, Paul. 1931. *Regards sur le monde actuel* et autres essais. 305 pages, Editions Gallimard. EAN : 9782070324941
- Valle, Alejandro del, Mathilda Eriksson, Oscar A. Ishizawa, and Juan Jose Miranda. 2020. 'Mangroves Protect Coastal Economic Activity from Hurricanes'. *Proceedings of the National Academy of Sciences* 117 (1): 265–70. <https://doi.org/10.1073/pnas.1911617116>.
- Valle, Alejandro del, Alain de Janvry, and Elisabeth Sadoulet. 2020. 'Rules for Recovery: Impact of Indexed Disaster Funds on Shock Coping in Mexico'. *American Economic Journal: Applied Economics* 12 (4): 164–95. <https://doi.org/10.1257/app.20190002>.
- Virk, Gurdane, Antonia Jansz, Anna Mavrogianni, Anastasia Mylona, Jenny Stocker, and Michael Davies. 2015. 'Microclimatic Effects of Green and Cool Roofs in London and Their Impacts on Energy Use for a Typical Office Building'. *Energy and Buildings* 88 (February):214–28. <https://doi.org/10.1016/j.enbuild.2014.11.039>.
- Waters, Colin N., Jan Zalasiewicz, Colin Summerhayes, Anthony D. Barnosky, Clément Poirier, Agnieszka Gałuszka, Alejandro Cearreta, et al. 2016. 'The Anthropocene Is Functionally and Stratigraphically Distinct from the Holocene'. *Science (New York, N.Y.)* 351 (6269): aad2622. <https://doi.org/10.1126/science.aad2622>.
- WMO. 2023. *Guidelines on the Definition and Characterisation of Extreme Weather and Climate Events*. World Meteorological Organization, WMO-No. 1310. Geneva. Switzerland.
- WMO. 2024. *State of the Global Climate, 2023*. World Meteorological Organization, WMO-No. 1347. Geneva, Switzerland.
- Wooldridge J. 2002. *Econometric Analysis of Cross Section and Panel Data*. Cambridge, MA: MIT Press
- Xu, Zhiwei, Ruth A. Etzel, Hong Su, Cunrui Huang, Yuming Guo, and Shilu Tong. 2012. 'Impact of Ambient Temperature on Children's Health: A Systematic Review'. *Environmental Research* 117 (August):120–31. <https://doi.org/10.1016/j.envres.2012.07.002>.
- Yang, Yang, Theodore A. Endreny, and David J. Nowak. 2015. 'Simulating the Effect of Flow Path Roughness to Examine How Green Infrastructure Restores Urban Runoff Timing

- and Magnitude'. *Urban Forestry & Urban Greening* 14 (2): 361–67.
<https://doi.org/10.1016/j.ufug.2015.03.004>.
- Yao, Lei, Wei Wei, and Li-Ding Chen. 2016. 'How Does Imperviousness Impact the Urban Rainfall-Runoff Process under Various Storm Cases?' *Ecological Indicators* 60 (January):893–905. <https://doi.org/10.1016/j.ecolind.2015.08.041>.
- Ye, Xiaofang, Rodney Wolff, Weiwei Yu, Pavla Vaneckova, Xiaochuan Pan, and Shilu Tong. 2012. 'Ambient Temperature and Morbidity: A Review of Epidemiological Evidence'. *Environmental Health Perspectives* 120 (1): 19–28.
<https://doi.org/10.1289/ehp.1003198>.
- York, Richard, Eugene A Rosa, and Thomas Dietz. 2003. 'STIRPAT, IPAT and ImPACT: Analytic Tools for Unpacking the Driving Forces of Environmental Impacts'. *Ecological Economics* 46 (3): 351–65. [https://doi.org/10.1016/S0921-8009\(03\)00188-5](https://doi.org/10.1016/S0921-8009(03)00188-5).
- Zhao, Naizhuo, Feng-Chi Hsu, Guofeng Cao, and Eric L. Samson. 2017. 'Improving Accuracy of Economic Estimations with VIIRS DNB Image Products'. *International Journal of Remote Sensing* 38 (21): 5899–5918.
<https://doi.org/10.1080/01431161.2017.1331060>.
- Zhao, Xizhi, Bailang Yu, Yan Liu, Shenjun Yao, Ting Lian, Liujia Chen, Chengshu Yang, Zuoqi Chen, and Jianping Wu. 2018. 'NPP-VIIRS DNB Daily Data in Natural Disaster Assessment: Evidence from Selected Case Studies'. *Remote Sensing* 10 (10): 1526.
<https://doi.org/10.3390/rs10101526>.
- Zhou, Chunshan, and Shaojian Wang. 2018. 'Examining the Determinants and the Spatial Nexus of City-Level CO2 Emissions in China: A Dynamic Spatial Panel Analysis of China's Cities'. *Journal of Cleaner Production* 171 (January):917–26.
<https://doi.org/10.1016/j.jclepro.2017.10.096>.
- Ziter, Carly D., Eric J. Pedersen, Christopher J. Kucharik, and Monica G. Turner. 2019. 'Scale-Dependent Interactions between Tree Canopy Cover and Impervious Surfaces Reduce Daytime Urban Heat during Summer'. *Proceedings of the National Academy of Sciences of the United States of America* 116 (15): 7575–80.
<https://doi.org/10.1073/pnas.1817561116>.